UNCERTAIN INFERENCE, ESTIMATION, AND DECISION-MAKING IN INTEGRATED ASSESSMENTS OF GLOBAL CLIMATE CHANGE

by

L. JAMES VALVERDE A., JR.

M.S., Stanford University (1988)
S.M., Massachusetts Institute of Technology (1996)

SUBMITTED TO THE DEPARTMENT OF CIVIL AND
ENVIRONMENTAL ENGINEERING
IN PARTIAL FULFILLMENT OF THE REQUIREMENTS FOR THE DEGREE OF

DOCTOR OF PHILOSOPHY IN TECHNOLOGY, MANAGEMENT, AND POLICY

at the

MASSACHUSETTS INSTITUTE OF TECHNOLOGY

September 1997

Author.....................
Technology, Management, and Policy Program and
Department of Civil and Environmental Engineering
June 11, 1997

Certified by...............
Henry D. Jacoby
William F. Pounds Professor of Management
Sloan School of Management
Thesis Supervisor

Certified by.........................
Gordon M. Kaufman
Professor of Operations Research and Management
Sloan School of Management
Thesis Supervisor

Accepted by .
David H. Marks
James Mason Crafts Professor of Civil and Environmental Engineering

Accepted by ....
Joseph M. Sussman
Chairman, Departmental Committee on Graduate Studies

Uncertain Inference, Estimation, and Decision-Making in Integrated Assessments of Global Climate Change

by

L. James Valverde A., Jr.

Submitted to the Department of Civil and Environmental Engineering
on June 11, 1997, in partial fulfillment of the
requirements for the degree of
Doctor of Philosophy in Technology, Management, and Policy

Abstract

Current efforts to confront the prospect of anthropogenic global warming present policy analysts, decision-makers, and intergovernmental negotiators with a host of challenges. The technically-intensive nature of the policy debates that surround the climate change problem are complex and multifaceted. Much of the uncertainty that underlies the greenhouse debate arises, in part, from an incomplete understanding of critical features of atmospheric and climate science. Difficulties in predicting future levels of anthropogenic emissions of key greenhouse gases (GHGs), and their effects on the global carbon cycle, make it difficult to reliably assess the potential magnitude and timing of global climate change. Moreover, there are inherent difficulties in drawing reliable inferences as to the potential socio-economic impacts of climatic change, as well as the likely costs, benefits, and effectiveness of possible response strategies.

In this dissertation, we approach the problem of greenhouse warming from two complementary perspectives: (i) uncertain *inference* or *prediction*; and (ii) *decision-making under uncertainty*. Proceeding from these two vantage points, we set forth an integrated decision analysis (IDA) framework for structuring and evaluating complex policy decisions concerning global climate change and its potential socio-economic consequences. Our model formulation and discussion proceeds in four parts. First, we derive two *reduced-scale* models of the global climate system. These computationally-efficient models represent those processes that have the greatest influence on climatic change, and they permit nimble execution of long-term policy-dependent projections of global climate change. Second, we use econometric and statistical time series estimation techniques to numerically *calibrate* the reduced-scale models so that they essentially mimic the transient behavior of a larger global climate model that is contained within the MIT Integrated Global System Model (IGSM). Third, we develop *static* and *sequential* decision models for evaluating several GHG abatement policies that are currently being debated under the United Nations Framework Convention on Climate Change. The IDA framework draws structural linkages between the reduced-scale representations of the global climate system and the MIT IGSM. In addition, the framework provides a computational vehicle for exploring the role of *learning* in climate change decision-making. Finally, we conclude with an assessment of the policy relevance of our findings.

Thesis Supervisor: Henry D. Jacoby
Title: William F. Pounds Professor of Management
Sloan School of Management

Thesis Supervisor: Gordon M. Kaufman
Title: Professor of Operations Research and Management
Sloan School of Management

Acknowledgments

An undertaking such as this is not successfully completed without the assistance, encouragement, and support of many people, several of whom I would like to explicitly acknowledge here.

Since coming to MIT in the Fall of 1991, it has been my great fortune to have the opportunity to work under the direction of Gordon M. Kaufman. Working alongside Gordon has been the high point of my academic life, and I have learned much from him, both in and out of the classroom. His co-supervision of this dissertation has been thoughtful, precise, and always supportive.

Henry D. Jacoby has been an active supporter of the work presented here from the outset. Jake's leadership of the MIT Joint Program on the Science and Policy of Global Change is truly exemplary, and it has been my pleasure to have had an association with this world-class group of scholars. Jake's co-supervision of this dissertation was instrumental in helping me give the work a policy-relevant context and orientation. I owe Jake a debt of gratitude for providing me with detailed comments and suggestions on several early drafts of the dissertation, which did much to strengthen the clarity of the presentation.

John R. Ehrenfeld has had a tremendous influence on my intellectual development at MIT, and I am very fortunate to have had the opportunity to learn from him all these years. John's keen grasp of a range of disciplines, including technology, policy, risk analysis, philosophy of science, and social theory, combined with his uncanny ability to ask deep, penetrating questions, did much to help further my own understanding of these disciplines. Equally important, I think, is John's deep-seated humanity, which always came through in our conversations. MIT's Technology and Policy Program is truly fortunate to have an individual of John's calibre among its ranks.

Andrei Sokolov and Mort Webster extended themselves far beyond the call of duty in assisting me with various aspects of the work presented here. Andrei did much to further my knowledge and understanding of atmospheric science and climate modeling. In addition, I am grateful to Andrei for providing me with the time series data used in Chapter 4. Mort has been an excellent sounding board for new ideas, and I am fortunate to have had the benefit of his expertise in all matters pertaining to the MIT EPPA model; I am particularly grateful to Mort for his assistance with the sixteen sequential climate policies analyzed in Chapter 6.

Many friends and classmates have added much to my experiences at MIT. I am particularly grateful to Eugene Bae, Joanne Brown, Liberty Clinton, Debra Cash, Andrew Greco, Lindsay Haugland, Linda Kato, Alfonso Lopez-Arteaga, Sekhar Ramanathan, Karen Rothkin, Hitendra Wadhwa, and Kent Yan.

I owe a warm, heartfelt thanks to two-thirds of what aptly came to be known as the *Spanish Troika*: Jonathan Ladinsky and Ramon Vela Cordova, wonderful friends who helped me—each in his own way—through a difficult period in my life.

I am, of course, forever grateful to my parents and family for all that they have given me. My parents instilled in me a love for learning that has enriched my life beyond measure, and my brother, Omar, has been my best friend for 31 years.

The love and support given to me by Larry and Corrine Finnegan has made all the difference in the world.

Most important of all, this dissertation is dedicated in loving memory of Kristen Ellen Finnegan (1965-1995), the kindest, gentlest, most beautiful soul I have ever known.

L.J.V.A.
London

In Loving Memory of Kristen Ellen Finnegan

Contents

List of Figures

List of Tables

13

Chapter 1

Introduction

Current efforts to confront the prospect of anthropogenic global warming present policy analysts, decision-makers, and intergovernmental negotiators with a host of challenges. The technically-intensive nature of the policy debates that surround the climate change problem are complex and multifaceted. Much of the uncertainty that underlies the greenhouse debate arises, in part, from an incomplete understanding of critical features of atmospheric and climate science. Difficulties in predicting future levels of anthropogenic emissions of key greenhouse gases (GHGs), and their effects on the global carbon cycle, make it difficult to reliably assess the potential magnitude and impacts of global climate change. The climate change problem is, in addition, characterized by several unique features, all of which complicate efforts to arrive at reasoned responses to the prospect of anthropogenic global warming. For example, the time horizons that must be considered in the evaluation of climate change response strategies are on the order of one or more centuries. And although the climate change problem is global in scale, the spatial and temporal distribution of impacts is likely to be non-uniform. Moreover, the physical inertias that drive the global climate system are such that the potential social-economic and environmental impacts associated with climatic change are, to varying degrees, irreversible.

It is interesting to note that the history of scientific study of global warming is, in fact, long and varied. Fourier [22] was, perhaps, the first to notice—more than a century ago—that the Earth is a greenhouse, kept warm by an atmosphere that reduces the loss of infrared radiation. The overriding importance of water vapor as a greenhouse gas was recognized even then. In the late 1890s, Arrhenius [3] was the first to quantitatively relate the concentration of carbon dioxide (CO_2) in the atmosphere to global surface temperature. Scientific understanding has, of course, increased since then, particularly stimulated in the latter half of this century by the conclusion of Revelle and Suess [64] that anthropogenic emissions of CO_2 would, in

the near-term, exceed the rate of uptake by natural sources. Also stimulating interest in the scientific community was the demonstration by Keeling et al. [39] that atmospheric CO_2 is steadily increasing. These scientists' warnings had little effect on public opinion or policy until the summer of 1988, at which time it was noted that five out of the previous six summers in the United States were the hottest on record. In addition, the long-term global temperature record was presented to the United States Congress, suggesting that a global-mean warming had emerged above the natural background variation [27].

Most of the observed warming in this century occurred before 1940, when anthropogenic emissions of greenhouse gases were much lower than they are today. Observations such as this have led some scientists to question the reality, or at least the imminence, of global warming.[1] Although the cooling caused by anthropogenic aerosols seems likely to have masked the effect of rising CO_2 emissions, the explanations presented to Congress were viewed as cause for concern by many people. In the ensuing policy debates, few proponents have enunciated clearly how—in their view—society should proceed in the face of large scientific uncertainty concerning the prospect of global warming. Should society ignore the prospect of global warming, until there is more definitive and direct evidence for its occurrence, and until there is a better understanding of the potential adverse consequences associated with its occurrence? Or, rather, should society argue for immediate action to prevent anthropogenic changes that are comparable to natural disasters, and that might have dramatic effects at a future time when society has developed habits that may be difficult to curtail or reverse?

Present-day efforts to confront and, ultimately, manage the prospect of anthropogenic climate change have lead researchers to propose a broad range of analytical frameworks and methodologies for characterizing and evaluating the various dimensions of the problem. In recent years, it has become commonplace and fashionable for economists, policy analysts, and climate researchers to focus their efforts on the development of a class of models commonly referred to as *integrated assessment* models of global climate change. Integrated assessment models (IAMs) are characterized by their broad-based, comprehensive approach to the analysis of the climate change problem. IAMs seek to represent the most salient features of the climate change problem, and are typically comprised of analytically-tractable linkages between (i) models of atmospheric, oceanic, and biological processes; (ii) models of the global climate system; and (iii) models of the socio-economic processes that influence, and are affected by, climatic change.[2] In order to inform climate policy choice, IAMs seek to provide policy analysts and decision-makers with answers to the following sorts of questions:

---

[1] See, e.g., Balling [4] and Seitz [68].

[2] For insightful discussions on current approaches to climate-change-related integrated assessment modeling, see, e.g., Dowlatabadi [17], Parson [58], and Toth [76].

- When, and by how much, should GHG emissions be reduced to achieve specific levels of atmospheric GHG concentrations or climatic change?

- Should governments wait for more information about key uncertainties before allocating scarce resources?

In this dissertation, we set forth an integrated assessment methodology that is seen to consist of two complementary components: uncertain *inference* or *prediction*, on the one hand, and *decision-making under uncertainty*, on the other. Long-term projections of future climate are an important aspect of integrated assessments of global climate change. Such predictions are, however, characterized by large degrees of uncertainty, which, in turn, makes it difficult to draw reliable inferences as to the potential socio-economic impacts associated with climatic change. Reasoned decision-making about the prospect of anthropogenic global warming requires that we integrate this type of information with additional knowledge and information concerning the risks, costs, and benefits that characterize the range of possible climate change response options.

Integrated assessment modeling is, in many respects, an emerging discipline and practice. In recent years, researchers have proposed a number of approaches for the development of such models. In its latest report, Working Group III of the Intergovernmental Panel on Climate Change (IPCC) highlights two challenges currently facing integrated assessment modelers [9]:

- Integrating and managing a large and diverse array of data and models from many researchers and a range of disciplines;

- Improving the relevance of the models to policy needs, as well as the presentation of model results to policymakers.

In this dissertation, we address these concerns in the context of a policy-oriented, integrated decision analysis (IDA) framework for structuring and evaluating GHG abatement policies under uncertainty. The IDA framework is intended to aid policymakers and negotiators in their efforts to formulate and evaluate reasoned responses to the prospect of greenhouse warming. The framework integrates knowledge and information concerning the magnitude, timing, and impacts of climate change, as well as information concerning the likely effectiveness and cost of possible response options.

Given the scale and complexity of the climate change problem, there are, of course, a plurality of approaches that can be taken in the formulation and evaluation of GHG abatement strategies.[3] The modeling approach that we adopt here is markedly *decision-oriented*, in that

---

[3]See, e.g., Nordhaus [55] for an insightful overview of the range of analytical frameworks and economic models that have been brought to bear on the problem of evaluating climate change response strategies.

the methodology imposes a formal decision-theoretic frame on the manner in which climate change response options are structured and evaluated. Our motivation for pursuing a decision-oriented approach to integrated assessment modeling stems, in part, the IPCC's recent commentary that "treatments of decision making under uncertainty... are at present poorly developed in international environmental economics, and especially in the climate change literature" [9, p. 7]. Moreover, the IPCC makes the expectant claim that "decision analysis can be a powerful tool for understanding the barriers to making optimal choice. Thinking about climate choices as decision analysis problems may highlight those aspects most likely to affect the decision process" [9, p. 62]. The methodology and analysis that we set forth here can, in the context of these remarks, be seen to provide answers to the following closely-related set of questions:

- What does modern decision science have to contribute to the emerging theory and practice of integrated assessment modeling of global climate change?

- Viewed from a decision-theoretic perspective, what policy actions—if any—should be taken in response to the prospect of anthropogenic climate change?

In this light, the contributions made here to the climate change literature are both *methodological* and *policy-analytic* in character.

The structure of our IDA framework attempts to incorporate the most salient aspects of the greenhouse problem. In Figure 1-1, we provide a schematic representation of the framework's key components. The framework breaks down the evaluation of climate change response options into six basic components: (1) changes in anthropogenic carbon emissions; (2) changes in atmospheric CO_2 concentrations; (3) changes in the radiative balance of the global climate system; (4) changes in global-mean surface temperature; (5) physical outcomes associated with changes in global-mean surface temperature; and (6) economic valuation of climate-change-related impacts.

Our IDA framework serves as a bridge—conceptual and otherwise—between two different ways of approaching the task of integrated assessment modeling. In particular, the modeling approach set forth here draws explicit linkages between (i) the *policy evaluation* capabilities of the MIT Global System Model (IGSM), which is rich in physical and biogeochemical detail;[4] and (ii) the *policy optimization* capabilities of a complementary set of decision-theoretic models for evaluating climate change response options under uncertainty.

The MIT IGSM is designed to seek the best tradeoff between scientific detail and computational performance. However, even given this attention to computational efficiency, bottlenecks arise, because the IGSM contains subcomponent models that require substantial storage and

---

[4]Specific components of the MIT IGSM are described in more detail in subsequent chapters of this dissertation. For a comprehensive overview and description of the IGSM, see Prinn et al. [62].
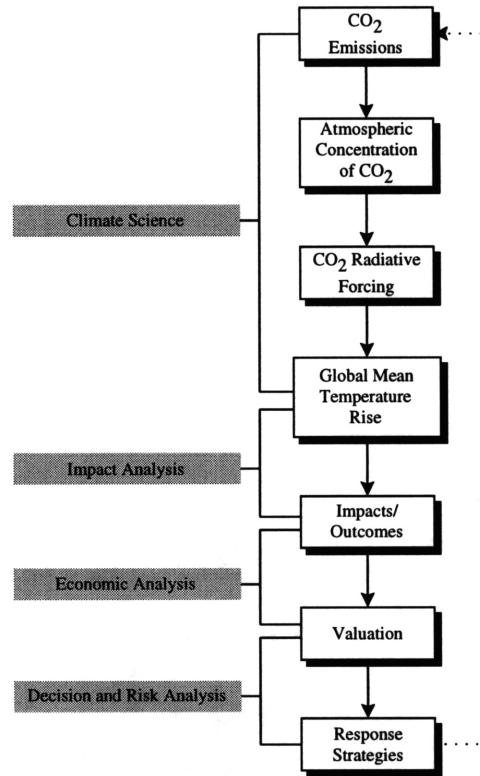
Figure 1-1: Schematic representation of the integrated decision analysis framework for evaluating global climate change response strategies.

execution time. In order to deal effectively with the limitations that computational constraints such as these impose on our ability to systematically trace-out the effects of policy choice on future climate, an important feature of our integrated modeling approach is the development of *reduced-scale* representations of the global climate system. As we discuss in the next several chapters, these computationally-efficient models represent those processes that have the greatest influence on climatic change, and they permit nimble execution of long-term policy-dependent projections of global climate change. These models are, in addition, numerically *calibrated* in such a way that they essentially mimic the transient behavior of a larger, more complex global climate model that is maintained within the MIT IGSM.

Because of their ability to mimic the transient behavior of their larger counterpart, these small and nimble models are capable of informing our understanding of the characteristic behavior of the IGSM. The reduced-scale models can, in this way, be used in an exploratory or experimental fashion to specify or design IGSM simulations and experiments. The modeling approach that we describe here is iterative in character: A study of climate policy using the IGSM produces a set of system outputs; the reduced-scale models are, in turn, calibrated against the integrated system output; the nimble models are then used to explore wider domains of
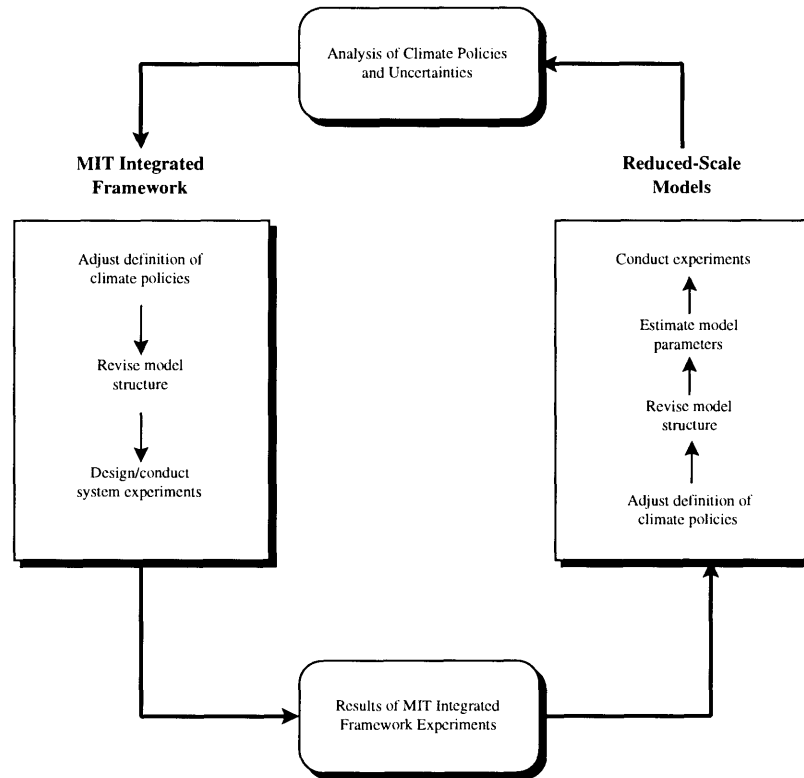
Figure 1-2: Interplay between the reduced-scale models and the MIT IGSM (Source: Jacoby, Kaufman, and Valverde (1995)).

policy choice than can be easily done with the computationally expensive IGSM (e.g., uncertainty analysis, sensitivity analysis, etc.); finally, this exploration of policy choice can, in turn, guide future decisions concerning which policies should be explored using the IGSM.

Figure 1-2 provides a schematic illustration of the interplay that exists between the IGSM and our reduced-scale modeling approach. In explaining this figure, we begin with the arrow at the lower left. The arrow represents the results of system experiments (e.g., GHG emission scenario studies, sensitivity analysis, etc.) that are conducted on the IGSM. These results are then used to (i) calibrate the reduced-scale models; (ii) inform the definition of policies to be studied; (iii) guide subsequent revisions of model structure; and (iv) estimate key model parameters.

Proceeding around the top of Figure 1-2, the reduced-scale models can also be used to inform subsequent analyses of climate policy, using the limited numbers of runs that are feasible within the larger integrated framework. The reduced-scale results can also provide information as to which uncertainties are most likely to be important to policy choice. This information can, in turn, lead to a judicious selection of cases to run using the more computationally expensive parts of the IGSM's interactive set of models. And so the analysis proceeds around the diagram, so long as the expected learning from additional rounds is perceived to be worth the cost of

analysis.

In the chapters that follow, we lay out the individual components that, together, comprise our IDA framework. The organization of our presentation follows the transition diagram shown in Figure 1-1. We begin, in Chapter 2, with a discussion of the nature of the relationship between global carbon emissions, changes in atmospheric CO_2 concentrations, and changes in CO_2-induced radiative forcing. As part of this discussion, we describe the nature of the global carbon cycle, and, in addition, we present several simplified carbon cycle models.

In Chapter 3, we address the related problems of climate modeling and prediction. We begin with a discussion of the major components of the global climate system, and then move to a discussion of the types of models that are used in its prediction. We then derive two reduced-scale global climate models that serve as key inputs to our IDA framework. The chapter concludes with the presentation of a simultaneous equations model for global climate change assessment.

In Chapter 4, we address the problem of numerically calibrating the reduced-scale global climate models presented in Chapter 3 to transient simulations of the MIT 2D-LO global climate model. Our calibration procedure utilizes econometric and statistical time series techniques to estimate key reduced-scale model parameters. The calibrated reduced-scale models are subsequently used to compute long-term, policy-dependent projections of global climate change.

In Chapters 5 and 6, we present *static* and *sequential* analyses, respectively, of several GHG abatement policies that are currently being debated under the United Nations Framework Convention on Climate Change. Chapter 5 begins with a brief discussion of the decision-theoretic concepts that underlie our modeling approach. We follow this discussion with the formal specification of a decision basis for evaluating GHG abatement policies under uncertainty. We then implement and numerically evaluate the decision basis within a graphically-based decision framework. As part of our analysis, we use deterministic and probabilistic sensitivity analyses to identify key uncertainties in the decision model. Finally, we consider the problems of valuing information and control, and we discuss the relevance of these concepts to climate change decision-making.

In Chapter 6, we consider the problem of climate change decision-making from a multi-period or sequential perspective. The chapter begins with an introduction to the basic concepts that underlie our sequential modeling approach. We then extend the static decision model presented in Chapter 5 to two periods. The chapter concludes with an in-depth examination of the role of *learning* in climate change decision-making.

Finally, in Chapter 7, we conclude with a summary of our research findings, and we propose several possible directions for future research.

Chapter 2

Radiative Forcing of Climate Change

A central feature of the integrated modeling approach that we set forth in this dissertation is the ability to assess the likely influence of policy choice on future climate. As an incremental step towards achieving this predictive capability, in this chapter we consider the first two linkages of the global climate change transition diagram shown in Figure 2-1. In particular, we consider the nature of the relation between global CO_2-equivalent emissions, changes in atmospheric CO_2 concentrations, and changes in radiative forcing. Our presentation is organized along the following lines. We begin with a brief introduction to the concept of radiative forcing, and from there we go on to consider the topic of CO_2-induced radiative forcing. We then discuss several key features of the global carbon cycle. As part of this discussion, we present three analytically-tractable frameworks for modeling the gradual accumulation of CO_2 concentrations in the Earth's atmosphere.

2.1   Introduction

Radiative forcing is formally defined as a change in the *average net radiation* at the tropopause, brought about by changes in either the incoming solar radiation, or in the outgoing infrared radiation. Radiative forcing therefore disturbs the balance that exists between incoming and outgoing radiation. As the climate system evolves over time, it responds to the perturbation by slowly re-establishing the radiative balance. In general, positive radiative forcing tends (on average) to give rise to surface warming, whereas negative forcing tends (on average) to give rise to surface cooling.

The Earth's climate is influenced largely by changes in radiative forcing that arise from changes in the concentrations of radiatively-active gases in the troposphere and the stratosphere. As Figure 2-2 illustrates, the global climate system is driven primarily by incoming
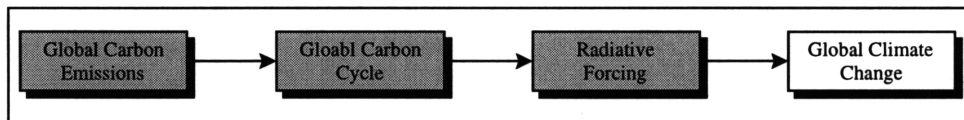
Figure 2-1: Transition between global carbon emissions, atmospheric CO_2 concentrations, and radiative forcing.

solar radiation. On an annually-averaged global scale, roughly one-third of the incoming solar radiation is reflected back out into space. Some of the outgoing (infrared) radiation is partially absorbed, and is then re-emitted by naturally-occurring GHGs. This so-called *natural greenhouse effect* warms the surface temperature of the Earth by approximately 33°C more than it would otherwise be if naturally-occurring GHGs were not present. The remaining two-thirds of the incoming radiation is absorbed by the atmosphere, land, ice, and ocean surfaces. In Figure 2-2, we see that the solar radiation that is absorbed by the Earth's atmosphere and surface (~ 240 Wm^{-2}) is—in the long run—balanced by outgoing infrared radiation. Thus, in *equilibrium*, the absorbed solar energy is balanced by the radiation that is emitted to space by the planet surface and atmosphere. Any factor that disturbs this balance is called a *radiative forcing agent* [32]. In the discussion that follows, we focus on the changes in radiative forcing that are brought about by changes in atmospheric CO_2 concentrations.

2.2 Carbon Dioxide Radiative Forcing

Long-term predictions of anthropogenic emissions of key GHGs play an important role in current efforts to obtain reliable predictions of future concentrations of radiatively and chemically important trace species. Emissions of the long-lived gases—CO_2, methane (CH_4), nitrous oxide (N_2O), and chlorofluorocarbons (CFCs)—are central to assessing changes in radiative forcing. Because of their influence on atmospheric chemistry, emissions of several short-lived gases, such as nitrogen oxides (NO_x), sulfur dioxide (SO_2), and carbon monoxide (CO), are also important. Carbon dioxide is the most important anthropogenic GHG. The importance of CO_2 as a GHG stems, in part, from the fact that its emissions are directly influenced by human activities. Moreover, ignoring the uncertain effects of the CFCs and changes in ozone, increases in CO_2 have, to date, contributed to roughly 70% of the enhanced greenhouse effect, with CH_4 and N_2O accounting for the remaining $\sim 23\%$ and $\sim 7\%$, respectively. Carbon dioxide is therefore likely to play a dominant role in future warming, whereas, over the course of the next century, the role of other GHGs is expected to be relatively minor.

Long-term projections of non-CO_2 GHGs are, at present, highly uncertain. Given this con-
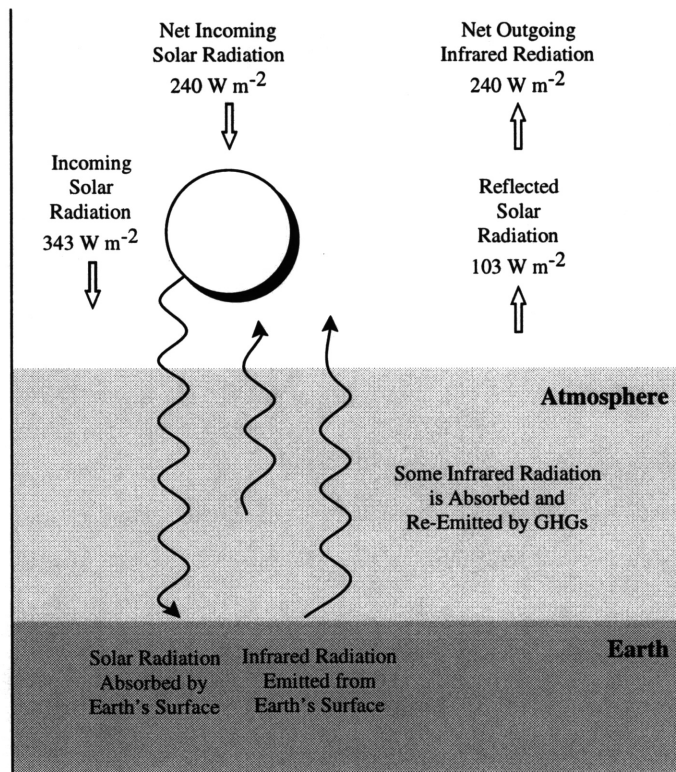
Figure 2-2: Schematic representation of the global long-term radiative balance of the Earth's atmosphere.

sideration, together with those outlined above, it is common practice to take these other gases and convert them to equivalent amounts of CO_2. These so-called *CO_2-equivalents* represent the amounts of CO_2 that would give rise to the same radiative forcing. In this dissertation, we adopt this CO_2-equivalent emissions approach, in that it provides a reasonable approximation to more computationally-burdensome and expensive analyses that treat each GHG in an individual fashion.

GHGs are typically classified in terms of their levels of concentration in the atmosphere, and in terms of the strength of their absorption of infrared radiation. Since pre-industrial times, CO_2 levels in the atmosphere have increased by more than 25%, from approximately 280 ppmv[1] to approximately 356 ppmv [7]. At present levels of atmospheric CO_2 concentrations, the relation between changes in GHG concentration levels and radiative forcing is strongly nonlinear [7]. This relation is typically expressed in terms of changes in *net radiative flux* at the tropopause (i.e., the top of the troposphere). In formal terms, we can represent these changes as

---

[1] 1 ppmv $\equiv$ 1 part per million by volume.

$$\Delta F(t) = f\left(\, C(t_0), \, C(t) \, \right),$$

where $\Delta F(t)$ denotes the change in net flux measured in Watts per square meter (Wm^{-2}) corresponding to a volumetric concentration change from the initial concentration level at time period t_0 to the concentration level at some later time period t.

Climate modelers utilize detailed radiative transfer models to explore the relationships that exist between radiative forcing and the atmospheric concentration levels of key GHGs. These radiative transfer models attempt to simulate the variation of the absorption and emission for specific GHGs, as a function of wavelength. These models also account for any overlap that exists between the absorption bands of the gases, as well as for the effects that clouds have on radiative transfer [32].

The concentration-forcing relationships that are derived from radiative transfer models are typically characterized by complicated functional forms. These complicated representations can, however, be used to derive simpler analytical expressions. For carbon dioxide, the functional form of f is well approximated by presuming a logarithmic dependence of $\Delta F(t)$ on $C(t)$. Specifically,

$$\Delta F(t) = 6.3 \ln \left(\frac{C(t)}{C(t_0)} \right), \tag{2.1}$$

where $C(t_0)$ and $C(t)$ are the atmospheric concentrations of CO_2 in ppmv at times t_0 and t, respectively. Equation (2.1) yields reasonable approximations of CO_2-induced radiative forcing for values of $C(t)$ less than 1000 ppmv.[2]

It is worth noting that the uncertainty that underlies the specification of the CO_2 forcing-concentration relationship arises from several sources. First, the radiative transfer models that are used to derive the complicated functional forms that ultimately give rise to Eq. (2.1) are themselves uncertain. For example, Shine et al. [71] cite a 1984 study that places the uncertainties at around $\pm 10\%$. In a more recent study, Cess et al. [12] document the uncertainties

---

[2]We note that in a recent study, Nordhaus [57] uses a somewhat different CO_2 forcing equation than that given by Eq. (2.1). The relationship between GHG accumulation and increased radiative forcing used by Nordhaus is given by

$$\Delta F(t) = 4.1 \, \frac{\log[C(t)/590]}{\log 2},$$

where $C(t)$ denotes the atmospheric concentration of CO_2 in ppmv at time period t. Nordhaus states that this forcing equation is "not controversial." As we discuss below, this statement is not altogether accurate. Also, Nordhaus states erroneously that this equation is used by the Intergovernmental Panel on Climate Change in their 1990 report [32]; in fact, the IPCC report uses Eq. (2.1). In comparing these two equations, it is important to recognize that each implies a different level of forcing in response to a static doubling of atmospheric CO_2, and will lead—other things being equal—to a different climate sensitivity. Specifically, the Nordhaus equation implies a climate sensitivity of 4.1 Wm^{-2}, whereas Eq. (2.1) implies a climate sensitivity of 4.4 Wm^{-2}.

in carbon dioxide radiative forcing in 15 GCMs. A series of CO_2 doubling experiments revealed substantial differences among the 15 models. In accounting for these differences, Cess et al. suggest several hypotheses:

- Differences in the lapse rate among the models;

- Differences in the atmospheric water vapor distributions among the models;

- Differences in the parameterization of radioactive overlap in the radiation codes of the models;

- Differences in the GCM cloud fields.

Cess et al. found that the largest contributor to the observed model-to-model variations was the carbon dioxide radiation parameterizations used in the GCMs. In addition, they found that the models used in the study gave a global warming average of approximately 4°C, and produced an average CO_2 forcing of 4.0 Wm^{-2}. These results are equivalent to an average climate sensitivity of 1°C of warming for each 1 Wm^{-2} of radiative forcing. In discussing the implications of this finding, Cess et al. make the following observation: Imagine that the 15 GCMs used in the study possess the same climate sensitivity of 1°C warming per 1 Wm^{-2} and, in addition, possess the same observed forcing variation. Under this set of assumptions, for presumed CO_2 concentration levels, the global warming projections given by the 15 GCMs would range from 3.4°C to 4.7°C *just because of their forcing differences*. This is an important observation, in that the range is substantial and, moreover, constitutes nearly half of the often-quoted IPCC climate sensitivity range of 1.5° - 4.5°C. We note that the IPCC range is based only on *feedback uncertainties*, and assumes no differences in the forcing. Also, the 3.4°C lower bound specified by Cess et al. is well above the IPCC "best estimate" of 2.5°C. Findings such as this provide an initial basis for explaining the degree of scientific uncertainty that surrounds current climate sensitivity estimates.[3]

2.3   Modeling the Global Carbon Cycle

An important aspect of global climate change assessment concerns the manner in which the carbon cycle is modeled. The storage and transport of carbon in the atmosphere is a process that is only partially understood. During the course of the past decade, atmospheric scientists have improved their understanding of how the removal of CO_2 from the atmosphere is distributed between sinks in the ocean and on land. In this biological, chemical, and physical

---

[3]For a discussion concerning the range of scientific opinion about climate sensitivity, as well as other key climate-change-related quantities, see Morgan and Keith [53].

process, carbon is transferred or exchanged between the atmosphere, oceans, and terrestrial biosphere. In the global climate system, the net uptake of anthropogenic CO_2 by the deep oceans occurs very slowly. Consequently, anthropogenic CO_2 has a long-lasting effect on atmospheric concentrations and future climate. In the 1980s, the average rate of increase in atmospheric CO_2 concentrations was on the order of 1.5 ppmv/year, which is equivalent to 3.2 GtC/year [7]. Viewed on a decadal time-scale, the proportion of anthropogenic emissions remaining in the atmosphere has stayed relatively constant at approximately 50%.

In order to model the global carbon cycle, there are several key processes that need to be considered [7]:

- The exchange of CO_2 between the atmosphere and the ocean;

- The exchange of CO_2 between surface waters and long-term storage in the deep ocean;

- The net release or uptake of CO_2 from changes in land-use practices;

- Photosynthetic uptake, storage, and transfer of CO_2 by soil and plants.

Current efforts to negotiate so-called *quantified emission limitation and reduction objectives* (QEL-ROs) require an understanding of the nature of the relation between carbon emissions and atmospheric CO_2 concentrations. Naturally, climate-change-related targets can be defined in a number of ways. Say, for example, that an international agreement is reached whereby Annex I countries[4] abate GHG emissions so as to achieve an emissions target, E^*, by the year 2010. Figure 2-3 illustrates three separate emission time-paths that achieve this target. Though each path leads to the same target, the accumulation of CO_2 concentrations in the atmosphere will differ for each carbon emission path.

Alternatively, QELRO-type agreements can be cast in terms of *cumulative* emission targets, where a cap or upper bound is placed on the total sum of carbon emissions that are allowed within a particular time frame. We illustrate this concept in Figure 2-4. Although the cumulative emissions from 1990 to 2100 are (roughly) the same for paths A and B, the concentration trajectories associated with each of these emission paths (illustrated in Figure 2-5) differ from one another, as do their implied commitments to warming. In this way, the specification of a cumulative emission target gives rise to various possible emission time-paths that achieve the target. For this reason, the *shape* of the emission time-path is an important consideration, in that early reductions may give rise to potentially beneficial outcomes.

Recent policy proposals for confronting the prospect of anthropogenic global warming have focused on the goal of *stabilizing* atmospheric concentrations of carbon dioxide. In order to evaluate CO_2 stabilization policies, we must pose two fundamental questions [7]:

---

[4]Annex I countries consist of the OECD nations (except Mexico), plus 12 so-called "economies in transition" in the former Soviet Union and Eastern Europe.

Figure 2-3: Three alternative carbon emission time-paths that achieve the same emission target, E^*, in the year 2010.

- For a given CO_2 emission time-path, in what way are atmospheric CO_2 concentrations likely to evolve in the future?

- For a given atmospheric CO_2 concentration trajectory leading to *stabilization* at some predefined level, what anthropogenic carbon emission time-path is implied?

In light of these questions, an important task in the evaluation of CO_2 stabilization policies is the identification of emission time-paths that—over the course of a predefined time horizon—achieve a desired level of stabilization. Early efforts to explore this problem were first carried out under the auspices of the IPCC. Specifically, two types of calculations were performed. In the first type of calculation, "forward" projections were used to determine the atmospheric CO_2 concentrations that would result from a specified carbon emission time-path. Looking, first, at a broad range of carbon emission scenarios—each encompassing a diverse range of assumptions concerning factors such as economic growth and demographics—global carbon cycle models showed marked increases in projected atmospheric CO_2 concentrations well above pre-industrial levels by the year 2100.[5]

---

[5]In fact, several of the IPCC scenarios are characterized by a doubling of pre-industrial CO_2 levels before the year 2070.
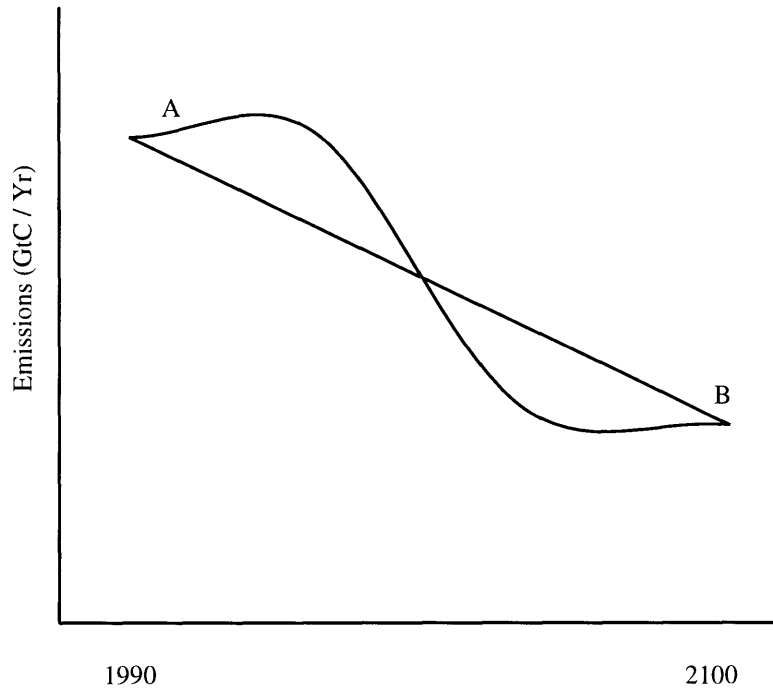
Figure 2-4: The area under carbon emission paths A and B are roughly the same over the 110 year time horizon.

In the second type of calculation, the IPCC computed the carbon emission time-paths required to achieve particular CO_2 concentration stabalization levels via specified pathways. In a series of analyses presented in its 1994 report [7], the IPCC used "inverse" carbon cycle calculations to determine the emission time-paths that would be required to achieve stabalization of atmospheric CO_2 concentrations at levels ranging from 350 ppmv to 750 ppmv via specified pathways.[6] The IPCC inverse calculations suggest that major reductions in global carbon emissions will be required in order to stabalize atmospheric CO_2 levels, even at 750 ppmv.

In order to assess the influence that policy choice is likely to have on future climate, it is necessary to model the global carbon cycle in a computationally-tractable manner. In the discussion that follows, we consider three simplified models of the global carbon cycle.

2.3.1 Three Simple Carbon Cycle Models

The three carbon cycle models that we present below for modeling the accumulation of carbon dioxide in the Earth's atmosphere are computationally-tractable and, in addition, are easily

---

[6]According to the IPCC, "the selection of the range of concentrations from 350 ppmv to 750 ppmv was *arbitrary* and should not be construed as having any policy implications," and "many different stabilization levels, time-scales for achieving these levels, and routes to stabilization could have been chosen" [7, p. 15, emphasis added].
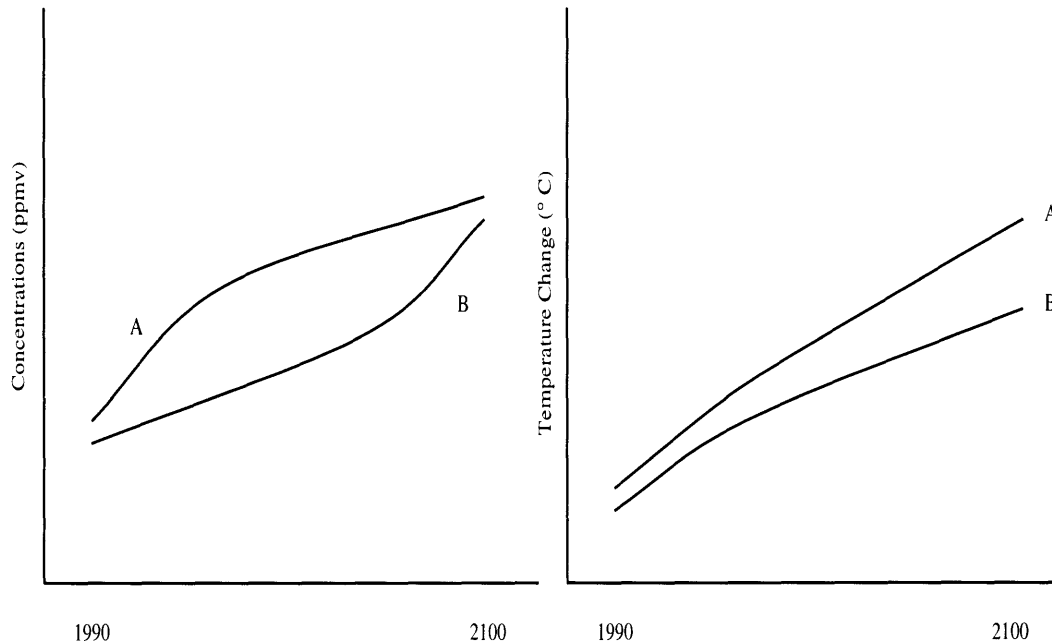
Figure 2-5: Carbon emissions paths A and B lead to different concentration and temperature change trajectories.

implementable within an integrated assessment framework.

Model I

In order to link anthropogenic emissions of carbon dioxide to atmospheric concentrations, we begin by stating the problem in terms of *sources* and *sinks*. Specifically, we construe the process of accumulation of carbon as a *trend*, defined as the difference of all sources and sinks:

$$\text{Trend} = \text{Source} - \text{Sink}.$$

In more formal terms, this relationship can be expressed as

$$\frac{\Delta C}{\Delta t} = E(t) - \frac{C(t)}{\tau}, \tag{2.2}$$

where E denotes the carbon source, C denotes the atmospheric concentration of CO_2 in ppmv, and τ denotes the *atmospheric lifetime* of CO_2. For our purposes here, let $E(t)$ denote the amount of anthropogenic CO_2 that is emitted at time t, specified in units of GtC/year. Let $\Delta C(t) = C(t + h) - C(t)$ denote the change in atmospheric CO_2 concentrations during the finite time interval $[t, t + h)$. If we now define the time step $\Delta t = h$, then Eq. (2.2) becomes

$$\lim_{h \to 0} \frac{\Delta C(t)}{h} = \frac{dC(t)}{dt} = k_{CO_2} E(t) - \frac{C(t)}{\tau}, \tag{2.3}$$

where the constant k_{CO_2} converts CO_2 concentrations in GtC to ppmv.

We are typically interested in estimating observed changes in CO_2 concentration levels relative to some arbitrarily-specified time period or baseline, which we denote by t_0. At equilibrium, the time derivative $dC(t)/dt$ evaluated at time $t = t_0$ is equal to zero. For $t \geq t_0$, let $C(t) = C(t_0) + [C(t) - C(t_0)]$. Also, to simplify notation, let

$$\delta C(t) \equiv C(t) - C(t_0)$$

denote the difference between atmospheric CO_2 concentrations at time periods t and t_0, respectively. Equation (2.3) can now be written as

$$\begin{aligned} \frac{dC(t)}{dt} &= \frac{d}{dt}[C(t) - C(t_0)] = \frac{d\delta C(t)}{dt} \\ &= k_{CO_2} E(t) - \frac{C(t) - C(t_0)}{\tau}. \end{aligned} \tag{2.4}$$

In terms of a finite time interval $[t, t + h)$, for some time-step $h > 0$, when h is small, Eq. (2.4) can be approximated by

$$[\delta C(t + h) - \delta C(t)] \approx h \left[k_{CO_2} E(\xi) - \frac{C(\xi) - C(\xi_0)}{\tau} \right], \tag{2.5}$$

for any $t \leq \xi < t + h$. If we choose $h = 1$, and let $\xi = t$ and $\xi_0 = t_0$, then Eq. (2.5) becomes

$$\delta C(t + 1) - \delta C(t) \approx k_{CO_2} E(t) - \frac{C(t) - C(t_0)}{\tau},$$

which gives rise to

$$\delta C(t + 1) \approx \delta C(t) + k_{CO_2} E(t) - \frac{\delta C(t)}{\tau}. \tag{2.6}$$

Equivalently, Eq. (2.6) can be expressed as

$$\delta C(t) \approx \delta C(t - 1) + k_{CO_2} E(t - 1) - \frac{\delta C(t - 1)}{\tau}. \tag{2.7}$$

Model II

A second model of the global carbon cycle is quite similar to the model we described above. This model is used by Nordhaus [57] in his DICE model, and was originally put forth by Machta [43]. The model assumes that the *accumulation* and *transportation* of carbon emissions follow the equation

32

$$C(t) = (1 - \frac{1}{\tau_e}) C(t-1) + \beta E(t-1), \tag{2.8}$$

where $C(t)$ represents the deviation of atmospheric CO_2 concentrations from its preindustrial equilibrium, $E(t)$ represents anthropogenic CO_2 emissions, τ_e is the *e-folding* or turnover time (in years) for the deep oceans, and β is the *marginal atmospheric retention rate.* Most estimates place τ_e between 100 and 500 years. Missing in this model is an explicit treatment of the uptake and release of CO_2 by the terrestrial biosphere.

In Eq. (2.8), atmospheric concentrations of CO_2 are calculated as deviations from an equilibrium preindustrial level, which, for our purposes here, is taken to be 590 GtC. Intuitively, Eq. (2.8) states that deviations in the total carbon mass in the atmosphere are increased by carbon emissions, but are reduced as carbon diffuses into the deep ocean [57].

It is possible to recast Eq. (2.8) so as to represent the accumulation and transport of atmospheric CO_2 on a *decadal* time scale. Specifically, Eq. (2.8) can be written as

$$C(t) = (1 - \gamma) C(t-1) + \beta E(t-1), \tag{2.9}$$

where γ is the decadal rate of transfer to the deep oceans, which are treated as an infinite sink. Equation (2.9) therefore assumes that, in the short run, the fraction β of an emission remains in the atmosphere, and that GHGs are transported to the deep oceans at a rate γ [57].

Model III

The carbon cycle models described above are relatively simple representations of the storage and transport of carbon in the global climate system. There are, however, several key facets of the global carbon cycle that these models do not consider. Central in this regard is the manner in which we represent the uptake of CO_2 by the ocean. In the models presented earlier, there are, for example, no factors that dampen the rate at which carbon dioxide is removed from the atmosphere when there are exponential increases in carbon emissions. Also missing from these models are explicit treatments of the uptake and release of CO_2 by the terrestrial biosphere.

In an attempt to address these shortcomings, in recent years attention has focused on the development of realistic ocean CO_2 storage models that are, at the same time, computationally-tractable. Maier-Reimer and Hasselmann [45], for example, put forth a relatively simple global carbon cycle model that attempts to accurately represent the transport and storage of CO_2 in the oceans. This model is used in several recent integrated assessments of the climate change

problem.[7]

The Maier-Reimer and Hasselmann carbon cycle model provides a computationally tractable means by which to estimate the atmospheric CO_2 concentration trajectories associated with specific CO_2 emission time-paths. The essential component of the model involves summarizing the response of a coupled three-dimensional global ocean circulation model and carbon cycle model in terms of a simple *linear impulse response function*, which we denote by $G(t)$.[8] For an arbitrarily-specified carbon emission trajectory, $E(t)$, specified in terms of GtC/year, the change in *atmospheric mass* of CO_2, $\Delta M(t)$, is given by

$$\Delta M(t) = 2.13 \, \Delta C(t) \quad = \quad \int_{t_0}^{t} E(t - u) \, G(u) \, du$$

$$= \quad \int_{t_0}^{t} E(u) \, G(t - u) \, du, \qquad (2.10)$$

where $\Delta C(t)$ denotes the change in atmospheric CO_2 concentration in ppmv from time period t_0 to period t, and the constant term 2.13 converts concentrations in ppmv to masses in GtC. Alternatively, the atmospheric concentration of CO_2 at time t can be expressed as

$$C(t) = C(t_0) + k_{CO_2} \int_{t_0}^{t} E(u) \, G(t - u) \, du, \qquad (2.11)$$

where $k_{CO_2} = 1/2.13 = 0.4695$ ppmv/GtC.

In their model formulation, Maier-Reimer and Hasselmann express the impulse response function, $G(t)$, as the sum of several exponential decay terms, each of which represents different time scales that characterize the ocean mixing portion of the carbon cycle. In particular,

$$G(t) = a_0 + \sum_{i=1}^{4} a_i \exp\left(-\frac{t}{\tau_i}\right). \qquad (2.12)$$

In this equation, the amplitude a_0 denotes the asymptotic airborne fraction for the equilibrium response of the ocean-atmosphere system to any finite-duration unit integral input function [45]. The a_j terms are interpreted as the relative capacity of other reservoirs; these reservoirs are filled independently by atmospheric input, at rates that are characterized by the relaxation time scales τ_j (in years).

Maier-Reimer and Hasselmann fit the linear impulse response function given by Eq. (2.12) via a least-squares procedure to the computed response of the ocean carbon cycle model for a step-function change in the initial CO_2 concentration. Table 2.1 provides the fitted response function

---

[7]See, e.g., Dowlatabadi and Morgan [18, 19], Hammitt [26], and Lempert et al. [41].

[8]As Maier-Reimer and Hasselmann point out, the linearity assumption is reasonable for small deviations from a *stationary* equilibrium state.

a_0	a_1	τ_1	a_2	τ_2	a_3	τ_3	a_4	τ_4
0.131	0.201	362.9	0.321	73.6	0.249	17.3	0.098	1.9

Table 2.1: Exponential fits to the computed impulse response function for a step-function increase of initial atmospheric CO_2 concentration level by a factor of 1.25.

parameters for a sudden step-function initial change of a 25% increase in the initial (1800) atmospheric CO_2 concentration level.[9]

Having specified the fitted response function parameters described above, substituting Eq. (2.12) into Eq. (2.11) yields

$$C(t) = C(t_0) + k_{CO_2} \int_{t_0}^{t} E(u) \left(a_0 + \sum_{i=1}^{4} a_i \exp\left[-\frac{(t-u)}{\tau_i} \right] \right) du. \qquad (2.13)$$

In recent years, researchers have developed numerical methods that avoid the computationally-intensive task of constructing time series for $C(t)$ by successive iteration of Eq. (2.13). By exploiting the functional form of $G(t)$, it has been possible to develop computationally-efficient algorithms that avoid the direct calculation of the convolution integral.[10]

2.4 Summary

In this chapter, we discussed a number of issues relating to the topic of radiative forcing of climate change. The set of integrated model linkages discussed here represent a crucial step in our efforts to assess the influence that policy choice is likely to have on future climate. In the following chapter, we consider the next linkage in our IDA framework, namely, the relation between changes in radiative forcing and changes in global-mean surface temperature.

---

[9]Maier-Reimer and Hasselmann [45] also specify the fitted response function parameters for step-function initial changes representing static doublings and quadruplings of initial atmospheric CO_2 concentrations.

[10]See, e.g., Harvey [29] and Wigley [79].

Chapter 3

Climate Modeling and Prediction

In the previous chapter, we considered the first two linkages in our integrated framework, namely, the relation between global carbon emissions, changes in atmospheric CO_2 concentrations, and changes in radiative forcing. In this chapter, we consider the third linkage in our integrated framework, namely, the relation between changes in CO_2-induced radiative forcing and changes in the global-mean surface temperature. This linkage is illustrated in Figure 3-1. We divide our presentation into three parts. In Section 3.1, we begin with a brief description of the basic components of the global climate system, as well as the various types of models that are used in its prediction. In Section 3.2, we describe the *reduced-scale* climate modeling approach that is utilized in this dissertation. As part of this discussion, we derive two globally-averaged reduced-scale climate models that are used in our IDA framework to generate long-term policy-dependent projections of global climate change. In Section 3.3, we present a simultaneous equations model for global climate change assessment. We close with a numerical test of the stability of the coupled system.

3.1 Modeling the Global Climate System

The global climate system is comprised of several major components, all of which interact with one another in complex and often unpredictable ways. The fundamental process that drives the climate system is *heating* by incoming short-wave radiation and *cooling* by long-wave radiation into space. In general, the climate system of the Earth can be seen to consist of the following five basic components:

- **Atmosphere**. Absorbs and emits infrared radiation; clouds promote cooling by reflecting sunlight.

36

```
┌─────────────────────────────────────────────────────────────────────────┐
│  ┌──────────────┐      ┌──────────────┐      ┌──────────────┐      ┌──────────────┐  │
│  │ Global Carbon│ ───▶ │ Gloabl Carbon│ ───▶ │   Radiative  │ ───▶ │ Global Climate│  │
│  │   Emissions  │      │    Cycle     │      │    Forcing   │      │    Change    │  │
│  └──────────────┘      └──────────────┘      └──────────────┘      └──────────────┘  │
└─────────────────────────────────────────────────────────────────────────┘
```
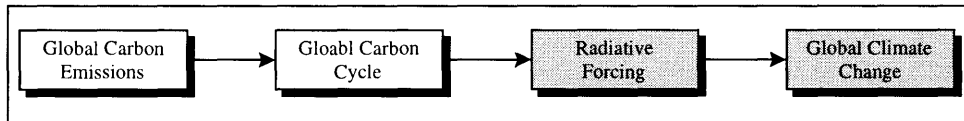
Figure 3-1: Transition between radiative forcing and global climate change.

- **Oceans.** Exert a large influence on current climate conditions; absorb over half of the solar radiation reaching the Earth's surface. The heat capacity of the ocean delays the response of the climate system.

- **Land.** Atmospheric processes are strongly coupled to the land surface of the planet. The soil interacts with the atmosphere via exchanges of aerosols, gases, and moisture. Such exchanges are influenced by soil type and vegetation, and are strongly dependent on soil wetness.

- **Ice.** Reflects sunlight; sea-ice reduces heat exchange between the ocean and atmosphere, and affects climate on time-scales of seasons and longer.

- **Biosphere.** Affects climate by influencing atmospheric composition, albedo, and hydrology. Also controls the magnitude of the fluxes of several GHGs, including CO_2 and methane.

We illustrate these basic components of the global climate system in Figure 3-2.

Modeling the components and processes that, together, makeup the global climate system is a complicated task. Numerical models attempt to mimic or simulate the physical processes that give rise to climatic change. In order to simulate the dynamic behavior of the climate system, modelers utilize simplified representations, most of which are based on physical laws governing such factors as mass, momentum, and energy flows and exchanges in the atmosphere.

The task of arriving at realistic representations of the global climate system's main components and processes is complicated by a number of factors. First, many of the physical laws that govern the processes that influence climate change are poorly understood. For example, as Lindzen [42] points out, very little is known about the factors that determine the equator-to-pole temperature distribution. Knowledge about this distribution bears directly on our understanding of the processes that determine the mean surface temperature of the Earth.

The uncertainties that underlie modern atmospheric science's best physical representations of clouds and oceans limit the predictive capability of even the most sophisticated climate models. Most climate models are extremely sensitive to the manner in which clouds are represented. Intuitively, clouds have both a positive and a negative effect on warming: Clouds exert a negative effect on temperature by reflecting sunlight off into space, and they have a positive effect

37

Space
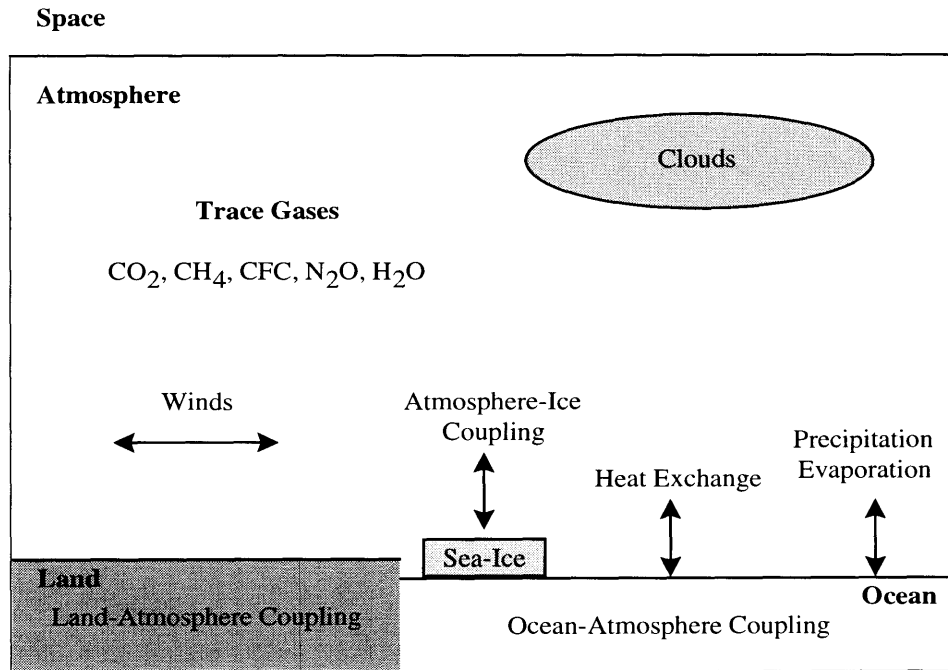
Figure 3-2: Simplified representation of the global climate system.

by trapping heat from below. It is generally accepted that cloud feedback is an important determinant of observed differences in estimates of global warming [53]. Conjectures about the direction and magnitude of cloud feedback effects vary significantly; also, the factors that most influence cloud behavior (e.g., type, amount, height distribution, etc.) are poorly understood, and realistic models are several years away.

The role of the oceans in absorbing CO_2, as well as in storing and transporting heat, is also poorly understood. The Earth's oceans transport roughly 50% of the heat carried from the equator to the pole. The oceans also slow temperature change, though—as we discuss in Chapter 4—fundamental uncertainty exists as to the rate at which heat is transported downward in the ocean.

The task of modeling the global climate system is complicated by other factors, as well. For example, the specification of the climate system's initial conditions is an inherently problematic task. Equally important, the global climate system is characterized by a complex array of interactions and feedbacks, knowledge of which is also highly uncertain. Complicating matters further is the fact that these climatic interactions and feedbacks occur at different levels of both spatial and temporal resolution.

38

3.1.1 Types of Climate Models

There are, of course, many ways to model the global climate system. In general, all numerical climate models must address the following set of issues [30]:

- **Radiation.** The input and absorption of incoming solar radiation; emission of outgoing infrared radiation.

- **Dynamics.** The movement of energy around the globe, from low to high latitudes, as well as vertical movements.

- **Surface Processes.** The role of land/ocean/ice interactions and the resultant change(s) in albedo, emissivity, and surface-atmosphere energy interchanges.

- **Resolution in Space and Time.** The time-step of the model, as well as the resolution of the horizontal and vertical scales.

The manner and degree to which these facets of the climate system are represented in numerical climate models depends, in large measure, upon the climate model type. In general, there are four basic types of climate models:

- **Energy Balance Models.** Zero- and one-dimensional models that are used to predict either globally-averaged temperature or the variation of the Earth's surface temperature with latitude. Models of this type are useful for evaluating scenarios of future climate change, as well as for developing parameterizations that explore climate system sensitivities.

- **One-Dimensional Radiative-Convective Models.** Models that make explicit calculations of the fluxes of solar and terrestrial radiation. Models of this type usually include detailed representations of radiative transfer and atmospheric chemistry. Such models usually compute vertical globally-averaged temperature profiles by modeling the radiative process with a "convective adjustment" that re-establishes a predetermined lapse rate.[1]

- **Two-Dimensional Statistical Dynamical Models.** Models that represent surface processes and dynamics in a zonally-averaged manner, and with a vertically resolved atmosphere. Such models typically represent either the two horizontal dimensions, or the vertical and horizontal dimensions.

- **General Circulation Models.** Utilize fundamental equations that describe flows of mass, momentum, and heat, to model the three-dimensional nature of the atmosphere and ocean; such models typically have a higher spatial resolution than other types of climate models.

---

[1]The *lapse rate* is the rate at which temperature decreases as a function of height in the atmosphere.

3.1.2 Climate Sensitivity and Intermodel Comparisons

An important scientific uncertainty in the greenhouse debate concerns the expected change in global-mean surface temperature that results from increases in atmospheric concentrations of key GHGs. The models described above all play a role in present-day efforts to assess the influence of GHGs on climatic change. These gases include—in addition to CO_2—methane (CH_4), nitrous oxide (N_2O), the CFCs, and, most importantly, water vapor.[2] Factors that determine the atmospheric concentrations of GHGs from known emissions are moderately well understood, though current forecasts of CFC concentrations are thought to be much more certain than forecasts of CO_2, CH_4, and N_2O.

A useful benchmark for comparing models is the so-called *climate sensitivity* value, which is defined as the *equilibrium response* of the global climate system to a static doubling of atmospheric CO_2 concentrations. Most scientists believe that the range 1–5°C is likely to contain the true climate sensitivity value.[3] If there were no change in the concentration of water vapor, a static doubling of atmospheric CO_2 would give rise to a global mean surface temperature increase of $\Delta T_d \approx 1.2°C$.[4] However, as water evaporates with increasing temperature, the concentration of water vapor in the Earth's atmosphere is expected to increase; this effect could, in turn, amplify warming. In addition, water can introduce interactive feedbacks into the climate system, such as water vapor, clouds (especially cirrus clouds), and snow-ice albedo. Feedbacks such as these introduce considerable uncertainty into long-term predictions of global-mean surface temperature changes resulting from increases in atmospheric concentrations of key GHGs.

Global-mean surface temperature, ΔT_s, is roughly related to ΔT_d by the formula

$$\Delta T_s = \Delta T_d / (1 - f),$$

where f denotes the sum of all climate feedbacks. The water vapor feedback is relatively simple, in that a warmer atmosphere is likely to contain more water vapor. This process gives rise to a positive feedback: An increase in one greenhouse gas, CO_2, induces an increase in another greenhouse gas, namely, water vapor. Cloud feedback, however, is harder to evaluate, because it depends on the difference between the warming caused by the reduced emission of infrared radiation from the Earth into outer space and the cooling through reduced absorption of solar

---

[2] The concentration of water vapor varies rapidly in space and time, and this variation arises from climate feedback mechanisms that are currently not well understood.

[3] See, e.g., National Academy of Sciences [54] and the Intergovernmental Panel on Climate Change [31]. Cf. Jacoby and Prinn [36, p. 13–16] for an insightful discussion of the various interpretations that can be attached to the Intergovernmental Panel's climate sensitivity range.

[4] This estimate depends on the assumption that the cooling of the Earth is from the stratosphere, and that there is a fixed air temperature distribution with height.

radiation. The net effect is determined by the amount of clouds, their altitude, and their water content. Estimates for ΔT_s from different models vary from 1.9°C to 5.2°C [15].

It is worth noting that two models which give similar values for ΔT_s values can differ in the effects of various feedback mechanisms. For example, two GCM models—GFDL and GISS[5]— show an unequal temperature increase as clouds are included (from 1.7°C and 2.0°C to 2.0°C and 3.2°C, respectively). The effects of ice albedo in these two models are different, but opposite, so that the results converge (4.0°C versus 4.2°C, respectively). What this example shows is that agreement between models may be spurious and potentially misleading. In addition, many climate experts believe that f is high enough (~ 0.70) that even small increases in this value could result in a runaway warming that is not predicted by current models [46, 74].

3.1.3 The MIT 2D-LO Global Climate Model

The prediction of anthropogenic climate change is an important facet of the MIT Joint Program on the Science and Policy of Global Change. Within this research program, efforts are currently underway to develop a large-scale integrated assessment framework for addressing various aspects of the greenhouse debate, including carbon emissions projection, climate prediction, economic analysis of control policies, and the assessment of social and environmental impacts.[6]

An important component of the MIT framework is a sophisticated land- and ocean-resolving two-dimensional (2D-LO) climate model that simulates various climate processes and variables that relate to environmental and societal impacts. The 2D-LO model simulates zonally-averaged climate separately over land and ocean, as a function of both latitude and height. The radiation code that is contained within the 2D-LO model includes all significant GHGs (H_2O, CO_2, CH_4, N_2O, CFCs, etc.), and twelve types of aerosols.

The choice of the 2D-LO model is motivated, in part, by the observation that latitudinal variations play a stronger role than longitudinal variations in determining climate, and that transport by large-scale 3-D eddies can be parameterized using dynamical theory. Projections of climate change are based on changes in the zonal-mean climate over land and ocean, with more detailed longitudinal variations being based on current climate, or on transient 3-D model simulations of climate change.

The 2D-LO climate model solves the primitive system equations as an initial value problem. There are nine vertical layers: two in the planetary boundary layer, five in the troposphere, and two in the stratosphere. There are 24 grid points in latitude, corresponding to a resolution of 7.826°. A schematic of the model is shown in Figure 3-3. In the verification and validation

---

[5]See, e.g., Hansen et al. [28].

[6]For a detailed description of the issues that underlie the conceptual design, model selection, and development of the MIT Integrated Framework, see, e.g., Ref. [38] and Prinn et al. [62].
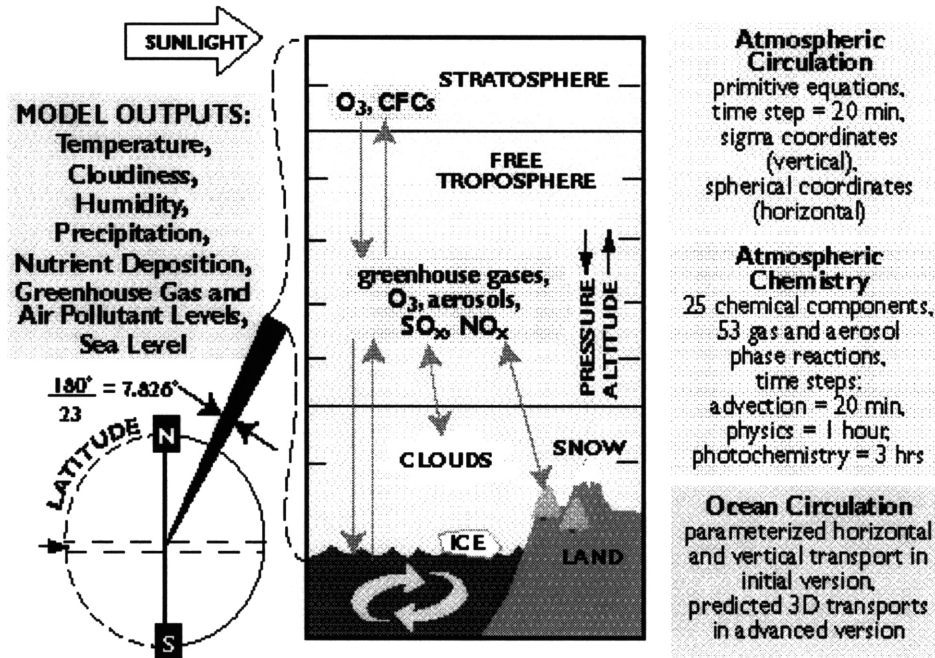
Figure 3-3: Schematic representation of the MIT 2D-LO global climate model. Using predictions of atmospheric composition obtained from an associated biogeochemistry model, the 2D-LO model simulates the zonally-averaged climate separately over land and ocean, as a function of latitude and height (Source: MIT Joint Program on the Science and Policy of Global Change).

of the 2D-LO model, model numerics and physics (e.g., long and shortwave radiation, cumulus convection, large-scale condensation, clouds, surface fluxes, and the oceans) have closely paralleled those of the NASA GISS three-dimensional GCM.[7]

As with any global climate model, the 2D-LO model requires that numerical values be assigned to model parameters before it can be used to generate long-term projections of future climate. Of course, even conditional upon having specified a particular model's functional form, modelers are almost always uncertain *a priori* about what numerical values to assign to its parameters. The continuing controversy about the numerical value to assign to the feedback multiplier in the computation of equilibrium change in global-mean surface temperature is an example of a parameter uncertainty that gives rise to a large spread in expert judgements about climate sensitivity. Within the MIT Integrated Framework, further examples of important parameter uncertainties include the following:

- **Cloud Feedback.** The cloud feedback simulated by the MIT 2D-LO global climate model depends on the parameterizations of cloud cover. Letting $n(\phi, z)$ denote cloud cover at

---

[7]Detailed technical discussions of the MIT 2D-LO climate model, and its relation to other sub-models in the MIT Integrated Global System Model (IGSM), are found in Refs. [62] and [72].

latitude ϕ and height z, the parameterization of cloud cover takes the functional form

$$n(\phi, z) = \max \left\{ 0, \frac{A\,[r(\phi, z) - r_c]}{(1 - r_c)} \right\},$$

where

r = Relative humidity at (ϕ, z);

r_c = Critical humidity threshold;

A = Empirical constant.

This parameterization is similar to that used in many GCMs. Given this prescription for cloud cover as a function of humidity, the change in $n(\phi, z)$ over location and time will determine cloud feedback behavior. Conditional on accepting this model structure, knowledge of one of A or of r_c would allow us to compute a reasonable value of the other from observed data. Unfortunately, which values of A or of r_c most adequately represent cloud cover are not well-understood.

- **Rapidity of Deep Ocean Mixing.** Both heat and CO_2 mixing within the deep ocean are represented as simple diffusion with the MIT 2D-LO climate model. The magnitude of the diffusion coefficient, which is a function $K(\phi)$ of latitude, is uncertain, but lies within a broad , finite range, $0 < K(\phi) < 10 \text{ cm}^2/\text{sec}$. Heat flux $F(\phi, z)$ at a given ϕ and z is directly proportional to K in the diffusion equation

$$F(\phi, z) = -\rho\, C\, K(\phi)\, \frac{\partial T(\phi, z)}{\partial z},$$

where ρ is the water density, C is water heat capacity, and $\partial T(\phi, z)/\partial z$ is the temperature gradient in the vertical direction. If $K(\phi)$ is uncertain, it follows that heat flux $F(\phi, z)$ is also uncertain.

- **Initial Temperature of the Deep Ocean.** Current scientific knowledge does not allow us to know with certainty if the deep ocean temperature is, in actuality, an equilibrium temperature. If $T_0(\phi)$ is the deep ocean temperature for current climate and $T_e(\phi)$ is the corresponding deep ocean equilibrium temperature, then the future evolution of temperature depends on $T_0(\phi) - T_e(\phi) = \delta T(\phi)$. But, $\delta T(\phi)$ is not known with certainty.

Naturally, computational capacity places boundaries on our ability to perform systematic and exhaustive analyses of policy. Even though the 2D-LO model is more than one hundred times faster than the GISS GCM at 4° × 5° resolution, the computational costs involved in

running this model are sufficiently high to make its integration into formal decision-analytic frameworks, such as those which we present in Chapters 5 and 6, a practical impossibility.

In order to deal effectively with these computational restrictions, an important aspect of our integrated modeling approach is the development of *reduced-scale* representations of the global climate system. In the following section, we present two reduced-scale global climate models. Later, in Chapter 4, these models are numerically calibrated against the larger, more complex 2D-LO climate model.

3.2 Reduced-Scale Modeling of Global Climate Change

Global energy balance models (EBMs) constitute the simplest means by which to model the climate system of the Earth. Historically, such models have played an important role in our understanding of the various components and processes that influence climatic change. The earliest EBMs date back to the late 1960s, beginning with the work of Budyko [10] and Sellers [69] demonstrating that equator-to-pole energy transport and radiation streams are fundamental processes of the global climate system.

The fundamental principle underlying all EBMs is that the *incoming* and the *outgoing* radiation for the globe is—in the long run—balanced. In more formal terms, the rate of change of the surface temperature, T, with time, t, is represented as the difference between *net incoming* and *net outgoing* radiant energies. This relationship between time, temperature, and radiant energies can be stated informally as follows:

$$K \frac{\Delta T}{\Delta t} = R \downarrow - R \uparrow, \tag{3.1}$$

where K is the "thermal inertia" or *heat capacity*[8] of the system, and $R \downarrow$ and $R \uparrow$ are the incoming and outgoing radiation fluxes, respectively.

3.2.1 Globally-Averaged One-Box Model

Equation (3.1) serves as the conceptual basis for a variety of EBMs. Schneider and Mass [67], for example, propose a one-box time-dependent globally averaged model of the Earth's climate system. The model they put forth is *zero-dimensional*, in that the Earth is treated as a single point in space, characterized by a global-mean surface temperature whose value at time t is denoted $T(t)$. The model is formally specified in terms of a global energy balance equation, with heat storage expressed in terms of solar energy absorbed minus infrared energy emitted to

---

[8]The *heat capacity* of a body is defined as the ratio of the amount of heat energy that a body is supplied with to its corresponding temperature rise.

space. If we let $\Delta T(t) = T(t + h) - T(t)$ denote the change in *global-mean surface temperature* during the finite time interval $[t, t+h)$, and define the time-step $\Delta t = h$, then the *global energy balance* for this model is given by

$$K \lim_{h \to 0} \frac{\Delta T(t)}{h} = K \frac{dT(t)}{dt} = Q[1 - \alpha(T(t))] - R_{ir} \!\uparrow\! (T(t)), \tag{3.2}$$

where K is the heat capacity coefficient, Q is the annually averaged solar radiation received by the earth (a constant with respect to both time and temperature), $\alpha(T(t))$ is the *planetary albedo*,[9] and $R_{ir} \!\uparrow\! (T(t))$ is the outgoing infrared radiation to space.

In order to render Eq. (3.2) more amenable to analysis, we linearize $\alpha(T(t))$ and $R_{ir} \!\uparrow\! (T(t))$ as follows [67, 77]:

$$\alpha(T(t)) = a + b\,T(t), \tag{3.3}$$

$$R_{ir} \!\uparrow\! (T(t)) = x + y\,T(t). \tag{3.4}$$

Typically, the real-valued coefficients a, b, x, and y in Eqs. (3.3) and (3.4) are treated as empirically-determined constants that account for the greenhouse effect of clouds, water vapor, and CO_2 [30].

Equation (3.4) provides a conceptually simple means by which to combine the effects of surface emissivity and atmospheric transmisivity. For our purposes here, it is useful to modify this equation slightly. Specifically, in order to explore the response of the one-box model to external CO_2 forcing, we generalize Eq. (3.4) by lumping together the effects of increasing atmospheric CO_2 concentrations due to anthropogenic CO_2-equivalent emissions into the coefficient x. If we treat anthropogenic CO_2 as an exogenously-specified variable that is dependent on time, but not on $T(t)$, then Eq. (3.4) can be rewritten as

$$R_{ir} \!\uparrow\! (t, T(t)) = x(t) + y\,T(t), \tag{3.5}$$

where the function $R_{ir} \!\uparrow\!$ is now defined on a domain that consists of both time, t, and global mean surface temperature, $T(t)$. Intuitively, Eq. (3.5) states that the outgoing infrared radiation to space can, in principle, change over time, even if global-mean temperature remains constant.

Now, substituting Eqs. (3.3) and (3.5) into Eq. (3.2) yields

$$K \frac{dT(t)}{dt} = Q[1 - (a + b\,T(t))] - [x(t) + y\,T(t)]$$

---

[9] *Planetary albedo* is defined as the ratio of reflected to incident radiation, and provides a measure of the *reflectivity* of the earth's surface and its atmosphere.

$$= (1-a)Q - (bQ + y)T(t) - x(t). \tag{3.6}$$

In order to estimate the impact of rising CO_2 concentrations on climate, relative to some pre-industrial baseline which we denote by t_0, at time $t = t_0$, we assume that the system is in a state of *climatic equilibrium*; that is, the time derivative $dT(t)/dt$ evaluated at time $t = t_0$ is equal to zero. At equilibrium, we are able to establish the following initial condition for Eq. (3.6):

$$(bQ + y)T(t_0) = (1-a)Q - x(t_0). \tag{3.7}$$

For $t \geq t_0$, let $T(t) = T(t_0) + [T(t) - T(t_0)]$. Also, to simplify notation, let

$$\tau(t) = T(t) - T(t_0)$$

denote the difference between global-mean surface temperature T at times t and t_0, respectively. Equation (3.6) can now be written as

$$
\begin{aligned}
K\frac{dT(t)}{dt} &= K\frac{d}{dt}[T(t_0) + \tau(t)] = K\frac{d\tau(t)}{dt} \\
&= (1-a)Q - (bQ + y)T(t_0) - (bQ + y)\tau(t) - x(t). \tag{3.8}
\end{aligned}
$$

Now, substituting Eq. (3.7) into Eq. (3.8) yields

$$
\begin{aligned}
K\frac{d\tau(t)}{dt} &= (1-a)Q - [(1-a)Q - x(t_0)] - (bQ + y)\tau(t) - x(t) \\
&= x(t_0) - x(t) - (bQ + y)\tau(t). \tag{3.9}
\end{aligned}
$$

By defining $F(t) = x(t_0) - x(t)$ and $\lambda = y + bQ$, Eq. (3.9) can be expressed as

$$K\frac{d\tau(t)}{dt} = F(t) - \lambda\tau(t), \tag{3.10}$$

where $F(t)$ denotes the change (from equilibrium) of that part of the time-dependent outgoing longwave radiation that is independent of temperature. Intuitively, we recognize that as concentrations of CO_2 in the atmosphere increase, the values that $x(t)$ takes on decrease and $F(t) > 0$, which agrees with our intuition about the effects of increased CO_2 in the atmosphere.

In terms of a finite time interval $[t, t + h)$, for some time-step $h > 0$, when h is small, Eq. (3.10) can be approximated by

$$K\left[\tau(t+h) - \tau(t)\right] \approx h\left[F(\xi) - \lambda\,\tau(\xi)\right], \tag{3.11}$$

for any $t \le \xi < t + h$. Now, if we choose $h = 1$ and let $\xi = t$, then Eq. (3.11) becomes

$$K\left[\tau(t+1) - \tau(t)\right] \approx F(t) - \lambda\,\tau(t),$$

which gives rise to

$$\tau(t+1) \approx \tau(t) + \frac{1}{K}\left[F(t) - \lambda\,\tau(t)\right]. \tag{3.12}$$

Equivalently, Eq. (3.12) can be expressed as

$$\tau(t) \approx \tau(t-1) + \frac{1}{K}\left[F(t-1) - \lambda\,\tau(t-1)\right].^{10} \tag{3.13}$$

3.2.2 Globally-Averaged Two-Box Model

The climate model given by Eq. (3.13) is concerned only with the atmosphere of the Earth. Most atmospheric processes, however, are strongly coupled to the Earth's oceans. In what follows, we extend the model presented above to include ocean-atmosphere interactions.

The globally-averaged two-box model that we consider here was originally developed by Schneider and Thompson [67], and versions of it are used by Nordhaus [57] and others in several recent integrated assessments of global climate change.

In this globally-averaged model, the ocean-atmosphere system is represented by two "boxes" or layers: one layer for land and another for the world ocean. The upper box consists of a land fraction, f_L, and is characterized by a globally- and annually-averaged temperature, $T(t)$; the lower box consists of an ocean fraction, $1 - f_L$, and is characterized by a globally- and annually-averaged temperature, $T^*(t)$. Each of these layers is assumed to be internally well-mixed. As in the case of the one-box model, the two-box model is driven by external solar forcing, Q — the absorbed portion of which is scaled by the planetary albedo $\alpha(T(t))$ — and emits infrared

---

[10]It bears mentioning that if we choose $\xi = t + h - \epsilon$, for small ϵ satisfying $h > \epsilon > 0$, then, letting $h = 1$, Eq. (3.11) becomes

$$K\left[\tau(t) - \tau(t-1)\right] \approx \left[F(t-\epsilon) - \lambda\,\tau(t-\epsilon)\right],$$

in which case

$$\tau(t) \approx \tau(t-1) + \frac{1}{K}\left[F(t-\epsilon) - \lambda\,\tau(t-\epsilon)\right].$$

As $\epsilon \to 0$, we obtain

$$\tau(t) \approx \tau(t-1) + \frac{1}{K}\left[F(t) - \lambda\,\tau(t)\right].$$

Thus, from a purely analytical vantage point, there exists some degree of flexibility as to whether F and τ are treated as contemporaneous or lagged variables.

radiation, $R_{ir} \uparrow (t, T(t))$, to space. The *heat transfer rate* between the upper and the lower box is proportional to the *volume rate*, $\dot{V}(t)$, of water exchange between the two boxes.

The global energy balance for the two-box model is formally specified by the following system of equations:

$$K_1 \frac{dT(t)}{dt} = Q\left[1 - \alpha(T(t))\right] - R_{ir} \uparrow (t, T(t))$$
$$- \frac{c_w}{\sigma_g} \dot{V}(t) \left[T(t) - T^*(t)\right], \tag{3.14}$$

$$K_2 \frac{dT^*(t)}{dt} = \frac{c_w}{\sigma_g} \dot{V}(t) \left[T(t) - T^*(t)\right], \tag{3.15}$$

where K_1 and K_2 are the thermal inertias for the upper and lower box, respectively, c_w is the volumetric heat capacity of water, and σ_g is the global surface area.[11]

The thermal inertias K_1 and K_2 are given by

$$K_1 = \frac{c_w}{\sigma_g} V, \tag{3.16}$$

$$K_2 = \frac{c_w}{\sigma_g} V^*, \tag{3.17}$$

where V and V^* are the water-equivalent volumes of the upper and the lower box, respectively. Note that in this model, the water-equivalent volumes are fixed with respect to both time and temperature.

As in the case of the one-box model, we are ultimately interested in examining the behavior of the two-box model to external, anthropogenic CO_2 forcing. Looking, first, at Eq. (3.14), we use the linearized forms for $\alpha(T(t))$ and $R_{ir} \uparrow (t, T(t))$ given previously by Eqs. (3.3) and (3.5), respectively, to rewrite Eq. (3.14) as

$$K_1 \frac{dT(t)}{dt} = Q\left[1 - (a + bT(t))\right] - \left[x + yT(t)\right]$$
$$- \frac{c_w}{\sigma_g} \dot{V}(t) \left[T(t) - T^*(t)\right]$$
$$= (1 - a)Q - (bQ + y)T(t) - x(t)$$

---

[11]We note that the two-box model described by Eqs. (3.14) and (3.15) can be viewed intuitively as a generalization of the one-box model developed in Section 3.2.1. Specifically, the model can be specified in terms of the weighted sum

$$K_1 \frac{dT(t)}{dt} + K_2 \frac{dT^*(t)}{dt} = Q\left[1 - \alpha(T(t))\right] - R_{ir} \uparrow (t, T(t)),$$

where $K_2 \frac{dT^*(t)}{dt}$ is defined by Eq. (3.15).

$$- \frac{c_w}{\sigma_g} \dot{V}(t) \left[T(t) - T^*(t) \right]. \tag{3.18}$$

As before, the variable t_0 denotes some pre-industrial baseline relative to which we wish to measure climatic change. At time t_0, we assume that the system is in a state of climatic equilibrium. At equilibrium, two conditions obtain: first, the time derivative $dT(t)/dt$ evaluated at time $t = t_0$ is equal to zero; second, the surface temperature at time $t = t_0$, $T(t_0)$, is equal to the ocean temperature at time $t = t_0$, $T^*(t_0)$. Thus, at time $t = t_0$, in equilibrium, Eq. (3.18) yields

$$(bQ + y)T(t_0) = (1 - a)Q - x(t_0). \tag{3.19}$$

Now, let $\tau(t) = T(t) - T(t_0)$ denote the difference between global-mean surface temperature at times t and t_0, respectively; similarly, let $\tau^*(t) = T^*(t) - T^*(t_0)$ denote the difference between ocean temperature at times t and t_0, respectively. Using these definitions, the two-box model specified by Eqs. (3.18) and (3.15) becomes

$$
\begin{aligned}
K_1 \frac{dT(t)}{dt} \;=\;& K_1 \frac{d}{dt}[T(t_0) + \tau(t)] = K_1 \frac{d\tau(t)}{dt} \\[2mm]
=\;& (1 - a)Q - (bQ + y)[T(t_0) + \tau(t)] - x(t) \\[2mm]
& - \frac{c_w}{\sigma_g} \dot{V}(t) \left[T(t_0) - T^*(t_0) + \tau(t) - \tau^*(t) \right] \\[2mm]
=\;& (1 - a)Q - (bQ + y)T(t_0) - (bQ + y)\tau(t) - x(t) \\[2mm]
& - \frac{c_w}{\sigma_g} \dot{V}(t) \left[T(t_0) - T^*(t_0) + \tau(t) - \tau^*(t) \right],
\end{aligned}
$$

$$
\begin{aligned}
K_2 \frac{dT^*(t)}{dt} \;=\;& K_2 \frac{d}{dt}\left[T^*(t_0) + \tau^*(t) \right] = K_2 \frac{d\tau^*(t)}{dt} \\[2mm]
=\;& \frac{c_w}{\sigma_g} \dot{V}(t) \left[T(t_0) - T^*(t_0) + \tau(t) - \tau^*(t) \right].
\end{aligned}
$$

Since, in equilibrium, $T(t_0)$ equals $T^*(t_0)$, these two equations can be rewritten as

$$
\begin{aligned}
K_1 \frac{d\tau(t)}{dt} \;=\;& (1 - a)Q - (bQ + y)T(t_0) - (bQ + y)\tau(t) - x(t) \\[2mm]
& - \frac{c_w}{\sigma_g} \dot{V}(t) \left[\tau(t) - \tau^*(t) \right], \tag{3.20}
\end{aligned}
$$

$$K_2 \frac{d\tau^*(t)}{dt} = \frac{c_w}{\sigma_g} \dot{V}(t) \left[\tau(t) - \tau^*(t)\right]. \tag{3.21}$$

At equilibrium, Eq. (3.19) obtains, in which case Eq. (3.20) becomes

$$
\begin{aligned}
K_1 \frac{d\tau(t)}{dt} &= (1-a)Q - [(1-a)Q - x(t_0)] - (bQ + y)\tau(t) - x(t) \\
&\quad - \frac{c_w}{\sigma_g} \dot{V}(t) \left[\tau(t) - \tau^*(t)\right] \\
&= x(t_0) - x(t) - (bQ + y)\tau(t) - \frac{c_w}{\sigma_g} \dot{V}(t) \left[\tau(t) - \tau^*(t)\right]. \tag{3.22}
\end{aligned}
$$

As before, letting $F(t) = x(t_0) - x(t)$ and $\lambda = y + bQ$, Eq. (3.22) can be rewritten as

$$K_1 \frac{d\tau(t)}{dt} = F(t) - \lambda\tau(t) - \frac{c_w}{\sigma_g} \dot{V}(t) \left[\tau(t) - \tau^*(t)\right]. \tag{3.23}$$

In this equation, $F(t)$ is again interpreted as the change—from a specified baseline—of that portion of the outgoing longwave radiation, $R_{ir}\uparrow$, that is dependent upon time, but is independent of temperature.

In this representation, we are interested in exploring the effects that upper and lower box mixing have on the climate variable of interest, namely, the upper box temperature, $T(t)$. Following Broecker [8] and Schneider and Thompson [67], we use the following parameterization for upper and lower box mixing:

$$\dot{V}(t) = \frac{V^*}{v_d}, \tag{3.24}$$

where V^* is defined as before, and v_d is the *ventilation time* of the world deep ocean. Substituting Eqs. (3.24) and (3.17) into Eqs. (3.23) and (3.21), the system of equations for the two-box model becomes

$$K_1 \frac{d\tau(t)}{dt} = F(t) - \lambda\tau(t) - \frac{K_2}{v_d} \left[T(t) - T^*(t)\right], \tag{3.25}$$

$$K_2 \frac{d\tau^*(t)}{dt} = \frac{K_2}{v_d} \left[T(t) - T^*(t)\right]. \tag{3.26}$$

As in the case of the one-box model, for computational purposes, it is useful to express the two-box model in finite-difference form. To this end, consider a finite time interval $[t, t+h)$, for some nonzero time-step h. For small values of h, Eqs. (3.25) and (3.26) are approximated by

$$K_1 \left[\tau(t+h) - \tau(t) \right] \approx h \left(F(\xi) - \lambda \tau(\xi) - \frac{K_2}{v_d} \left[\tau(\xi) - \tau^*(\xi) \right] \right),$$

$$K_2 \left[\tau^*(t+h) - \tau^*(t) \right] \approx h \left(\frac{K_2}{v_d} \left[\tau(\xi) - \tau^*(\xi) \right] \right),$$

for any $t \le \xi < t + h$. If we let $\xi = t$, and make our time-step unity, then this system of equations becomes

$$\tau(t+1) \approx \tau(t) + \frac{1}{K_1} \left(F(t) - \lambda \tau(t) - \frac{K_2}{v_d} \left[\tau(t) - \tau^*(t) \right] \right),$$

$$\tau^*(t+1) \approx \tau^*(t) + \frac{1}{K_2} \left(\frac{K_2}{v_d} \left[\tau(t) - \tau^*(t) \right] \right).$$

Equivalently, if we let $t = t - 1$, then the two-box model can be expressed as

$$\tau(t) \approx \tau(t-1) + \frac{1}{K_1} \left(F(t-1) - \lambda \tau(t-1) \right.$$
$$\left. - \frac{K_2}{v_d} \left[\tau(t-1) - \tau^*(t-1) \right] \right), \tag{3.27}$$

$$\tau^*(t) \approx \tau^*(t-1) + \frac{1}{v_d} \left[\tau(t-1) - \tau^*(t-1) \right]. \tag{3.28}$$

Equations (3.27) and (3.28) can be represented succinctly in matrix form as

$$\begin{pmatrix} \tau(t) \\ \tau^*(t) \end{pmatrix} = \begin{pmatrix} \Gamma_{11} & \Gamma_{12} \\ \Gamma_{21} & \Gamma_{22} \end{pmatrix} \begin{pmatrix} \tau(t-1) \\ \tau^*(t-1) \end{pmatrix} + \frac{1}{K_1} \begin{pmatrix} F(t-1) \\ 0 \end{pmatrix}, \tag{3.29}$$

where

$$\Gamma_{11} = -\frac{1}{K_1} \left(\lambda + \frac{K_2}{v_d} \right),$$
$$\Gamma_{12} = \frac{K_2}{K_1 v_d},$$
$$\Gamma_{21} = \frac{1}{v_d},$$
$$\Gamma_{22} = -\frac{1}{v_d}.$$

In this structural representation, we note that thermal forcing due to changes in atmospheric CO_2 concentrations is decoupled from the climatic variables, and is treated as an *exogenous*

51

input to the system.

In order to simplify notation, we define a (2×1) column vector $\mathbf{y}_t$ and a (2×2) *parameter matrix* Γ as

$$\mathbf{y}_t \equiv \begin{pmatrix} \tau(t) \\ \tau^*(t) \end{pmatrix},$$

and

$$\Gamma \equiv \begin{pmatrix} \Gamma_{11} & \Gamma_{12} \\ \Gamma_{21} & \Gamma_{22} \end{pmatrix},$$

where the matrix elements Γ_{ij} are defined as above. In addition, we define a (2×1) vector $\mathbf{u}_t$ as

$$\mathbf{u}_t \equiv \begin{pmatrix} \frac{1}{K_1} F(t) \\ 0 \end{pmatrix}.$$

Using the above definitions, system (3.29) can be expressed succinctly as

$$\mathbf{y}_t = \Gamma \mathbf{y}_{t-1} + \mathbf{u}_{t-1}. \tag{3.30}$$

Intuitively, we recognize that Eq. (3.30) holds true for all values of t, in which case

$$\mathbf{y}_{t-1} = \Gamma \mathbf{y}_{t-2} + \mathbf{u}_{t-2}. \tag{3.31}$$

If we let $(\Gamma)^k$ denote the kth power of the parameter matrix Γ and, in addition, define $(\Gamma)^0$ to be the identity matrix, then substituting Eq. (3.31) into Eq. (3.30) yields

$$\begin{aligned} \mathbf{y}_t &= \Gamma(\Gamma \mathbf{y}_{t-2} + \mathbf{u}_{t-2}) + \mathbf{u}_{t-1} \\ &= (\Gamma)^2 \mathbf{y}_{t-2} + \Gamma \mathbf{u}_{t-2} + \mathbf{u}_{t-1}. \end{aligned}$$

By induction, it is easily verified that

$$\mathbf{y}_t = (\Gamma)^t \mathbf{y}_0 + \sum_{j=1}^{t} (\Gamma)^{j-1} \mathbf{u}_{t-j}. \tag{3.32}$$

Equation (3.32) provides a computationally simple means by which to compute numerical values of the vector time series $\mathbf{y}_t$.

3.3   A Simultaneous Equations Model

In the previous section, we derived two reduced-scale global climate models. These simplified models provide a computationally-tractable means by which to simulate the response of the

global climate system to CO_2-induced thermal forcing. Earlier, in Chapter 2, we described several simplified representations of the global carbon cycle. In this section, we analyze these simplified representations as a *coupled* or *integrated* system. Our motivation for explicitly linking these models together is three-fold in nature. First, we are interested in exploring the dynamic properties of the coupled system. Second, insofar as we are interested in using these simplified models for evaluating climate policy choice, the manner and degree to which the system's variables interact with one another has important implications for how the behavior of the overall system is estimated and interpreted. Lastly, in exploring the formal properties of the coupled system, we hope to better understand the characteristic structure and dynamic behavior of the individual models that comprise the system.

Our presentation is organized along the following lines. In Section 3.3.1, we begin with a description of the coupled system of equations. In Sections 3.3.2 and 3.3.3, we explore the dynamic properties and numerical stability of the coupled system. Lastly, in Section 3.3.4, we present a simple numerical test of the stability of the coupled system.

3.3.1 Coupled System of Equations

In Table 3.1, we summarize the individual equations that we use in the specification of our simultaneous equations model. The equations listed in this table are for the global carbon cycle, CO_2-induced radiative forcing, and the globally averaged two-box climate model.[12] In the context of our discussion here, we view these equations as the *structural equations* of global climate change, in that each equation describes a particular facet of the global climate system, and each equation is, in some measure, derived from first principles or physical theory.

In the absence of uncertainty, the four climate-related equations in Table 3.1 imply the following system of equations:

$$\begin{pmatrix} C_t \\ \tau_t \\ \tau_t^* \end{pmatrix} = \begin{pmatrix} \Gamma_{11} & 0 & 0 \\ 0 & \Gamma_{22} & \Gamma_{23} \\ 0 & \Gamma_{32} & \Gamma_{33} \end{pmatrix} \begin{pmatrix} C_{t-1} \\ \tau_{t-1} \\ \tau_{t-1}^* \end{pmatrix} + \beta \begin{pmatrix} E_{t-1} \\ 0 \\ 0 \end{pmatrix} + \frac{1}{K_1} \begin{pmatrix} 0 \\ \rho(C_{t-1}) \\ 0 \end{pmatrix}, \qquad (3.33)$$

where

---

[12]In the previous sections, time-indexed variables were explicitly represented in a functional manner so as to emphasize the time-dependent nature of the climate system variables. To simplify notation, in this chapter all time-indexed variables are represented in a subscripted manner.

$$C_t = (1 - \frac{1}{\tau_e})C_{t-1} + \beta E_{t-1}$$

$$F_t = 6.3 \ln\left(\frac{C_t}{C_{t_0}}\right)$$

$$\tau_t = \tau_{t-1} + \frac{1}{K_1}\left[F_{t-1} - \lambda \tau_{t-1} - \frac{K_2}{v_d}(\tau_{t-1} - \tau_{t-1}^*)\right]$$

$$\tau_t^* = \tau_{t-1}^* + \frac{1}{v_d}(\tau_{t-1} - \tau_{t-1}^*)$$

Table 3.1: Finite-difference equations for the global carbon cycle, CO_2-induced radiative forcing, and the globally-averaged two-box climate model.

$$\Gamma_{11} = (1 - \frac{1}{\tau_e}),$$

$$\Gamma_{22} = -\frac{1}{K_1}\left(\lambda + \frac{K_2}{v_d}\right),$$

$$\Gamma_{23} = \frac{K_2}{K_1 v_d},$$

$$\Gamma_{32} = \frac{1}{v_d},$$

$$\Gamma_{33} = -\frac{1}{v_d},$$

and

$$\rho(C_{t-1}) \equiv F_{t-1} = 6.3 \ln\left(\frac{C_{t-1}}{C_{t_0}}\right).$$

In this system of equations, we note that the variables C_t, τ_t, and τ_t^* are *jointly dependent* or *endogenous*, whereas the variable E_t is *exogenously* specified. This particular representation of the climate system provides an at-a-glance view of the elements and structure of the overall system.

To simplify notation, we define a (3×1) column vector $\mathbf{y}_t$ and a (3×3) *parameter matrix* Γ as

$$\mathbf{y}_t \equiv \begin{pmatrix} C_t \\ \tau_t \\ \tau_t^* \end{pmatrix}$$

and

$$\Gamma \equiv \begin{pmatrix} \Gamma_{11} & 0 & 0 \\ 0 & \Gamma_{22} & \Gamma_{23} \\ 0 & \Gamma_{32} & \Gamma_{33} \end{pmatrix}, \tag{3.34}$$

54

where the matrix elements Γ_{ij} in (3.34) are defined as before. In order to exploit the *block* form of (3.34), we partition Γ in the following manner:

$$\Gamma \equiv \begin{pmatrix} \Gamma_{11} & \mathbf{0}^T \\ \mathbf{0} & \Gamma_{22} \end{pmatrix},$$

where Γ_{11} is a scalar (as defined previously), $\mathbf{0}$ is a (2×1) zero vector, $\mathbf{0}^T$ is a (1×2) transposed zero vector, and Γ_{22} is a (2×2) submatrix whose elements come from the lower right-hand corner of matrix (3.34), i.e.,

$$\Gamma_{22} = \begin{pmatrix} \Gamma_{22} & \Gamma_{23} \\ \Gamma_{32} & \Gamma_{33} \end{pmatrix}. \tag{3.35}$$

Finally, combining the last two terms of system (3.33), we define a (3×1) vector $\mathbf{u}_t$ as

$$\mathbf{u}_t \equiv \begin{pmatrix} \beta E_t \\ \frac{1}{K_1} \rho(C_t) \\ 0 \end{pmatrix}.$$

Using these four definitions, system (3.33) can now be expressed succinctly as

$$\mathbf{y}_t = \Gamma \mathbf{y}_{t-1} + \mathbf{u}_{t-1}. \tag{3.36}$$

3.3.2   Dynamic Properties of the System

We now examine some of the dynamic properties of system (3.36). To begin, we recognize that Eq. (3.36) holds true for all values of t, in which case

$$\mathbf{y}_{t-1} = \Gamma \mathbf{y}_{t-2} + \mathbf{u}_{t-2}. \tag{3.37}$$

If we now define the kth power of the parameter matrix Γ as

$$\underbrace{\Gamma \cdot \Gamma \cdots \Gamma}_{k \text{ terms}} \equiv (\Gamma)^k,$$

and, also, define $(\Gamma)^0 \equiv \mathbf{I}$, where $\mathbf{I}$ denotes the identity matrix, then substituting Eq. (3.37) into Eq. (3.36) yields

$$\begin{aligned} \mathbf{y}_t &= \Gamma(\Gamma \mathbf{y}_{t-2} + \mathbf{u}_{t-2}) + \mathbf{u}_{t-1} \\ &= (\Gamma)^2 \mathbf{y}_{t-2} + \Gamma \mathbf{u}_{t-2} + \mathbf{u}_{t-1}. \end{aligned}$$

Proceeding by induction, it is easily verified that

55

$$\mathbf{y}_t = (\mathbf{\Gamma})^t\,\mathbf{y}_0 + \sum_{j=1}^{t}(\mathbf{\Gamma})^{j-1}\,\mathbf{u}_{t-j}. \qquad (3.38)$$

Equation (3.38) provides a computationally simple means by which to compute numerical values of the vector time series $\mathbf{y}_t$. In this equation, $\mathbf{y}_t$ is seen as the sum of two components. The first component is $(\mathbf{\Gamma})^t\,\mathbf{y}_0$, which is the solution to the system $\mathbf{y}_t = (\mathbf{\Gamma})\,\mathbf{y}_{t-1}$. In this way, the first component of Eq. (3.38) represents what $\mathbf{y}_t$ would be if it were influenced only by its own lagged values. As for the second component of Eq. (3.38), rearranging terms, we note that the difference

$$\mathbf{y}_t - (\mathbf{\Gamma})^t\,\mathbf{y}_0 = \sum_{j=1}^{t}(\mathbf{\Gamma})^{j-1}\,\mathbf{u}_{t-j}$$

can be interpreted as the *combined effects* of an exogenously-specified CO_2 emissions path $E_0, E_1, \ldots, E_t$ and the radiative forcing trajectory $\rho(C_0), \rho(C_1), \ldots, \rho(C_t)$ associated with this carbon emissions path.[13]

As a preliminary step in our exploration of the dynamic properties of Eq. (3.38), we begin by exploiting the fundamental structure of the parameter matrix $\mathbf{\Gamma}$. In particular, given its distinctive "block" form, it is possible to specify matrix *decompositions* or *factorizations* of $\mathbf{\Gamma}$ which—after some mathematical manipulation—allow useful inferences to be drawn about the *dynamic behavior* and *stability* of the overall system.

The approach that we take in decomposing the parameter matrix $\mathbf{\Gamma}$ has two parts. We begin by decomposing submatrix $\mathbf{\Gamma}_{22}$. This decomposition is then used in the ensuing decomposition of the parameter matrix, $\mathbf{\Gamma}$. For submatrix $\mathbf{\Gamma}_{22}$, it is easily shown that if the eigenvalues of this matrix are distinct, then there exists a *nonsingular*[14] (2×2) matrix $\mathbf{T}$ such that

$$\mathbf{\Gamma}_{22} = \mathbf{T}\mathbf{\Lambda}\mathbf{T}^{-1}, \qquad (3.39)$$

where $\mathbf{\Lambda}$ is a (2×2) diagonal matrix with the eigenvalues of $\mathbf{\Gamma}_{22}$ along the principal diagonal and zeros elsewhere. Thus, $\mathbf{\Lambda}$ is defined as

$$\mathbf{\Lambda} \equiv \begin{pmatrix} \lambda_1 & 0 \\ 0 & \lambda_2 \end{pmatrix},$$

where λ_1 and λ_2 denote the distinct eigenvalues of submatrix $\mathbf{\Gamma}_{22}$. Using decomposition (3.39), we can express the parameter matrix $\mathbf{\Gamma}$ as

$$\mathbf{\Gamma} = \begin{pmatrix} \mathbf{\Gamma}_{11} & \mathbf{0}^{\mathrm{T}} \\ \mathbf{0} & \mathbf{T}\mathbf{\Lambda}\mathbf{T}^{-1} \end{pmatrix}.$$

---

[13]In Appendix A, we present a simple means by which to compute an upper bound for CO_2-induced radiative forcing.

[14]Any square matrix with full rank is called a *nonsingular* matrix.

The diagonal structure of Γ necessarily implies that powers of this matrix are also diagonal matrices. In general, the kth power of Γ, $(\Gamma)^k$, is given by

$$(\Gamma)^k = \begin{pmatrix} \Gamma_{11}^k & \mathbf{0}^{\mathrm{T}} \\ \mathbf{0} & (\mathbf{T}\Lambda\mathbf{T}^{-1})^k \end{pmatrix}. \tag{3.40}$$

Given the nature of decomposition (3.39), powers of $(\mathbf{T}\Lambda\mathbf{T}^{-1})$ are given by

$$
\begin{aligned}
\left(\mathbf{T}\Lambda\mathbf{T}^{-1}\right)^k &= \underbrace{\left(\mathbf{T}\Lambda\mathbf{T}^{-1}\right)\left(\mathbf{T}\Lambda\mathbf{T}^{-1}\right)\cdots\left(\mathbf{T}\Lambda\mathbf{T}^{-1}\right)}_{k \text{ terms}} \\
&= \mathbf{T}\Lambda\mathbf{I}\cdots\mathbf{I}\Lambda\mathbf{T}^{-1} \\
&= \mathbf{T}\Lambda^k\mathbf{T}^{-1}, \tag{3.41}
\end{aligned}
$$

where

$$\Lambda^k = \begin{pmatrix} \lambda_1^k & 0 \\ 0 & \lambda_2^k \end{pmatrix}.$$

Thus, substituting Eq. (3.41) into Eq. (3.40) yields

$$(\Gamma)^k = \begin{pmatrix} \Gamma_{11}^k & \mathbf{0}^{\mathrm{T}} \\ \mathbf{0} & \mathbf{T}\Lambda^k\mathbf{T}^{-1} \end{pmatrix}.$$

Turning our attention, now, to the parameter matrix Γ, we recognize that it, too, can be decomposed in a similar fashion. Using the same diagonalization procedure outlined above, the matrix Γ can be decomposed as

$$\Gamma = \mathbf{SDS}^{-1}, \tag{3.42}$$

where the matrix $\mathbf{S}$ is a nonsingular (3×3) matrix and $\mathbf{D}$ is a (3×3) diagonal matrix consisting of the distinct eigenvalues of Γ. For our purposes here, let

$$\mathbf{S} = \begin{pmatrix} 1 & \mathbf{0}^{\mathrm{T}} \\ \mathbf{0} & \mathbf{T} \end{pmatrix} \qquad\qquad \mathbf{S}^{-1} = \begin{pmatrix} 1 & \mathbf{0}^{\mathrm{T}} \\ \mathbf{0} & \mathbf{T}^{-1} \end{pmatrix}$$

and

$$\mathbf{D} = \begin{pmatrix} \Gamma_{11} & \mathbf{0}^{\mathrm{T}} \\ \mathbf{0} & \Lambda \end{pmatrix}.$$

In this way, the decomposition of Γ_{22} has, in a simple and direct way, motivated the ensuing decomposition of the parameter matrix Γ. As a check on the assumptions that underlie this decomposition, we note that

$$SS^{-1} = \begin{pmatrix} 1 & \mathbf{0}^T \\ \mathbf{0} & \mathbf{T} \end{pmatrix} \begin{pmatrix} 1 & \mathbf{0}^T \\ \mathbf{0} & \mathbf{T}^{-1} \end{pmatrix} = \mathbf{I}.$$

Given decomposition (3.42), it is easily verified that $(\Gamma)^t = \mathbf{SD}^t\mathbf{S}^{-1}$, in which case system (3.38) becomes

$$
\begin{aligned}
\mathbf{y}_t &= (\Gamma)^t \, \mathbf{y}_0 + \sum_{j=1}^{t} (\Gamma)^{j-1} \, \mathbf{u}_{t-j} \\
&= \mathbf{SD}^t\mathbf{S}^{-1}\mathbf{y}_0 + \sum_{j=1}^{t} \mathbf{SD}^{j-1}\mathbf{S}^{-1} \, \mathbf{u}_{t-j} \\
&= \begin{pmatrix} 1 & \mathbf{0}^T \\ \mathbf{0} & \mathbf{T} \end{pmatrix} \begin{pmatrix} \Gamma_{11}^t & \mathbf{0}^T \\ \mathbf{0} & \Lambda^t \end{pmatrix} \begin{pmatrix} 1 & \mathbf{0}^T \\ \mathbf{0} & \mathbf{T}^{-1} \end{pmatrix} \mathbf{y}_0 \\
&\quad + \sum_{j=1}^{t} \begin{pmatrix} 1 & \mathbf{0}^T \\ \mathbf{0} & \mathbf{T} \end{pmatrix} \begin{pmatrix} \Gamma_{11}^{j-1} & \mathbf{0}^T \\ \mathbf{0} & \Lambda^{j-1} \end{pmatrix} \begin{pmatrix} 1 & \mathbf{0}^T \\ \mathbf{0} & \mathbf{T}^{-1} \end{pmatrix} \mathbf{u}_{t-j}.
\end{aligned}
\tag{3.43}
$$

Equation (3.43) provides a computationally efficient means by which to compute values of $\mathbf{y}_t$ for specified values of t. We note, however, that the formulation arrived at above is predicated on the assumption that the parameter matrix Γ consists of linearly independent eigenvectors. It must be stressed that *not all matrices are diagonalizable in the manner described above.*

In addressing this problem, we approach the decomposition of Γ from a somewhat different vantage point. To begin, we again focus our attention on submatrix Γ_{22} of matrix Γ. Using the so-called *singular value decomposition*[15] procedure, it can be shown that there exists *orthogonal matrices*[16] $\mathbf{R}_1$ and $\mathbf{R}_2$ of order (2×2) such that

$$\Gamma_{22} = \mathbf{R}_1 \Lambda \mathbf{R}_2^T, \tag{3.44}$$

where Λ is a (2×2) diagonal matrix. The columns of $\mathbf{R}_1$ are eigenvectors of $\Gamma_{22}\Gamma_{22}^T$; similarly, the columns of $\mathbf{R}_2$ are eigenvectors of $\Gamma_{22}^T\Gamma_{22}$. The so-called *singular values* of Λ are defined as the square roots of the nonzero eigenvalues of both $\Gamma_{22}\Gamma_{22}^T$ and $\Gamma_{22}^T\Gamma_{22}$.

Using decomposition (3.44), the parameter matrix Γ can be expressed as

$$\Gamma = \begin{pmatrix} \Gamma_{11} & \mathbf{0}^T \\ \mathbf{0} & \mathbf{R}_1 \Lambda \mathbf{R}_2^T \end{pmatrix}.$$

As before, since Γ is a diagonal matrix, the kth power of Γ, $(\Gamma)^k$ is given by

$$(\Gamma)^k = \begin{pmatrix} \Gamma_{11}^k & \mathbf{0}^T \\ \mathbf{0} & \left(\mathbf{R}_1 \Lambda \mathbf{R}_2^T\right)^k \end{pmatrix}. \tag{3.45}$$

---

[15] See, e.g., Strang [75, Appendix A].

[16] An orthogonal matrix is defined as a square matrix whose columns are orthonormal.

In contrast with the previous case, Eq. (3.45) does not lend itself to a simple factorization in the way that Eq. (3.40) did. In order to push the decomposition further, we must impose an additional constraint on the matrices R_1 and R_2, namely, we require that

$$R_2^T R_1 = I.$$

Proceeding from this assumption, it is easily verified that $(R_1 \Lambda R_2^T)^k = R_1 \Lambda^k R_2^T$, in which case Eq. (3.45) becomes

$$(\Gamma)^k = \begin{pmatrix} \Gamma_{11}^k & 0^T \\ 0 & R_1 \Lambda^k R_2^T \end{pmatrix}.$$

As before, the parameter matrix Γ can be written in spectral form as

$$\Gamma = Q_1 D Q_2^T,$$

where Q_1 and Q_2 are orthogonal matrices, and D is a diagonal matrix. For our purposes here, we let

$$Q_1 = \begin{pmatrix} 1 & 0^T \\ 0 & R_1 \end{pmatrix} \qquad\qquad Q_2 = \begin{pmatrix} 1 & 0^T \\ 0 & R_2 \end{pmatrix}$$

and

$$D = \begin{pmatrix} \Gamma_{11} & 0^T \\ 0 & \Lambda \end{pmatrix}.$$

Since $(\Gamma)^t = Q_1 D^t Q_2^T$, Eq. (3.38) becomes

$$
\begin{aligned}
y_t &= (\Gamma)^t y_0 + \sum_{j=1}^{t} (\Gamma)^{j-1} u_{t-j} \\
&= Q_1 D^t Q_2^T y_0 + \sum_{j=1}^{t} Q_1 D^{j-1} Q_2^T u_{t-j} \\
&= \begin{pmatrix} 1 & 0^T \\ 0 & R_1 \end{pmatrix} \begin{pmatrix} \Gamma_{11}^t & 0^T \\ 0 & \Lambda^t \end{pmatrix} \begin{pmatrix} 1 & 0^T \\ 0 & R_2^T \end{pmatrix} y_0 \\
&\quad + \sum_{j=1}^{t} \begin{pmatrix} 1 & 0^T \\ 0 & R_1 \end{pmatrix} \begin{pmatrix} \Gamma_{11}^{j-1} & 0^T \\ 0 & \Lambda^{j-1} \end{pmatrix} \begin{pmatrix} 1 & 0^T \\ 0 & R_2^T \end{pmatrix} u_{t-j}. \quad\quad (3.46)
\end{aligned}
$$

As in the previous case, for any admissible set of parameter values, Eq. (3.46) provides a computationally-efficient means by which to compute specific values for the vector y_t.

3.3.3 Stability of the System

We now briefly explore the numerical *stability* of Eqs. (3.43) and (3.46). Given the unique structure of these equations, it is useful to invoke a *change of basis*. Without loss of generality, we confine our attention to Eq. (3.46). Premultiplying both sides of Eq. (3.46) by Q_1^T yields

$$
\begin{aligned}
Q_1^T y_t &= Q_1^T Q_1 D^t Q_2^T y_0 + \sum_{j=1}^{t} Q_1^T Q_1 D^{j-1} Q_2^T u_{t-j} \\
&= D^t Q_2^T y_0 + \sum_{j=1}^{t} D^{j-1} Q_2^T u_{t-j} \\
&= \begin{pmatrix} \Gamma_{11}^t & 0^T \\ 0 & \Lambda^t \end{pmatrix} \begin{pmatrix} 1 & 0^T \\ 0 & R_2^T \end{pmatrix} y_0 \\
&\quad + \sum_{j=1}^{t} \begin{pmatrix} \Gamma_{11}^{j-1} & 0^T \\ 0 & \Lambda^{j-1} \end{pmatrix} \begin{pmatrix} 1 & 0^T \\ 0 & R_2^T \end{pmatrix} u_{t-j}.
\end{aligned}
\tag{3.47}
$$

If we now denote the individual elements of the matrix R_2 as

$$
R_2 = \begin{pmatrix} r_{11(2)} & r_{12(2)} \\ r_{21(2)} & r_{22(2)} \end{pmatrix}
$$

and, as before, let $\Lambda = \mathrm{Diag}(\lambda_1, \lambda_2)$, then $Q_1^T y_t$ can be written explicitly as

$$
\begin{aligned}
Q_1^T y_t &= \begin{pmatrix} \Gamma_{11}^t & 0 & 0 \\ 0 & r_{11(2)}\lambda_1^t & r_{21(2)}\lambda_1^t \\ 0 & r_{12(2)}\lambda_2^t & r_{22(2)}\lambda_2^t \end{pmatrix} \begin{pmatrix} C_0 \\ \tau_0 \\ \tau_0^* \end{pmatrix} \\
&\quad + \sum_{j=1}^{t} \begin{pmatrix} \beta \Gamma_{11}^{j-1} & 0 & 0 \\ 0 & \frac{r_{11(2)}\lambda_1^{j-1}}{K_1} & 0 \\ 0 & 0 & \frac{r_{12(2)}\lambda_2^{j-1}}{K_1} \end{pmatrix} \begin{pmatrix} E_{t-j} \\ \rho\left(C_{t-j}\right) \\ \rho\left(C_{t-j}\right) \end{pmatrix}.
\end{aligned}
\tag{3.48}
$$

Intuitively, we see that Eq. (3.48) recasts system (3.38) in terms of the *characteristic roots* of the parameter matrix Γ. By inspection, it is easily seen that a *necessary* (though not sufficient) *stability condition* for system (3.46) is that all of the eigenvalues of the parameter matrix Γ must be less than one in absolute value.

3.3.4 A Numerical Example

We now consider a simple numerical test of the stability of Eqs. (3.43) and (3.46). For this example, let

$$\Gamma = \begin{pmatrix} 0.9917 & 0 & 0 \\ 0 & -0.1690 & 0.0493 \\ 0 & 0.0017 & -0.0017 \end{pmatrix} \tag{3.49}$$

denote a set of illustrative values for the parameter matrix.[17]

Following our discussion in the previous section, we are interested in specifying the columns of the orthogonal matrices Q_1 and Q_2. To this end, we first compute the eigenvectors of $\Gamma\Gamma^T$ and $\Gamma^T\Gamma$, respectively. Thus, for the matrices

$$\Gamma\Gamma^T = \begin{pmatrix} 0.9835 & 0 & 0 \\ 0 & 0.0310 & -0.0004 \\ 0 & -0.0004 & 5.78 \times 10^{-6} \end{pmatrix}$$

and

$$\Gamma^T\Gamma = \begin{pmatrix} 0.9835 & 0 & 0 \\ 0 & 0.0286 & -0.0083 \\ 0 & -0.0083 & 0.0024 \end{pmatrix},$$

we specify the matrices Q_1 and Q_2 as follows:

$$Q_1 = \begin{pmatrix} 1 & 0 & 0 \\ 0 & -0.9999 & 0.0120 \\ 0 & 0.0120 & 0.9999 \end{pmatrix}$$

and

$$Q_2 = \begin{pmatrix} 1 & 0 & 0 \\ 0 & 0.9600 & -0.2801 \\ 0 & -0.2801 & -0.9600 \end{pmatrix}.$$

Computing the eigenvalues of Γ yields the values 0.9917, 0.1761, and 0.0012. Thus, the diagonal matrix D is specified as

$$D = \begin{pmatrix} 0.9917 & 0 & 0 \\ 0 & 0.1761 & 0 \\ 0 & 0 & 0.0012 \end{pmatrix}.$$

Inspection of this diagonal matrix reveals that the stability condition described earlier is, indeed, satisfied for this particular set of parameter values. The parameter matrix Γ can now be written in spectral form as the product of the matrices Q_1, D, and Q_2:

$$\Gamma = Q_1 D Q_2^T$$

---

[17]For this example, we assume that $v_d = 590$ years, $K_2/v_d = 0.675$, and, following Maier-Reimer and Hasselman [45], $\tau_e = 120$ years. We also assume that $1/K_1 = 0.073$, a value which we numerically estimate in Chapter 4.

$$
= \begin{pmatrix} 1 & 0 & 0 \\ 0 & -0.9999 & 0.0120 \\ 0 & 0.0120 & 0.9999 \end{pmatrix} \begin{pmatrix} 0.9917 & 0 & 0 \\ 0 & 0.1761 & 0 \\ 0 & 0 & 0.0012 \end{pmatrix} \begin{pmatrix} 1 & 0 & 0 \\ 0 & 0.9600 & -0.2801 \\ 0 & -0.2801 & -0.9600 \end{pmatrix}
$$

$$
= \begin{pmatrix} 0.9917 & 0 & 0 \\ 0 & -0.1690 & 0.0493 \\ 0 & .00017 & -0.0017 \end{pmatrix}.
$$

The numerical procedure outlined above can be used to test the stability of the coupled system of equations, for any specified set of model parameter values.

3.4 Summary

In this chapter, we explored a number of issues pertaining to the closely-related topics of climate modeling and prediction. Central to our presentation was the derivation of two reduced-scale models of the global climate system. The reduced-scale climate modeling approach presented here provides a computationally-efficient means by which to obtain policy-dependent projections of future climate. As we discuss later in Chapter 6, this capability is an important aspect of our IDA framework. In the chapter that follows, we address the technical problem of calibrating these reduced-scale models to transient simulations of the MIT 2D-LO global climate model.

Chapter 4

Reduced-Scale Model Calibration

The preceding chapters have sought to emphasize the centrality of long-term climate predictions in integrated assessments of global climate change. General Circulation Models—by far the most sophisticated tools for performing global climate simulations—are ill-suited for the task of policy-oriented global climate change assessment, in that the computational costs required to perform long-term simulations are largely prohibitive. Large-scale global climate models are, in addition, unable to provide the degree of flexibility, ease-of-use, and transparency that policy-oriented modeling requires. Moreover, it is impossible to incorporate large-scale climate models into decision-analytic frameworks such as those which we present later in Chapters 5 and 6.

Policy-oriented assessments of global climate change necessarily entail trade-offs between model adequacy or realism, on the one hand, and computational efficiency, on the other. The reduced-scale global climate models put forth previously in Chapter 3 attempt to strike an instrumental balance between these competing needs. In particular, each of these models posses a sound theoretical basis, and each represents those processes that—for our purposes here—have the greatest influence on global climate change. In order to render such models suitable for policy analysis, it is desirable that the *output* of these reduced-scale models resemble—as closely as possible—the characteristic output of larger, more realistic climate models. In this chapter, we address the problem of *calibrating* the reduced-scale climate models in such a way that they essentially mimic the transient behavior of the MIT 2D-LO global climate model.[1] In what follows, we address a number of technical issues surrounding the problem of numerically calibrating the one- and two-box models to transient simulations of the 2D-LO climate model.

---

[1] The MIT 2D-LO global climate model was described earlier in Chapter 3.

4.1 Calibration of the One-Box Model

In Chapter 3, we derived the following globally-averaged one-box climate model:

$$\tau_t = \tau_{t-1} + \frac{1}{K} \left(F_{t-1} - \lambda \tau_{t-1} \right), \tag{4.1}$$

where τ_t is the change in global-mean surface air temperature at time t, K is the heat capacity or thermal inertia of the climate system, F_t is the change in radiative forcing at time t, and λ is a feedback parameter. Equation (4.1) is *dynamic* in character, in that non-contemporaneous relationships exist between the variables in the model. Specifically, the time-lagged values of τ and F are *explanatory* variables for changes in global-mean surface air temperature, and $1/K$ and λ are physically-determined parameters that influence the *rate* and *magnitude* of climatic change. For our purposes here, Eq. (4.1) is construed as a *structural time series model*, in the sense that each variable has a direct, physical interpretation. In this section, we address the problem of calibrating Eq. (4.1) to transient simulations of the 2D-LO global climate model, where each simulation assumes a gradual increase in atmospheric CO_2 concentrations.

Intermodel comparisons of long-term climate simulations using large-scale GCMs reveal significant differences in the transient response of these models to gradual increases of GHG concentrations in the atmosphere. Our calibration of Eq. (4.1) draws upon a series of sensitivity studies carried out at MIT using the Integrated Global System Model.[2] In particular, we examine a set of 2D-LO transient model runs that are characterized by different numerical values for the following pair of climate-related variables:

- **Climate Sensitivity.** Formally defined as the difference in global-average surface temperature between equilibrium climates for current and doubled CO_2 levels;

- **Ocean Diffusion Coefficient.** Influences the global climate system's rate of warming.[3]

In Figure 4-1, we summarize the climate sensitivity and ocean diffusion coefficient values that characterize the transient 2D-LO simulations that are used here to calibrate the one- and two-box models. In this figure, we note that each transient simulation assumes that climate sensitivity takes on the value 1.5°C, 2.5°C, or 4.5°C, representing the lower, "best guess," and upper values, respectively, of the IPCC climate sensitivity range [32]. Each transient simulation is also characterized by an ocean diffusion coefficient, which is assumed to range between 1/50 and 50, with 1 and 5 as middle values.[4]

---

[2] See, e.g., Sokolov and Stone [73]. For a detailed description of the MIT Integrated Global System Model, see Prinn et al. [62].

[3] In the 2D-LO climate model, different climate sensitivities are obtained by imposing cloud-feedback parameterizations that depend on increases in surface air temperature. Also, heat uptake by the deep ocean is parameterized by diffusive mixing of mixed-layer temperature perturbations (A. P. Sokolov, Private Communication).

[4] Nordhaus [57] calibrates the climate portion of his DICE model to single transient runs of three separate GCMs, each of which is characterized by a different climate sensitivity value.
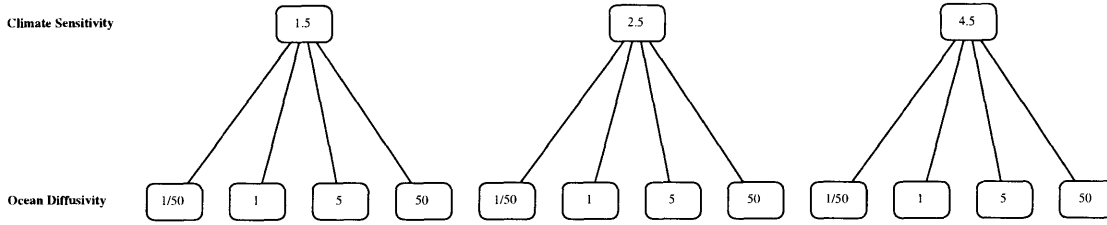
Figure 4-1: Structure of transient simulations of the MIT 2D-LO global climate model used to calibrate the reduced-scale climate models. Each simulation assumes a specific climate sensitivity and ocean diffusivity value.

As illustrated in Figure 4-2, our calibration of the reduced-scale climate models proceeds along the following lines. We begin with an exogenously-specified radiative forcing scenario. The forcing trajectory is used to drive a series of transient simulations of the 2D-LO climate model, where two of the model's parameters—climate sensitivity and ocean diffusivity—are varied successively in the manner described above. This procedure gives rise to twelve long-term projections of global-mean surface temperature change. As discussed below, we utilize econometric and statistical time series techniques to estimate key reduced-scale model parameters.

In arriving at an appropriate numerical representation for Eq. (4.1), we begin by examining a set of 2D-LO transient simulations of global-mean surface air temperature change, where each simulation assumes that atmospheric CO_2 concentrations grow at a rate of 1.2% per year. In addition, we focus on the case where climate sensitivity is 2.5°C. In Figure 4-3, we plot the atmospheric CO_2 concentration and radiative forcing time-paths used for this set of simulations, for the period 1977–2077. The four global-mean surface temperature trajectories associated with this forcing scenario are plotted in Figure 4-4; in this figure, we plot one simulated temperature trajectory for each individual ocean diffusion coefficient value.
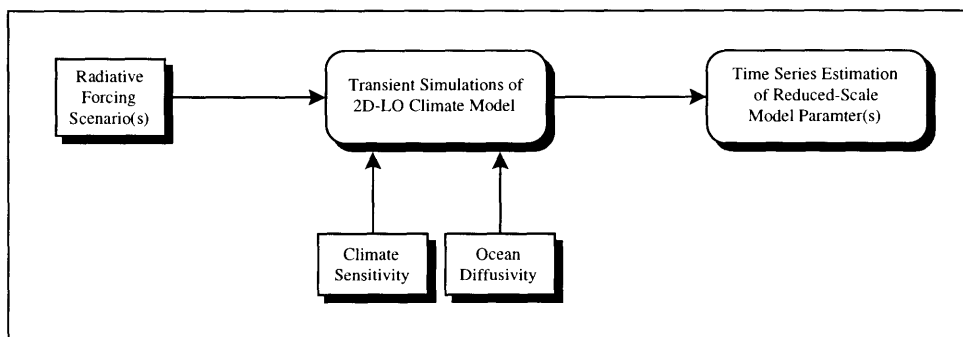
Figure 4-2: Reduced-scale model calibration procedure.
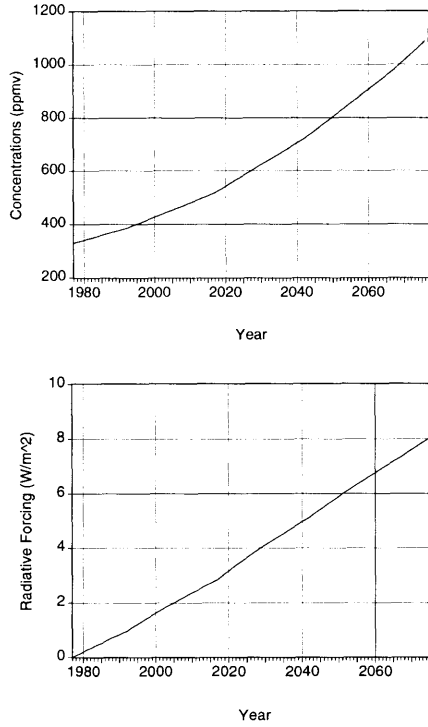
Figure 4-3: CO_2 concentration and radiative forcing time-paths for the period 1977–2077. Atmospheric CO_2 concentrations are assumed to grow at the rate of 1.2% per year.

In using this set of temperature change trajectories to calibrate the one-box climate model, we first re-write Eq. (4.1) as

$$\tau_t = \tau_{t-1} + C_1 \left(F_{t-1} - C_2 \tau_{t-1} \right), \tag{4.2}$$

where $C_1 = 1/K$ and $C_2 = \lambda$. At equilibrium, it is easily shown that the feedback parameter, λ, is related to climate sensitivity and radiative forcing via the equation

$$\lambda = \frac{\Delta F_{2\times}}{\Delta T_{2\times}}, \tag{4.3}$$

where $\Delta F_{2\times}$ denotes the change in radiative forcing brought about by a static doubling of atmospheric CO_2 concentrations, and $\Delta T_{2\times}$ denotes climate sensitivity. Following Nordhaus [57], we assume that $\Delta F_{2\times}$ is equal to 4.1 Wm^{-2}. Since $\Delta T_{2\times}$ is, for this particular set of transient model runs, equal to 2.5°C, λ equals $4.1/2.5 = 1.64$, in which case Eq. (4.2) becomes

$$\tau_t = \tau_{t-1} + C_1 \left(F_{t-1} - 1.64\, \tau_{t-1} \right). \tag{4.4}$$

Using the global-mean surface temperature change time series data presented in Figure 4-4,

Figure 4-4: Projections of global-mean surface air temperature change derived from the MIT 2D-LO global climate model. The projections assume that atmospheric CO_2 concentrations increase at a rate of 1.2% per year. Each temperature trajectory assumes a climate sensitivity value of 2.5°C, but differs in the value used for the ocean diffusion (OD) coefficient.

in Table 4.1 we summarize the ordinary least-squares[5] (OLS) estimates of the inertial parameter, $C_1 = 1/K$. Inspection of this table reveals that the OLS estimation procedure yields estimates of C_1 that range from 0.012 to 0.052. In Figures 4-5 - 4-8, we plot the actual, fitted, and residual values for global-mean surface temperature change, for the period 1977-2077. Visual inspection of these values, together with a cursory examination of the summary statistics, reveals that—for this set of transient runs—the one-box climate model reasonably mimics the transient behavior of the larger 2D-LO model.

An alternative to the estimation procedure outlined above is to compute a *pooled estimate* of the inertial parameter, $C_1 = 1/K$. To compute such an estimate, we begin by re-writing Eq. (4.2) as

$$\tau_{it} = \tau_{it-1} + C_1 \left(F_{it-1} - C_2 \tau_{it-1} \right),$$
(4.5)

---

[5]For technical discussions of ordinary least-squares estimation with lagged dependent variables, see, e.g., Greene [23, pp. 419-420; 435-436] and Hamilton [24].

67

$\Delta T_{2\times}$	Ocean Diffusivity	$C_1 = \frac{1}{K}$	R^2	SER
2.5°C	1/50	0.052 (0.007)	0.998	0.061
	1	0.024 (0.004)	0.997	0.058
	5	0.015 (0.003)	0.995	0.063
	50	0.012 (0.002)	0.995	0.056

Table 4.1: Inertial parameter estimates for the globally-averaged one-box climate model, with climate sensitivity of 2.5°C. Values in parentheses denote standard errors.
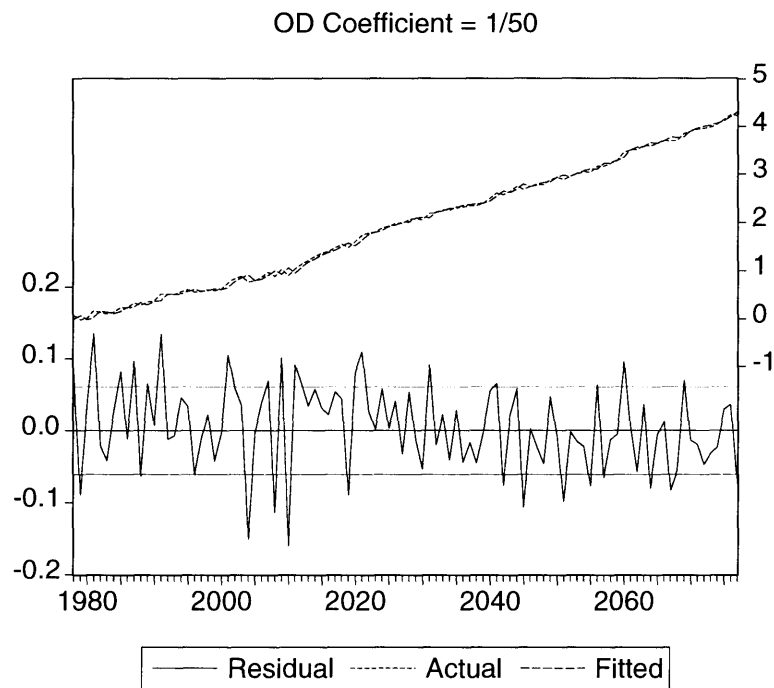
OD Coefficient = 1/50

Figure 4-5: Actual, fitted, and residual values for global-mean surface air temperature change for the period 1977-2077, with climate sensitivity of 2.5°C and OD coefficient of 1/50.
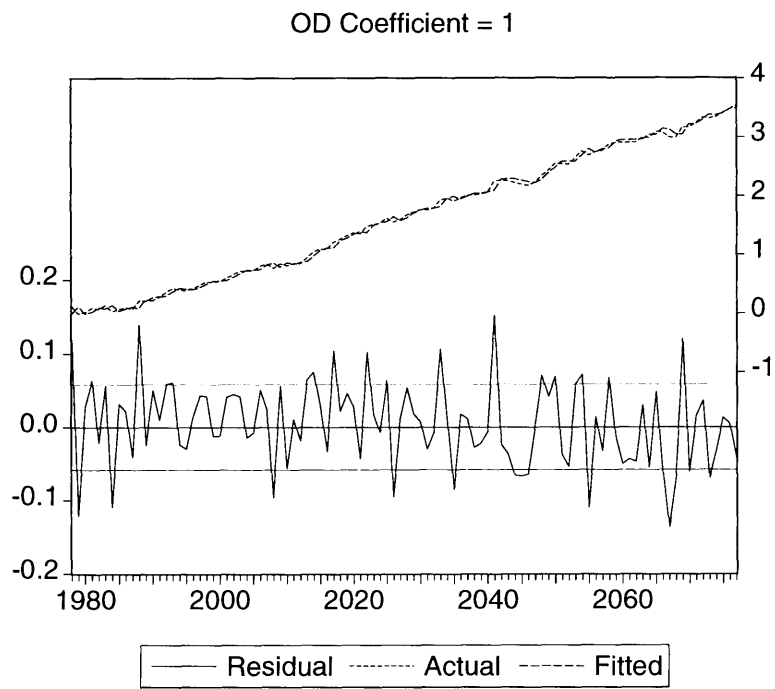
OD Coefficient = 1

Figure 4-6: Actual, fitted, and residual values for global-mean surface air temperature change for the period 1977-2077, with climate sensitivity of 2.5°C and OD coefficient of 1.
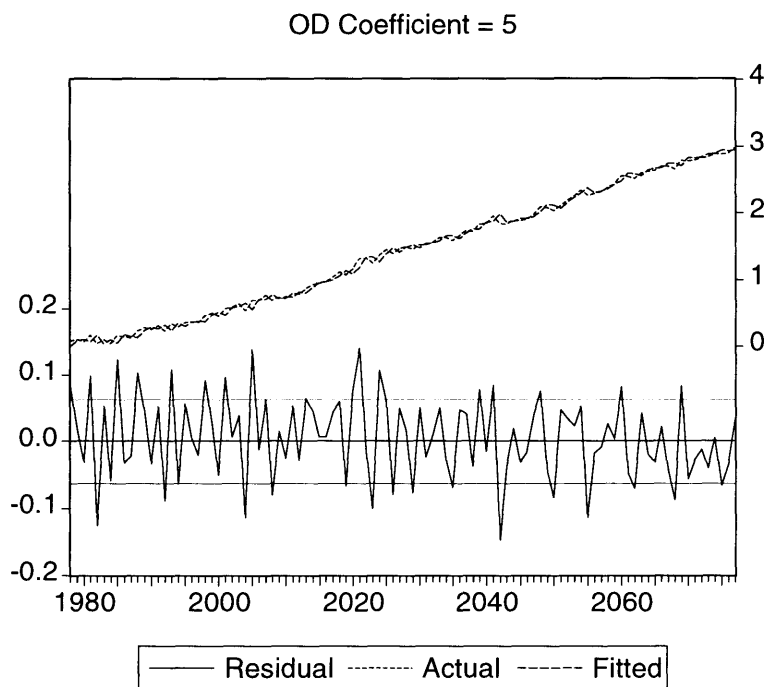
OD Coefficient = 5

Figure 4-7: Actual, fitted, and residual values for global-mean surface air temperature change for the period 1977-2077, with climate sensitivity of 2.5°C and OD coefficient of 5.
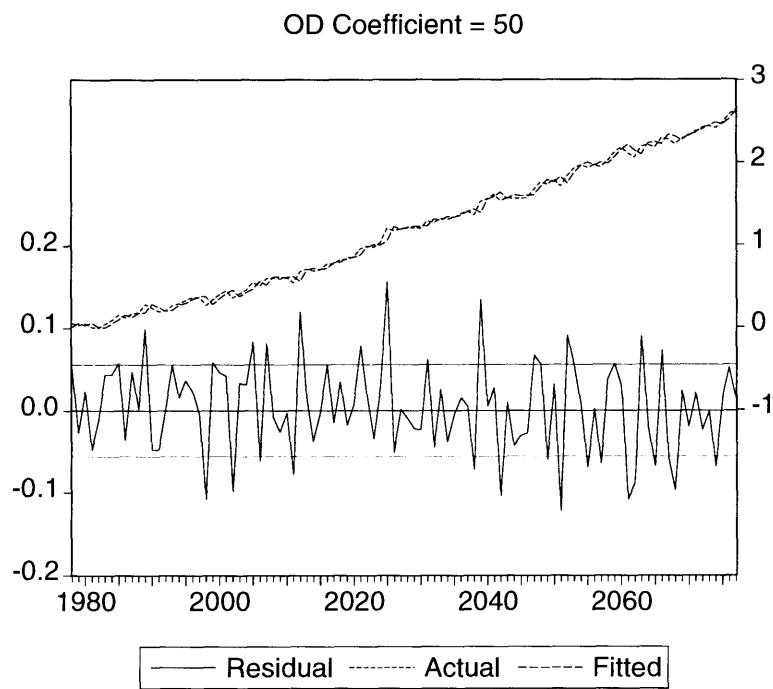
Figure 4-8: Actual, fitted, and residual values for global-mean surface air temperature change for the period 1977-2077, with climate sensitivity of 2.5°C and OD coefficient of 50.

where $i = 1, \ldots, 4$ indexes the four temperature time series associated with each ocean diffusion coefficient value; the parameters C_1 and C_2 are defined as before, and remain constant for all i. Equation (4.5) interprets the four temperature change trajectories described above as *cross-sectional units*, observed at each discrete time period $t = 1977, \ldots, 2077$. For the radiative forcing scenario described above, with $\Delta T_{2\times} = 2.5°C$, we obtain the following OLS pooled estimate[6] for C_1:

$$\tau_t = \tau_{t-1} + 0.017 \ (F_{t-1} - 1.64 \, \tau_{t-1}),$$

$$(0.002)$$

where $R^2 = 0.99$ and SER= 0.06. As expected, the pooling procedure yields an estimate for C_1 that lies between the low and high inertial parameter estimates obtained previously.

The numerical estimates obtained above for the inertial parameter, $1/K$, are derived from a set of transient simulations of the 2D-LO climate model that assume the IPCC "best guess" climate sensitivity estimate of $2.5°C$. Naturally, it is important to explore the manner and degree to which these parameter estimates vary when climate sensitivity takes on values that span the IPCC range. To this end, we now explore a set of transient simulations of the 2D-LO model that assume the full range of climate sensitivity and ocean diffusion coefficient values shown in Figure 4-1. For this particular set of transient simulations, atmospheric CO_2 concentrations are assumed to grow at a rate of 1% per year. In Figure 4-9, we plot the radiative forcing scenario used for this set of transient simulations. In Figures 4-10 – 4-12, we plot the temperature change time series associated with each climate sensitivity-ocean diffusivity pair. In Table 4.2, we summarize the OLS estimates of the inertial parameter, for each possible climate sensitivity-ocean diffusivity pair. In this table, we also summarize the pooled inertial parameter estimates, as a function of climate sensitivity.

4.1.1 Serial Correlation

The OLS estimates obtained above for the inertial parameter in Eqs. (4.2) and (4.5) are based on the assumption that the errors corresponding to different observations generated by the 2D-LO climate model are uncorrelated. Correlation among error terms from different time periods is referred to as *serial correlation*. In the context of our discussion here, an important concern is that in utilizing the reduced-scale climate models to make long-term projections of global-mean surface temperature change, we wish to identify instances where overestimation of the magnitude of temperature change in one year may lead to overestimation in succeeding years.

---

[6]The use of OLS in the estimation of cross-sectional time series is discussed by Greene [23, pp. 444-464].
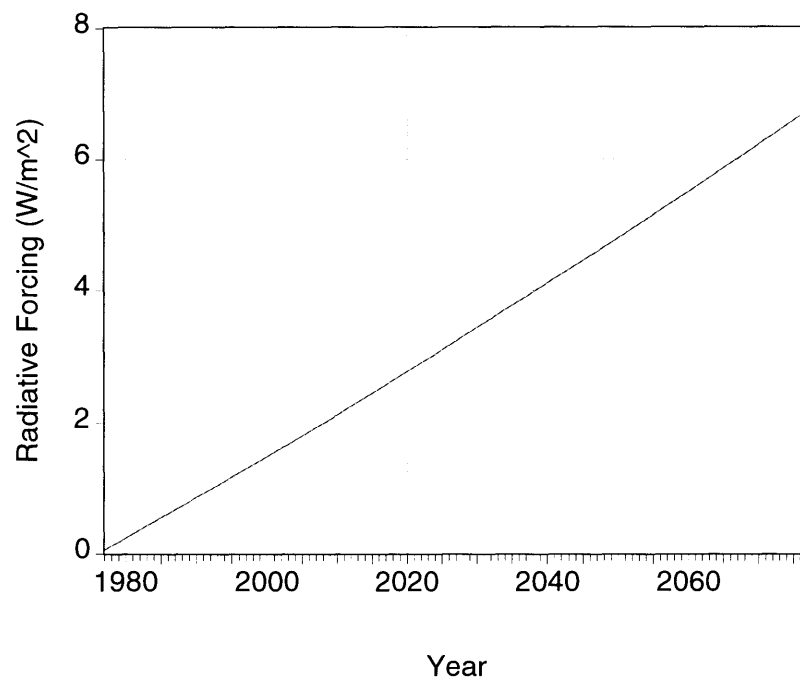
Figure 4-9: Radiative forcing time paths for the period 1977–2077. Atmospheric CO_2 concentrations are assumed to grow at the rate of 1% per year.

$\Delta T_{2\times}$	Ocean Diffusivity	$C_1 = \frac{1}{K}$	Durbin-Watson	Pooled Estimate
1.5°C	1/50	0.028 (0.004)	1.295	0.015 (0.001)
	1	0.019 (0.002)	1.765	
	5	0.014 (0.002)	0.815	
	50	0.012 (0.001)	1.251	
2.5°C	1/50	0.048 (0.004)	0.390	0.017 (0.001)
	1	0.025 (0.006)	2.331	
	5	0.015 (0.002)	0.624	
	50	0.010 (0.001)	1.295	
4.5°C	1/50	0.053 (0.003)	0.784	0.016 (0.001)
	1	0.021 (0.001)	0.666	
	5	0.013 (0.001)	0.703	
	50	0.010 (0.001)	0.851	

Table 4.2: Inertial parameter estimates for the globally-averaged one-box climate model, as a function of climate sensitivity and ocean diffusivity. Values in parentheses denote standard errors.
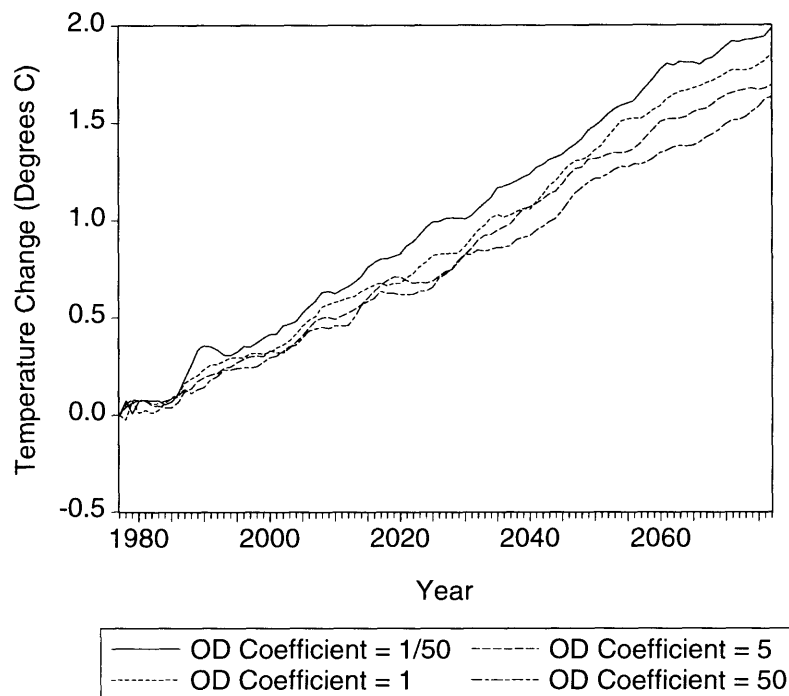
Figure 4-10: Projections of global-mean surface air temperature change derived from the MIT 2D-LO global climate model. The projections assume that atmospheric CO_2 concentrations increase at a rate of 1% per year. Each temperature trajectory assumes a climate sensitivity of 1.5°C, but differs in the value used for the ocean diffusion (OD) coefficient.
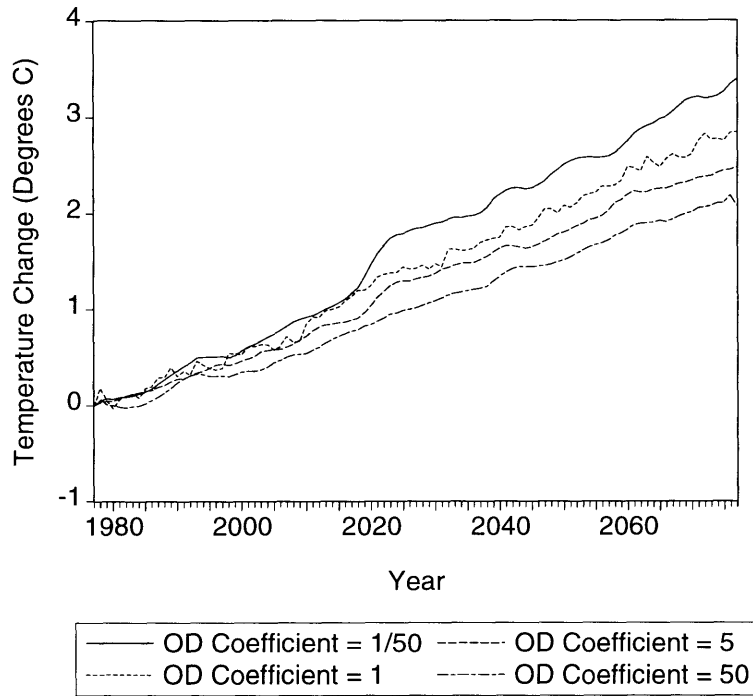
Figure 4-11: Projections of global-mean surface air temperature change derived from the MIT 2D-LO global climate model. The projections assume that atmospheric CO_2 concentrations increase at a rate of 1% per year. Each temperature trajectory assumes a climate sensitivity of 2.5°C, but differs in the value used for the ocean diffusion (OD) coefficient.
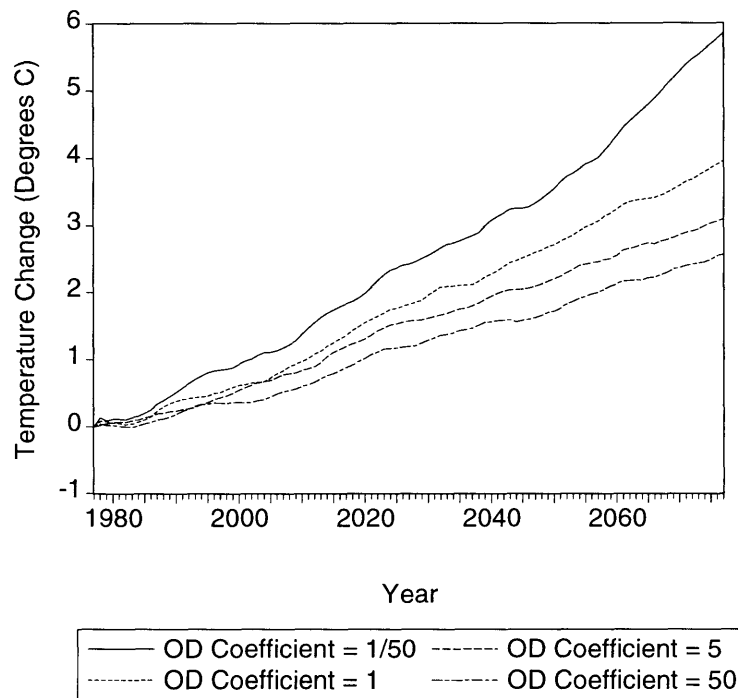
Figure 4-12: Projections of global-mean surface air temperature change derived from the MIT 2D-LO global climate model. The projections assume that atmospheric CO_2 concentrations increase at a rate of 1% per year. Each temperature trajectory assumes a climate sensitivity of 4.5°C, but differs in the value used for the ocean diffusion (OD) coefficient.

Durbin-Watson Test

A commonly used procedure for identifying serial correlation is the so-called *Durbin-Watson* test. This test is based on the assumption that serial correlation in the true disturbances is likely to manifest itself in the residuals, e_t, that are derived from the least-squares estimation procedure. The Durbin-Watson test statistic, dw, is defined as follows:

$$dw = \frac{\sum_{t=2}^{100} (e_t - e_{t-1})^2}{\sum_{t=1}^{100} e_t^2}.$$

For this equation, successive values of e_t that are close to each other give rise to a low Durbin-Watson statistic—an indication of positive serial correlation. The Durbin-Watson statistic is defined on the interval 0 to 4, with values near 2 indicating that first-order serial correlation is not present. Values above and below 2 are indicative of negative serial correlation and positive serial correlation, respectively. In the fourth column of Table 4.2, we provide the Durbin-Watson statistic value for each of the inertial parameter estimates. For the high climate sensitivity cases, we note that the Durbin-Watson values are indicative of positive serial correlation. The Durbin-Watson values obtained for the low and "best guess" climate sensitivity cases are indicative of both negative and positive serial correlation.

Breusch-Godfrey

The Durbin-Watson has been shown to be biased against finding serial correlation when there is a lagged dependent variable, as is the case in Eqs. (4.2) and (4.5).[7] An alternative procedure is the so-called *Breusch-Godfrey* (BG) test. The BG test is a Lagrange multiplier test of the hypothesis

$$H_0 \equiv \text{No Autocorrelation,}$$
$$H_1 \equiv e_t = \text{AR}(r),$$

where r is specified as a positive order.[8] The test has power against all types of serial correlation, and is applicable to equations that have lagged values of the dependent variable. The test is carried out by regressing the OLS residuals on the right-hand variables, together with r lagged residuals. The BG statistic is calculated as the product TR^2, where T denotes the total number of observations. We then refer BG statistic values to tabled critical values for the chi-squared distribution, with r degrees of freedom. In Table 4.3, we tabulate the BG statis-

---

[7]See, e.g., Dezhbaksh [16] and Durbin [20].
[8]For our purposes here, we assume that $r = 2$.

$\Delta T_{2\times}$	Ocean Diffusivity	Breusch-Godfrey	p-Value
1.5°C	1/50	14.307	0.001
	1	9.225	0.010
	5	26.754	0.000
	50	10.680	0.005
2.5°C	1/50	62.326	0.000
	1	9.136	0.010
	5	43.071	0.000
	50	14.596	0.001
4.5°C	1/50	28.630	0.000
	1	35.079	0.000
	5	36.195	0.000
	50	32.976	0.000

Table 4.3: Breusch-Godfrey statistic values and their associated p-values for the calibration of the globally-averaged one-box climate model.

tic values, and their associated p-values,[9] for the 12 climate sensitivity-ocean diffusivity pairs tabulated in Table 4.2. The BG statistic values listed in Table 4.3 indicate that we can reject the null hypothesis (no autocorrelation) at significance levels less than or equal to 1%.

4.1.2 Corrections for Serial Correlation

In order to correct for serial correlation in our calibration of the one-box model, we introduce a first-order autoregressive error process of the form

$$\varepsilon_t = \rho \, \varepsilon_{t-1} + u_t,$$

where ρ denotes the first-order serial correlation coefficient, and u_t is distributed as $N(0, \sigma_u^2)$, and is assumed to be i.i.d. By introducing this error process, we are able to reflect the possibility of mis-specification in our basic model structure. Given this assumption, our one-box model becomes

$$\tau_t = \tau_{t-1} + C_1 \left(F_{t-1} - C_2 \tau_{t-1} \right) + \varepsilon_t,$$

$$\varepsilon_t = \rho \, \varepsilon_{t-1} + u_t, \qquad 0 \le |\rho| < 1.$$

---

[9]For a given test statistic, the p-value or *attained significance level* is the smallest level of significance for which the observed data indicates that the null hypothesis should be rejected.

$\Delta T_{2\times}$	Ocean Diffusivity	$C_1 = 1/K$	ρ
1.5°C	1/50	0.030 (0.005)	0.308 (0.092)
	1	0.019 (0.002)	0.110 (0.100)
	5	0.014 (0.003)	0.540 (0.079)
	50	0.012 (0.002)	0.341 (0.092)
2.5°C	1/50	0.054 (0.013)	0.798 (0.064)
	1	0.024 (0.004)	-0.213 (0.095)
	5	0.016 (0.003)	0.679 (0.073)
	50	0.010 (0.002)	0.240 (0.118)
4.5°C	1/50	0.054 (0.004)	0.510 (0.075)
	1	0.021 (0.002)	0.612 (0.073)
	5	0.013 (0.002)	0.645 (0.077)
	50	0.009 (0.001)	0.555 (0.083)

Table 4.4: Inertial parameter estimates for the globally-averaged one-box climate model, as a function of climate sensitivity and ocean diffusivity, with corrections for serial correlation. Values in parentheses denote standard errors.

In Table 4.4, we summarize the inertial parameter estimates for the globally-averaged one-box climate model, as a function of climate sensitivity and ocean diffusivity, with corrections for serial correlation. Inspection of these values reveals that the revised estimates for this parameter range from 0.009 to 0.054.

As a means of visualizing the numerical results of our calibration procedure, in Figure 4-13 we provide a three-dimensional surface plot of the inertial parameter estimates, as a function of climate sensitivity and ocean diffusivity. This *calibration response surface* shows how the inertial parameter estimate responds to changes in both climate sensitivity and ocean diffusivity. Inspection of the response surface reveals that, for small values of ocean diffusivity, the inertial parameter rises sharply across the range 1.5–4.5°C. We note, also, that as ocean diffusivity increases, the response of the inertial parameter estimate to increases in climate sensitivity is dampened, until at ocean diffusivity levels of ~ 20 and above, variations in climate sensitivity have little effect on the value of the parameter estimate. Graphical displays such as Figure 4-13 help summarize qualitative features of the behavior of the inertial parameter estimate to simultaneous changes in climate sensitivity and ocean diffusivity; such features are difficult to identify solely by visual inspection of tabular data such as that presented in Table 4.4.
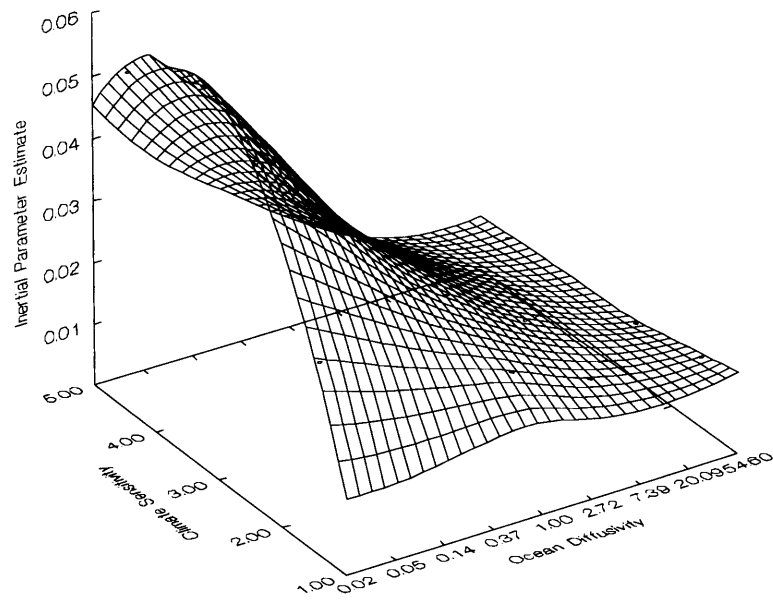
Figure 4-13: Calibration response surface for the globally-averaged one-box climate model inertial parameter estimates, as a function of climate sensitivity and ocean diffusivity. The scale for ocean diffusivity is logarithmic, but is displayed with untransformed values.

4.2 Calibration of the Two-Box Model

The globally-averaged two-box climate model put forth previously in Chapter 3 is specified as follows:

$$\tau_t = \tau_{t-1} + \frac{1}{K_1} \left(F_{t-1} - \lambda \tau_{t-1} - \frac{K_2}{v_d} \left[\tau_{t-1} - \tau^*_{t-1} \right] \right),$$ (4.6)

$$\tau^*_t = \tau^*_{t-1} + \frac{1}{v_d} \left(\tau_{t-1} - \tau^*_{t-1} \right),$$ (4.7)

where τ_t and τ^*_t denote the changes, at time t, in global-mean surface air temperature and deep ocean temperature, respectively. As before, F_t denotes the change in radiative forcing at time t, and λ is a feedback parameter. The parameters K_1 and K_2 denote the thermal inertias for land and ocean, respectively, and v_d is the ventilation time of the deep ocean.

Numerical calibration of the two-box model to transient runs of the 2D-LO climate model proceeds in a manner similar to that which we outlined earlier for the one-box model, with one notable exception: Equation (4.7) requires that we specify temperature change time series for the deep ocean. In Figures 4-14 – 4-16, we plot the transient simulations of deep ocean temperature change that correspond to the transient simulations of global-mean surface air temperature change depicted earlier in Figures 4-10 – 4-12.

Each transient simulation of the 2D-LO model is characterized by a fixed climate sensitivity value, from which we are able to derive — via Eq. (4.3) — a corresponding value for λ. The 2D-LO transient simulations of deep ocean temperature change assume that the deep ocean is 3,000 meters in depth. Given this assumption, it follows that $K_2 = 398 \, \mathrm{J m^{-2} \, K^{-1} \, yr^{-1}}$.[10] Most published estimates of the transient coefficient, v_d, lie between 500 and 550.[11] Rather than assume a single value for v_d, we assume a range of possible values, each of which is functionally dependent on the ocean diffusion coefficient values defined previously. In Table 4.5, we summarize the values used for v_d, K_2/v_d, and $1/v_d$ in the calibration of the two-box model.

For the purposes of calibration, we rewrite Eqs. (4.6) and (4.7) as

$$\tau_t = \tau_{t-1} + C_1 \left(F_{t-1} - C_2 \tau_{t-1} - C_3 \left[\tau_{t-1} - \tau^*_{t-1} \right] \right),$$ (4.8)

$$\tau^*_t = \tau^*_{t-1} + C_4 \left(\tau_{t-1} - \tau^*_{t-1} \right),$$ (4.9)

where $C_1 = 1/K_1$, $C_2 = \lambda$, $C_3 = K_2/v_d$, and $C_4 = 1/v_d$. Estimation of this system of equations is, in general, a problematic task. The presence of lagged dependent variables with serial

---

[10]A. P. Sokolov, Private Communication.
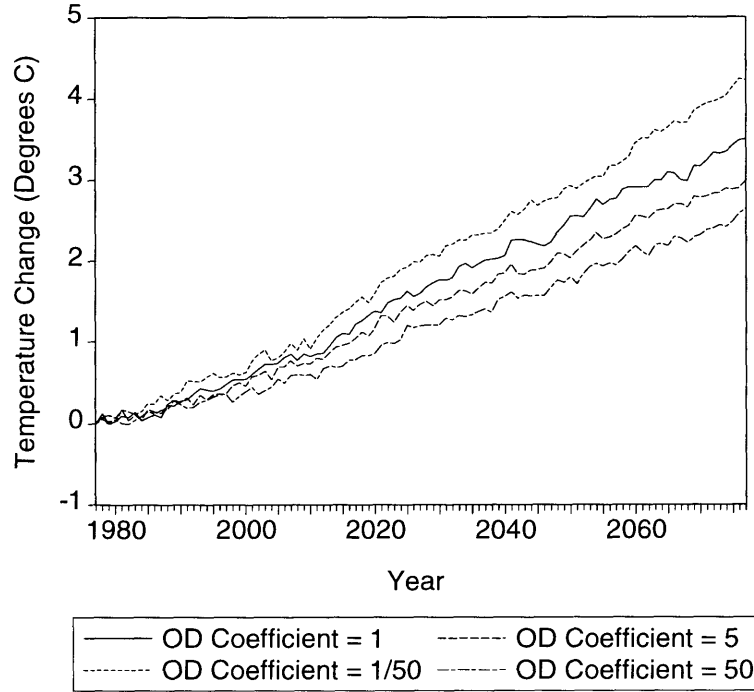[11]See, e.g., Nordhaus [57], who uses $v_d = 500$ in his DICE model.
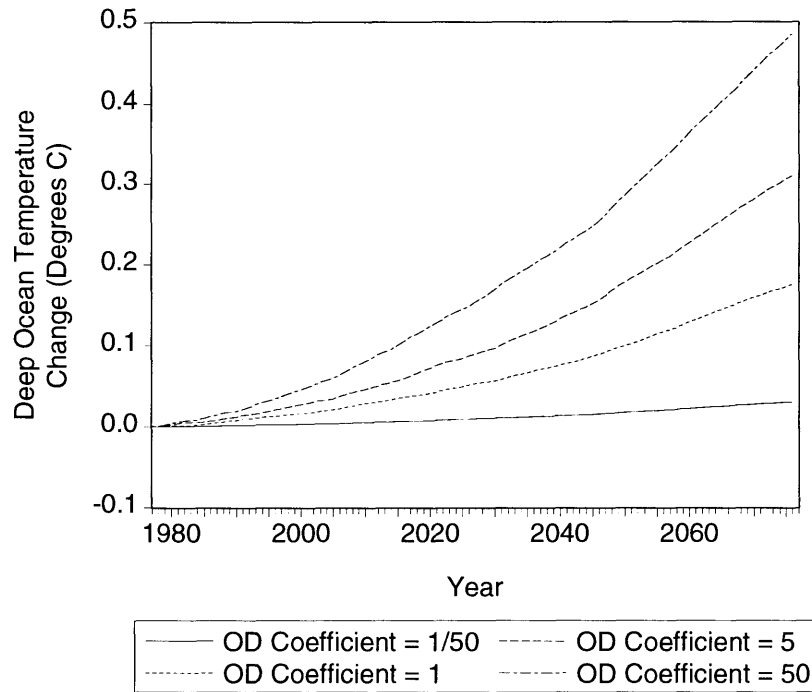
Figure 4-14: Projections of deep ocean temperature change derived from the MIT 2D-LO global climate model. The projections assume that atmospheric CO_2 concentrations increase at a rate of 1% per year. Each temperature trajectory assumes a climate sensitivity of 1.5°C, but differs in the value used for the ocean diffusion (OD) coefficient.

Ocean Diffusivity	ν_d	K_2/ν_d	$1/\nu_d$
1/50	29,500	0.013	0.000034
1	590	0.675	0.0017
5	118	3.373	0.0085
50	11.8	33.729	0.0847

Table 4.5: Parameter values for the globally-averaged two-box climate model, as a function of ocean diffusivity.

82
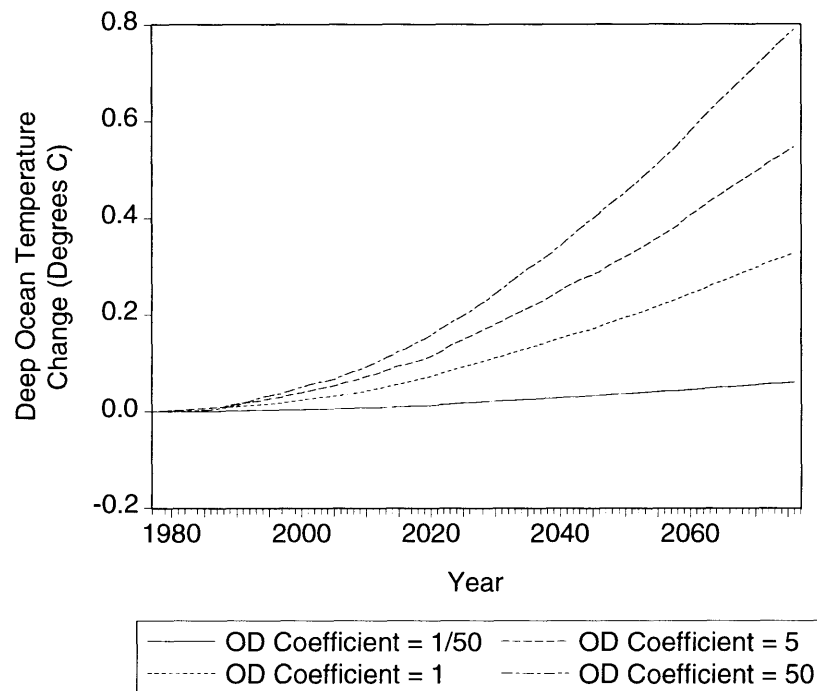
Figure 4-15: Projections of deep ocean temperature change derived from the MIT 2D-LO global climate model. The projections assume that atmospheric CO_2 concentrations increase at a rate of 1% per year. Each temperature trajectory assumes a climate sensitivity of $2.5°C$, but differs in the value used for the ocean diffusion (OD) coefficient.
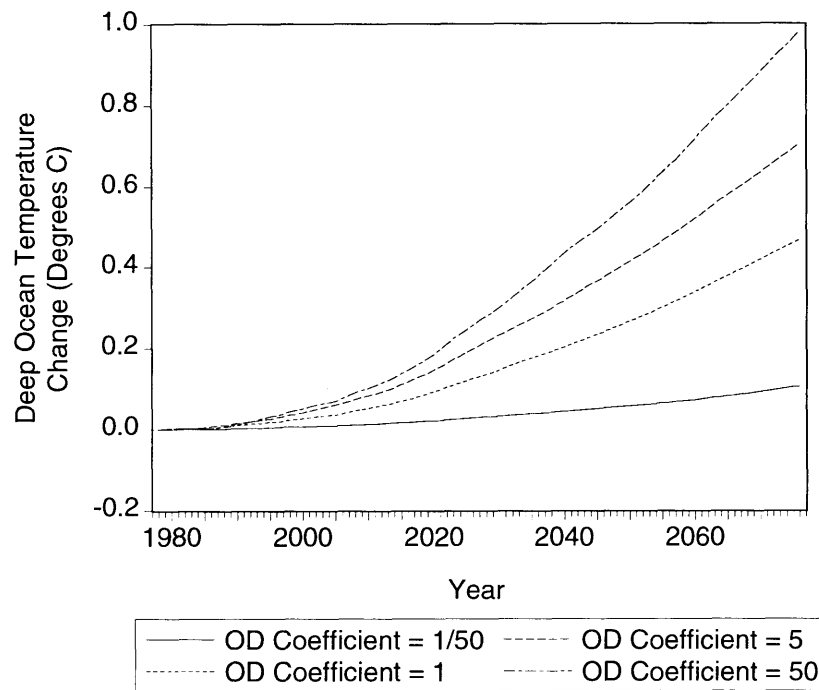
Figure 4-16: Projections of deep ocean temperature change derived from the MIT 2D-LO global climate model. The projections assume that atmospheric CO_2 concentrations increase at a rate of 1% per year. Each temperature trajectory assumes a climate sensitivity of 4.5°C, but differs in the value used for the ocean diffusion (OD) coefficient.

correlation complicates our efforts to estimate the inertial parameter, $C_1 = 1/K_1$. If it were the case that our temperature change time series were not serially correlated, then OLS estimates of C_1 would be consistent, but biased.

To obtain consistent estimates of the inertial parameter, we re-write the system defined by Eqs. (4.8) and (4.9) so as to include an autoregressive error term:

$$\tau_t \;=\; \tau_{t-1} + C_1 \; (F_{t-1} - C_2 \tau_{t-1} - C_3 \left[\tau_{t-1} - \tau_{t-1}^* \right]) + \varepsilon_t, \tag{4.10}$$

$$\varepsilon_t \;=\; \rho \, \varepsilon_{t-1} + u_t, \tag{4.11}$$

$$\tau_t^* \;=\; \tau_{t-1}^* + C_4 \; (\tau_{t-1} - \tau_{t-1}^*), \tag{4.12}$$

where ρ denotes the first-order serial correlation coefficient, and u_t is distributed as $N(0, \sigma_u^2)$, and is assumed to be i.i.d. In obtaining numerical estimates of the inertial parameter, $C_1 = 1/K_1$, we use a three-stage least squares (3SLS) procedure, which applies two-stage least squares (2SLS), together with a full treatment of the cross-equation correlations of residuals.[12] Each iteration of the 3SLS procedure transforms Eqs. (4.10) and (4.12) so as to eliminate cross-equation correlation, and then applies 2SLS. Following Fair [21], we include as first-stage "instruments" the lagged dependent variables, τ_{t-1} and τ_{t-1}^*, as well as the exogenously-specified lagged values for F_{t-1}. Since Eqs. (4.10) and (4.12) contain endogenous variables on the right-hand side, 3SLS yields asymptotically efficient results.[13]

In Table 4.6, we summarize the 3SLS estimates for $C_1 = 1/K_1$. In Figure 4-17, we plot the calibration response surface for this set of inertial parameter estimates. The corresponding isocontour plot shown in Figure 4-18 allows for a precise reading of the parameter estimate values shown in Figure 4-17. Clearly, the response surface shown here is quite different from that which we presented earlier for the globally-averaged one-box climate model. Obtaining a meaningful *physical* interpretation for the observed differences between these two surfaces is problematic, because, in reality, the inertial parameter $C_1 = 1/K_1$ is not *directly* influenced by climate sensitivity and ocean diffusivity.[14]

The most striking feature of the calibration response surface shown in Figure 4-17 is the presence of a relatively flat plateau or "tabletop," where, for climate sensitivity values ranging from roughly 2.4–4.5°C, and for ocean diffusivity values ranging from roughly 0.02–1.0, the value of the inertial parameter estimate exhibits only slight variation. As in the one-box model,

---

[12]For technical discussions of the 3SLS estimation procedure, see, e.g., Greene [23], Hamilton [24], and Pindyck and Rubinfeld [61].

[13]For a discussion of the efficiency of the 3SLS estimation procedure, see, e.g., Madansky [44].

[14]A. P. Sokolov, Private Communication.

$\Delta T_{2\times}$	Ocean Diffusivity	$C_1 = 1/K_1$
1.5°C	1/50	0.015 (9.23×10^{-6})
	1	0.015 (0.0003)
	5	0.008 (0.0007)
	50	0.001 (0.0001)
2.5°C	1/50	0.070 (0.0172)
	1	0.073 (0.0175)
	5	0.009 (0.0008)
	50	0.005 (0.0014)
4.5°C	1/50	0.053 (0.0041)
	1	0.062 (0.0058)
	5	0.015 (0.0013)
	50	0.013 (0.0018)

Table 4.6: Inertial parameter estimates for the globally-averaged two-box model, as a function of climate sensitivity and ocean diffusivity. Values in parentheses denote standard errors.

we note that for ocean diffusivity values greater than ~ 20, variations in climate sensitivity have only a small effect on the value of the inertial parameter estimate.

4.3 Summary

In this chapter, we utilized econometric and statistical time series estimation techniques to numerically calibrate the globally-averaged one- and two-box climate models presented earlier in Chapter 3. By calibrating these reduced-scale models against transient simulations of the larger, more complex MIT 2D-LO global climate model, we are able to mitigate the tension that is seen to exist between two competing objectives in integrated assessment modeling. In particular, the reduced-scale modeling approach set forth here provides a conceptually powerful means by which to balance the obvious need for scientific adequacy and model realism, on the one hand, and computational efficiency, on the other. Later, in Chapter 6, we utilize portions of the calibration exercise presented here as part of our IDA framework for evaluating sequential climate policies under uncertainty.
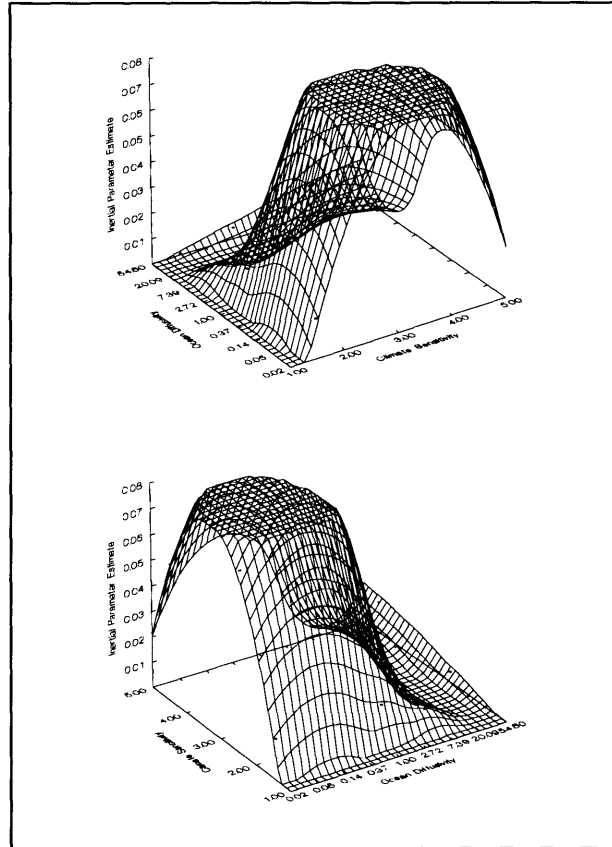
Figure 4-17: Two views of the calibration response surface for the globally-averaged two-box climate model inertial parameter estimates, as a function of climate sensitivity and ocean diffusivity. The scale for ocean diffusivity is logarithmic, but is displayed with untransformed values.
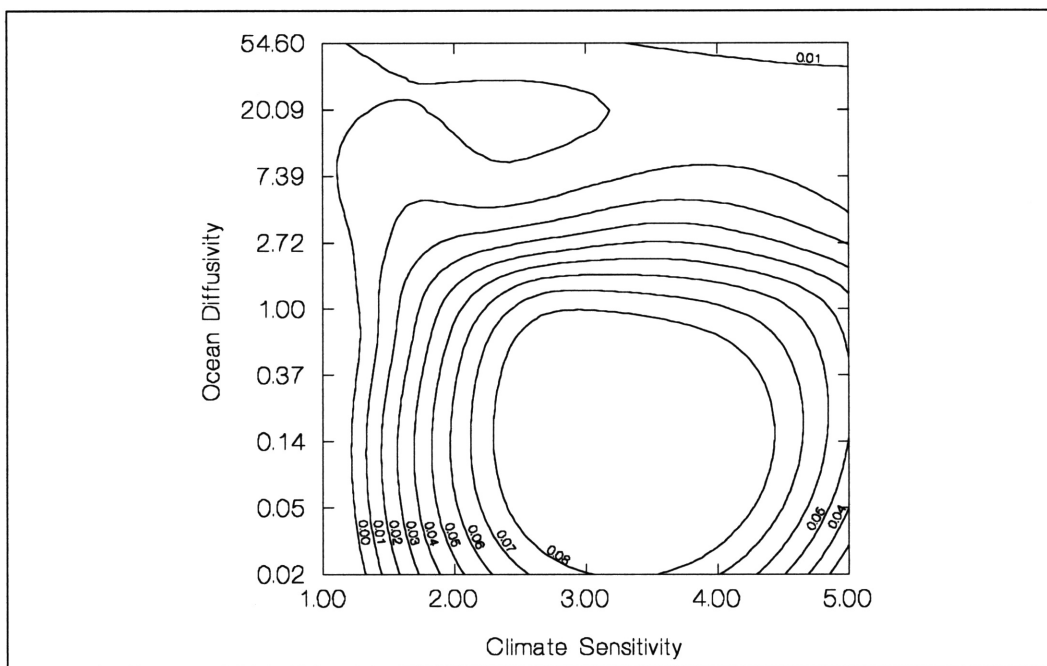
Figure 4-18: Isocontour plot for the globally-averaged two-box climate model calibration response surface.

Chapter 5

Climate Change Decision-Making Under Uncertainty

Current policy debates surrounding the issue of global climate change are complex and multifaceted. Much of the complexity that underlies the greenhouse debate arises, in part, from an incomplete understanding of critical features of atmospheric science, as well as from scientific uncertainty concerning the causes and consequences of human interaction with the global climate system. In addition, difficulties in predicting future levels of anthropogenic emissions of key GHGs complicate efforts to reliably assess the potential magnitude and timing of anthropogenically-induced climate change. Moreover, there are inherent difficulties in drawing reliable inferences as to the potential socio-economic impacts of climatic change, as well as the likely costs, benefits, and effectiveness of possible response strategies.

In this chapter, we set forth a formal decision-analytic framework for *structuring* and *evaluating* global climate change response options. The model formulation that we present here is *static* in design, and serves as the conceptual basis for a *dynamic* formulation which we present in Chapter 6. Our presentation is organized along the following lines. We begin, in Section 5.1, with a brief discussion of the decision-theoretic concepts that underlie our decision modeling approach. We follow this discussion with the specification of a formal decision basis for evaluating an illustrative set of GHG abatement policies. In Section 5.2, we implement and numerically evaluate the decision basis within a graphical structure for modeling uncertain variables and decisions. We then use this analytical framework to evaluate an optimal course of GHG abatement action. As part of this analysis, we use deterministic and probabilistic sensitivity analyses to identify key uncertainties in our model formulation. In Section 5.3, we consider the related problems of valuing information and control, and we discuss the relevance of these concepts to climate change decision-making. Finally, in Section 5.4, we conclude with a brief

89

summary of our findings, and we offer some tentative conclusions as to the policy relevance of our analysis.

5.1 Decision-Making Under Uncertainty

Governmental and intergovernmental decisions as to what actions, if any, should be taken in response to the prospect of anthropogenic climate change are characterized by conflicting criteria and large degrees of uncertainty. In addition, policymakers must evaluate a range of possible response options in a decision context where the effects of climate change may be recognized only decades hence. In addition to being characterized by long lead-times, some of these effects may, in fact, be irreversible. Also complicating efforts to arrive at a robust set of climate change response options are the inherent nonlinearities that characterize the global climate system. The existence of such nonlinearities force decision-makers to consider the possibility of "shocks" or "surprises" in the climate system, some of which could potentially give rise to catastrophic consequences.

The formal evaluation of climate change response options requires that we consider a number of interrelated factors. Our focus here is on the evaluation of *mitigation options* that seek, ultimately, to minimize or prevent climatic change. In order to slow or prevent global warming, it is necessary to reduce net emissions of key GHGs. Such reductions can be achieved in one of two ways: (i) reducing the *sources* of GHGs; or (ii) increasing the *sinks* (natural or otherwise) of GHGs. In this way, climate change response options are typically broken down into those options that reduce or eliminate GHG emissions, and those that measurably offset GHG emissions.

As with any complex, real-world problem, there are a plurality of ways to frame the greenhouse problem. In this section, we explore how the evaluation of GHG abatement options can be framed as a decision problem under uncertainty. The decision basis that we set forth below provides a formal and explicit means by which to structure and evaluate alternative GHG abatement policies.

5.1.1 Formal Elements of Decision Theory

For our purposes here, any situation in which a climate policy choice must be made among alternative courses of action with uncertain consequences will be referred to as a *decision problem under uncertainty*. Following Leonard Savage's [66] classic formulation of decision theory, a decision problem under uncertainty is seen to consist of four basic elements:

(i) A set $A = \{a_1, \ldots, a_m\}$ of alternative *policy options*, one of which will be selected;

(ii) For each policy option $a_i \in A$, a set $U_j = \{X_1, \ldots, X_n\}$ of *uncertain events* that describe the possible outcomes associated with the selection of policy option a_i;

(iii) Corresponding to each set U_j, a set of *consequences* $C_j = \{c_1, \ldots, c_r\}$;

(iv) A *preference order*, $\leq$, defined as a binary relation between some of the elements of A.

Given this formulation, having chosen a policy action a_i, we observe the occurrence of uncertain events in the set U_j. Each uncertain event in the set U_j has associated with it a corresponding consequence set C_j. In this way, the set of uncertain events $U_j = \{X_1, \ldots, X_n\}$ forms a *partition* of the total set of possibilities, with each policy option a_i mapping elements of U_j to the elements $c_k \in C_j$, i.e., $a_i(\cdot) : U_j \to C_j$ or $a_i(U_j) = c_k$.

In this chapter, we focus on the problem of identifying GHG abatement policies that *minimize expected social loss* over all policy options $a \in A$. Assume that we are interested in only one uncertain quantity X. Assume, further, that our *degree of belief* that the uncertain quantity X will assume the value x, given our background state of information, ξ, is $\Pr(x \mid \xi)$, the probability mass function for X. If x occurs, and if policy option a is adopted, then the resulting payoff or social loss is represented by the function $l(x, a)$. Let l^* denote the minimum expected social loss. When x is a discrete random variable,[1] our decision problem is formally stated as follows:

$$l^* = \min_{a \in A} E\left[\, l(X, a) \mid \xi \,\right]$$
$$= \min_{a \in A} \sum_x l(x, a) \Pr(x \mid \xi).$$

A policy option a^* that minimizes expected social loss is called a *Bayes decision*.[2]

5.1.2 A Single-Period Decision Model

In what follows, we put forth a single-period decision model for the evaluation of GHG abatement strategies. As alluded to earlier, this single-period model serves as the conceptual basis for a sequential model formulation—which we present in Chapter 6—that integrates the reduced-scale climate modeling approach that we described earlier in Chapters 3 and 4, with time-series outputs drawn from the MIT IGSM. The single-period model that we describe below provides a nimble, flexible framework for evaluating climate policy choice under uncertainty, as well as for assessing the relative importance of the various factors that are considered as part of our formal evaluation of optimal policy choice.

---

[1] The problem is easily formulated for the case where X is characterized as a continuous random variable.

[2] We note that the probability distribution for X may be conditioned on policy option a, as well as on our background state of information, ξ. The relevance of this type of probabilistic dependence to climate-change decision-making is discussed by Jacoby, Kaufman, and Valverde [34].

For the purposes of illustration, we consider a set of GHG abatement policies that are currently being debated under the United Nations Framework Convention on Climate Change.[3] We focus on three aspects of the climate change problem that are particularly relevant to the evaluation of GHG abatement strategies:

- The economic costs of pursuing a range of GHG abatement strategies;

- The economic benefits of abating global climate change;

- Uncertainty concerning the level or magnitude of global climate change.

In this way, GHG abatement actions are construed as *hedges* against what could possibly be unacceptable levels of global climate change.

5.1.3 Specification of the Decision Basis

We now formally specify the individual components that, together, comprise the *decision basis* of our single-period model. The decision basis consists of three parts: (i) specification of the decision alternatives; (ii) specification of the possible states of nature and their associated probabilities; and (iii) specification of abatement costs and possible climate change impacts.

Decision Alternatives

In our decision model formulation, we assume a *single* or *unitary* decision-maker, who wishes to choose among a finite set of possible *abatement strategies*.[4] Each of these abatement strategies differ in their severity and timing.[5] We begin our formulation with the definition of a finite set of possible abatement options

$$\text{Abatement Decision} = \{a_1, a_2, a_3, a_4\},$$

---

[3]We discuss the United Nations Framework Convention on Climate Change in Chapter 7.

[4]The greenhouse debate is, of course, characterized by *multiple stakeholders*, all of whom are likely to value the various facets of the problem differently. Our motivation for adopting the perspective of a unitary decision-maker is twofold in nature. First, given the *global* character of the problem, it is reasonable to suppose that *unilateral* responses to the prospect of global warming are unlikely to be effective in mitigating climatic change and its potential adverse consequences. For this reason, a global perspective such as the one which we adopt here seeks, at a base level, to inform our conception of what climate-change-related goals and objectives might be achievable within a particular time horizon. Second, much of the policy-oriented dialogue surrounding the greenhouse debate is global in character, though researchers are now beginning to explore the difficult problem of assessing the *regional* implications of global warming. These efforts notwithstanding, the usefulness of pursuing *multi-actor* formulations of the climate change problem is severely limited by the inability of modern climate science to provide reliable, long-term predictions of regional climate change. The analytical frameworks and methodology that we set forth here can, of course, be utilized by *individual* stakeholders, who may be part of a larger, multi-actor policymaking and negotiation process.

[5]All of the decision models presented in this dissertation are evaluated on an *expected-value* or *risk neutral* basis. The role that risk preferences should play in societal decision-making is, of course, a contentious issue, and it is not our intent to enter into these debates here. Suffice it to say that extensions to the analyses put forth here to include the risk preferences of decision-makers are, for the most part, straightforward and easily implemented.

where

$$a_1 \equiv \text{Reference Baseline-No Controls Strategy,}$$

$$a_2 \equiv \text{AOSIS Protocol,}$$

$$a_3 \equiv \text{Delayed AOSIS Protocol,}$$

$$a_4 \equiv \text{Stringent Abatement Strategy.}$$

Strategy a_1 represents a carbon emissions baseline that is unconstrained by a GHG abatement policy. The economic costs of mitigation are defined as the difference in costs between the baseline scenario and a new scenario that is characterized by lower GHG emissions. Strategy a_2 represents a protocol recently proposed by the Alliance of Small Island States (AOSIS) and Germany [1]. Under the terms of the AOSIS protocol,

- All Annex I[6] countries agree to reduce CO_2 emissions to 20% below 1990 levels by the year 2005;

- There are *no* commitments to reduction or limitation of GHG emissions by non-Annex I countries or by Economies in Transition.

Under Strategy a_3, we extend the original AOSIS target date from the year 2005 to 2015. Lastly, under Strategy a_4, we assume that GHG emissions are reduced to 40% of 1990 levels.

Naturally, there are a host of other abatement options that we could consider as part of this analysis. Our intent here, however, is to illustrate the formal concepts and methods that—in Chapter 6—serve as the basis for an integrated decision analysis framework for evaluating sequential GHG abatement policies under uncertainty.

Possible States of Nature

For the purposes of our static analysis, we focus on the possible states of nature associated with the *level* or *magnitude* of global-mean surface temperature change. We assume that the level of warming is observed in the year 2050. In our single-period model, we define a chance variable Climate Change, consisting of four mutually exclusive and collectively exhaustive events:

$$\text{Climate Change} = \{\text{Small, Medium-Low, Medium-High, Large}\},$$

where

---

[6] Annex I countries consist of the OECD nations (except Mexico), plus 12 so-called "economies in transition" in the former Soviet Union and Eastern Europe.

$$\text{Small} \quad \equiv \quad < 1°C,$$

$$\text{Medium-Low} \quad \equiv \quad 1-5°C \text{ (on the low side)},$$

$$\text{Medium-High} \quad \equiv \quad 1-5°C \text{ (on the high side)},$$

$$\text{Large} \quad \equiv \quad > 5°C.$$

The chance variable **Climate Change** represents a broad range of possibilities concerning the extent or magnitude of future climate change. The probability distribution associated with this uncertain quantity is influenced by the decision variable **Abatement Decision**. In this way, *policy action to abate GHG emissions influences the likelihood of each possible state of nature.* In our model formulation, we therefore specify probabilities of the form

$$p(s_j \mid a_i) = \Pr\{\textbf{Climate Change} = s_j \mid \textbf{Abatement Decision} = a_i\}, \tag{5.1}$$

where $a_i \in$ **Abatement Decision** and $s_j \in$ **Climate Change**.

In assessing subjective probability distributions for Eq. (5.1), we utilize outputs from the MIT IGSM to assess the likely influence of policy choice on global-mean surface temperature change. In Figure 5-1, for example, we plot the MIT IGSM temperature change projections for Strategies a_1 and a_2. Using long-term climate projections such as these as a source of data in probability elicitation exercises directed at Eq. (5.1), we are able to specify the discrete distributions shown in Table 5.1. In this way, expert judgement is used to summarize the best available knowledge and information about the likely effects of policy choice on climatic change.

In specifying subjective probability distributions for Eq. (5.1), we recognize that scientific uncertainty concerning key climate-change-related quantities is treated in an *implicit* fashion. For instance, we note that the global climate model used to generate the policy-dependent temperature change projections shown in Figure 5-1 is characterized by a particular climate sensitivity value, in this case, 2.9°C. As we discussed earlier in Chapters 3 and 4, considerable scientific uncertainty currently surrounds this particular quantity. By imposing subjective probability distributions on the categorical states of nature defined above, we are, in effect, making indirect assertions about this uncertain quantity, as well as others. Suppose, for example, that the expert who provides subjectively-assessed values for Eq. (5.1) believes that the energy-economic model within the MIT IGSM makes "optimistic" assumptions about the availability and cost of so-called "carbon-free" backstop technologies. Suppose, further, that the expert believes that the *true* climate sensitivity value is 4.5°C, rather than 2.9°C. In order to reflect this set of beliefs in the assessed values for Eq. (5.1), the expert wishes to represent the idea that, by assuming a low climate sensitivity value in long-term temperature change
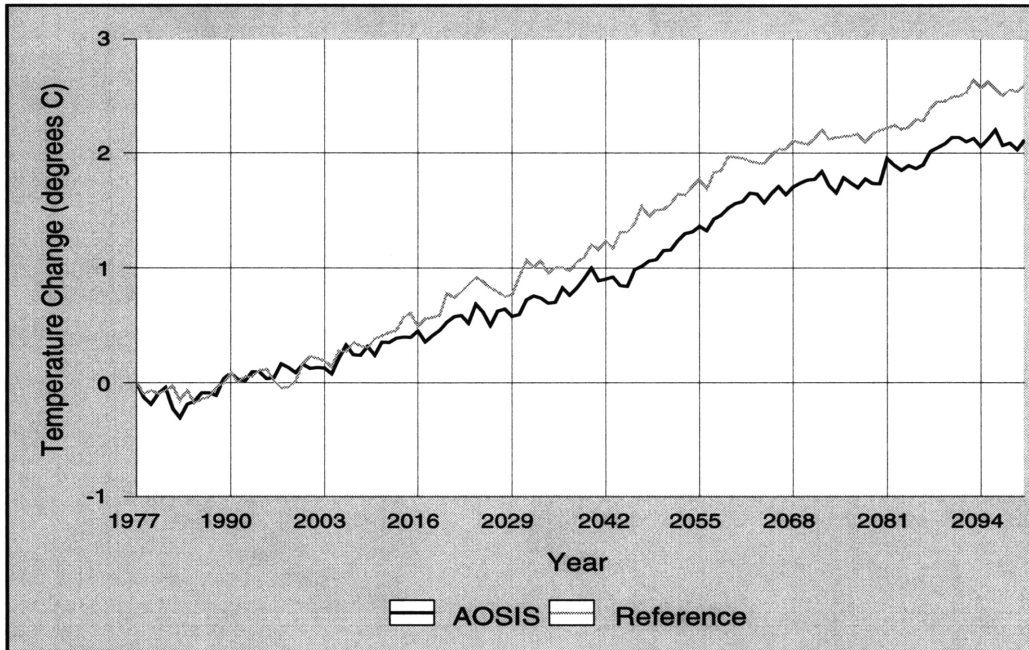
Figure 5-1: MIT IGSM projections of global-mean surface temperature change for the Reference scenario and the AOSIS Protocol.

projections such as those shown in Figure 5-1, the climate model is, at any particular point in time, likely to *underestimate* the true magnitude of observed climatic change. To "correct" for this underestimation, the expert assigns the 'Medium-High' and 'High' states higher likelihoods of occurrence. The modeling approach outlined here is, of course, just one of many that are possible. Later, in Chapter 6, we treat uncertainty concerning climate sensitivity (and other climate-change-related quantities) in an explicit fashion.

In Table 5.1, the probability distribution imposed on the variable Climate Change, given that Strategy a_1 (i.e., no controls on carbon emissions) is adopted, is defined as follows: 'Small' and 'Large' climate change are each assigned probabilities of 0.2, and 'Medium-Low' and 'Medium-High' are each assigned probabilities of 0.3. Consistent with the temperature change projections shown in Figure 5-1, this probability distribution captures the qualitative belief that the range 1–5°C is most likely to contain the true magnitude of the observed level of warming. Strategy a_2 constitutes a relatively moderate abatement policy; looking, again, at Figure 5-1, the probability mass for the chance variable Climate Change is, for this strategy, allocated so as to favor the likelihood of 'Small' or 'Medium-Low' climate change. Adopting Strategy a_3 is presumed to increase the likelihood that Climate Change falls into either the 'Medium-High' or the 'Large' category. Lastly, Strategy a_4 is presumed to increase the likelihood of observing either 'Small' or 'Medium-Low' climate change. Later, in Section 5.2.5, we examine the effects

95

Climate Change	Abatement Decision			
	Strategy a_1	Strategy a_2	Strategy a_3	Strategy a_4
Small	.2	.2	.2	.4
Medium-Low	.3	.4	.3	.3
Medium-High	.3	.3	.4	.2
Large	.2	.1	.1	.1

Table 5.1: Probability distributions for the Climate Change chance variable.

that alternative probability specifications have on the policy prescriptions of our static decision model.

Abatement Costs and Climate Change Impacts

In our model formulation, *abatement costs* and *climate change impacts* are measured in terms of *percentage of gross domestic product (GDP) loss*.[7] The economic cost of pursuing a specific climate change abatement strategy depends, in large measure, upon the *stringency* of the policy, the adjustment time, and the expected technological improvements in energy sources and renewables.[8]

The costs of emissions control for Strategies a_1, a_2, and a_3 are introduced in the form of a data structure that is drawn from output of the MIT Emissions Prediction and Policy Analysis (EPPA) model. EPPA is a global, applied general equilibrium model, derived in part from the OECD General Equilibrium Environmental (GREEN) model. The model projects anthropogenic GHG emissions based on analysis of economic development and patterns of technical development. Like GREEN, the EPPA model is divided into twelve geopolitical regions, each of which is linked with bilateral trade. There are four OECD regions (USA, EEC, Japan, and other OECD), and eight non-OECD regions (China, India, Brazil, Dynamic Asian Economies, Energy Exporting LDCs, Former Soviet Union, Central and Eastern Europe, and Rest of World). In version 1.6 of the EPPA model used here,[9] each region has ten production sectors (five energy, two future energy backstops, and three non-energy) and four consumption sectors. The various components

---

[7]GDP is a measure of all currently produced final goods and services evaluated at market prices, and is typically broken down into four basic components: (i) consumption; (ii) investment; (iii) government purchases; and (iv) net exports. While GDP is arguably the most comprehensive measure of a nation's economic activity, it is important to recognize two salient limitations of this aggregate measure. First, GDP leaves out *nonmarket* productive activities. Second, GDP is not a welfare measure. Since non-market effects have no observable prices, they must be valued using alternative measures, the most common measure being *willingness to pay*. Another practical consideration concerns the manner in which cross-country comparisons of costs/impacts should be conducted (e.g., nominal exchange rates vs. trade-weighted rates). These limitations notwithstanding, GDP remains a useful means by which to aggregate a number of goods and services that contribute to welfare.

[8]For a detailed survey of the economic dimensions of the climate change problem, see, e.g., Cline [14] and Ref. [9].

[9]See Yang et al. [80].
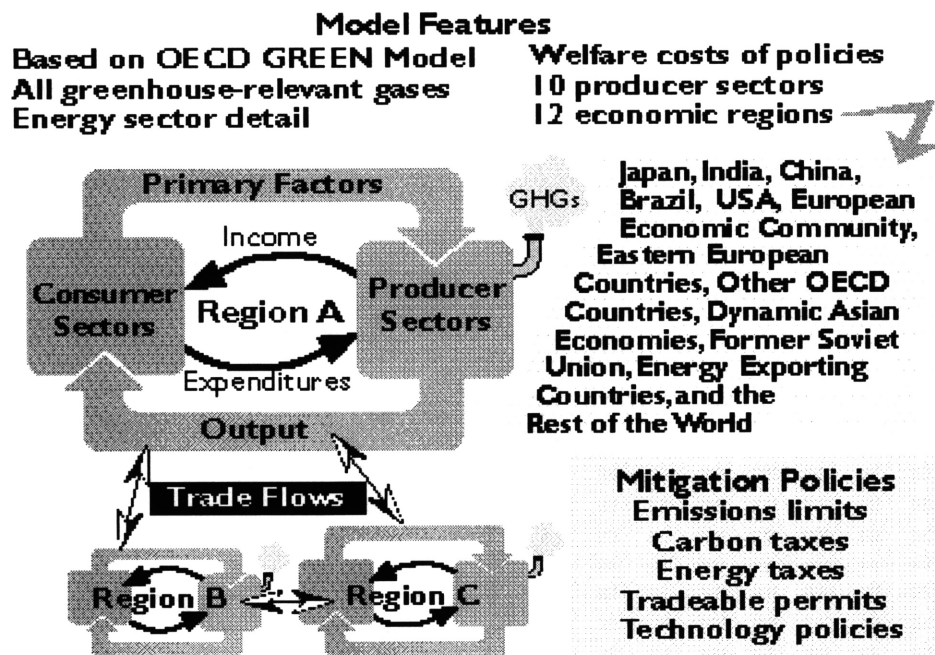
Figure 5-2: Features of the MIT EPPA model (Source: MIT Joint Program on the Science and Policy of Global Change).

of the EPPA model are illustrated in Figure 5-2.

Because of its importance for greenhouse emissions, the overall energy sector is modeled in the greatest detail. The EPPA model contains sectors for oil, gas, coal, and electricity. The model also includes non-fossil technologies (e.g., solar and advanced nuclear power) and new carbon-based sources that might replace conventional fossil fuels in the long term. The model projects emissions of CO_2, CO, CH_4, SO_2, NO_x, and N_2O from the twelve geopolitical regions, taking account of inter-regional trade in energy and other goods. The regional structure also allows consideration of the geographic distribution of emissions of short-lived trace gases (NO_x, SO_2, CO).[10]

The EPPA model solves for equilibrium in five-year time-steps for the period 1985 to 2100, and the model is calibrated with 1985 data. For the purposes of policy analysis, carbon emission constraints can be imposed on any of the 12 regions, in any time period. Control policies may be modeled in the form of price instruments (taxes or subsidies) or quantitative controls (quotas). The price instruments may be *ad valorem* energy or carbon taxes. The quantitative instruments that the EPPA model can handle include CO_2 emission quotas imposed globally, or imposed on a single region, or a block of regions. These constraints may be *fixed* (i.e., no trading), or specified

---

[10]The distribution of these gases is important, in that they drive atmospheric chemistry (HO_x, etc.) and radiative forcing (sulfate production, O_3 production, CH_4 destruction), which is regional in effect.

Reference Case	OECD	Non-OECD	Global
Annualized GDP 2000–2050 (billion 1985$)	10,100	7,300	17,400
GDP NPV 1985–2050 (billion 1985$)	278,600	185,500	464,100
Carbon Emissions in 2050 (GtC)	7.0	8.9	15.9
Carbon Emissions 1985–2050 (GtC)	315.9	385.1	701.1

Table 5.2: Reference case GDP and carbon emissions data.

as *tradable* with other regions, which reallocates the quotas so as to minimize cost.

For the single-period decision model, we specify the abatement costs for each response option as follows:

$$\text{Abatement Costs} = \begin{cases} 0\%, & \text{if Abatement Decision} = a_1; \\ 2.03\%, & \text{if Abatement Decision} = a_2; \\ 1.85\%, & \text{if Abatement Decision} = a_3; \\ 10\%, & \text{if Abatement Decision} = a_4. \end{cases}$$

The economic and carbon emissions data that underlie these cases are summarized in Tables 5.2 and 5.3. Table 5.2 summarizes the GDP and carbon emissions conditions of the Reference case, broken down in terms of OECD, Non-OECD, and global values. Table 5.3 shows the annualized costs for Strategies a_2 and a_3 for the period 2000–2050, their NPVs for the period 1985–2050 (in billions of 1985 dollars), a percentage change in GDP (annualized) from the Reference case, and carbon emissions results. The abatement cost specified for Strategy a_4 is hypothetical, but is, nonetheless, consistent with published estimates of the economic costs associated with this level of GHG abatement.

The economic valuation of the potential social and environmental losses associated with anthropogenic global warming is an inherently problematic task. Most published damage estimates are for benchmark warming studies for $2\times CO_2$, with the majority of estimates focusing primarily on the United States and OECD countries.[11]

In our single-period model, estimates of the percentage of GDP loss associated with the possible levels of climate change that we outlined previously are specified as follows:[12]

$$\text{Climate Change Impacts} = \begin{cases} 0\%, & \text{if Climate Change} = \text{Small}; \\ 0.5\%, & \text{if Climate Change} = \text{Medium-Low}; \\ 3\%, & \text{if Climate Change} = \text{Medium-High}; \\ 30\%, & \text{if Climate Change} = \text{Large}. \end{cases}$$

---

[11] A useful summary of the social costs of global climate change is found in Chapter 6 of Ref. [9].

[12] The values used here are consistent with various published damage estimates. See, e.g., Cline [14] and Nordhaus [56].

AOSIS Protocol	Global
Annualized Costs 2000–2050 (billion 1985$)	-353
NPV 1985–2050 (billion 1985$)	-6,500
Percent Change in Annualized GDP from Base	-2.03%
Change in Carbon Emissions in 2050 (GtC)	11.5
Carbon Emissions 1985–2050 (GtC)	158.1

Delayed AOSIS Protocol	Global
Annualized Costs 2000–2050 (billion 1985$)	-322
NPV 1985–2050 (billion 1985$)	-5,600
Percent Change in Annualized GDP from Base	-1.85%
Carbon Emissions in 2050 (GtC)	11.5
Change in Carbon Emissions 1985–2050 (GtC)	152.5

Table 5.3: Global results from the MIT EPPA model for Strategies a_2 and a_3.

This set of values implies that climate change falling below the 1–5°C range is expected to have negligible effects on social and environmental costs, whereas a change greater than 5°C is expected to have a very large effect. The economic impact of climate change that falls within the 1–5°C range is expected to range between 0.5% and 3% of GDP reduction.

Having specified the decision basis for the single-period model, we now address the task of constructing a formal decision-analytic framework that provides a computationally-efficient means by which to structure and numerically evaluate the GHG abatement policies outlined above.

5.2 Influence Diagram Representation of the Decision Model

The construction of formal decision models generally necessitates the integration of three types of knowledge [59]:

- *Causal* knowledge about how events influence, or relate to, one another;

- Knowledge about what *action sequences* are possible in a particular circumstance or decision context;

- Knowledge about how *desirable* the potential consequences are.

Central to our decision model formulation is the concept of an *influence diagram*, which serves as the formal means by which we structure and numerically evaluate the global climate

change response options outlined above. The language of influence diagrams (IDs) provides an elegant, robust, and computationally powerful means by which to represent decision problems under uncertainty, at several levels of abstraction. As we discuss later in Chapter 6, it is this last feature—computational efficiency—that serves as an important motivating factor in our decision to use IDs as a modeling language for our decision-analytic framework.

At their simplest and, perhaps, most transparent level, IDs provide a graphical means by which to *qualitatively* represent the key elements and components of a decision problem. At this qualitative level of abstraction—often referred to as the *relational* or *topological* level—we are able to graphically depict the flow of information among those actions and distinctions that are thought to characterize the decision problem in question. At a deeper level of abstraction, IDs are used to represent the *functional* and *numeric* relationships that characterize a decision problem.

5.2.1 Formal Elements of Influence Diagrams

Influence diagrams possess a rich underlying mathematical structure. In real-world decision problems, we are typically interested in modeling relationships in a *domain* consisting of *decision variables D* and *chance variables U*. Influence diagrams provide a convenient means by which to represent the relationships that exist between these variables. Formally defined, an ID is an *directed acyclic graph* whose vertices represent either decision variables, random variables, or value functions. Influence diagrams therefore consist of three types of nodes:

- **Decision Nodes.** Represent those actions that are under the full control of the decision-maker, and are depicted graphically as squares (□);

- **Chance Nodes.** Represent the random or uncertain variables in a decision problem, and are depicted graphically as circles or ovals (○);

- **Value Nodes.** Depicted graphically as diamonds or rounded squares (▱).

The arcs in an ID have different meanings and interpretations. Specifically, arcs can be of two types: (i) *information* arcs; and (ii) *relevance* arcs. As Figure 5-3 illustrates, an arc from a chance or decision node A *to* a decision node B is said to be "informational," in the sense that the arc implies a time precedence, and states that the variable A is known to the decision-maker at the time that decision B is made. A relevance arc from a chance or decision node A to a chance node B denotes a probabilistic or functional dependency. The absence of a relevance arc represents *conditional independence* between the variables in question.

Identifying relevance is an important task in the construction of an ID. In order to identify relevance arcs, we begin by ordering the variables in $U = (X_1, \ldots, X_n)$, and for each variable X_i,

Information Arcs   **Relevance Arcs**
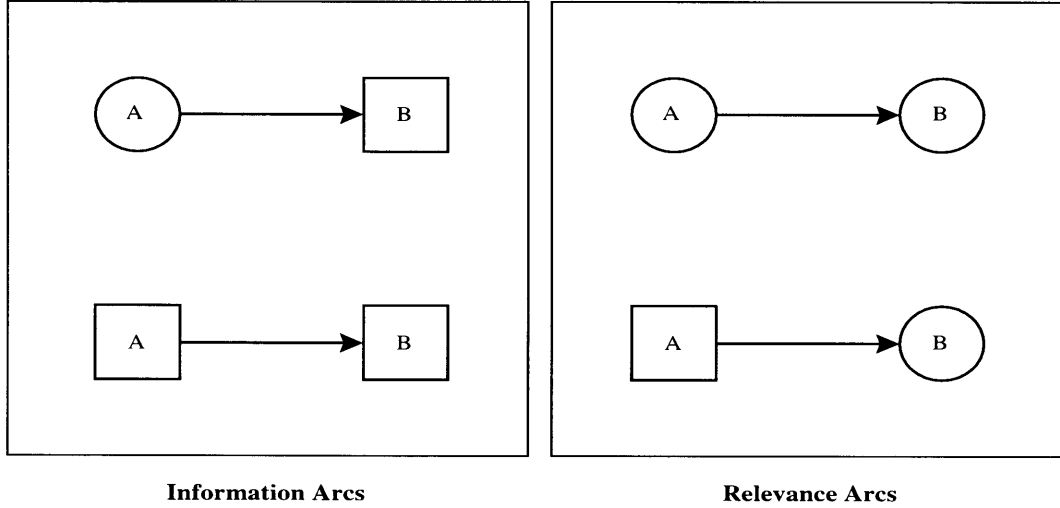
Figure 5-3: Information and relevance arcs in influence diagrams.

specify a set $\text{par}(X_i) \subseteq \{X_1, \ldots, X_{i-1}, D\}$ such that

$$\Pr\{X_i \mid X_1, \ldots, X_{i-1}, D\} = \Pr\{X_i \mid \text{par}(X_i)\}. \tag{5.2}$$

In constructing the ID, for every variable $z \in \text{par}(X_i)$, we place a relevance arc from z to X_i in the diagram. The nodes that belong to the set $\text{par}(X_i)$ are referred to as the *parents* of X_i.

Following this procedure, associated with each chance node X_i in an ID are the probability distributions $\Pr\{X_i \mid \text{par}(X_i)\}$. The so-called "chain rule" of probability states that

$$\Pr\{X_1, \ldots, X_n \mid D\} = \prod_{i=1}^{n} \Pr\{X_i \mid X_1, \ldots, X_{i-1}, D\}. \tag{5.3}$$

Given Eqs. (5.2) and (5.3), it follows that any ID for $U \cup D$ uniquely determines the following joint probability distribution for U given D [5]:

$$\Pr\{X_1, \ldots, X_n \mid D\} = \prod_{i=1}^{n} \Pr\{X_i \mid \text{par}(X_i)\}.$$

In recent years, a number of numerical procedures have been developed for computing the *optimal decision policy* from an ID. A large class of ID solution procedures eliminate nodes from the diagram via a series of so-called *value-preserving* transformations.[13] These transformations preserve the joint distribution of the chance variables in the diagram, but they do not influence the *expected value* of the diagram. In this way, at every step in the solution process, the modified graph remains a *well-formed* ID.

---

[13]For detailed, technical presentations of algorithms for evaluating IDs, see, e.g., Pearl [59, pp. 309-313] and Shachter [70]. Lucid and accessible presentations of these and related topics are found in Clemen [13, pp. 81-83] and Matzkevich and Abramson [51].
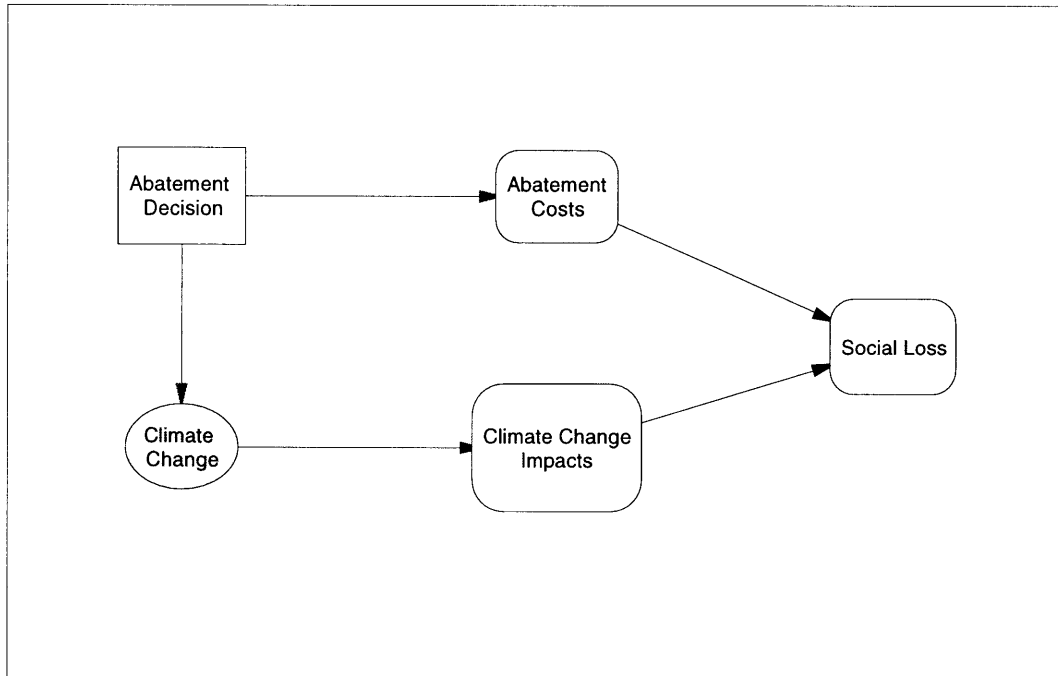
Figure 5-4: Influence diagram representation of the single-period decision model.

5.2.2 Single-Period Decision Model

Figure 5-4 depicts a single-period ID for the decision basis that we specified earlier. The diagram uses three types of nodes to represent each of the individual elements of the decision problem. In particular, the diagram is seen to consist of one decision node (Abatement Decision), one chance node (Climate Change), and three value nodes (Abatement Costs, Climate Change Impacts, and Social Loss). Beginning at the top-left portion of the diagram, the choice of an abatement strategy is seen to influence Abatement Costs, i.e., each abatement strategy has associated with it an economic cost. In addition, the choice of an abatement strategy is seen to influence the probabilities associated with the chance variable Climate Change. The value node Climate Change Impacts is seen to depend on the observed magnitude of the chance node Climate Change. The right-most node, Social Loss, aggregates the expected costs and benefits of pursuing a particular abatement strategy. Specifically, the value nodes Abatement Costs and Climate Change Impacts are aggregated via the equation

$$\text{Social Loss} = \text{Abatement Costs} + \text{Climate Change Impacts.}$$

In interpreting the structure of the ID in Figure 5-4, we first note that there are no information arcs in the diagram. Consequently, the diagram depicts what Manne and Richels [48] call an *act-then-learn* decision strategy. Under such a strategy, an abatement decision is made in

102
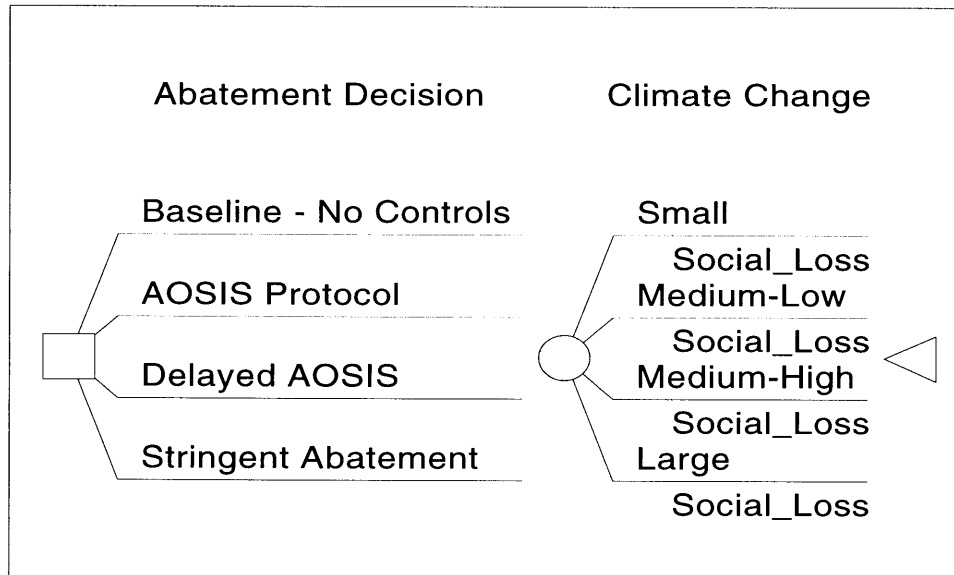
Figure 5-5: Schematic decision tree for the single-period model.

the near-term, without knowing which possible states of nature will obtain in the future. This structure becomes readily apparent when we examine the model's corresponding schematic decision tree, shown in Figure 5-5. This figure depicts a situation where an abatement decision is made in the near-term, and then, at some point in the future, the magnitude of climate change is observed. Associated with each possible state of nature is an economic consequence, measured in terms of aggregate social loss.

5.2.3 Evaluation of the Single-Period Model

Having fully specified the single-period model, we now numerically evaluate the ID in Figure 5-4 so as to determine an optimal decision policy. Figure 5-6 summarizes the optimal decision policy for the ID.[14] We observe that the optimal policy is to pursue Strategy a_2, i.e., AOSIS Protocol. This abatement action has an expected social loss of 6.13%, whereas the other three abatement strategies—No Abatement, Delayed AOSIS Protocol, and Stringent Abatement—have expected social losses of 7.05%, 6.20%, and 13.75%, respectively.

Figure 5-7 depicts the so-called *cumulative risk profile* for the single-period model. The risk profile depicts a cumulative probability distribution of possible outcomes for the optimal policy, Strategy a_2. In this profile, we see that our model specification is such that there is no chance that aggregate social loss will be less than zero. Also, the risk profile rises quickly

---

[14]All of the decision models developed in this dissertation are implemented and numerically evaluated using the *Decision Programming Language* (*DPL*) modeling environment. The technical details that underlie this decision modeling environment are described in Call and Miller [11] and in Ref. [2].

```
                                                          Small              [0]
                                                    .200                      0
                                   Climate_Change    Medium_Low         [0.5]
              Baseline___No_Controls    [7.05]      .300                  0.5
                                                    Medium_High           [3]
                                                    .300                    3
                                                    Large                 [30]
                                                    .200                   30
                                                    Small              [2.03]
                                                    .200                 2.03
                                   Climate_Change    Medium_Low         [2.53]
              AOSIS_Protocol          [6.13]        .400                 2.53
                                                    Medium_High         [5.03]
                                                    .300                 5.03
                                                    Large             [32.03]
  Abatement_Decision                                .100                32.03
      [6.13]                                        Small              [1.85]
                                                    .200                 1.85
                                   Climate_Change    Medium_Low         [2.35]
              Delayed_AOSIS           [6.2]         .300                 2.35
                                                    Medium_High         [4.85]
                                                    .400                 4.85
                                                    Large             [31.85]
                                                    .100                31.85
                                                    Small               [10]
                                                    .400                  10
                                   Climate_Change    Medium_Low       [10.5]
              Stringent_Abatement    [13.75]        .300                 10.5
                                                    Medium_High          [13]
                                                    .200                   13
                                                    Large                [40]
                                                    .100                   40
```

Figure 5-6: Decision policy summary for the single-period model.

between (roughly) 1.25% and 5%, and then levels off.

5.2.4 Sensitivity Analysis: Identifying Key Uncertainties

We now explore the manner and degree to which the policy prescriptions of the single-period decision model are sensitive to changes in the input data. The results of this type of analysis can be used to identify key linkages and variables in the model, as well as to motivate subsequent extensions and improvements to the model. We begin by examining the sensitivity of the model outputs to changes in the values specified for Abatement Costs and Climate Change Impacts.

Estimates of the economic costs of GHG reductions are most sensitive to assumptions about (i) appropriate model structure; (ii) demographic and economic growth; (iii) the cost and availability of energy demand- and supply-side options; (iv) the desired level and timing of abatement; and (v) choice of policy instruments. Different assumptions about these and related issues lead to a wide range of emissions reduction cost estimates. Similarly, estimates of the economic impacts of climate change are likely to *underestimate* the true impacts of climate change, the reason being that many of the effects that we associate with climatic change are not fully quantifiable. Moreover, it is difficult to incorporate the effects that adaptation may have on damage estimates.

The values that we use in the sensitivity analysis of Abatement Costs and Climate Change Impacts are presented in Tables 5.4 and 5.5. Ideally, it would be useful to have some knowledge about the underlying statistical variation in these values. In the absence of concrete knowledge

104
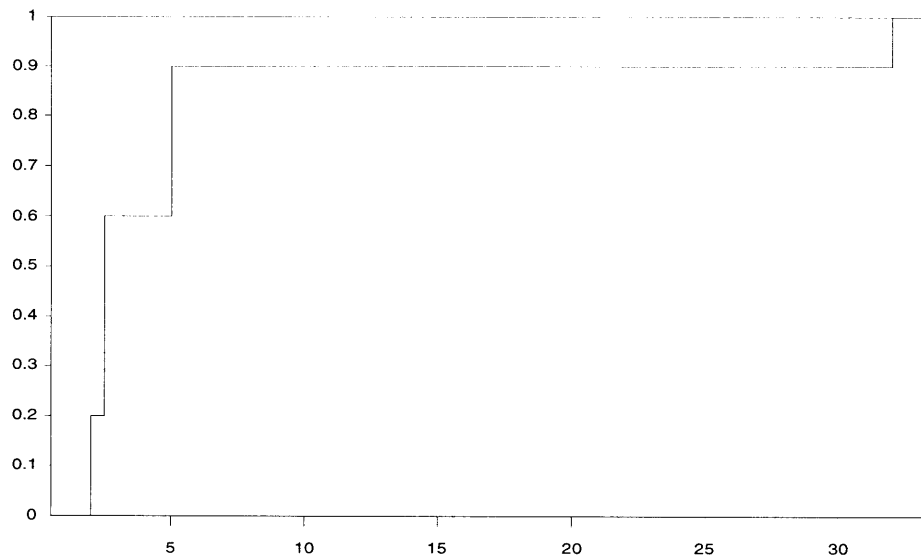
Figure 5-7: Risk profile for the optimal static climate policy, Strategy a_2.

Abatement Decision	Abatement Costs		
	Low Value	Nominal Value	High Value
No Abatement	0	**0**	0
AOSIS Protocol	1	**2.03**	3
Delayed AOSIS Protocol	.9	**1.85**	2.8
Stringent Abatement	5	**10**	15

Table 5.4: Range of **Abatement Costs** for the single-period decision model.

of this sort, the values in both of these tables are specified so as to reflect a roughly three-fold variation between the nominal value and the low-high extremes.

Figure 5-8 depicts a *tornado diagram* of our sensitivity analysis results. Tornado diagrams are a convenient means by which to communicate and explore the relative impacts that alternative value specifications have on the *expected value* and *policy prescriptions* of a decision model. In a tornado diagram, the horizontal bars are sorted from top to bottom, from most important to least important. *Importance* is measured in terms of the relative impact that a particular quantity has on the expected value of the optimal policy. Each of the horizontal bars in a tornado diagram depicts a so-called *value sensitivity analysis*, which calculates the change in expected value and optimal policy that is brought about by varying one variable in the model, while holding all of the other variables fixed. In effect, a value sensitivity analysis requires that we evaluate the model twice: once using the low value and once using the high

105

Climate Change	Climate Change Impacts		
	Low Value	Nominal Value	High Value
Small	0	**0**	0
Medium-Low	0.25	**0.5**	0.75
Medium-High	1.5	**3**	4.5
Large	15	**30**	45

Table 5.5: Range of Climate Change Impacts for the single-period decision model.

value. The length of the bars indicate the difference in the expected value between the two runs; the expected value of the original model is indicated by a vertical line; shifts in optimal policy are denoted by a change in color.

In Figure 5-8, we note that the optimal decision policy is most sensitive to the climate change impacts associated with the large and medium-high levels of climatic change. The decision model is, in addition, sensitive to the abatement costs specified for Strategies a_2 and a_3. The remaining value sensitivities depicted in Figure 5-8 have little or no effect on the policy prescriptions, or the expected value, of the model.

5.2.5 Probabilistic Sensitivity Analysis

We now examine the sensitivity of the single-period model's policy prescriptions to changes in the probability distributions specified for the Climate Change chance variable. In particular, looking again at Eq. (5.1), we specify—in Table 5.6—four alternative probability distributions for $p(s_j \mid a_2)$, the probability distribution for Climate Change, given that optimal Strategy a_2 is adopted. These subjective probability distributions span a broad range of possible beliefs concerning the influence that Strategy a_2 is likely to have on future climate change. Evaluating our primary model with each of the probability distributions shown in Table 5.6 reveals that the model is, indeed, sensitive to the distributions specified for the Climate Change chance node, given that Strategy a_2 is adopted. The bottom of Table 5.6 summarizes the optimal climate policy choice and expected social loss that each probability distribution induces in the decision model.

5.3 Valuing Information and Control

Information is, at a fundamental level, central to the evaluation of policy proposals. Formal policy analysis often requires that we address issues concerning the *cost, reliability, source,* and
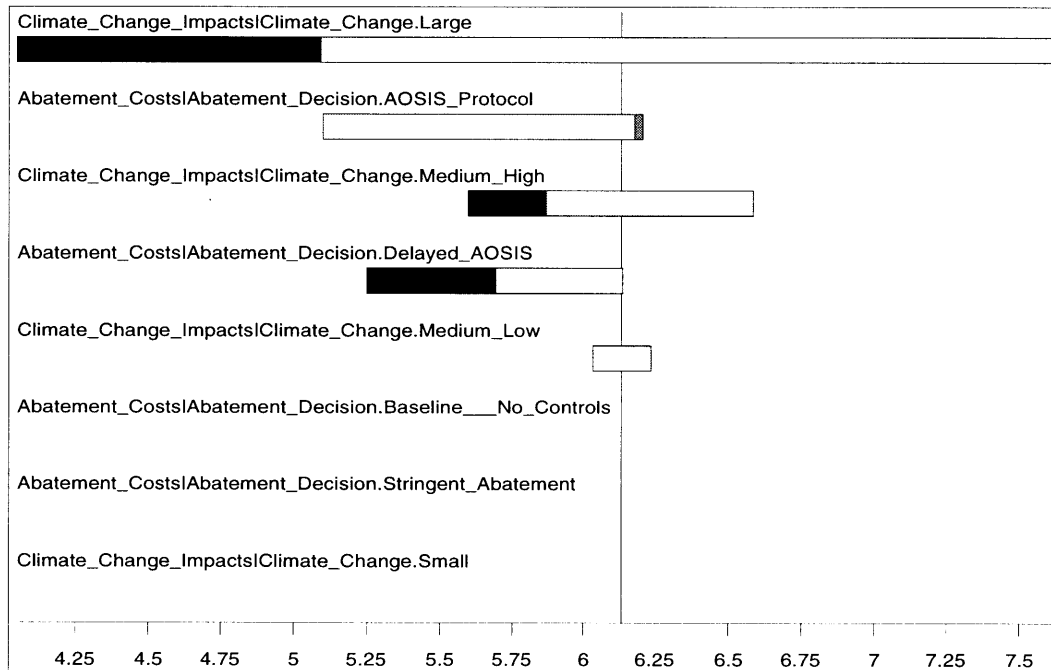
Figure 5-8: Tornado diagram for Abatement Costs and Climate Change Impacts.

timing of information. In modern decision analysis, the notions of *value of information* and *value of control* provide important conceptual schemes for systematically evaluating possible opportunities for gathering information, and for gaining insights about the value of considering alternatives that provide decision-makers with some measure of control over key variables [50].

In this section, we explore how the single-period decision model presented earlier can be modified so as to lend itself to the exploration of issues concerning the valuation of information and control. We begin our discussion with the notion of *clairvoyance* or *perfect information*, and from there we go on to consider the more general notion of *imperfect information*. We follow this presentation with a discussion of the concept of the value of control and its relevance to

Climate Change	Distribution$_1$	Distribution$_2$	Reference	Distribution$_3$	Distribution$_4$
Small	0	0	.2	.25	.75
Medium-Low	0	.25	.4	.50	.25
Medium-High	.25	.50	.3	.25	0
Large	.75	.25	.1	0	0
Optimal Policy	a_3 [6.2]	a_3 [6.2]	a_2 [6.13]	a_2 [3.03]	a_2 [2.16]

Table 5.6: Alternative policy-dependent probability distributions for $p(s_j|a_2)$.

107

climate change decision-making.

5.3.1 Computing the Value of Clairvoyance

The value of clairvoyance or perfect information is typically construed as an *upper bound* on the value of obtaining a specific piece of information. The basic question that concerns us here is, "What is the *value* of knowing the outcome of an uncertain climate-change-related quantity *now* rather than *later*?" We pose this question so as to gain insight about whether it is economically viable or desirable to pursue specific policy actions or research programs that could potentially resolve key scientific uncertainties in the greenhouse debate.

By definition, the expected value of perfect information (EVPI) can be zero or positive. If the EVPI is zero, then the decision is said to be *invariant* to the information that we may receive. Suppose that we wish to compute the EVPI for the chance variable Climate Change in our single-period decision model. Looking, again, at the ID shown in Figure 5-4, we recognize that before we can perform a determinate value of clairvoyance calculation on Climate Change, we must modify the basic structure of the diagram: Were it not for the influence arc from Abatement Decision to Climate Change, the addition of an information arc from Climate Change to Abatement Decision would allow us to calculate the value of the primary model with perfect information about the magnitude of climate change.[15] However, the addition of such an arc in Figure 5-4 would introduce an illegal cycle into the diagram. In addition to this problem, there is a conceptual difficulty with this approach that merits mention, namely, before revealing the value of the uncertain quantity that interests us—in this case, Climate Change—the clairvoyant must know what decision alternative has been chosen. As Howard [33] points out, if the clairvoyant were able to answer our query in the absence of knowledge concerning which course of GHG abatement action we have taken (or plan to take), then our actions would, in effect, be *predetermined.*

In order to sidestep this dilemma, we modify our basic model so that it is represented in *canonical form.*[16]

Definition 1 *An influence diagram for uncertain variables U and decisions D is said to be in* canonical form *if*

> *1. Every chance node that is not a descendant of a decision node is unresponsive to D;*

> *2. Every chance node that is a descendant of a decision node is a deterministic node.*

---

[15]Such a procedure is typical of the manner in which determinate value of information calculations are performed in formal policy analyses of global climate change. See, e.g., Hammitt [25], Manne and Richels [48], and Peck and Teisberg [60].

[16]See, e.g., Howard [33] and Matheson [50].

Climate Change

Abatement Strategy	Small	Medium-Low	Medium-High	Large
No Abatement	☐	☐	☐	☐
AOSIS Protocol	☐	☐	☐	☐
Delayed AOSIS	☐	☐	☐	☐
Stringent Abatement	☐	☐	☐	☐

Figure 5-9: Clairvoyant Form for the chance variable Climate Change.

An ID that is in canonical form allows modelers to represent all of the causal dependencies that exist in a given domain. In order to recast our single-period decision model in canonical form, we begin by imagining that the clairvoyant is able to fill out a form such as the one depicted in Figure 5-9. When filled out by the clairvoyant, the form indicates—for every course of action that the decision-maker can take—whether or not the event will occur. Since there are four possible abatement strategies that can be adopted, and four possible outcomes associated with the chance variable Climate Change, there are $4^4 = 256$ possible ways for the clairvoyant to fill out the form.

In modifying our original ID, we assume that the answer the clairvoyant provides, given that the decision-maker chooses to follow a particular abatement strategy, is probabilistically relevant to the answers he would provide if the decision-maker were to follow another course of action [33]. Such a characterization requires that we assign probabilities to receiving particular reports from the clairvoyant. In order to explicitly model this probabilistic dependency, we replace the chance node Climate Change with four separate chance nodes, which we label (Climate Change | a_1), (Climate Change | a_2), (Climate Change | a_3), and (Climate Change | a_4). In this characterization, each of the four chance nodes for the variable Climate Change is conditioned by one of the four possible abatement strategies. What this characterization does is separate the variables under the decision-makers control from the variables he cannot influence [50]. To complete our specification, we represent any *mutual relevance* that exists between these four random quantities, as well as specify the probabilities that are associated with each of these

109
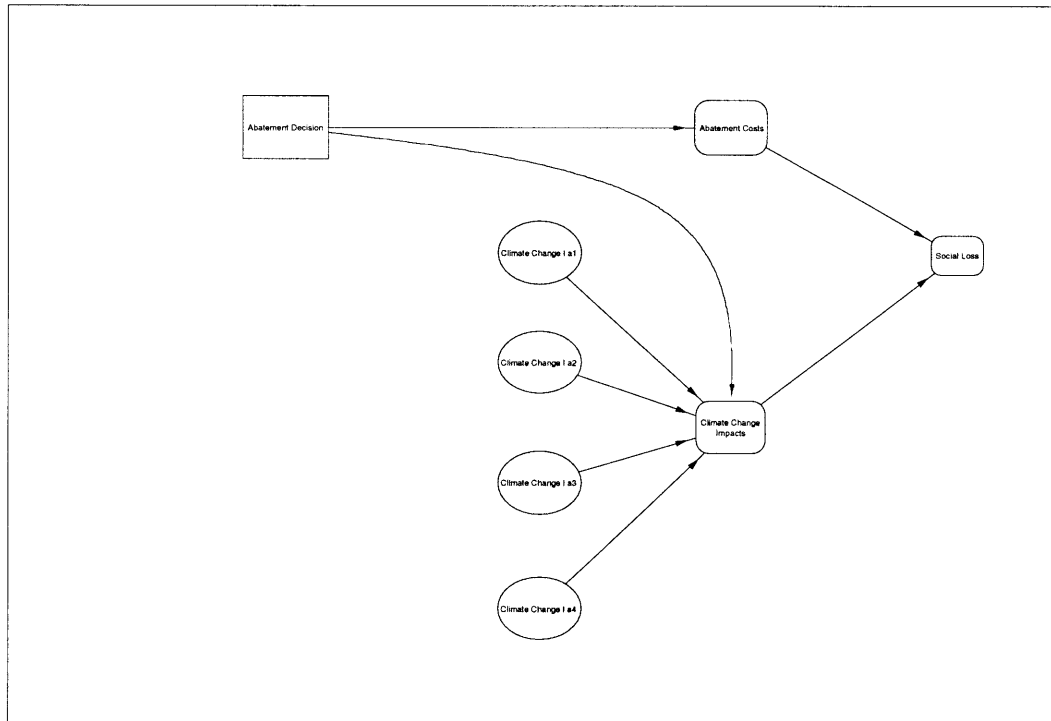
Figure 5-10: Single-period decision model in canonical form.

chance nodes.

Figure 5-10 illustrates one possible way in which our single-period decision model can be modified so as to reflect these ideas. We note that there are 4! = 24 possible assessment orders for the uncertain variables in the revised model. For the purposes of illustration, we single out the simplest possible assessment order: We assume that no mutual relevance exists between the four random quantities. For each chance variable (Climate Change | a_i), for $i \in \{1,\ldots,4\}$, we use the probability distributions listed in Table 5.1.[17] Having specified the required probability distributions, we compute the value of *complete* clairvoyance on Climate Change—as illustrated in Figure 5-11—by drawing an information arc from each of the four chance nodes to the Abatement Decision node. Adding these information arcs stipulates that the decision-maker has *perfect information* concerning the chance variables (Climate Change | a_i) at the time that the abatement decision is made, i.e., the outcomes of these chance variables are known *prior* to making the abatement decision. The model therefore assumes that the decision-maker follows what Manne and Richels [48] call a *learn-then-act* decision strategy, in the sense that the magnitude of climate change is learned prior to choosing an abatement strategy.

---

[17]Given these assumptions, the IDs in Figures 5-4 and 5-10 are *decision equivalent*, i.e., the two diagrams share the same optimal policy and expected value.
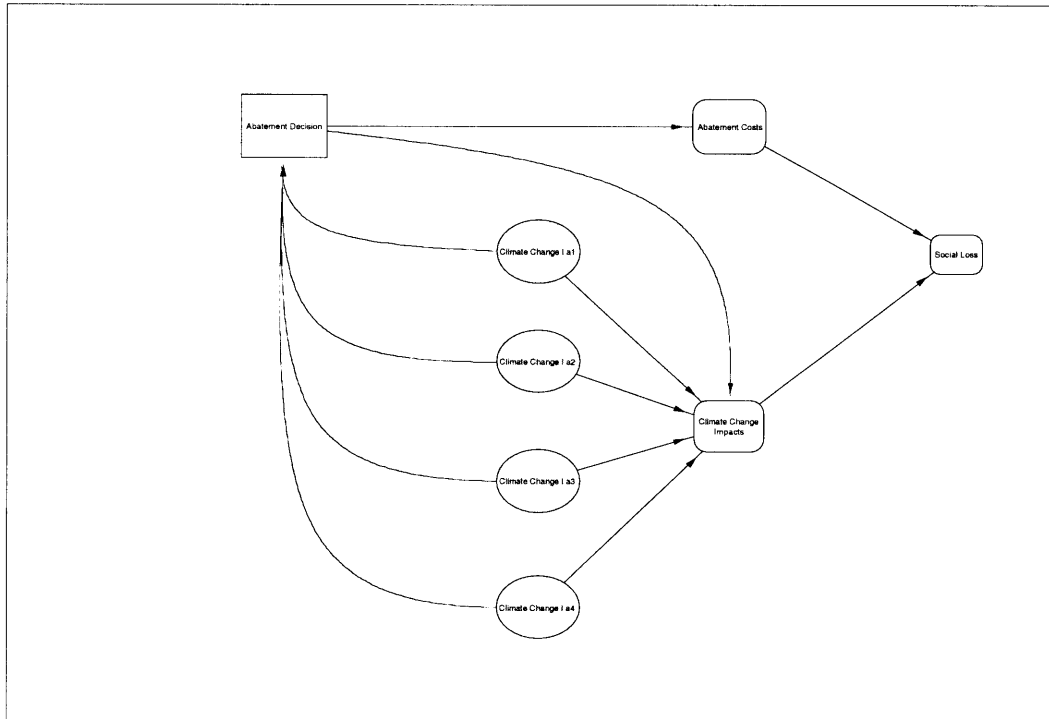
Figure 5-11: Complete value of clairvoyance on Climate Change using the canonical form representation of the single-period decision model.

In order to compute the value of complete clairvoyance on Climate Change, we first evaluate the ID in Figure 5-11. The solution for this model yields an expected social loss of 1.42%. Subtracting from this amount the expected social loss of the primary decision model shown in Figure 5-10 yields an EVPI of 1.42% − 6.13% = −4.71%. This value can be interpreted as the maximum amount that the decision-maker should be willing to pay a clairvoyant for perfect information concerning the magnitude of climate change.

The canonical form ID described above can also be used to compute the value of *partial* clairvoyance, i.e., the value of clairvoyance on Climate Change for each abatement policy individually. This computation is achieved by adding only those information arcs that are of most interest to the decision-maker. For example, looking again at the ID shown in Figure 5-10, in order to compute the value of cost-free clairvoyance on Climate Change for Strategy a_1, we draw an arc from the node labeled (Climate Change | a_1) to the Abatement Decision node. Evaluating the revised diagram yields an expected social loss of 2.28%. Subtracting from this amount the expected social loss of the original model yields an EVPI of 2.28% − 6.13% = −3.85%. In Table 5.7, we summarize the expected value of cost-free clairvoyance on Climate Change, for each abatement policy individually.

Abatement Decision	Value of Partial Clairvoyance
a_1	-3.85%
a_2	-2.58%
a_3	-2.50%
a_4	0.00%

Table 5.7: Value of cost-free partial clairvoyance on Climate Change, for each individual abatement option.

5.3.2 Computing the Value of Imperfect Information

Human decision-makers rarely find themselves in situations where they have access to *perfect* information concerning uncertain quantities of interest. In truth, the notion of clairvoyance or perfect foresight can, in many ways, be seen to be little more than a convenient fiction. The more realistic case arises when the decision-maker has the option of consulting an *imperfect* *information source* that is, for whatever reason, limited in it's ability to foresee the course of future events.

The value of *imperfect information* is defined mathematically as the difference between the expected utilities associated with two optimal decision strategies: one decision path allows the decision-maker to choose an information source, whereas the other decision path does not allow this opportunity. The expected value of the information source is computed as the (posterior) expected difference between the utilities (or monetary values) that correspond to optimal decisions with and without the information source.

In practice, decision-makers are often faced with situations where they must choose among competing sources of information. The canonical approach to evaluating an information source is depicted in the decision tree shown in Figure 5-12.[18] Reading the tree from left to right, we first decide whether to consult the information source in question, or to act without it. If we choose to consult the information source, we then observe potential reports, r, from the information source. Next, we choose a possible course of action, a. Having chosen a decision path, nature then chooses a state, s.

The numerical procedure that we use to compute a determinate value of the information source has two parts. We begin by focusing on the upper portion of the tree in Figure 5-12. Using the process of *backward induction*,[19] the utility of report r, $U(r)$, is given by

$$U(r) = \max_a \sum_s \Pr(s \mid r) U(a,s).$$

---

[18]This figure is adapted from Bernardo and Smith [6] and Pearl [59].
[19]See, e.g., Bernardo and Smith [6] and Raiffa [63].
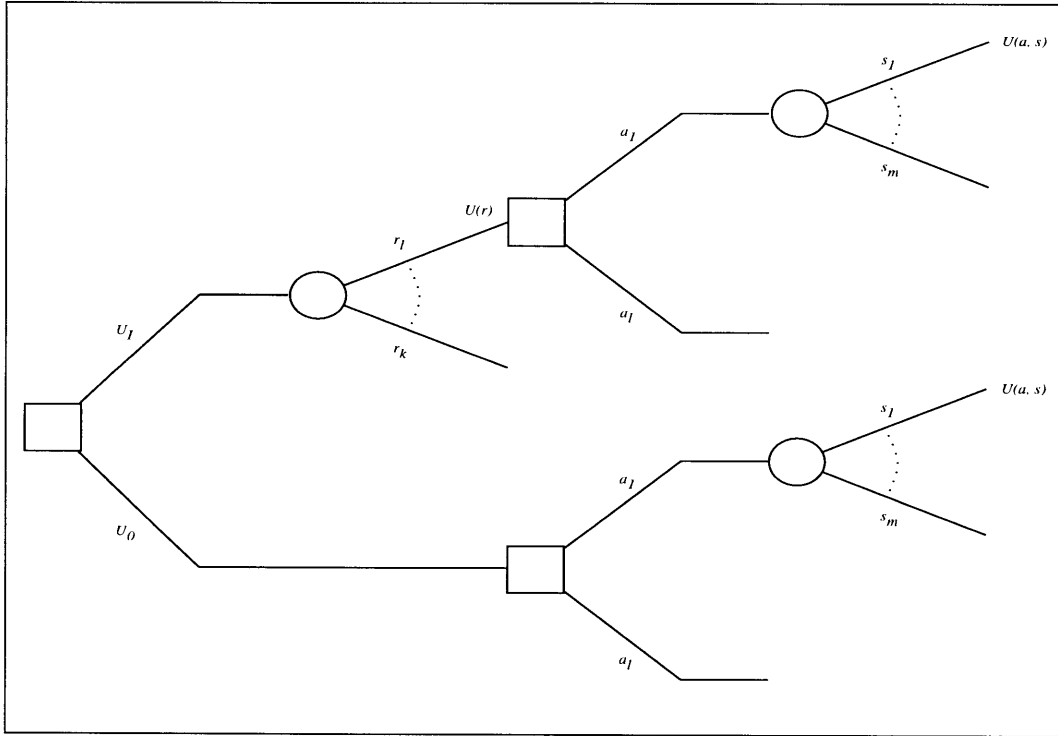
Figure 5-12: Assessment of an imperfect information source.

Thus, the expected utility of consulting the information source I is given by

$$U_I = \sum_r \Pr(r) \, U(r) = \sum_r \sum_s \Pr(r \mid s) \, \Pr(s) \, U(r),$$

which reflects the probability of obtaining report r, and the utility of acting optimally after receiving it. It is important to recognize that the conditional probability, $\Pr(r \mid s)$, *fully characterizes* the nature of the information source. This conditional probability measures what Pearl [59] calls the "fidelity" with which r "mirrors" s.

Looking, now, at the lower path in Figure 5-12, we see that U_0 reflects the utility of *not* consulting the information source, and is given by

$$U_0 = \max_a \sum_s \Pr(s) \, U(a, s).$$

The value of the information source $\eta = \Pr(r \mid s)$ is now defined as the difference between the upper and the lower paths in our decision tree. Specifically, we have that

$$
\begin{aligned}
V(\eta) \quad &= \quad U_I - U_0 \\[2ex]
&= \quad \sum_r \sum_s \max_a \left[\sum_{s'} \Pr(s' \mid r) \, U(a, s') \right] \Pr(r \mid s) \, \Pr(s)
\end{aligned}
$$

$$-\max_a \sum_s \Pr(s)\, U(a, s).$$

It is easily shown that the value of the information source is always nonnegative, i.e., $V(\eta) \geq 0$.

The canonical form ID shown in Figure 5-10 is easily modified so as to allow one to perform determinate value of imperfect information calculations in the manner described above. Suppose, for example, that we wish to compute the value of imperfect information on Climate Change for abatement policy a_3. To do so, we add a chance node to the diagram that represents an imperfect information source or *forecast* concerning the chance variable Climate Change, given that abatement policy a_3 is adopted. The revised ID is shown in Figure 5-13. In this diagram, we assume that the forecasts and the event outcomes are represented by the same categories that we defined earlier for the chance variable Climate Change. Thus, we define a chance variable

(Climate Forecast | a_3) = {"Small", "Medium-Low", "Medium-High", "Large"},

where the quotes denote forecasts of the four climate change categories. For this new ID, we must specify the relative frequency of each category, $\Pr\{$Climate Change $|\, a_3\}$. In addition, we must specify a likelihood matrix, **F**, whose i^{th} row and j^{th} column consists of the following conditional probabilities:

$$p(i \mid j) = \Pr\{(\text{Climate Forecast} \mid a_3) = r_i \mid (\text{Climate Change} \mid a_3) = s_j\},$$

where $r_i \in$ (Climate Forecast | a_3) and $s_j \in$ (Climate Change | a_3).

For the purposes of illustration, let us suppose that the chance variable (Climate Change | a_3) is characterized by the probability distribution that we specified earlier in Table 5.1. For the likelihood matrix **F**, we follow Manne and Richels [48] and assume that forecast errors are symmetrically distributed.[20] In this way, we assume that a climate forecast is equally likely to overestimate or underestimate the actual climate change outcome. Thus, for the chance variable (Climate Change | a_3), we assume that the likelihood matrix **F** takes the form depicted in Table 5.8. In this table, the parameter σ (labeled 'sigma' in the ID shown in Figure 5-13) is a measure of the *accuracy* of the climate forecast. By inspection, we see that if $\sigma = 1/4$, then all of the climate forecasts are characterized as being equally probable; consequently, the forecasts fail to provide the decision-maker with additional new information. Alternatively, if σ is equal to unity, then the climate forecasts represent *perfect* information concerning the

---

[20]This assumption should, of course, be modified if available evidence suggests that the climate forecast errors are characterized by a different distributional form. Also, we note that the analysis presented here differs from that of Manne and Richels [48] in one important respect, namely, we model the *probabilistic influence* that policy choice has on the possible states of nature associated with climatic change.
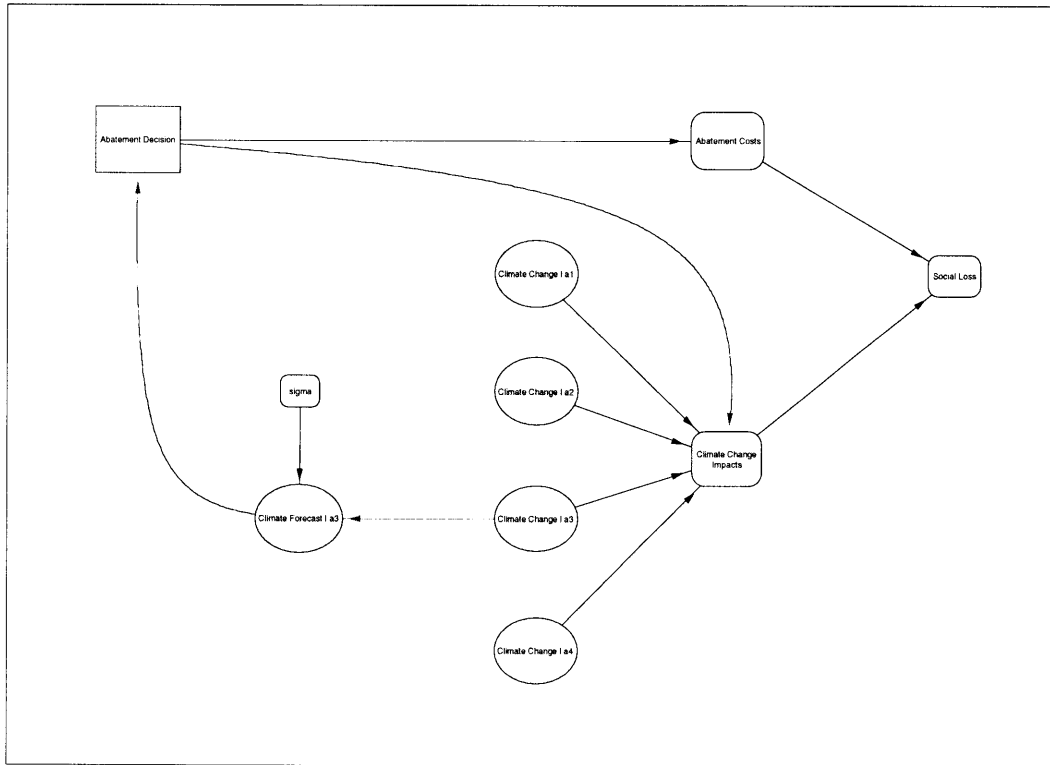
Figure 5-13: Canonical form ID for computing a determinate value of imperfect information on (Climate Change | a_3).

chance variable Climate Change. In this way, increasing values of σ in the interval 1/4 to 1 give rise to increases in the accuracy of the climate forecasts.

In order to evaluate the ID in Figure 5-13, we must specify a value for σ. For the purposes of illustration, we consider three separate cases: $\sigma = 0.4$, $\sigma = 0.6$, and $\sigma = 0.8$. Evaluating the diagram with each of these three values for σ yields expected social losses of 5.67%, 4.99%, and 4.31%, respectively. Subtracting from these values the expected social loss of the primary model (6.13%) yields expected values of imperfect information of -0.46%, -1.14%, and -1.82%, respectively. Clearly, the value of imperfect information increases with the accuracy of the climate forecast, which agrees with our intuition.

At this point, it is useful to explore the influence that receiving a particular climate forecast has on the policy-dependent prior probability judgements concerning climate change. Specifically, we now address the question of how the decision-maker's prior probability assessments concerning the level of climatic change are *revised* or *updated* in light of new information. In the context of our discussion here, this new information takes the form of categorical forecasts of climatic change, and the ID shown in Figure 5-13 provides a useful computational vehicle for exploring this issue.

115

Climate Forecast	Climate Change			
	Small	Medium-Low	Medium-High	Large
"Small"	σ	$\frac{1-\sigma}{3}$	$\frac{1-\sigma}{3}$	$\frac{1-\sigma}{3}$
"Medium-Low"	$\frac{1-\sigma}{3}$	σ	$\frac{1-\sigma}{3}$	$\frac{1-\sigma}{3}$
"Medium-High"	$\frac{1-\sigma}{3}$	$\frac{1-\sigma}{3}$	σ	$\frac{1-\sigma}{3}$
"Large"	$\frac{1-\sigma}{3}$	$\frac{1-\sigma}{3}$	$\frac{1-\sigma}{3}$	σ

Table 5.8: Likelihood matrix for value of imperfect information calculations.

As discussed previously in Section 5.2.1, it is possible to transform any well-formed ID by means of so-called *value-preserving* operations. Of interest to us here is an operation called *arc reversal*, which provides a computational means by which to perform *Bayesian inversion* calculations. Looking, again, at the ID shown in Figure 5-13, we are interested in reversing the arc that goes from (Climate Change | a_3) to (Climate Forecast | a_3), so as to compute the posterior probabilities, $\mathrm{Pr}\{$(Climate Change | a_3) | (Climate Forecast | a_3)$\}$. Calculation of coherent values for these updated probabilities are obtained via Bayes' rule, which, for this example, we state as follows:

$$\frac{\mathrm{Pr}\{\text{(Climate Forecast} \mid a_3) \mid \text{(Climate Change} \mid a_3)\} \, \mathrm{Pr}\{\text{(Climate Change} \mid a_3)\}}{\mathrm{Pr}\{\text{(Climate Change} \mid a_3)\}}.$$

In the ID, we specified the marginal distribution for (Climate Change | a_3), and the forecast likelihoods for (Climate Forecast | a_3). In order to perform the Bayesian inversion, we must also compute the marginal forecast probabilities, $\mathrm{Pr}\{$(Climate Forecast | a_3). These probabilities are easily obtained by means of the decomposition formula

$$\mathrm{Pr}\{\text{(Climate Forecast} \mid a_3)\} \;=\; \sum \big[\, \mathrm{Pr}\{\text{(Climate Forecast} \mid a_3) \mid \text{(Climate Change} \mid a_3)\}$$
$$\times \, \mathrm{Pr}\{\text{(Climate Change} \mid a_3)\} \,\big].$$

In Table 5.9, we summarize these marginal probabilities, for each level of forecast accuracy. Table 5.10 summarizes the posterior probabilities that we obtain using the Bayesian arc reversal procedure described above. In this table, we tabulate the posterior probabilities for the three forecast accuracy levels considered here: $\sigma = 0.4$, $\sigma = 0.6$, and $\sigma = 0.8$. For the purposes of comparison, in Figure 5-14 we plot these three sets of posterior probabilities, along with the original prior probability assessment.

Inspection of Table 5.10, together with the bar plots shown in Figure 5-14, reveals some interesting characteristics about the prior-to-posterior values. First, as expected, the posterior probabilities that lie along the diagonals of the three individual tables shown in Table 5.10

Climate Forecast	Marginal Probability Distribution		
	$\sigma = .4$	$\sigma = .6$	$\sigma = .8$
"Small"	.24	.23	.21
"Medium-Low"	.26	.27	.29
"Medium-High"	.28	.32	.36
"Large"	.22	.18	.14

Table 5.9: Marginal probability distributions for the Climate Forecast chance variable, as a function of forecast accuracy, σ.

increase with forecast accuracy, σ. For the specific values used here, some of these increases are quite dramatic. For example, when σ equals 0.6 and 0.8, the probability for small climate change, given that the climate forecast says "Small," goes from 0.20 to 0.52 and 0.75, respectively. We note, also, that the probability of small climate change, given that the forecast says "Large," decreases with increases in forecast accuracy.

5.3.3 Computing the Value of Control

The concept of the *value of control* is often used to gain insight into the value of considering new decision alternatives that enable decision-makers to assume some measure of control over uncertain variables of interest. To operationalize the concept of value of control, we posit the existence of a "wizard" that is capable of *controlling* or *setting* the value of a particular variable of interest.

In our single-period decision model, we envision a situation where we wish to determine the value of exercising *perfect* control over the level or magnitude of observed climate change. If, for example, our objective is to minimize climate change, then we would engage the wizard to ensure a 'Small' degree of climate change.

For our purposes here, we assume that our hypothetical wizard is cost-free and is capable of ensuring the best possible outcome. To calculate the value of complete control over the chance variable Climate Change, we do not need to revise the ID shown in Figure 5-10. Rather, within the internal representation of the model, we simply set the chance node Climate Change to the desired state, and then numerically re-evaluate the model.

For the model specification presented above, this numerical calculation is quite simple. Since the wizard is able to ensure that the event 'Climate Change = Small' will obtain with certainty, we are guaranteed that Climate Change Impacts will be 0%. Consequently, the abatement decision that minimizes aggregate social loss is Strategy a_1, which has an abatement cost equal to 0%. Subtracting from this amount the value of the primary problem yields an expected

$\sigma = .4$	Climate Forecast			
Climate Change	"Small"	"Medium-Low"	"Medium-High"	"Large"
Small	.33	.15	.14	.18
Medium-Low	.25	.46	.21	.28
Medium-High	.33	.31	.57	.36
Large	.09	.08	.08	.18

$\sigma = .6$	Climate Forecast			
Climate Change	"Small"	"Medium-Low"	"Medium-High"	"Large"
Small	.52	.10	.08	.15
Medium-Low	.18	.65	.13	.22
Medium-High	.24	.20	.75	.30
Large	.06	.05	.04	.33

$\sigma = .8$	Climate Forecast			
Climate Change	"Small"	"Medium-Low"	"Medium-High"	"Large"
Small	.75	.05	.04	.10
Medium-Low	.09	.84	.06	.14
Medium-High	.13	.09	.88	.19
Large	.03	.02	.02	.57

Table 5.10: Posterior probabilities obtained from the arc reversal procedure, for three different levels of climate forecast accuracy: $\sigma = .4$, $\sigma = .6$, and $\sigma = .8$.
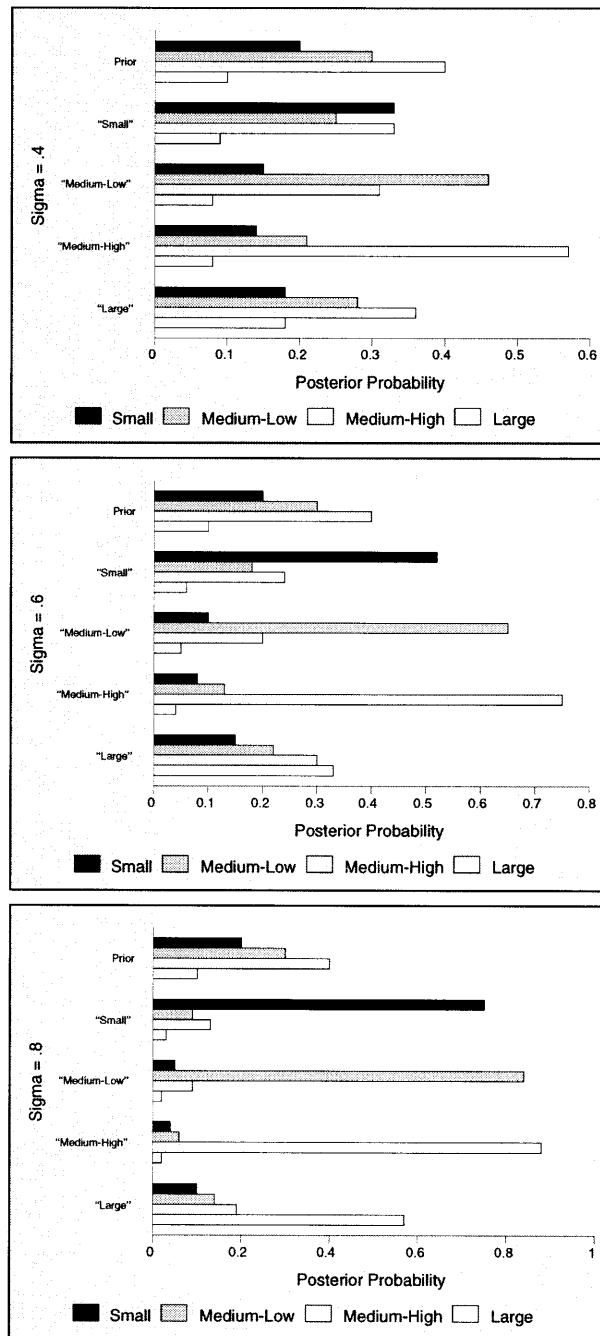
Figure 5-14: Prior and posterior probabilities for $\sigma = .4$, $\sigma = .6$, and $\sigma = .8$.

value of perfect control of 0% – 6.13% = –6.13%. This calculation demonstrates that the value of wizardry far exceeds the value of clairvoyance.

5.4 Summary

In this chapter, we examined how the problem of evaluating GHG abatement strategies can be framed as a decision problem under uncertainty. Analytical tools drawn from modern decision science served as the conceptual basis for an analytical framework for structuring and evaluating an illustrative set of GHG abatement policies. The decision-theoretic framework set forth here also provides a formal and explicit means by which to conduct sensitivity analyses of key model assumptions, inputs, and policy prescriptions, as well as to address issues concerning the valuation of information and control.

There can be little doubt that the decision models presented in this chapter represent a simplified picture of reality. Modeling efforts such as these are, as a matter of course, necessarily fraught with choices concerning which aspects of the human-climate system are most essential for the systematic appraisal of policy choice. Granting this point, the models presented here provide a convenient means by which to structure and integrate knowledge and information from a disparate range of sources.

To what end, then, can the decision models presented here be said to inform the climate policymaking process? Ultimately, our intention is to garner insights about the relative merits of adopting one GHG abatement action over another. Given the crudeness of even our best-available data, together with a sobering awareness of the myriad scientific and economic uncertainties that pervade the greenhouse debate, the most we can reasonably hope to achieve—at least in the near-term—is to assess relative *orders of magnitude*. In this context, the static decision models presented here are useful policy-analytic tools, in that they provide policymakers with nimble and computationally-efficient frameworks for exploring a broad range of climate change response options. As we discussed earlier in Chapter 1, the results of static analyses such as these can help guide the design and specification of subsequent analyses, which focus on more detailed or refined aspects of the greenhouse problem.

The static analysis presented here suggests that—relative to the other climate policies— the AOSIS Protocol represents an optimal course of GHG abatement action. We recognize, however, that this policy prescription is sensitive to the damages specified for medium-high to large degrees of climatic change, as well as the abatement costs specified for the AOSIS and Delayed AOSIS policies. The close proximity of the expected social loss associated with the AOSIS and Delayed AOSIS policies (6.12% vs. 6.2%) suggests that *delaying* implementation of the AOSIS Protocol by one decade is a policy alternative that deserves further analysis and

120

interpretation. In particular, given that the Delayed AOSIS policy is a static representation of what is, in actuality, a *sequential* climate policy, it seems reasonable to enquire how this policy would fare—relative to others—when evaluated from a multi-period or sequential perspective. In the following chapter, we address this question in the context of an integrated decision analysis framework for evaluating sequential GHG abatement policies under uncertainty.

Chapter 6

Integrated Frameworks for Sequential Decision-Making and Learning

In recent years, climate researchers, economists, and policy analysts have begun to study how the evaluation of climate change response options can be viewed as a sequential decision problem, where successive, interdependent GHG abatement decisions are made over a finite time horizon.[1] The single-period decision model put forth previously in Chapter 5 is essentially a *static* representation of the climate change problem, in that the model assumes a decision context where policymakers select a *single* GHG abatement policy in the short-term, *once-and-for-all*, with no future opportunities for amending or revising an adopted course of action.

In this chapter, we consider the problem of climate change decision-making from a *multi-period* or *sequential* perspective. Our presentation is divided into four parts. We begin, in Section 6.1, with an introduction to the basic concepts that underlie our sequential modeling approach. As part of this discussion, we review several analytical frameworks that climate researchers have, in recent years, put forth for the evaluation of sequential GHG abatement strategies. In Section 6.2, we extend the single-period decision model presented in Chapter 5 to two periods. Our sequential model formulation is seen to draw explicit linkages between the MIT IGSM and the reduced-scale climate modeling approach set forth earlier in Chapters 3 and 4. In Section 6.3, we turn our attention to the topic of *learning*, and we explore the relevance of this concept to climate change decision-making. Lastly, in Section 6.4, we briefly summarize the policy relevance of our findings.

---

[1] See, e.g., Manne and Richels [48] and Nordhaus [57].

6.1 Sequential Climate Change Decision-Making

Many real-world decision problems are characterized by *sequences* of successive and interdependent decisions. Viewing the problem of climate change decision-making from a sequential perspective requires that we first recognize that *an optimal course of abatement action will depend upon the optimal choices at subsequent decision points*. In this way, *near-term* GHG abatement action is not taken without first considering what climate change response options might be available in the future, as well as what might be observed in the *long-term* about important climate-change-related parameters. We recognize, also, that both mid- and long-term abatement actions will—in some measure—depend on the observed consequences of short-term policy action(s).

During the course of the past decade, economists and policy analysts have explored ways of formulating and evaluating sequential decision problems that are characterized by uncertainty and scarce resources.[2] In Chapter 4 of their landmark study, Manne and Richels [48] present a framework for dealing with uncertainty in the analysis of the economic costs of CO_2 emission reduction strategies. Their two-period, "Act-then-Learn" formulation assumes that decisions concerning CO_2 emission reductions are made at discrete ten-year time intervals. As illustrated in the schematic decision tree shown in Figure 6-1, as well as in the corresponding *temporal influence diagram* (TID) shown in Figure 6-2, near-term energy sector supply and demand decisions are made prior to knowing the true damage potential of global climate change. Manne and Richels assume that the damage potential is characterized by three possible states of nature: 'Low,' 'Moderate,' and 'High.' Associated with each possible state of nature is an assumed CO_2 emission reduction level. If, for example, the damage potential is 'Low,' then, from 2020 on, no limits are imposed on global carbon emissions. Alternatively, the 'Moderate' and 'High' damage potentials give rise to assumed carbon emission reductions of 20% and 50% below 1990 levels, respectively. By assigning a subjective probability distribution to the damage potential, the model is used to evaluate an optimal hedging policy for 2000 and 2010, without knowing which carbon emission scenario will obtain.[3] In this way, the framework makes explicit the idea of hedging against a range of possible future policy outcomes.

More recently, Hammitt, Lempert, and Schlesinger [26] put forth a sequential framework for evaluating GHG climate change abatement strategies. In Figure 6-3, we depict the basic structure of their framework in the form of a two-stage decision tree. In the tree, we see that two near-term abatement policies are evaluated: "Aggressive" and "Moderate." Under the aggressive

---

[2] In the field of environmental economics, e.g., Miller and Lad [52] develop a two-period model for evaluating resource development projects that are characterized by irreversible actions and consequences, and where learning is assumed to take place over a finite time horizon.

[3] In a recent paper, Manne [47] reports the results of a study that compares the optimal hedging strategies of seven models participating in Energy Modeling Forum Study 14.
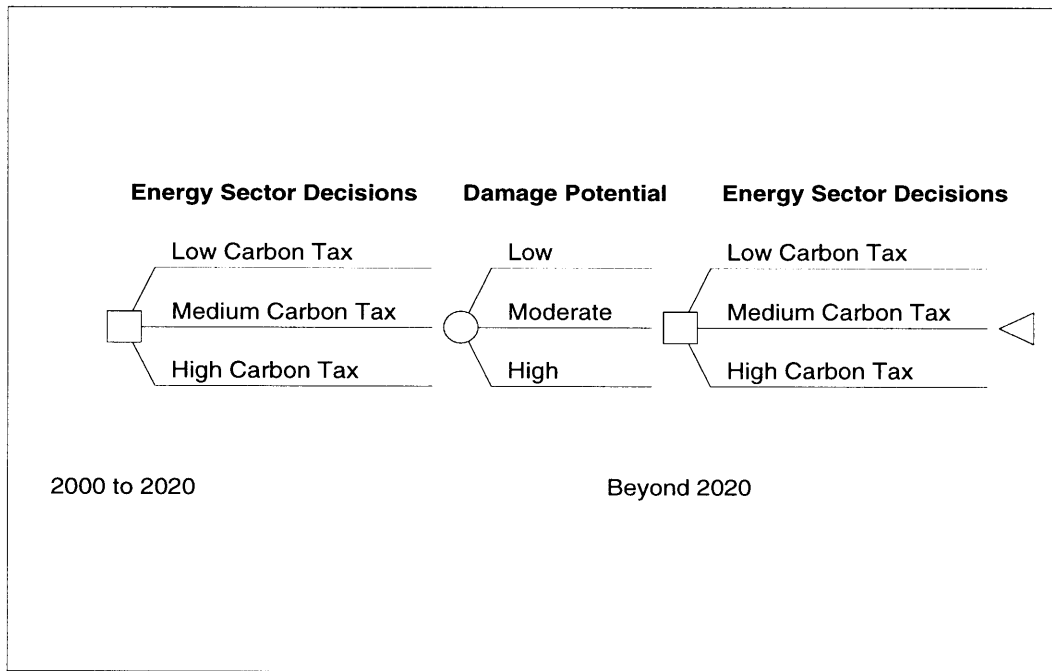
Figure 6-1: Act-then-learn decision framework proposed by Manne and Richels (1992).
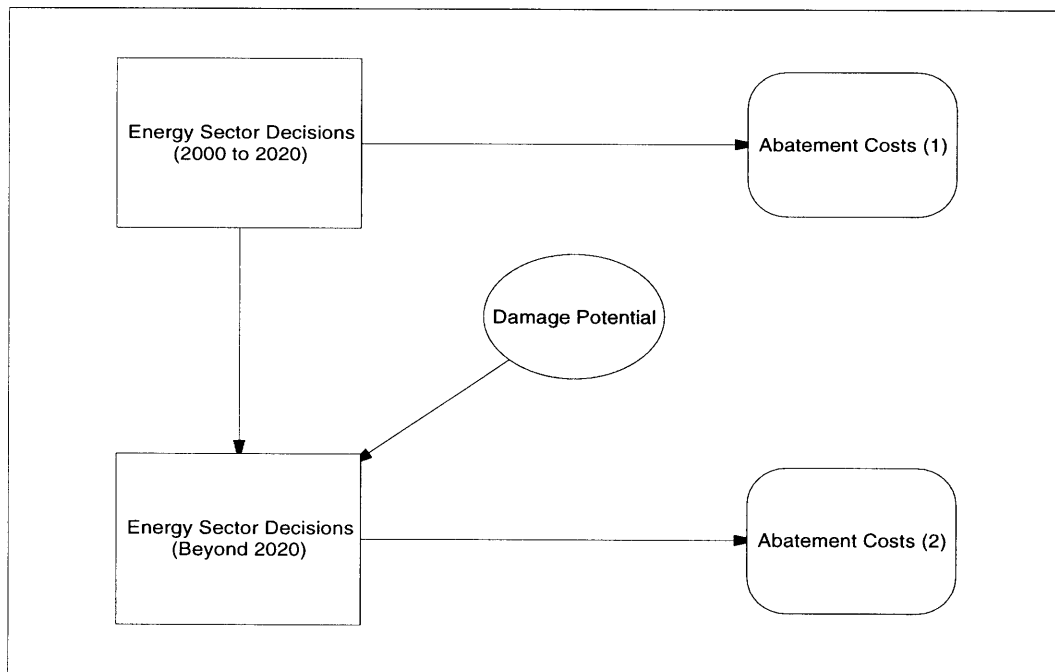
Figure 6-2: Temporal influence diagram representation of the act-then-learn decision framework proposed by Manne and Richels (1992).

124
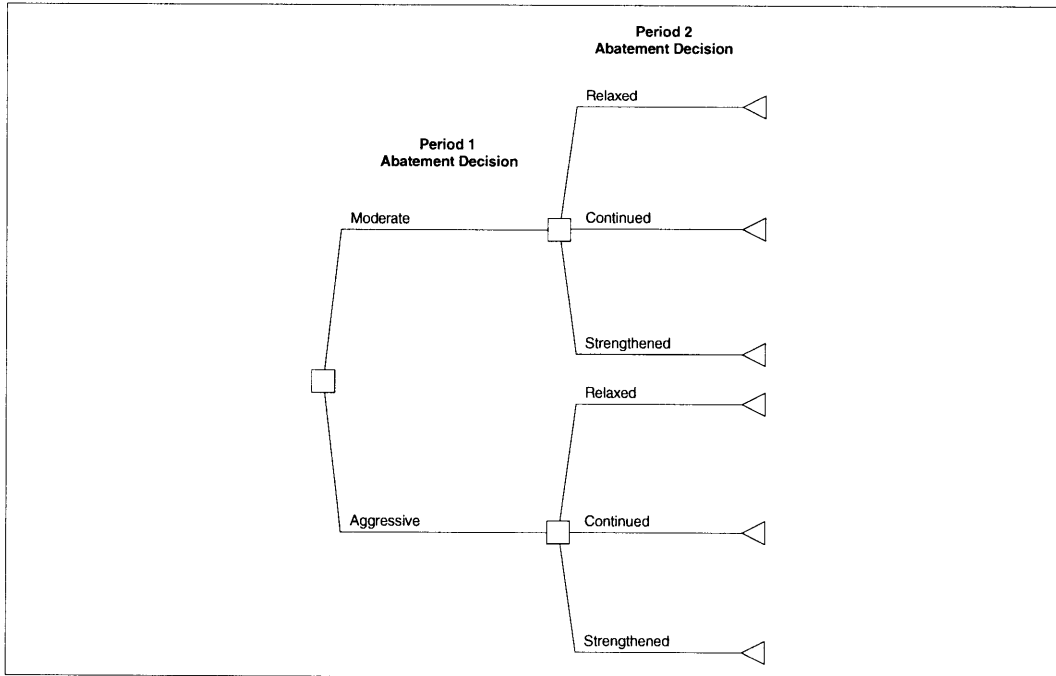
Figure 6-3: Two-stage decision tree proposed by Hammitt, Lempert, and Schlesinger (1992) for the evaluation of six sequential GHG abatement strategies.

abatement option, both energy conservation and fuel-switching measures are adopted at the beginning of Period 1; under the moderate option, only conservation measures are adopted at the beginning of Period 1. Regardless of which policy option is adopted in Period 1, at the beginning of Period 2, uncertainties concerning the climate sensitivity parameter, ΔT_{2x}, and a climate target, ΔT^*, are assumed to be fully resolved.[4] In Period 2, the rate of fuel switching is adjusted so that—for a given climate sensitivity value—observed temperature change at time t peaks at the revealed climate target, ΔT^*. In their model formulation, both climate sensitivity and the climate target are implicitly chosen so that the present value of the marginal costs of abatement is equal to that of the damages. In this way, abatement action in Period 1 is amended in Period 2 to limit the magnitude of climate change to some "optimal" level.

The salient features of the two-stage model put forth by Hammitt, Lempert, and Schlesinger are, for our purposes here, more adequately depicted in the form of a TID, which we show in Figure 6-4. In this alternative representation, we note that the level or magnitude of climate change at each time period is treated in a deterministic fashion. In their analysis, Hammitt, Lempert, and Schlesinger treat climate change uncertainty in an *implicit* fashion by examining

---

[4]It is important to note that, in this model formulation, ΔT_{2x} and ΔT^* serve as proxies or surrogates for the scientific uncertainty that surrounds the greenhouse debate. The uncertainty that characterizes these quantities is, however, treated in a deterministic fashion.
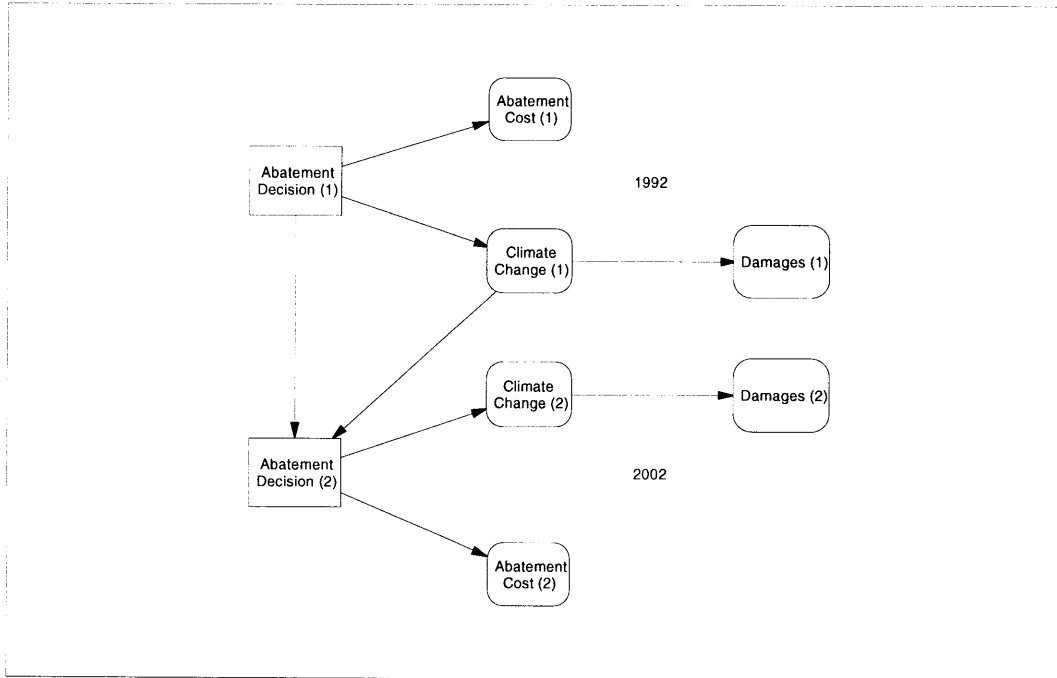
Figure 6-4: Temporal influence diagram representation of the sequential framework proposed by Hammitt, Lempert, and Schlesinger (1992).

the sensitivity of the model's policy prescriptions to a range of plausible climate sensitivity values, as well as to a range of possible climate targets.

The two-period formulation of Hammitt, Lempert, and Schlesinger, while useful in providing a basis for *comparing* an illustrative set of GHG abatement policies, fails to provide decision-makers with clear policy *prescriptions*, due, mainly, to the fact that key uncertainties in their model are not treated in an explicit, quantitative fashion.[5]

In what follows, we set forth an integrated decision analysis (IDA) framework for evaluating sequential GHG abatement policies under uncertainty. Our IDA framework seeks to improve upon the models discussed above in several respects, most notably, in the explicit treatment of uncertainty in key climate-change-related quantities and model parameters.

6.2 A Sequential Decision Model

In this section, we extend the single-period decision model presented earlier in Chapter 5 to two periods. The two-period formulation set forth here provides a formal and explicit means by

---

[5] It is worth noting that Hammitt, Lempert, and Schlesinger do not prescribe an "optimal" abatement path. Rather, they conclude that a "Moderate" control strategy is less costly than an "Aggressive" strategy if (i) climate sensitivity is low; or (ii) the allowable temperature change is above $3°C$.

which to represent several important features of the climate change decision-making problem:

1. The representation of possible mid-course corrections to near-term policy choice;

2. The representation of climatic change as a dynamic process that evolves over time;

3. The representation of uncertainty in key climate-change-related quantities;

4. The representation of uncertainty in the calibration and parameterization of the functions used to represent climate-induced damages or impacts.

As Jacoby, Kaufman, and Valverde [34] point out, there are several IAMs currently in use that incorporate some or all of these features. A key innovation of the analytical framework that we present here is the *integration* of these features into a nimble, transparent, and computationally-efficient scheme, with—as we discuss below—direct and tangible linkages to the larger, more complex MIT IGSM.

Our sequential model formulation begins with the TID shown in Figure 6-5; we shall refer to this diagram as the "primary" TID. As in the single-period case, the diagram represents the economic costs (in each period) of adopting particular GHG abatement policies, as well as the economic impacts associated with realized levels of climatic change. In contrast with the single-period formulation, however, global climate change is represented as a dynamic process that is functionally dependent on (i) the abatement policy adopted in each period; and (ii) chance variables representing the uncertainty that characterizes two important climate-related parameters.

The TID shown in Figure 6-5 provides a computationally-efficient framework for evaluating sequential climate policies. In its latest report, the IPCC rightly notes that "the intractability of complex decision trees has limited the application of [decision analysis] in environmental problems..." [9, p. 67]. To emphasize this point, we note that—for the sequential decision basis defined below—the decision tree equivalent for our primary TID contains over one thousand enumerated branches.

In the presentation that follows, we formally specify the sequential decision basis for the primary TID. As discussed below, we utilize quantified expert judgements to estimate the economic impacts associated with various levels of greenhouse warming, as well as to specify subjective probability distributions for key climate-change-related quantities and model parameters. The climate change experts who participated in this study are all affiliated with the MIT Joint Program on the Science and Policy of Global Change. Wherever possible, we have, in addition to these experts' opinions, drawn from published elicitations and surveys of expert opinions, most notably, Morgan and Keith [53] and Nordhaus [56].

127
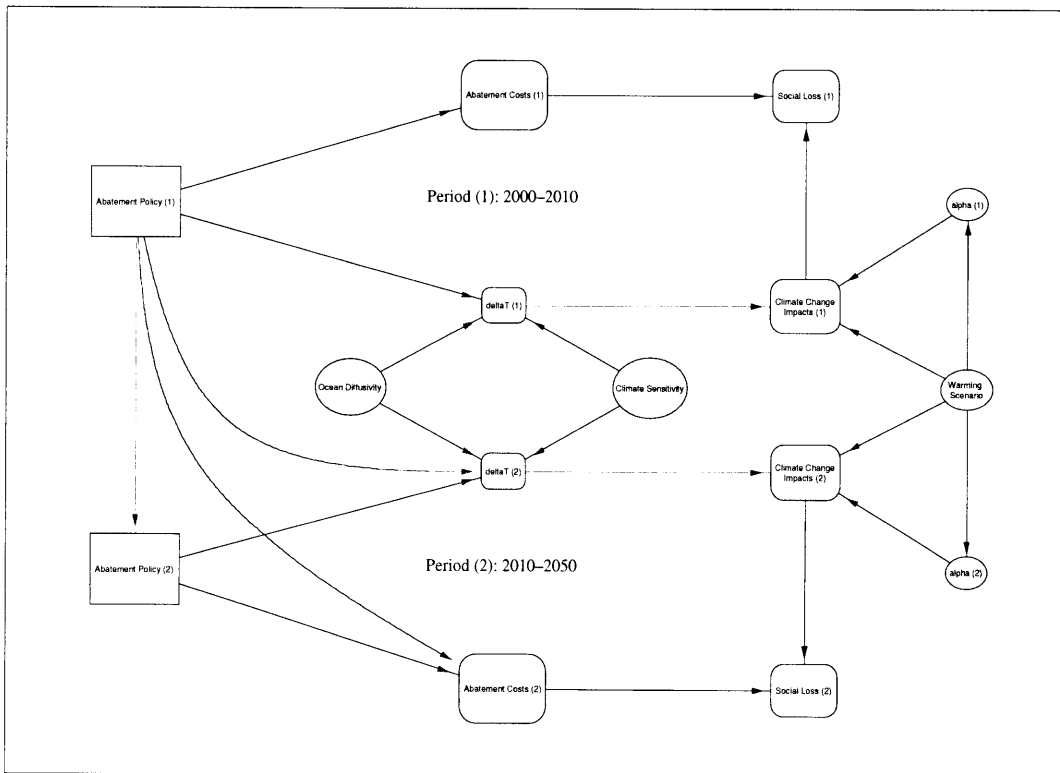
Figure 6-5: Temporal influence diagram representation of the sequential decision model.

6.2.1 Specification of the Sequential Decision Basis

The sequential decision basis for our two-period model consists of two stages: The first stage covers the years 2000–2010, and the second stage covers the years 2010–2050.[6] We now specify the sequential decision alternatives, possible states of nature, uncertain quantities, abatement costs, and climate change impacts that, together, comprise the decision basis for our sequential model.

Sequential Decision Alternatives

In our sequential model, we assume a unitary decision-maker, who wishes to choose among a finite set of possible abatement strategies.[7] In contrast, however, with the single-period model, our concern here is with the selection of optimal *sequential* decision strategies. Thus, we define two decision nodes, Abatement Policy (1) and Abatement Policy (2), denoting the model's first and second decision stages, respectively. In Figure 6-5, we observe that there is a directed arc from the first decision stage to the second decision stage. The addition of this so-called *no forgetting* arc introduces an explicit *time ordering* into the diagram. Specifically, in Period 1, an initial near-term abatement policy a_{1i} is selected from the set

$$\text{Abatement Policy (1)} = \{a_{11}, a_{12}, a_{13}, a_{14}\},$$

where

$$
\begin{aligned}
a_{11} &\equiv \text{Reference Baseline-No Controls,} \\
a_{12} &\equiv \text{Stabilize OECD Carbon Emissions at 1990 Levels,} \\
a_{13} &\equiv \text{AOSIS Protocol,} \\
a_{14} &\equiv \text{Stringent Abatement.}
\end{aligned}
$$

In a similar fashion, at the beginning of Period 2, a long-term abatement policy a_{2j} is selected from the set

$$\text{Abatement Policy (2)} = \{a_{21}, a_{22}, a_{23}, a_{24}\},$$

---

[6]The time horizon used here is consistent with the time horizon used earlier in our single-period model formulation.

[7]As in the single-period formulation, we stress that *unilateral* responses to the prospect of global warming are unlikely to be effective in the mitigation of climatic change and its potential socio-economic consequences. For this reason, a global, "single-actor" analysis such as that which we present here seeks to improve our understanding of what can potentially be achieved on a global scale, *given that opportunities for mutual cooperation are successfully negotiated in the geo-political arena.* Moreover, this type of analysis can provide useful insights about the relative importance of factors that are likely to influence the willingness of stakeholders to enter into, and abide by, politically-negotiated agreements concerning the abatement of key GHGs.

where

$$a_{21} \equiv \text{Reference Baseline-No Controls,}$$

$$a_{22} \equiv \text{Stabilize OECD Carbon Emissions at 1990 Levels,}$$

$$a_{23} \equiv \text{AOSIS Protocol,}$$

$$a_{24} \equiv \text{Stringent Abatement.}$$

Abatement policies a_{11} and a_{21} represent an unconstrained 'Reference' carbon emission baseline. As in the single-period case, abatement costs in our sequential framework are defined in terms of the difference in costs between the Reference Baseline scenario and an alternative policy scenario where carbon emissions are constrained. Under abatement policies a_{12} and a_{22}, OECD carbon emissions are stabilized at 1990 levels. The AOSIS Protocol, which we described earlier in Chapter 5, is represented by abatement policies a_{13} and a_{23}. Under abatement policies a_{14} and a_{24}, OECD carbon emissions are reduced to 30% of 1990 levels.

In Figure 6-6, we use a schematic decision tree to depict the abatement policies described above. In this tree, we observe that there are $4^2 = 16$ possible decision sequences in the model. We formally denote a *sequential climate policy* by the ordered pair, $< a_{1i}, a_{2j} >$, where $a_{1i} \in$ Abatement Policy (1) and $a_{2j} \in$ Abatement Policy (2). Using this notation, a complete enumeration of the sequential climate policies depicted in Figure 6-6 can be specified succinctly as follows:

$$< a_{11}, a_{21} > \quad < a_{12}, a_{21} > \quad < a_{13}, a_{21} > \quad < a_{14}, a_{21} >$$

$$< a_{11}, a_{22} > \quad < a_{12}, a_{22} > \quad < a_{13}, a_{22} > \quad < a_{14}, a_{22} >$$

$$< a_{11}, a_{23} > \quad < a_{12}, a_{23} > \quad < a_{13}, a_{23} > \quad < a_{14}, a_{23} >$$

$$< a_{11}, a_{24} > \quad < a_{12}, a_{24} > \quad < a_{13}, a_{24} > \quad < a_{14}, a_{24} >.$$

Inspection of this set of sequential climate policies reveals that the two-period formulation differs from the single-period formulation in some important respects. First, we note that an abatement policy that is adopted at the beginning of Period 1 can be *revised* or *amended* at the beginning of Period 2. If in Period 1, for example, abatement policy a_{12} is adopted, then in Period 2, the decision-maker can (i) abandon the policy and adopt a no-controls policy (Abatement Policy a_{21}); (ii) continue with the adopted policy (Abatement Policy a_{22}); or (iii) adopt a more stringent policy (Abatement Policies a_{23} or a_{24}). Also worth noting is the fact that the sequential model formulation allows for the explicit representation of *delayed* policy action. Specifically, we note that sequential climate policies $< a_{11}, a_{22} >$, $< a_{11}, a_{23} >$, and $< a_{11}, a_{24} >$ all represent delayed policy action in response to the prospect of anthropogenic global warming; also, sequential climate policy $< a_{11}, a_{23} >$ is an explicit representation of the 'Delayed AOSIS Protocol' option that we discussed earlier in Chapter 5.

Abatement Policy (1)   **Abatement Policy (2)**

No Controls   No Controls

Stabilize Emissions   Stabilize Emissions

AOSIS Protocol   AOSIS Protocol

Stringent Abatement   Stringent Abatement
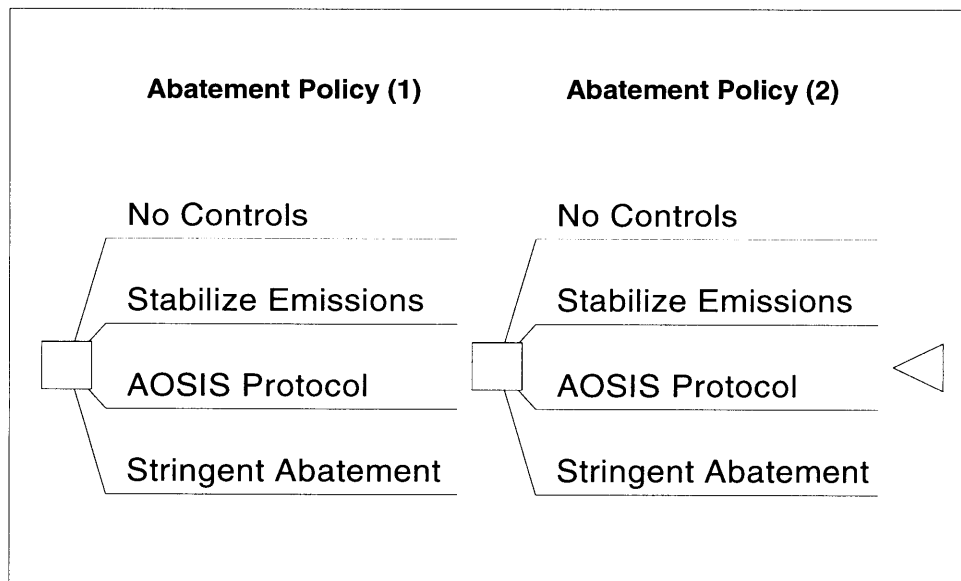
Figure 6-6: Schematic decision tree for the two-period model.

Representation of Possible States of Nature

In the static decision model presented earlier in Chapter 5, we utilized a single chance node to represent uncertainty in a set of categorical forecasts of future levels of climatic change. A more realistic representation construes climatic change as a *dynamic* process that evolves over time, and takes on a finite number of possible states. How this dynamic process evolves over time is, in our sequential framework, seen to depend on (i) what actions are taken—in both the short- and long-term—to mitigate climate change; and (ii) two key climate-related parameters: *climate sensitivity* and *ocean diffusivity*. As we discuss below, our formal representation of this dynamic process integrates the globally-averaged one-box climate model discussed previously in Chapters 3 and 4 with the TID shown in Figure 6-5.

Looking at the center portion of our primary TID, we note that the level or magnitude of climate change in Periods 1 and 2 is represented by two value nodes, labeled deltaT (1) and deltaT (2), respectively. The value nodes deltaT (1) and deltaT (2) represent the projected changes in global-mean surface temperature in the years 2010 and 2050, respectively. Each value node is seen to be a function of both the abatement policy that is adopted in each period, and two aleatory variables, Climate Sensitivity and Ocean Diffusivity, which we define as follows:

Climate Sensitivity = {Low, Medium, High},

where

Low $\equiv$ 1.5°C;

131

$$\text{Medium} \equiv 2.5°C;$$

$$\text{High} \equiv 4.5°C;$$

and

$$\text{Ocean Diffusivity} = \{od_1, od_2, od_3, od_4\},$$

where

$$od_1 \equiv 1/50;$$

$$od_2 \equiv 1;$$

$$od_3 \equiv 5;$$

$$od_4 \equiv 50.$$

We note that the possible states of nature for these two chance variables are defined in a manner that is consistent with the definitions used earlier in Chapter 4 for the numerical calibration of the globally-averaged reduced-scale climate models.

In Figure 6-5, we note that the TID asserts that Climate Sensitivity and Ocean Diffusivity are probabilistically independent.[8] Thus, the diagram requires that we assess subjective probability distributions for Climate Sensitivity and for Ocean Diffusivity. The probability distribution for Climate Sensitivity is specified as follows: 'Low' and 'High' are each assigned probabilities of 0.2, and 'Medium' is assigned a probability of 0.6. The probability distribution for Ocean Diffusivity is specified as follows: od_2 and od_3 are assigned probabilities of 0.6 and 0.199, respectively; od_1 and od_4 are assigned probabilities of 0.2 and 0.001, respectively.[9]

For each abatement policy $a_{1i} \in$ Abatement Policy (1), the functional dependence shown in Figure 6-5 of deltaT (1) on Climate Sensitivity and Ocean Diffusivity gives rise to a *value node data structure* of the form depicted in Figure 6-7. For this data structure, we note that the deltaT (1) value node is defined in terms of twelve separate projections of global-mean surface temperature change, one for each possible Climate Sensitivity-Ocean Diffusivity pair. The data structure for deltaT (2) is identical to that of deltaT (1), with the exception that the structure is conditioned by the abatement policy choices made in both Periods 1 and 2.[10]

We now address the problem of numerically specifying the data structures that correspond to the deltaT (1) and deltaT (2) value nodes. Recall that earlier, in Chapter 4, we used transient simulations of the MIT 2D-LO global climate model, together with econometric and statistical

---

[8] In doubled CO_2 experiments, the deep ocean is assumed to be at a temperature that is in equilibrium with the atmosphere. Since there is no physical process that "links" climate sensitivity and ocean diffusivity, we are able to assert that these two quantities are probabilistically independent.

[9] Expert judgement elicitation: A. P. Sokolov.

[10] This dual conditionality arises from the presence of the no-forgetting arc between the primary TID's two decision nodes.
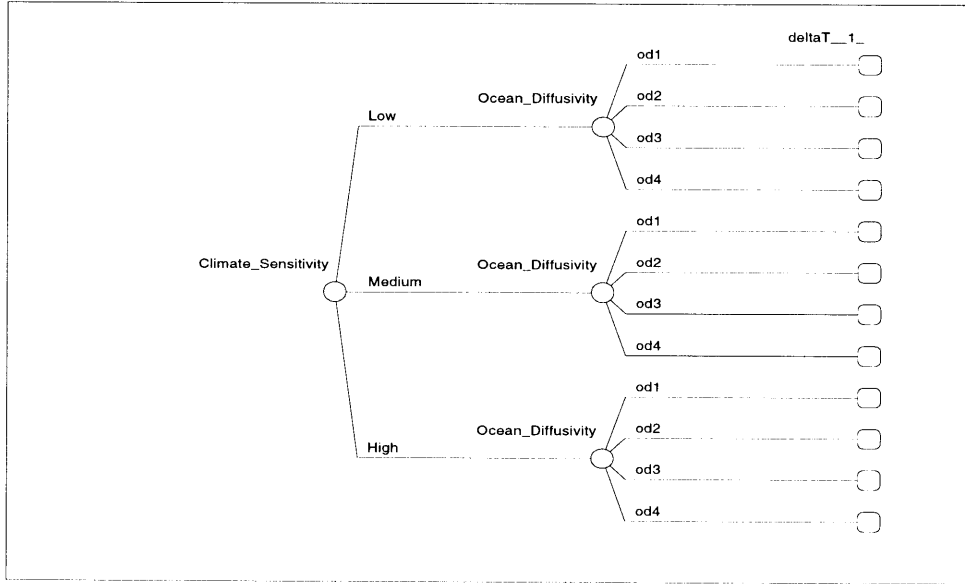
Figure 6-7: Data structure for the deltaT (1) value node, conditioned by the selection of an abatement policy $a_{1i} \in$ AbatementPolicy (1).

time series techniques, to compute a range of estimates for the globally-averaged one-box climate model's inertial parameter, $C_1 = 1/K.$[11] In these simulations, we varied the climate sensitivity and ocean diffusivity parameters across a discrete range of values. Specifically, three climate sensitivity values ($1.5°C$, $2.5°C$, and $4.5°C$), combined with four ocean diffusivity values ($1/50$, 1, 5, and 50), were seen to give rise to twelve separate estimates of the one-box model's inertial parameter. In this way, the one-box climate model can, for our purposes here, be restated as

$$\tau_t = \tau_{t-1} + C_1(\text{Climate Sensitivity, Ocean Diffusivity}) \left[F_{t-1} - \lambda \tau_{t-1} \right], \qquad (6.1)$$

where the inertial parameter, C_1, is now indexed by the possible states of nature associated with the Climate Sensitivity and the Ocean Diffusivity chance nodes.

The twelve estimates obtained earlier in Chapter 4 for the inertial parameter give rise to an equal number of numerical specifications for Eq. (6.1). Numerical implementation of this equation requires that we provide an exogenously-specified radiative forcing time series, $\{F_t\}_{t=1}^T$. For a given radiative forcing trajectory, the twelve numerical specifications for Eq. (6.1) give rise to twelve projections of global-mean surface temperature change, for times $t = 1, \ldots, T$.

In our primary TID, for each sequential climate policy, $< a_{1i}, a_{2j} >$, we assess a corresponding radiative forcing trajectory, $\{F_t\}_{t=1977}^{2050}$. As illustrated in Figure 6-8, we utilize elements of

---

[11]To simplify our presentation, we focus on the globally-averaged one-box climate model. Application of the globally-averaged two-box climate model proceeds in an analogous fashion.
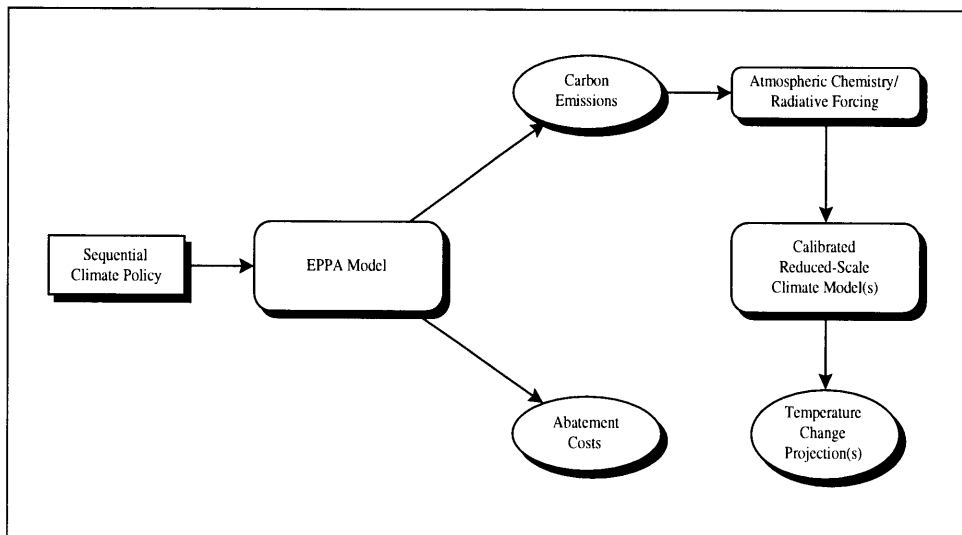
Figure 6-8: Linkages between the integrated decision analysis framework, the MIT Integrated Global System Model, and the reduced-scale global climate model(s).

the MIT IGSM to assess the radiative forcing time-paths and—as we discuss below—the abatement costs associated with each of the sixteen sequential climate policies outlined above.

Using Eq. (6.1), for each radiative forcing trajectory, $\{F_t\}_{t=1977}^{2050}$, we compute twelve separate projections for deltaT (1) and for deltaT (2). In Appendix B, we tabulate the global carbon emission, atmospheric CO_2 concentration, and radiative forcing time-paths associated with each sequential climate policy; in this appendix, we also tabulate, for each of the sixteen sequential climate policies, the one-box climate model projections for deltaT (1) and deltaT (2), as a function of Climate Sensitivity and Ocean Diffusivity.

Sequential Abatement Costs

The economic costs associated with each sequential climate policy are measured in terms of percentage of gross domestic product (GDP) loss. In our primary TID, abatement costs in each period are represented numerically in the form of a value node data structure. As illustrated in Figure 6-8, the values specified for this data structure are drawn from output of the MIT EPPA model.[12] In Table 6.1, we summarize the economic and carbon emissions data that underlie our Reference baseline scenario. In Table 6.2, we summarize the Period 1 and Period 2 abatement costs associated with each sequential climate policy, $< a_{1i}, a_{2j} >$. The costs in each period are stated in terms of *percentage of GDP loss* for the periods 2000-2010 and 2010-2050,

---

[12]The MIT EPPA model was discussed briefly in Chapter 5. Outputs derived from EPPA are deterministic in character. Recent work by Webster [78] represents one possible avenue for introducing uncertainty into the carbon emission forecasts and cost estimates that are derived from EPPA.

Reference Case	OECD	Non-OECD	Global
Annualized GDP 2000-2050 (billion 1985$)	13,107	10,560	23,667
GDP NPV 1985-2050 (billion 1985$)	248,107	199,902	448,010
Carbon Emissions in 2050 (GtC)	5.54	9.71	15.25
Carbon Emissions 1985-2050 (GtC)	61.84	83.43	145.27

Table 6.1: Reference case GDP and carbon emissions data.

respectively.[13]

Specification of Climate Change Impacts

As discussed briefly in Chapter 5, the literature on the economic valuation of climate change impacts is at an early stage of development.[14] The approach to damage valuation that we adopt here is, in some respects, similar to that used by Nordhaus [57], Peck and Teisberg [60], and others. Specifically, we are interested in specifying a *damage function*, D, whose domain is defined as the level or magnitude of climate change at time t. In general, the damage function is typically assumed to take the form

$$D(\tau_t) = (\tau_t)^y, \tag{6.2}$$

where, as before, τ_t denotes the change in global-mean surface temperature at time t, and y characterizes the order of the damage function. The parameter y is usually assumed to take on the values 1, 2, or 3.[15]

Though the use of Eq. (6.2) in integrated assessments of global climate change is relatively widespread, recent analyses suggest that its use can potentially give rise to counter-intuitive or pathological results. Webster[16] points out that there is an implied (and, it seems, unquestioned) assumption among policy analysts who utilize Eq. (6.2) that larger values of the parameter y necessarily entail larger damages. If, however, the temperature change over some finite time period is less than 1°C, then it follows that $(\tau_t) > (\tau_t)^2 > (\tau_t)^3$, in which case welfare loss is seen to *decrease* with increases in the order of the damage function.

In order to avoid this potential pitfall in our sequential framework, we assume that the damages in each of the model's two periods are characterized by an exponential function of the form

---

[13]Abatement costs in each period are stated in net present value terms, with an assumed discount rate of 5%.
[14]For a useful overview of this literature, see, e.g., Chapter 6 of Ref. [9].
[15]See, e.g., Nordhaus [57].
[16]Mort D. Webster, Private Communication.

Sequential Climate Policy	Abatement Cost (1)	Abatement Cost (2)
$< a_{11}, a_{21} >$	0%	0%
$< a_{11}, a_{22} >$		0.84%
$< a_{11}, a_{23} >$		1.16%
$< a_{11}, a_{24} >$		1.49%
$< a_{12}, a_{21} >$	0.32%	0.15%
$< a_{12}, a_{22} >$		0.84%
$< a_{12}, a_{23} >$		1.23%
$< a_{12}, a_{24} >$		1.47%
$< a_{13}, a_{21} >$	0.45%	0.25%
$< a_{13}, a_{22} >$		1.04%
$< a_{13}, a_{23} >$		1.43%
$< a_{13}, a_{24} >$		1.67%
$< a_{14}, a_{21} >$	0.55%	0.32%
$< a_{14}, a_{22} >$		1.11%
$< a_{14}, a_{23} >$		1.48%
$< a_{14}, a_{24} >$		1.78%

Table 6.2: Abatement costs incurred in Periods 1 and 2 for each sequential climate policy.

$$D(\tau_t) = e^{\alpha \tau_t} - 1, \tag{6.3}$$

where τ_t is defined as before, and α is a scaling constant. The functional form of Eq. (6.3) is seen to have an important advantage over Eq. (6.2), namely, for any two values $\alpha_1 < \alpha_2$, it follows that $e^{\alpha_1 \tau_t} < e^{\alpha_2 \tau_t}$, for all positive values of τ_t.

Typically, damage functions such as Eqs. (6.2) and (6.3) are calibrated so that, for particular levels of global-mean surface temperature change, damages are seen to equal a certain percentage of gross production. Peck and Teisberg [60], for example, assume that the damage associated with a 3°C surface temperature rise is 2% of gross production—a value which they refer to as the *adaptation/damage percent*.[17]

In our sequential framework, rather than assume a *single* deterministic specification for Eq. (6.3), we treat the calibration and parameterization of this damage function as an explicit uncertainty in the decision model. In particular, rather than anchoring the calibration of Eq. (6.3) to a single level of climatic change (say, e.g., 3°C), we calibrate the damage function against a *range* of possible warming levels. For our purposes here, we focus on two climate change scenarios: one scenario is characterized by a low level of warming, and the other is characterized by a high level of warming. For each warming scenario, we utilize quantified expert judgement to specify 'Low,' 'Medium,' and 'High' estimates for the expected adaptation/damage percent in the sequential model's two periods.

The two warming scenarios that we utilize for the calibration of Eq. (6.3) are drawn directly from the one-box climate model projections for global-mean surface temperature change under the Reference policy scenario. In particular, for the low warming scenario, we select the low values for deltaT (1) and deltaT (2) under sequential climate policy $< a_{11}, a_{21} >$; similarly, for the high warming scenario, we select the high values for deltaT (1) and deltaT (2) under the same sequential policy. Looking at Table B.1 in Appendix B, we see that the temperature change projections for the low warming scenario are 0.470°C and 0.876°C for Periods 1 and 2, respectively; the corresponding temperature change values for the high warming scenario are 1.340°C and 2.913°C.

An expert judgement elicitation of the expected adaptation/damage percentages associated with the low and high warming scenarios might yield a set of values such as those shown in Table 6.3.[18] The 'Low,' 'Medium,' and 'High' percentages associated with each warming scenario are, for our purposes here, interpreted as the 0.05-, 0.50-, and 0.95-fractiles of a cumulative probability distribution for the expected adaptation/damage percent in each period.[19] For

---

[17]For the purposes of sensitivity analysis, Peck and Teisberg vary the adaptation/damage percent from 0.5% to 3.5%.

[18]The expected damages that we utilize here are consistent with those reported by Nordhaus [56].

[19]The z-fractile is defined as the magnitude α_z of the uncertain quantity α such that there is a probability of z

137

Low Warming Scenario	Expected Adaptation/Damage Percent		
	Low	Medium	High
0.470°C rise by 2010	0.1%	0.75%	1%
0.876°C rise by 2050	0.2%	1.75%	3%

High Warming Scenario	Expected Adaptation/Damage Percent		
	Low	Medium	High
1.340°C rise by 2010	0.2%	2.25%	4%
2.913°C rise by 2050	0.3%	3.75%	10%

Table 6.3: Low, medium, and high estimates for the expected adaptation/damage percentages associated with the low and high warming scenarios.

Low Warming Scenario	Calibrated Scaling Parameter		
	Low	Medium	High
0.470°C rise by 2010	0.203	1.191	1.475
0.876°C rise by 2050	0.208	1.155	1.583

High Warming Scenario	Calibrated Scaling Parameter		
	Low	Medium	High
1.340°C rise by 2010	0.136	0.880	1.201
2.913°C rise by 2050	0.090	0.535	0.881

Table 6.4: Calibrated low, medium, and high values for the damage function scaling parameter, α.

each row of values in Table 6.3, we solve Eq. (6.3) for the corresponding 'Low,' 'Medium,' and 'High,' values of the scaling parameter, α. We summarize these values in Table 6.4. Using these calibrated parameter values, in Figures 6-9 and 6-10, we plot the damage functions associated with the low and high warming scenarios, respectively, for Periods 1 and 2.

As alluded to earlier, in our sequential framework, we treat the calibration and parameterization of the damage functions shown in Figures 6-9 and 6-10 as an explicit set of uncertainties in the model. In particular, consistent with our discussion above, we define a chance node

$$\text{Warming Scenario} = \{\text{Low, High}\},$$

where

---

that the true magnitude is less than or equal to α_z.

138
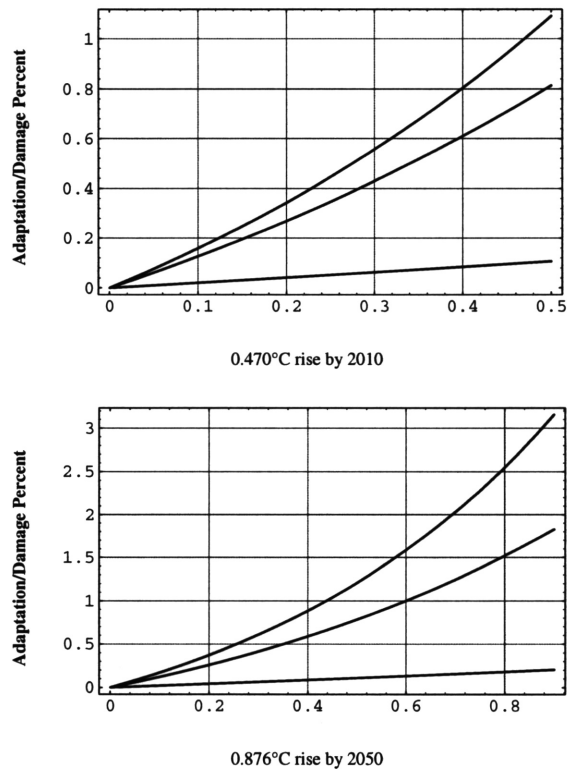
Figure 6-9: Damage functions for the low warming scenario, for Periods 1 and 2 of the sequential decision framework.

1.340°C rise by 2010

2.913°C rise by 2050
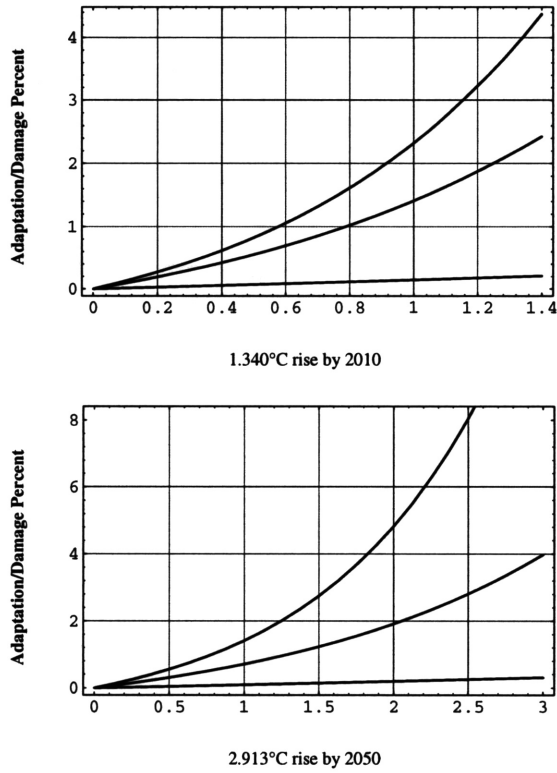
Figure 6-10: Damage functions for the high warming scenario, for Periods 1 and 2 of the sequential decision framework.

140

$$\text{Low} \equiv \begin{cases} 0.470°\text{C by } 2010; \\ 0.876°\text{C by } 2050; \end{cases}$$

$$\text{High} \equiv \begin{cases} 1.340°\text{C by } 2010; \\ 2.913°\text{C by } 2050. \end{cases}$$

As before, we utilize quantified expert judgement to specify a discrete probability distribution for this chance variable. The nominal values used for this distribution are as follows: the 'Low' warming scenario is assigned a probability of 0.7, and the 'High' warming scenario is assigned a probability of 0.3.

In our primary TID, the chance node Warming Scenario is seen to condition two chance nodes, alpha (1) and alpha (2), each defined in terms of three possible states of nature, corresponding to the 'Low,' 'Medium,' and 'High' values of the calibrated scaling parameter, α. Also, the chance nodes alpha (1) and Warming Scenario have directed arcs that lead into a value node labeled Climate Change Impacts (1); similarly, alpha (2) and Warming Scenario have directed arcs that lead into a value node labeled Climate Change Impacts (2). This set of functional specifications give rise to a pair of value node data structures—which we illustrate in Figure 6-11—for representing climate-change-related impacts.

In specifying probability distributions for alpha (1) and alpha (2), we simplify the assessment procedure by assuming that these two chance nodes are conditionally independent given Warming Scenario. In addition, the directed arcs from Warming Scenario to alpha (1), and from Warming Scenario to alpha (2), are—for our purposes here—interpreted as *non-conditioning* arcs. As discussed earlier, the 'Low,' 'Medium,' and 'High' values of the scaling parameter α are interpreted as the 0.05-, 0.50-, and 0.95-fractiles of a cumulative probability distribution. In specifying these distributions, we use the so-called *extended Pearson-Tukey method* to obtain a three-point approximation.[20] Using this approximation, the 'Low,' 'Medium,' and 'High' values of the chance nodes alpha (1) and alpha (2) are assigned probabilities of 0.185, 0.63, and 0.185, respectively.

Aggregating Abatement Costs and Climate Change Impacts

In our primary TID, abatement costs and climate change impacts are, in each period, aggregated via the following set of equations:

Social Loss (1) = Abatement Costs (1) + Climate Change Impacts (1);

---

[20]For a discussion of the Pearson-Tukey approximation method, see, e.g., Clemen [13, p. 278].
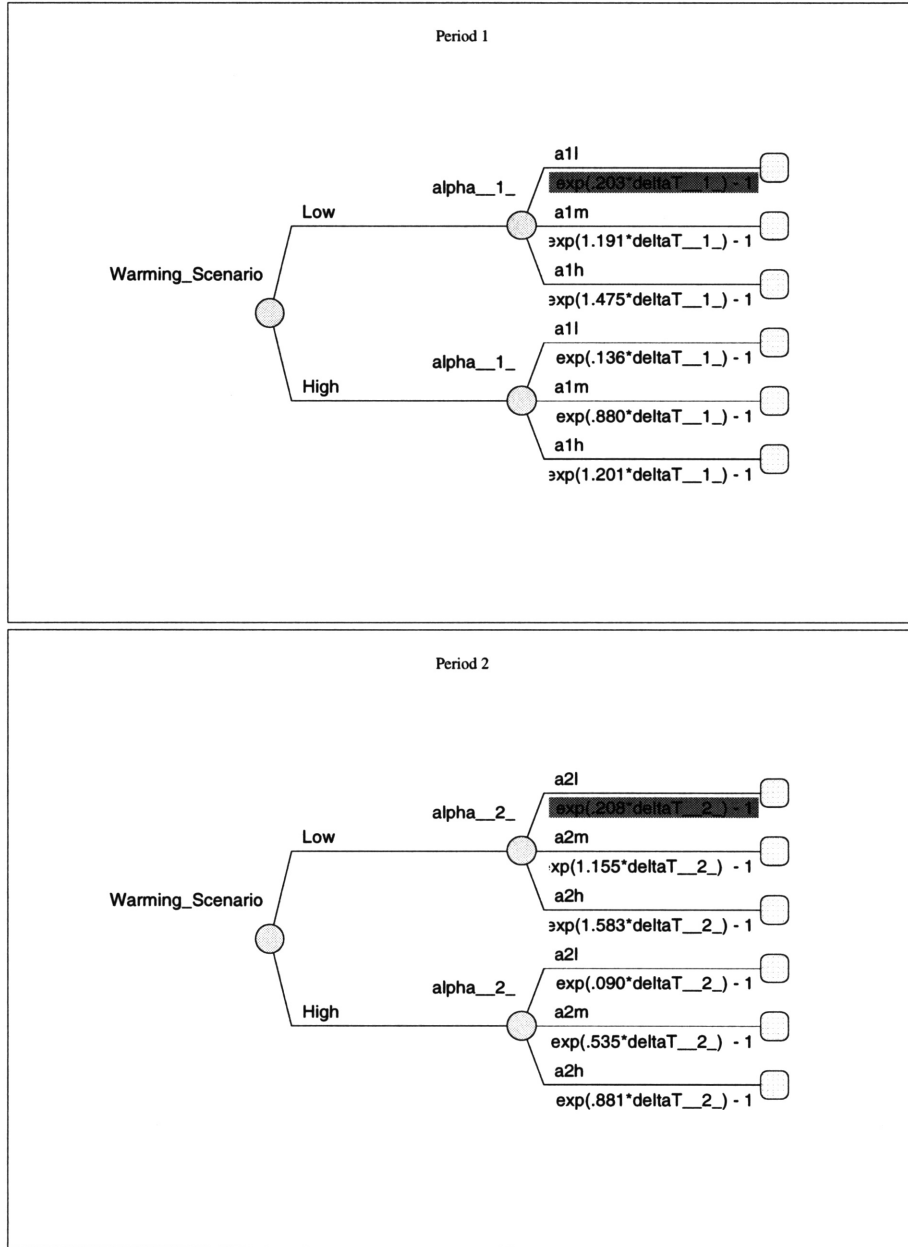
Figure 6-11: Data structures for the Climate Change Impacts (1) and Climate Change Impacts (2) value nodes.

and

Social Loss (2) = Abatement Costs (2) + Climate Change Impacts (2).

6.2.2 Evaluation of the Sequential Decision Model

We now numerically evaluate the TID shown in Figure 6-5 so as to determine the optimal sequential climate policy. Figure 6-12 summarizes the resulting optimal policy for the case where the uncertainties are resolved at the end of the model's presumed time horizon, i.e., 2050.[21] In this figure, we observe that the optimal course of GHG abatement action is to pursue sequential climate policy $< a_{11}, a_{22} >$, i.e., No Controls in Period 1 and Stabilize Emissions in Period 2. This sequential strategy is seen to have an expected social loss of 6.05%. In Figure 6-13, we plot the global carbon emission path for the optimal climate policy, and for the Reference policy scenario (i.e., sequential climate policy $< a_{11}, a_{21} >$).

In Figure 6-14, we plot the risk profile associated with the optimal sequential climate policy. As we discussed earlier in Chapter 5, this type of figure depicts a cumulative probability distribution of possible outcomes under the optimal climate policy. The risk profile reveals that—under the optimal policy—there is no chance that aggregate social loss will be less than zero. In addition, the risk profile is seen to rise quickly between (roughly) 1% and 10%, and then gradually levels off. If the optimal climate policy is adopted, what this particular profile implies is that the probability that the expected social loss will be less than or equal to 1% is quite small (~ 0.05), whereas the probability that the expected social loss will be less than or equal to 10% is much higher (~ 0.85).

As part of our analysis, it is useful to compare the projections of global-mean surface temperature change associated with the Reference policy scenario and the optimal sequential climate policy. Since, in our sequential model formulation, projected temperature change is functionally dependent on climate policy choice, as well as on the chance variables Climate Sensitivity and Ocean Diffusivity, it is possible to graphically depict the temperature change projections under sequential policies $< a_{11}, a_{21} >$ and $< a_{11}, a_{22} >$, as functions of these two uncertain quantities. In Figures 6-15 and 6-16, we plot the global-mean surface temperature change response surfaces associated with each of these sequential policies. Since the optimal climate policy is, in this case, characterized by unconstrained carbon emissions in the first period, the Period 1 response surfaces shown in Figures 6-15 and 6-16 are identical. In Period 2, however, we note that—relative to the Reference scenario—the temperature change response surface for the optimal policy is characterized by a gradual leveling-off for high climate sensitivity values and low to medium-high ocean diffusivity values. The differences between these

---

[21]Later, in Section 6.3, we consider alternative resolution schemes, where the sequential model's climate-change-related uncertainties are resolved at various points in the presumed time horizon.
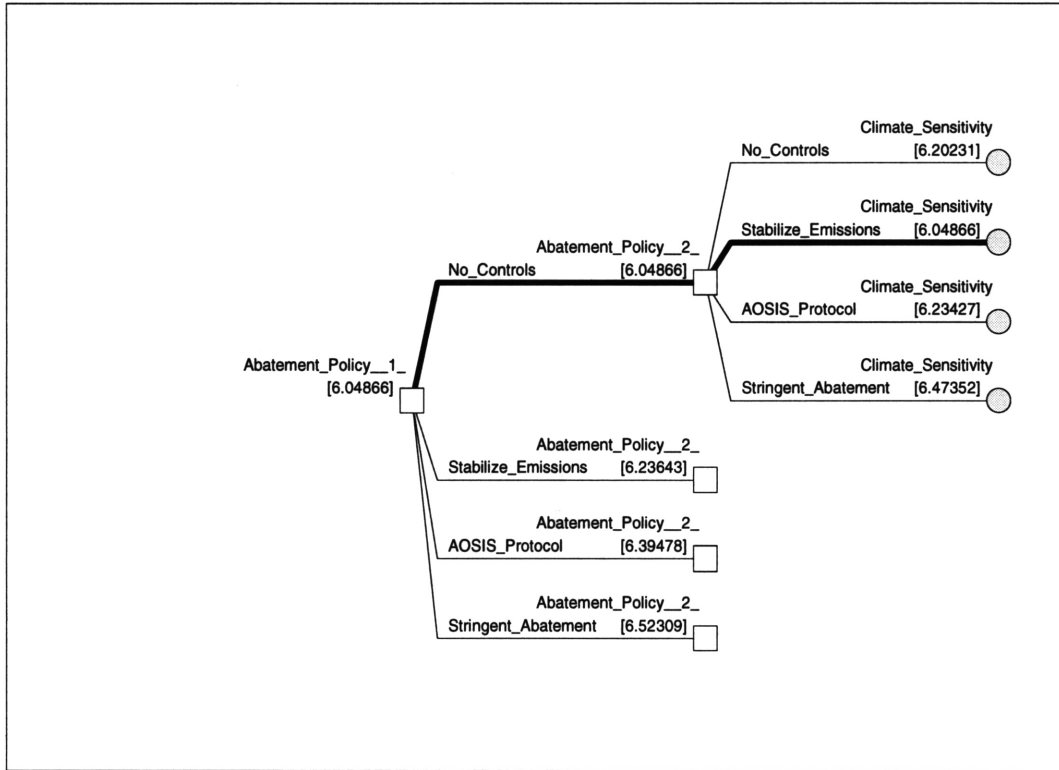
Figure 6-12: Decision policy summary for the sequential framework.
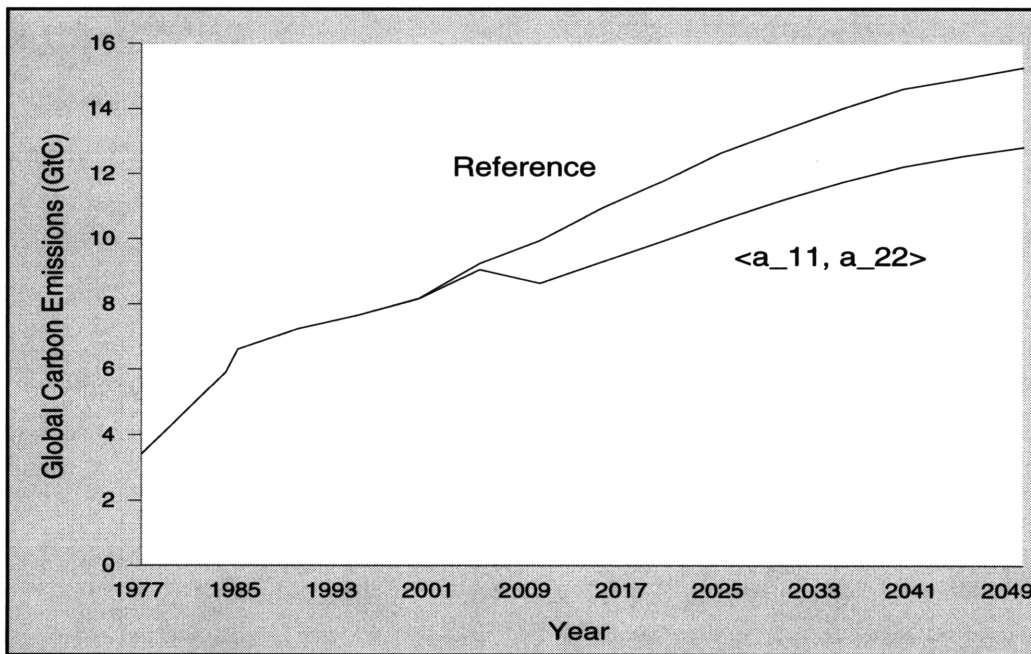
Figure 6-13: Global carbon emissions under the Reference policy scenario and optimal sequential climate policy $< a_{11}, a_{22} >$.

144
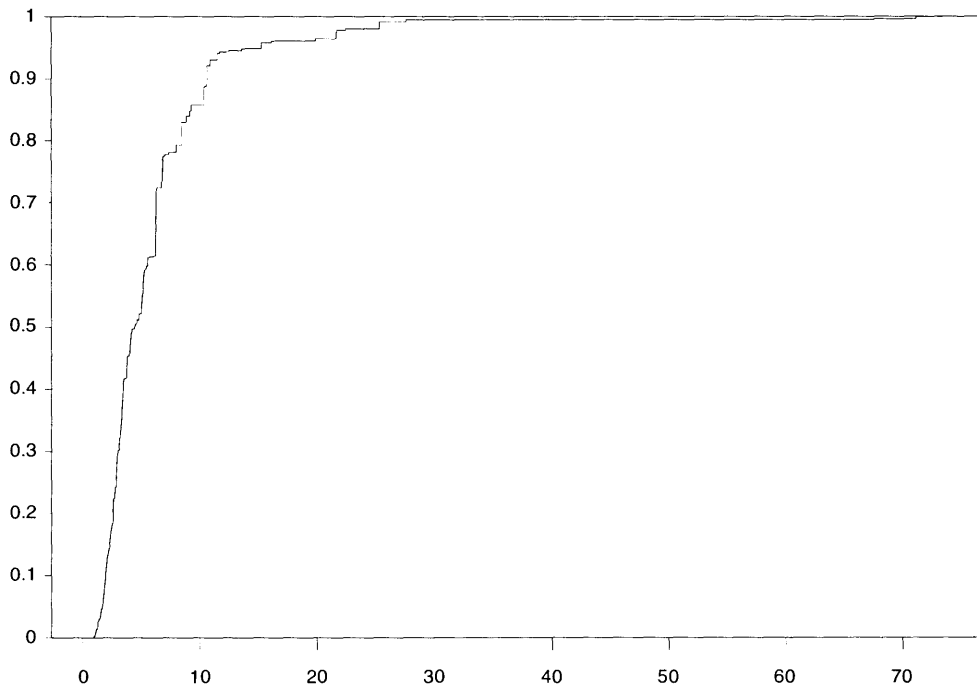
Figure 6-14: Risk profile for optimal sequential climate policy $< a_{11}, a_{22} >$.
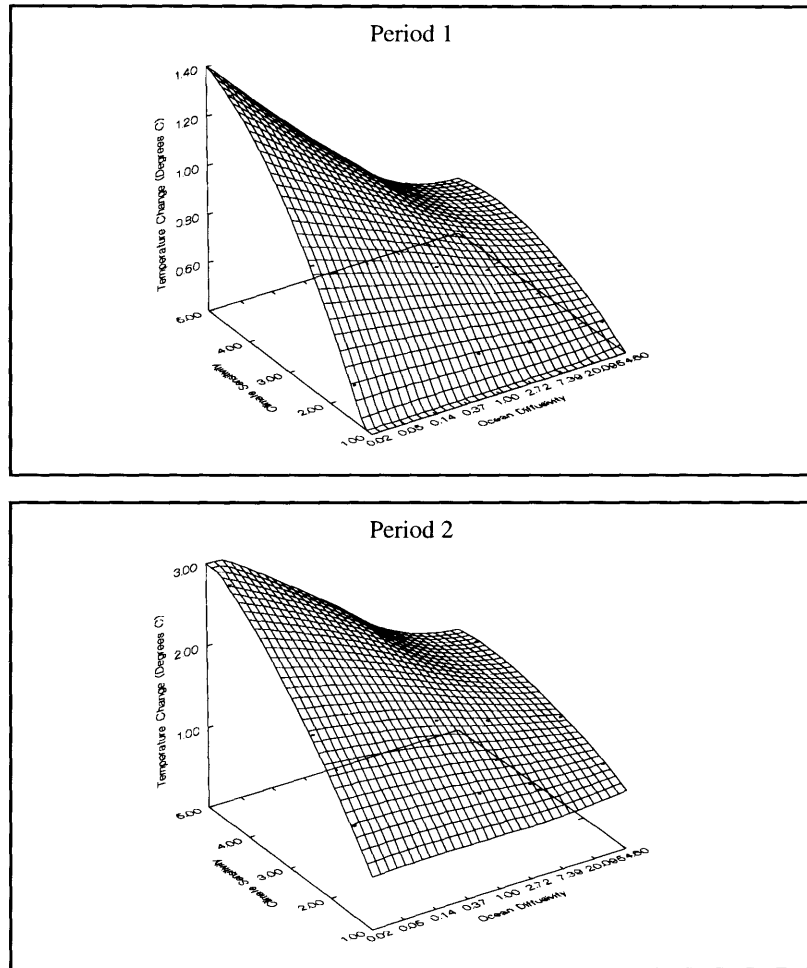
Figure 6-15: Global-mean surface temperature change response surfaces for Periods 1 and 2 of the Reference policy scenario, as a function of climate sensitivity and ocean diffusivity. The scale for ocean diffusivity is logarithmic, but is displayed with untransformed values.

two response surfaces are quite subtle, which suggests that the policy prescriptions described here are likely to be sensitive to the probability distributions specified for the chance variables Climate Sensitivity and Ocean Diffusivity.

6.2.3 Sensitivity Analysis

We now explore the robustness of the sequential policy prescriptions described above. In the discussion that follows, we consider two types of sensitivity analyses: (i) value sensitivity analysis of sequential abatement costs; and (ii) event sensitivity comparisons. These analyses play an instrumental role in our efforts to identify those variables and model parameters that have the greatest influence on the policy prescriptions presented here.

146
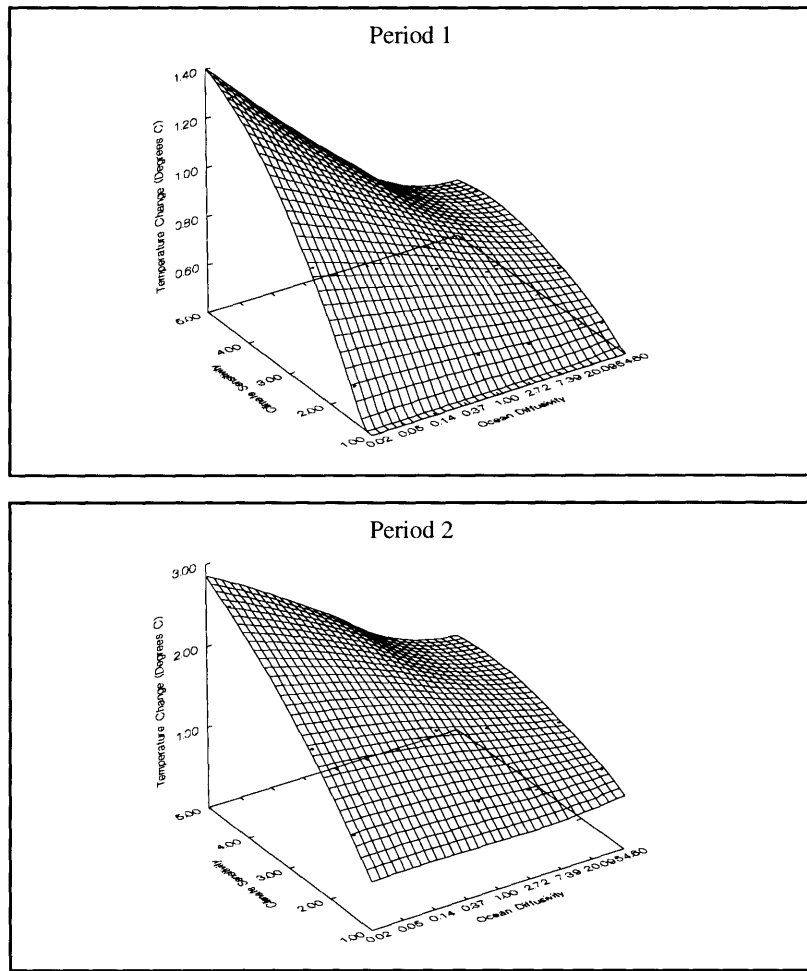
Figure 6-16: Global-mean surface temperature change response surfaces for Periods 1 and 2 of optimal sequential climate policy $< a_{11}, a_{22} >$, as a function of climate sensitivity and ocean diffusivity. The scale for ocean diffusivity is logarithmic, but is displayed with untransformed values.

147

Sequential Climate Policy	Abatement Costs (1)			Abatement Costs (2)		
	Low	Nominal	High	Low	Nominal	High
$< a_{11}, a_{21} >$		0%			**0**	
$< a_{11}, a_{22} >$				0.67%	**0.84%**	1%
$< a_{11}, a_{23} >$				0.93%	**1.16%**	1.39%
$< a_{11}, a_{24} >$				1.19%	**1.49%**	1.78%
$< a_{12}, a_{21} >$	0.16%	**0.32%**	0.48%	0.12%	**0.15%**	0.18%
$< a_{12}, a_{22} >$				0.67%	**0.84%**	1%
$< a_{12}, a_{23} >$				0.98%	**1.23%**	1.48%
$< a_{12}, a_{24} >$				1.18%	**1.47%**	1.76%
$< a_{13}, a_{21} >$	0.23%	**0.45%**	0.68%	0.2%	**0.25%**	0.3%
$< a_{13}, a_{22} >$				0.83%	**1.04%**	1.25%
$< a_{13}, a_{23} >$				1.14%	**1.43%**	1.72%
$< a_{13}, a_{24} >$				1.34%	**1.67%**	2%
$< a_{14}, a_{21} >$	0.28%	**0.55%**	0.83%	0.26%	**0.32%**	0.38%
$< a_{14}, a_{22} >$				0.89%	**1.11%**	1.33%
$< a_{14}, a_{23} >$				1.18%	**1.48%**	1.78%
$< a_{14}, a_{24} >$				1.42%	**1.78%**	2.14%

Table 6.5: Range of abatement costs incurred in Periods 1 and 2, for each sequential climate policy.

Value Sensitivity Analysis

We begin by exploring the sensitivity of the primary TID's expected value and optimal policy to changes in the values specified for Abatement Costs (1) and Abatement Costs (2). Recall that these values were obtained from the MIT EPPA model. The range of values utilized for this sensitivity analysis is shown in Table 6.5. We specify the Period 1 abatement costs so as to reflect a roughly three-fold variation between the nominal value and the low-high extremes; similarly, the Period 2 values are seen to reflect a roughly 1.5-fold variation. Using these low-high values, we conduct a series of value sensitivity analyses, which we then use to construct the tornado diagram shown in Figure 6-17. In this diagram, we observe that the model is most sensitive to the abatement costs specified in Period 2 for sequential climate policies $< a_{11}, a_{22} >$, $< a_{11}, a_{23} >$, and $< a_{12}, a_{22} >$. The sequential model is, in addition, sensitive to the abatement costs specified in Period 1 for abatement policy a_{12}. The remaining low-high values specified for Abatement Costs (1) and Abatement Costs (2) have no influence on the expected value and sequential policy prescriptions of the model.

Abatement_Costs__2_IAbatement_Policy__1_.No_Controls,Abatement_Policy__2_.Stabilize_Emissions

Abatement_Costs__2_IAbatement_Policy__1_.No_Controls,Abatement_Policy__2_.AOSIS_Protocol

Abatement_Costs__2_IAbatement_Policy__1_.Stabilize_Emissions,Abatement_Policy__2_.Stabilize_Emissions

Abatement_Costs__1_IAbatement_Policy__1_.Stabilize_Emissions

Abatement_Costs__1_IAbatement_Policy__1_.AOSIS_Protocol

Abatement_Costs__1_IAbatement_Policy__1_.Stringent_Abatement

Abatement_Costs__2_IAbatement_Policy__1_.No_Controls,Abatement_Policy__2_.Stringent_Abatement

Abatement_Costs__2_IAbatement_Policy__1_.Stabilize_Emissions,Abatement_Policy__2_.No_Controls

| 5.9 | 5.925 | 5.95 | 5.975 | 6 | 6.025 | 6.05 | 6.075 | 6.1 | 6.125 | 6.15 | 6.175 | 6.2 |

Figure 6-17: Tornado diagram for Abatement Costs (1) and Abatement Costs (2).

149

Event Sensitivity Comparisons

The value sensitivity analysis described above focused exclusively on the Period 1 and Period 2 abatement costs associated with each sequential climate policy, $< a_{1i}, a_{2j} >$. We now turn our attention to the uncertain quantities in our sequential framework. Our main objective here is to assess the influence that each uncertain quantity has on the expected value of the model.

We begin by performing a so-called *deterministic event sensitivity comparison* of our primary TID. In this type of analysis, we run the decision model once for every chance variable, each time replacing the lotteries on the remaining chance variables with their expected values. This type of sensitivity analysis yields information concerning the characteristic nature of the outcome distribution when the specified chance event is the *only* uncertain quantity in the model.

For the primary TID, the numerical procedure used in performing a deterministic event sensitivity comparison has six stages. First, we run the model once with all of the lotteries set to their expected values; this procedure establishes a *base case*, which is used as the basis for comparing the remaining cases. We then run the model in the manner described above, once for each of the five uncertain quantities, each time replacing the lotteries on the remaining uncertainties with their expected values. Following this procedure, we obtain the tornado diagram shown in Figure 6-18. In this diagram, we see a horizontal bar of zero-width labeled '*BASE CASE*,' which indicates that there is no variance in the outcome distribution of the base case. The remaining five bars in the tornado diagram depict the variance in the outcome distribution under the optimal policy. The width of each bar indicates the difference between the 10th and 90th percentiles of the outcome distribution. The 50th percentile is indicated by a change in color, and the vertical line indicates the expected value of the base case.

In interpreting the tornado diagram shown in Figure 6-18, we note, first, that the chance events whose bars lie furthest from the base case have the greatest influence on the outcome distribution of the sequential framework. Thus, the chance variables Climate Sensitivity, alpha (2), and Ocean Diffusivity are seen to have the greatest impact on the outcome distribution, whereas the chance variables Warming Scenario and alpha (1) are seen to contribute very little to this distribution.

In Figure 6-19, we plot the tornado diagram that corresponds to the *probabilistic* variant of the event sensitivity comparison described above. In performing a probabilistic event sensitivity comparison, we first run the sequential model with all of its lotteries present, thereby establishing a base case. We then run the model once for each uncertain quantity in the model. In contrast with the deterministic case, however, each bar in Figure 6-19 is obtained by replacing the corresponding chance event with its expected value; the lotteries for the remaining chance variables are left unchanged. Inspection of Figure 6-19 suggests that Ocean Diffusivity and Climate Sensitivity have the greatest influence on the outcome distribution of the decision

150
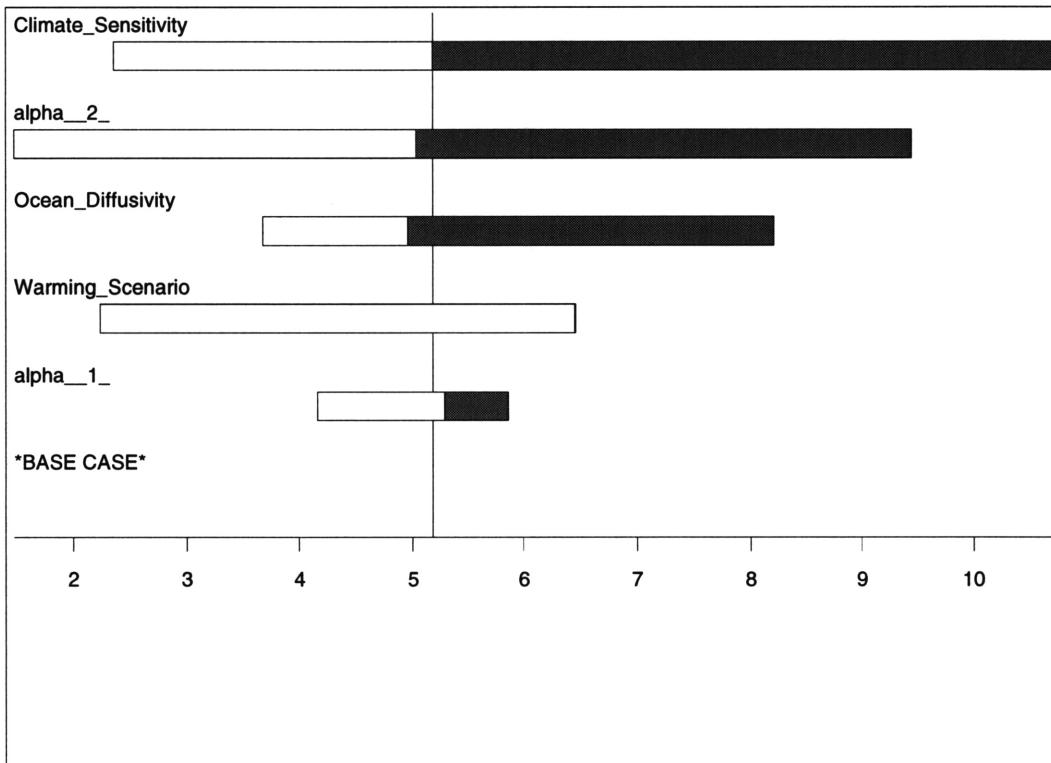
Figure 6-18: Tornado diagram for the deterministic event sensitivity comparison of the primary TID.
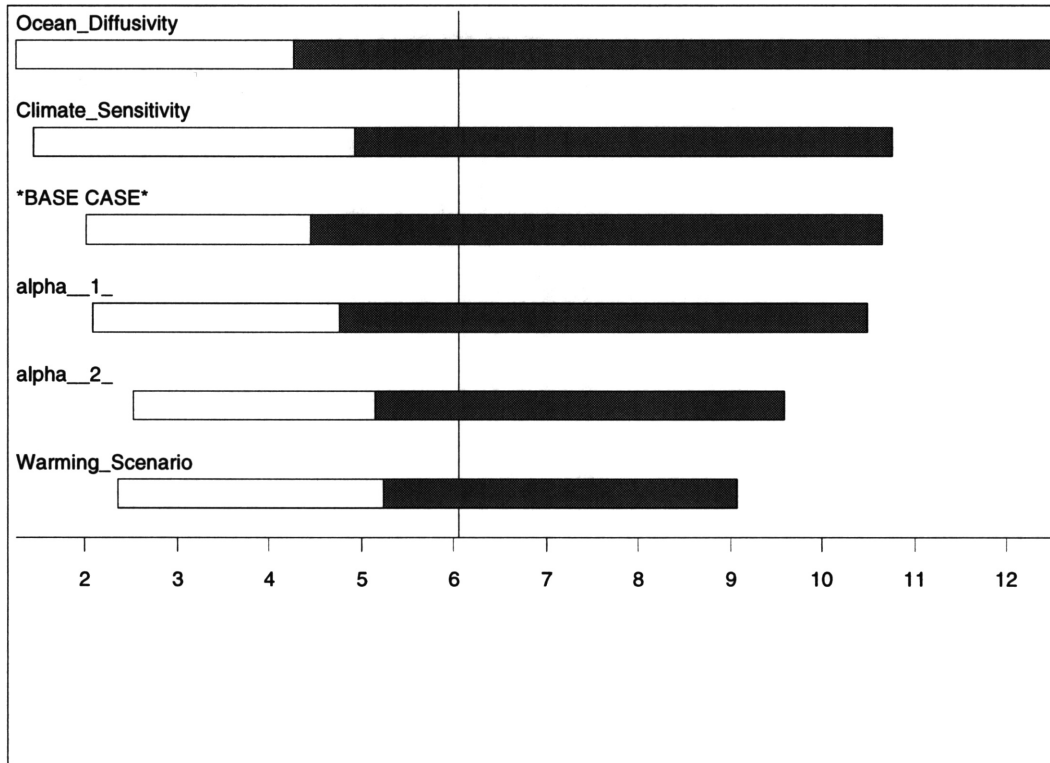
Figure 6-19: Tornado diagram for the probabilistic event sensitivity comparison of the primary TID.

model.

The sensitivity analyses described above highlight some important features about our sequential framework. First, the model's policy prescriptions are, indeed, sensitive to the abatement costs specified for the sequential GHG abatement policies which we have considered here. Second, the deterministic and probabilistic event sensitivity comparisons described above tend to bear-out our earlier intuitions about the sensitivity of the primary TID's policy prescriptions to the manner in which the chance variables Climate Sensitivity and Ocean Diffusivity are characterized. Ultimately, these results highlight the need for climate researchers and policy analysts to focus more attention and resources on efforts that seek to arrive at better characterizations of key climate-change-related uncertainties.

6.3 The Role of Learning

Learning is an intrinsic feature of the climate change problem, in that human knowledge and understanding about the various dimensions of the problem is continually evolving.[22] In this section, we explore the potential role that learning can play in the evaluation of GHG abatement policies. Our presentation is divided into three parts. We begin with an overview of the analytical approaches that researchers have, in recent years, put forth for addressing the topic of learning in climate change decision-making. We then explore how the sequential decision framework presented above can be used as a vehicle for representing learning about key climate-change-related uncertainties. We conclude our analysis with the presentation of a Bayesian learning model, where subjective beliefs concerning key scientific uncertainties are updated over time.

6.3.1 Past Approaches

The role of learning in climate change decision-making has, in recent years, sparked the interest of climate researchers, economists, and policy analysts, alike. As we discussed earlier in Chapter 5, Manne and Richels [48] were the first to explore so-called *learn-then-act* decision strategies for optimal GHG abatement. This type of decision strategy has also been explored by Nordhaus [57] in the context of his DICE model. We illustrate this characterization of climate-change-related learning in the schematic decision tree shown in Figure 6-20. In this decision tree, the damage potential associated with global climate change is treated as an uncertain quantity. Specifically, damages are seen to fall into one of three possible categories or states: 'Low,' 'Moderate,' or 'High.' In this learn-then-act formulation, it is assumed that the *true* damage potential is known to the decision-maker *prior* to choosing a carbon tax or a GHG emission reduction level.

More recently, Kolstad [40] develops a stochastic version of the DICE model that incorporates gradual learning over time about the extent of climate-induced damages.[23] The model assumes that the world can be in any one of a finite number of possible states, $s_1, \ldots, s_r$. Over time, the learning process is such that messages $m_1, \ldots, m_r$ are received concerning the true state of the world. The model further assumes an information structure that consists of two prior probability vectors, **P** and **Q**, defined over the set **S** of possible states of the world, and the set **M** of possible messages, respectively. These two vectors reflect the decision-maker's degree of

---

[22]Naturally, the term "learning" can take on many different meanings and connotations, depending on the application or circumstance in which it is used. For an insightful discussion of the notion of learning, and its relation to theories of cognition and human judgement, see Margolis [49].

[23]Kolstad's analysis assumes that climate change impacts fall into one of two possible states: (i) damages are five times as great as those assumed by Nordhaus in Ref. [57]; and (ii) there are no damages associated with climatic change.
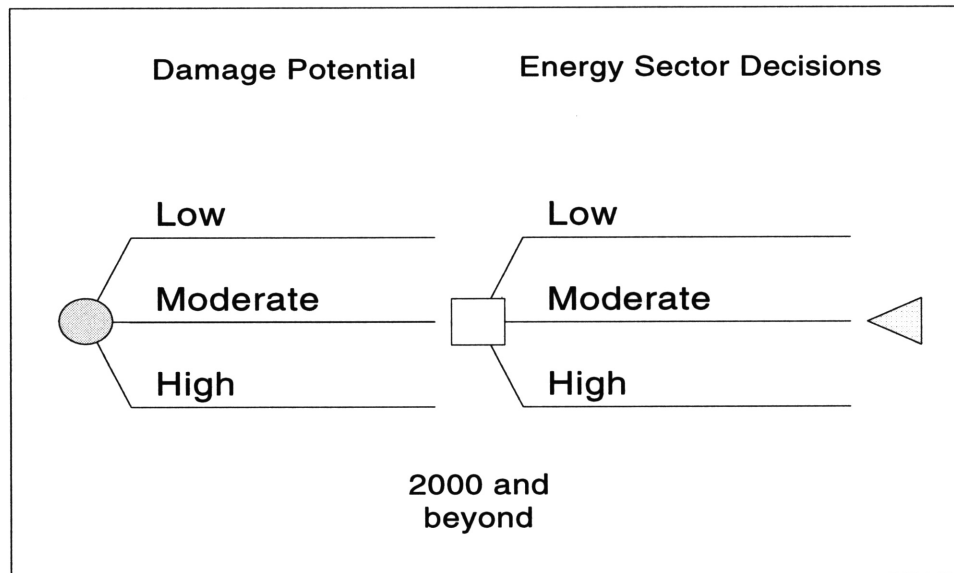
Figure 6-20: Learn-then-act decision framework proposed by Manne and Richels (1992).

belief concerning the relative likelihood of each possible state of the world, and the likelihood of receiving a particular message.

Each message, m_i, constitutes a "noisy signal" as to the true state of the world. In operationalizing this notion, Kolstad defines a parameter $\lambda \in [0, 1]$, which represents the quality of information in a particular message: A value of $\lambda = 0$ corresponds to "no information," and a value of $\lambda = 1$ corresponds to "perfect information." If a particular message is too noisy to contain any information, then the posterior probability of each possible state of the world, given that message, is equal to the prior probability associated with each state.[24] Using this parameterization, Kolstad is able to represent the "rate" of learning: $\lambda = 0$ denotes the situation where no learning takes place in a particular time period, whereas $\lambda = 1$ denotes complete resolution of uncertainty in a single period.

Kolstad's model formulation is somewhat limited in its ability to trace out the implications of learning for climate policy, due, mainly, to its myopic focus on climate-change-related damages, at the exclusion of factors that are likely to influence the magnitude and rate of climatic change. In what follows, we use the sequential framework presented earlier in Section 6.2 to explore an alternative set of frameworks for representing learning. Our modeling approach is seen to have some important advantages over the approaches described above, the most notable advantage being the ability to represent a broad range of learning schemes in a nimble, flexible, and

---

[24]This modeling approach is similar to the approach that we presented earlier in Section 5.3.2 for performing determinate value of imperfect information calculations.

transparent manner.

6.3.2 Modeling Learning

The policy-analytic treatments of learning described above are all conceptually predicated on the notion that learning essentially entails the acquisition of new evidence or information. How these models operationalize this conception of learning is, nevertheless, highly stylized. One consequence of this is that the models fail to provide decision-makers with accurate and convincing accounts of the potential role that learning can play in the evaluation of GHG abatement policies. The modeling approach that we set forth here is grounded in this general conception of learning, but focuses specifically on the problem of representing learning in sequential decision contexts that are characterized by uncertainty.

The acquisition of new information concerning anthropogenic climate change can occur in a number of ways, and can take many different forms (e.g., long-term climate forecasts, observed climate, risk analyses of socio-economic impacts, etc.).[25] In general, any systematic effort to assess or characterize the role of learning in the formal evaluation of GHG abatement strategies must address three basic questions:

1. What specific facets of the climate change problem might we expect to learn about in both the near- and long-term?

2. When will the learning occur?

3. How does learning influence the evaluation of optimal GHG abatement strategies?

In what follows, we use our sequential framework as a computational vehicle for exploring these questions.

Partial and Complete Learning Schemes

For the purposes of illustration, we focus on learning as it relates to the sequential framework's two climate-change-related variables: Climate Sensitivity and Ocean Diffusivity. Operationally, we model learning about these uncertain quantities by making assumptions about the *timing* of their occurrence. In particular, we utilize our sequential framework to explore various *learning schemes* for Climate Sensitivity and Ocean Diffusivity, where each scheme is characterized by a different set of assumptions concerning the timing of the resolution of uncertainty for these two quantities.

---

[25]Related to this point, Miller and Lad [52] make a semantically useful distinction between "active" and "inactive" learning. Active learning occurs when information obtained during a particular time period depends on what was actually done during that period, whereas inactive learning occurs with the mere passing of time.

The structure of our sequential framework is such that we are able to specify several possible *resolution points* for each of the uncertain quantities in the model. In particular, uncertainty concerning each chance variable can be resolved at one of three possible points:

1. Before Period 1;

2. At the end of Period 1;

3. At the end of Period 2.

In general, an n-period decision model consisting of p uncertain quantities is characterized by $(n + 1)^p$ possible learning schemes. The chance variables Climate Sensitivity and Ocean Diffusivity thus give rise to $(2 + 1)^2 = 9$ possible learning schemes. We denote each learning scheme by an ordered pair, $(rp_{\text{Climate Sensitivity}}, rp_{\text{Ocean Diffusivity}})$, where $rp_{\text{Climate Sensitivity}}$, $rp_{\text{Ocean Diffusivity}} \in \{1, 2, 3\}$ denote the resolution points for Climate Sensitivity and Ocean Diffusivity, respectively. Using this notation, we enumerate the following nine possible learning schemes for our sequential framework:

$$
\begin{array}{ccc}
(1, 1) & (1, 2) & (1, 3) \\
(2, 1) & (2, 2) & (2, 3) \\
(3, 1) & (3, 2) & (3, 3).
\end{array}
$$

We begin our discussion of the learning schemes outlined above by noting that our primary decision model—shown in Figure 6-5—is characterized by learning scheme (3, 3). In this learning scheme, uncertainty concerning both Climate Sensitivity and Ocean Diffusivity is resolved at the end of Period 2. As discussed below, this learning scheme is used as the reference case against which the remaining eight learning schemes are compared.

The topological structure of our primary TID is easily modified to represent the learning schemes outlined above. Such modifications are achieved by adding information arcs to the diagram. If, for example, in Figure 6-5 we include a directed arc from Climate Sensitivity to Abatement Policy (1), we are able to represent learning scheme (1, 3). The TID corresponding to this learning scheme is shown in Figure 6-21. Alternatively, if we draw an information arc from Ocean Diffusivity to Abatement Policy (1), we are able to represent learning scheme (3, 1). By evaluating each of these revised models, we are able to determine the value of knowing the outcome of the chance variables Climate Sensitivity or Ocean Diffusivity *prior to* choosing a GHG abatement policy in Period 1.

Suppose, now, that in Figure 6-21 we include a directed arc from Ocean Diffusivity to Abatement Policy (2). As shown in Figure 6-22, the addition of this arc gives rise to learning scheme (1, 2), which represents what we shall term *sequential learning* about Climate Sensitivity and Ocean Diffusivity, respectively. Learning scheme (2, 1) is specified in an analogous manner.

156
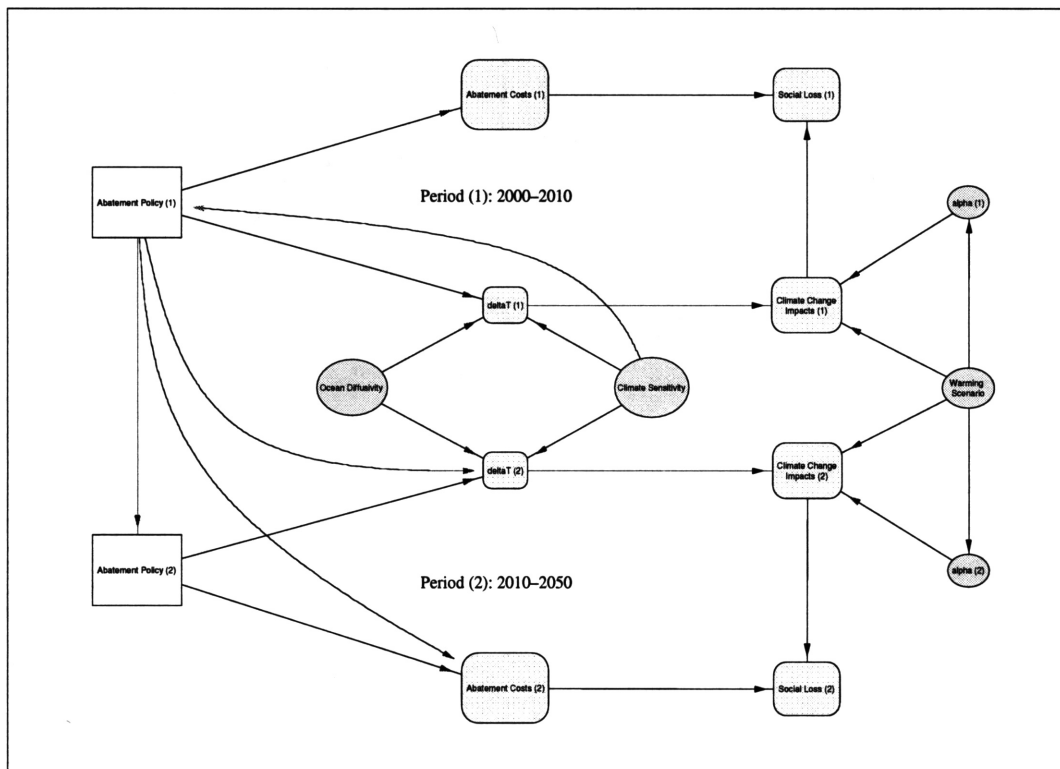
Figure 6-21: Temporal influence diagram with partial learning about Climate Sensitivity.
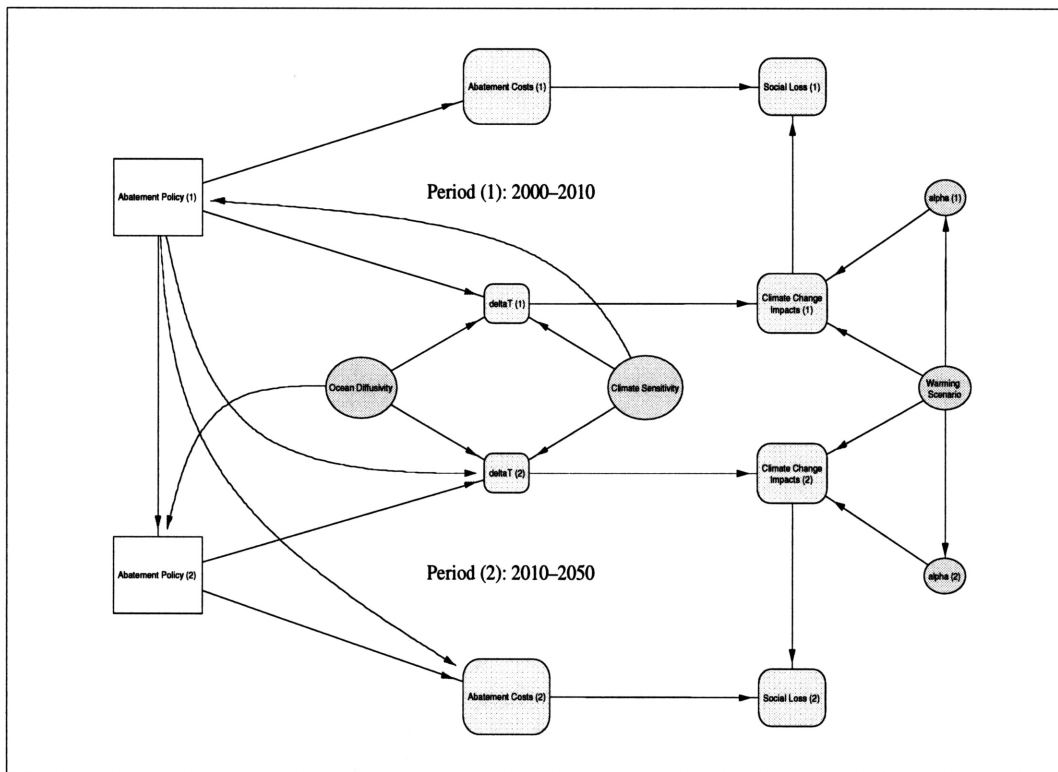
Figure 6-22: Temporal influence diagram with sequential learning about Climate Sensitivity and Ocean Diffusivity.
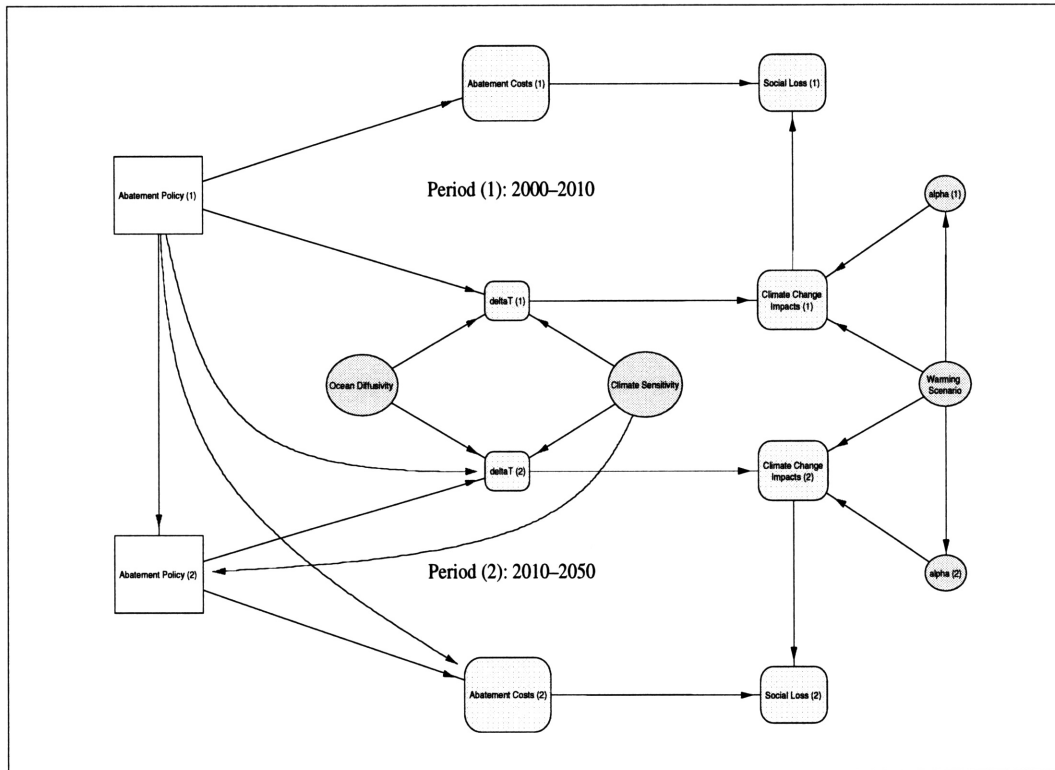
Figure 6-23: Temporal influence diagram with delayed learning about Climate Sensitivity.

An alternative to the learning schemes described above is to assess the influence that *delayed learning* has on the evaluation of both near- and long-term policy choice. Learning schemes (2, 3) and (3, 2) both represent this type of delayed learning. As shown in Figure 6-23, to specify learning scheme (2, 3), in our primary model we include a directed arc from Climate Sensitivity to Abatement Policy (2). Learning scheme (3, 2) is specified in an analogous fashion.

The frameworks described above are, for our purposes here, classified as *partial* learning schemes, in the sense that learning about the two climate-change-related quantities is assumed to take place *one variable at a time.* That is, prior to selecting an abatement policy in Periods 1 or 2, the decision-maker may learn about Climate Sensitivity or Ocean Diffusivity, *but not both at the same time.* The two remaining learning schemes — (1, 1) and (2, 2) — are representative of what we shall term *complete* learning schemes. Learning scheme (1, 1) is characterized by complete learning about the sequential model's two climate variables in Period 1, whereas learning scheme (2, 2) represents complete learning about these variables that is delayed by one period. The TIDs corresponding to these two learning schemes are shown in Figures 6-24 and 6-25.
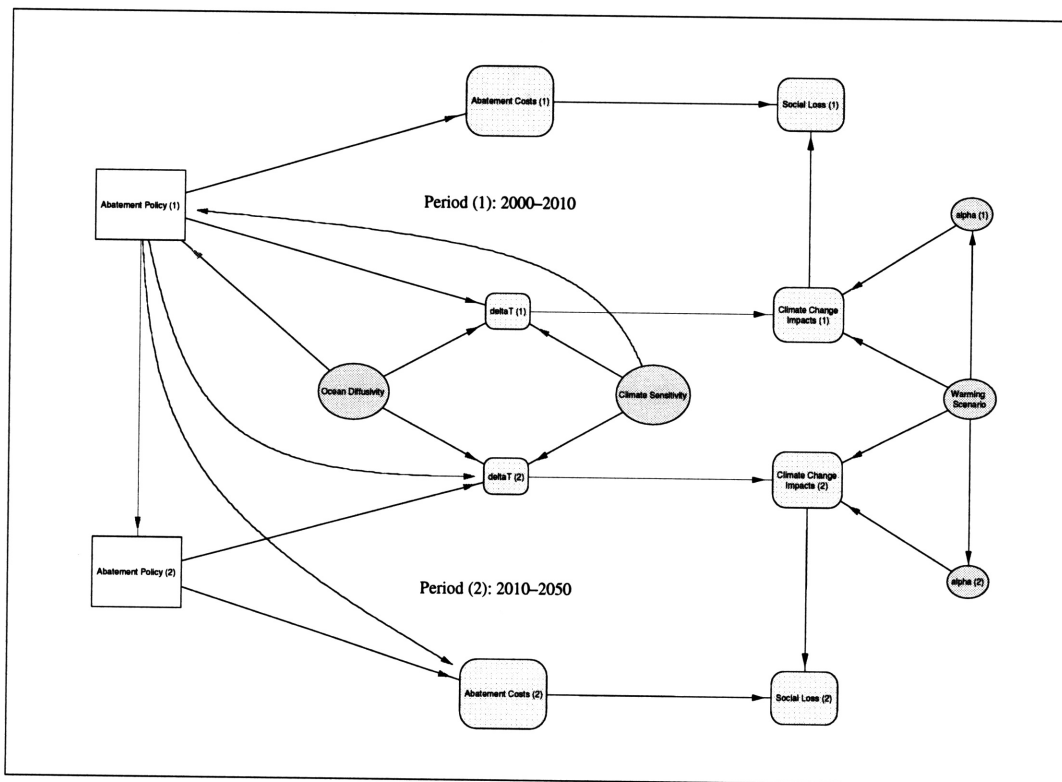
Figure 6-24: Temporal influence diagram with complete learning in Period 1 about Climate Sensitivity and Ocean Diffusivity.
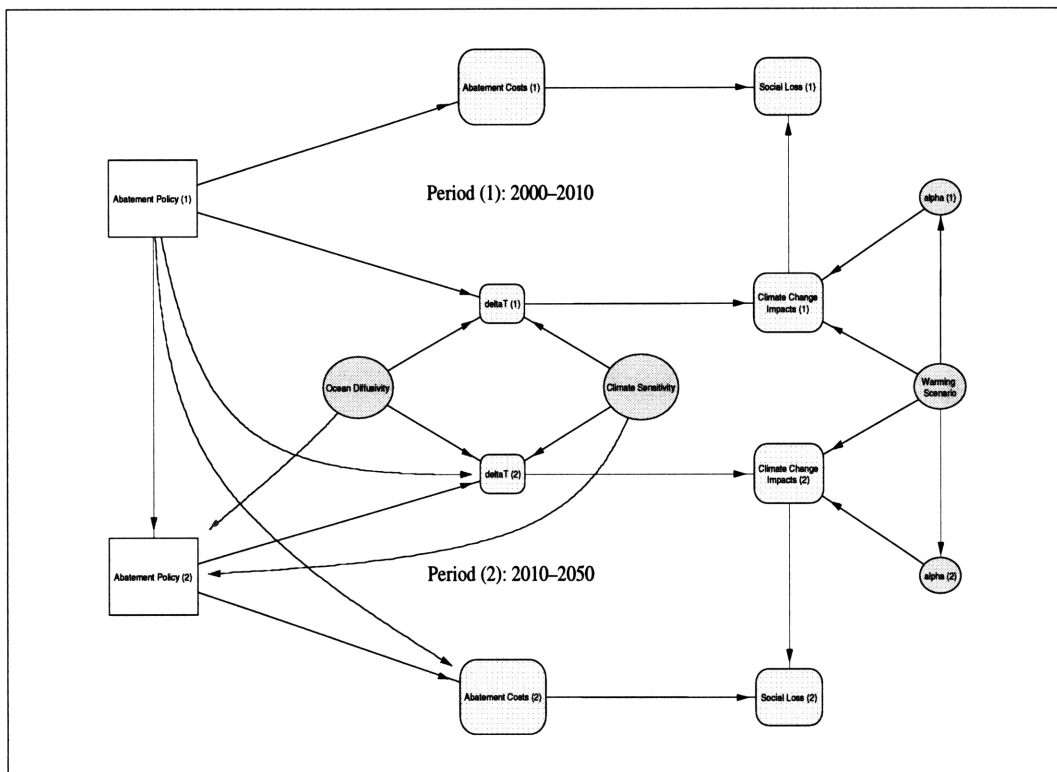
Figure 6-25: Temporal influence diagram with complete learning in Period 2 about Climate Sensitivity and Ocean Diffusivity.

Learning Scheme	Value of Learning
(1, 1)	-0.34%
(1, 2)	-0.31%
(1, 3)	-0.20%
(2, 1)	-0.34%
(2, 2)	-0.29%
(2, 3)	-0.18%
(3, 1)	-0.17%
(3, 2)	-0.17%

Table 6.6: Value of learning associated with each learning scheme.

6.3.3 Computing the Value of Learning

Numerically evaluating the TIDs associated with each of the learning schemes described above yields a set of expected values that can be used in a manner that is conceptually analogous to the determinate value of perfect information calculations that we performed earlier in Chapter 5. By computing the expected value of the TID corresponding to a particular learning scheme, and subtracting from this value the expected value of our primary decision model (6.05%), we are able to obtain an expected "value of learning."

In Table 6.6, we summarize the value of learning associated with each of the learning schemes described above. Looking at these values, we note that learning schemes (1, 1) and (2, 1) have the greatest value of learning (-0.34%). The fact that these two learning schemes share the same value of learning suggests that, from a policymaking perspective, there is no additional value to be gained by adopting a complete learning scheme in Period 1; learning about Ocean Diffusivity at resolution point 1, and then learning about Climate Sensitivity at resolution point 2, is seen to give rise to the same value of learning as the complete learning scheme. We note, also, that the value of learning associated with learning scheme (1, 2) (-0.31%) is close to the value of learning associated with learning scheme (2, 1), which suggests that if a sequential learning strategy is adopted, then Climate Sensitivity and Ocean Diffusivity are roughly interchangeable, in the sense that both learning schemes are seen to give rise to similar values of learning.

Looking, now, at the learning schemes that have the lowest values of learning, we note that learning schemes (3, 1) and (3, 2) both have values of learning of -0.17%. This result suggests that if uncertainty about Climate Sensitivity is not resolved until the end of Period 2, then there is no additional value to be gained by resolving uncertainty concerning Ocean Diffusivity before

Period 1, as opposed to at the end of Period 1. The values of learning associated with learning schemes (1, 3) and (2, 3) suggest that delayed learning about Ocean Diffusivity gives rise to a situation where there is only marginal benefit (-0.20% vs. -0.18%) in resolving uncertainty concerning Climate Sensitivity before Period 1, as opposed to at the end of Period 1. Lastly, we note that learning scheme (2, 2) has an expected value of learning of -0.29%, which suggests that complete learning about Climate Sensitivity and Ocean Diffusivity in Period 2 has moderate value, relative to the other learning schemes.

6.3.4 A Bayesian Learning Scheme

An alternative to the modeling approach described above is to posit a *Bayesian learning* scheme, where the decision-maker's beliefs about the chance variables Climate Sensitivity and Ocean Diffusivity are seen to change over time. Rather than assume a "static" representation for these two uncertain quantities, we now assume that the decision-maker's knowledge and information about these uncertain quantities evolves over the finite time horizon of the sequential framework. In formally representing this dynamic process, we generalize our earlier definitions for Climate Sensitivity and Ocean Diffusivity to two periods. Specifically, for climate sensitivity, we define two chance variables:

$$\text{Climate Sensitivity (1)} = \{\text{Low}_1, \text{Medium}_1, \text{High}_1\},$$

and

$$\text{Climate Sensitivity (2)} = \{\text{Low}_2, \text{Medium}_2, \text{High}_2\},$$

where, for $i = 1, 2$,[26]

$$\text{Low}_i \equiv 1.5°\text{C};$$
$$\text{Medium}_i \equiv 2.5°\text{C};$$
$$\text{High}_i \equiv 4.5°\text{C}.$$

In a similar fashion, for ocean diffusivity, we define two chance variables:

$$\text{Ocean Diffusivity (1)} = \{\text{od}_{11}, \text{od}_{12}, \text{od}_{13}, \text{od}_{14}\},$$

and

$$\text{Ocean Diffusivity (2)} = \{\text{od}_{21}, \text{od}_{22}, \text{od}_{23}, \text{od}_{24}\},$$

---

[26]To simplify our presentation, we assume that the state space for the chance variables defined here remains invariant over the finite time horizon of the model. This assumption is, of course, easily modified.

where, for $i = 1, 2,$

$$od_{i1} \equiv 1/50;$$
$$od_{i2} \equiv 1;$$
$$od_{i3} \equiv 5;$$
$$od_{i4} \equiv 50.$$

As we discuss below, in characterizing these chance variables, we assume that the *passage of experience*,[27] from Period 1 to Period 2, leads the decision-maker to change his degrees of belief concerning climate sensitivity and ocean diffusivity.

Incorporating these four chance variables into our sequential framework yields the TID shown in Figure 6-26. This revised diagram has several characteristic features that are worth noting. First, the diagram requires that we specify marginal probability distributions for Climate Sensitivity (1) and for Ocean Diffusivity (1), as well as conditional distributions for Climate Sensitivity (2), given Climate Sensitivity (1), and for Ocean Diffusivity (2), given Ocean Diffusivity (1). For our purposes here, the marginal distributions specified for Climate Sensitivity (1) and Ocean Diffusivity (1) are identical to those specified earlier in Section 6.2 for the chance variables Climate Sensitivity and Ocean Diffusivity.

In specifying the conditional probability distributions for

$$\text{Pr\{Climate Sensitivity (2) | Climate Sensitivity (1)\}} \tag{6.4}$$

and

$$\text{Pr\{Ocean Diffusivity (2) | Ocean Diffusivity (1)\}}, \tag{6.5}$$

we are interested in operationalizing the notion of "surprise" as it relates to the decision-maker's degrees of belief concerning the dynamic evolution of climate sensitivity and ocean diffusivity. For Eqs. (6.4) and (6.5), we assume the probability structures shown in Tables 6.7 and 6.8. Looking, first, at Table 6.7, we let the diagonal entries labeled p denote the conditional probability that Climate Sensitivity (2) is in a particular state in Period 2 (Low_2, $Medium_2$, or $High_2$), given that the chance variable was in the same state in Period 1. For our purposes here, we assume that $0.5 \leq p < 1$, which means that if Climate Sensitivity (1) is believed to be in a particular state in Period 1, then we assign at least better than even odds to the event that Climate Sensitivity (2) is in the same state in Period 2. In very general terms, we can think of

---

[27]This term is due to Richard Jeffrey. See, e.g., Jeffrey [37].
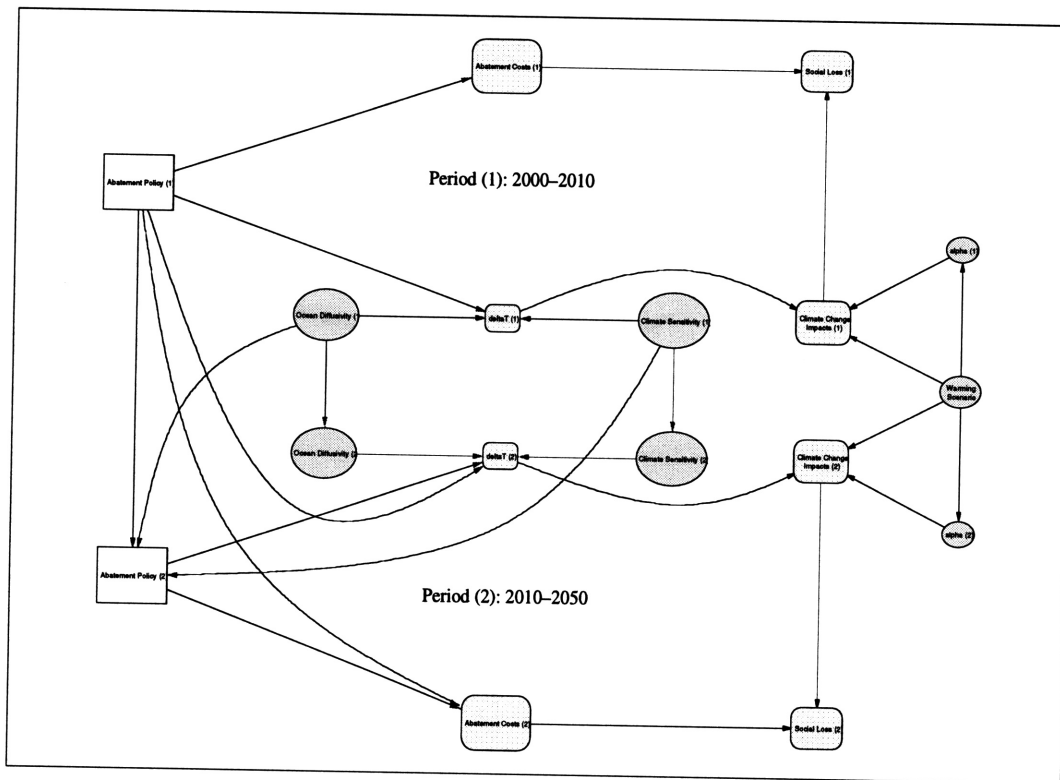
Figure 6-26: Temporal influence diagram with Bayesian learning about Climate Sensitivity and Ocean Diffusivity.

Climate Sensitivity (2)	Climate Sensitivity (1)		
	Low_1	$Medium_1$	$High_1$
Low_2	p	$\frac{1-p}{2}$	$\frac{1-p}{4}$
$Medium_2$	$\frac{3(1-p)}{4}$	p	$\frac{3(1-p)}{4}$
$High_2$	$\frac{1-p}{4}$	$\frac{1-p}{2}$	p

Table 6.7: Conditional probability distribution for Climate Sensitivity (2), given Climate Sensitivity (1).

Ocean Diffusivity (2)	Ocean Diffusivity (1)			
	od_{11}	od_{12}	od_{13}	od_{14}
od_{21}	q	$\frac{19(1-q)}{40}$	$\frac{1-q}{5}$	$\frac{1-q}{20}$
od_{22}	$\frac{3(1-q)}{4}$	q	$\frac{3(1-q)}{4}$	$\frac{1-q}{5}$
od_{23}	$\frac{1-q}{5}$	$\frac{19(1-q)}{40}$	q	$\frac{1-q}{4}$
od_{24}	$\frac{1-q}{20}$	$\frac{1-q}{20}$	$\frac{1-q}{20}$	q

Table 6.8: Conditional probability distribution for Ocean Diffusivity (2), given Ocean Diffusivity (1).

p as a measure of the *degree of entrenchment* of the decision-maker's beliefs concerning the dynamic evolution of climate sensitivity.

The off-diagonal elements of Table 6.7 are specified so as to reflect a range of probability judgements concerning the likelihood of moving from a particular state in Period 1 to a different state in Period 2. As alluded to earlier, these conditional probabilities are specified so as to reflect the degree of surprise that the decision-maker associates with these transitions. If, for example, in Period 1 climate sensitivity is in state 'Low$_1$,' then, for p = 0.6, Pr{Climate Sensitivity (2) = High$_2$ | Climate Sensitivity (1) = Low$_1$} = 0.1. In this way, we are able to represent the decision-maker's qualitative belief that it is unlikely that the passage of experience would give rise to a situation where climate sensitivity is believed to be 1.5°C in Period 1, and then believed to be 4.5°C in Period 2.

The presumed structure for Pr{Ocean Diffusivity (2) | Ocean Diffusivity (1)} is specified in an analogous manner. In Table 6.8, we let the diagonal entries labeled q denote the conditional probability that Ocean Diffusivity (2) is in a particular state (od_{21}, od_{22}, od_{23}, or od_{24}), given that the variable was in the same state in Period 1. Consistent with our discussion above, we assume that $0.5 \le q < 1$.

A characteristic feature of the TID shown in Figure 6-26 is the assumed timing of the climate-change-related uncertainties defined above. Specifically, in this dynamic formulation, we as-

sume that the outcomes of the chance variables Climate Sensitivity (1) and Ocean Diffusivity (1) are known to the decision-maker prior to choosing a GHG abatement policy in Period 2; furthermore, we assume that uncertainty concerning Climate Sensitivity (2) and Ocean Diffusivity (2) is resolved at the end of Period 2. This set of assumptions can, of course, be modified to reflect a range of possible timing assumptions, similar in character to those which we considered earlier.

6.3.5 Evaluation of Probabilistic Climate Policies

Numerical evaluation of the TID shown in Figure 6-26 require that we specify values for both p and q. For the purposes of illustration, we consider four separate cases, each reflecting a different set of assumptions concerning the dynamic evolution of the chance variables defined above:

1. $p = 0.5$ and $q = 0.5$;

2. $p = 0.5$ and $q = 0.75$;

3. $p = 0.75$ and $q = 0.5$;

4. $p = 0.75$ and $q = 0.75$.[28]

Having specified these values, in Table 6.9 we summarize the expected social loss associated with each of the four cases outlined above. Also summarized in this table are the policy prescriptions of the model. In the third and fourth columns of Table 6.9, we note that the abatement policies in each period have probabilities associated with their alternatives. Looking, first, at the case where $p = q = 0.5$, evaluation of our sequential Bayesian learning model yields an expected social loss of 6.38%. In Period 1, the optimal course of GHG abatement action is to pursue a 'No Controls' policy. Thus, for Abatement Policy (1), we see that the probability associated with the optimal choice, Strategy a_{11}, is 1.0; by the axioms of probability, it follows that the probabilities associated with the other abatement policies are 0. For Abatement Policy (2), the optimal climate policy is seen to depend on the outcomes of the chance events Climate Sensitivity (1) and Ocean Diffusivity (1). Since Abatement Policy (2) is preceded by these two chance events, it follows that the probability for each policy alternative in Period 2 may be less than 1.0. Hence, in Table 6.9, we note that the Period 2 abatement policies a_{21}, a_{22}, a_{23}, and a_{24} (i.e., 'No Controls,' 'Stabilize Emissions,' 'AOSIS Protocol,' and 'Stringent') have probabilities of 0.28, 0.68, 0.04, and 0, respectively. These probabilities reflect the likelihood that a particular

---

[28]The careful reader will note that, for the case where $p = q = 1$, our Bayesian learning scheme reduces to the TID associated with learning scheme (2, 2).

Case: (p, q)	Expected Social Loss	Probabilistic Climate Policies	
		Abatement Policy (1)	Abatement Policy (2)
(0.5, 0.5)	6.38%	a_{11} 1	a_{21} 0.28
		a_{12} 0	a_{22} 0.68
		a_{13} 0	a_{23} 0.04
		a_{14} 0	a_{24} 0
(0.5, 0.75)	6.27%	a_{11} 1	a_{21} 0.32
		a_{12} 0	a_{22} 0.64
		a_{13} 0	a_{23} 0.04
		a_{14} 0	a_{24} 0
(0.75, 0.5)	6.19%	a_{11} 1	a_{21} 0.32
		a_{12} 0	a_{22} 0.64
		a_{13} 0	a_{23} 0.04
		a_{14} 0	a_{24} 0
(0.75, 0.75)	6.09%	a_{11} 1	a_{21} 0.68
		a_{12} 0	a_{22} 0.28
		a_{13} 0	a_{23} 0
		a_{14} 0	a_{24} 0.04

Table 6.9: Probabilistic climate policies for four different combinations of p-q values.

policy choice will be made, *if the optimal policy is followed.* We shall refer to this type of policy as a *probabilistic* climate policy.

Examining the remaining three cases shown in Table 6.9, we note that the optimal course of GHG abatement action in Period 1 is 'No Controls.' This near-term abatement policy is therefore invariant under the range of learning assumptions considered here. It is also worth noting that, relative to the other cases, the case where $p = q = 0.75$ is seen to give rise to a dramatic increase in the probability associated with Strategy a_{21} (0.68 vs. 0.28 and 0.32). In contrast with the other cases, this case also gives rise to a 4% chance for Strategy a_{24}. These results suggest is that the more "entrenched" the decision-maker's beliefs about climate sensitivity and ocean diffusivity become, the more likely it is that sequential climate policy $< a_{11}, a_{21} >$, i.e., 'No Controls' in Periods 1 and 2, will represent an optimal course of GHG abatement action.

6.4 Summary

In this chapter, we presented an integrated decision analysis framework for evaluating sequential GHG abatement policies under uncertainty. Our sequential model formulation integrates the reduced-scale climate modeling approach set forth earlier in Chapters 3 and 4, and, in addition, is seen to include direct and tangible linkages to the MIT IGSM. In this way, the IDA framework presented here provides policy analysts and decision-makers with a nimble, computationally-efficient vehicle for evaluating a broad range of possible GHG abatement policies.

The sequential analysis presented here suggests that a ten year delay in taking GHG abatement action might be warranted, but only if followed, in Period 2, by the stabilization of global carbon emissions at their 1990 levels. As we discuss in the concluding chapter that follows, this policy prescription should not be construed as providing license for the explicit adoption of a "Do Nothing" greenhouse policy. *Delayed* policy action must, in the context of the type of analysis presented here, be clearly distinguished from *inaction* on the part of intergovernmental decision-makers and negotiators. Moreover, our assessment of the potential role of learning in the evaluation of GHG abatement policies suggests that there is positive value associated with pursuing policies and research programs aimed at reducing or resolving the uncertainty that currently underlies our knowledge and understanding of several key climate-change-related quantities. Learning strategies such as those evaluated here deserve explicit consideration in current efforts to arrive at reasoned responses to the prospect of anthropogenic global warming.

Chapter 7

Conclusion

In this chapter, we provide an executive summary of the main research findings presented in this dissertation. Following this summary, we discuss several possible directions for future research. Finally, we close with some concluding remarks.

7.1 Summary of Findings

The integrated assessment methodology set forth in this dissertation approaches the framing and evaluation of global climate change response options from two different though, in many ways, complementary perspectives: (i) *uncertain inference* or *prediction*; and (ii) *decision-making under uncertainty*. Proceeding from these two vantage points, the foregoing chapters outlined the main components of an integrated decision analysis (IDA) framework for evaluating GHG abatement policies under uncertainty. Structurally, the IDA model formulation consists of three major components:

- The derivation of two reduced-scale models of the global climate system. These models possess a reasonable balance of scientific adequacy/realism and computational efficiency.

- The numerical calibration of the reduced-scale climate models against a larger, more complex global climate model.

- The development of static and sequential frameworks for structuring and evaluating GHG abatement policies under uncertainty. These formal decision models utilize the reduced-scale climate modeling approach, and they utilize time-series outputs derived from the MIT IGSM.

In what follows, we summarize the key features of the IDA framework and, in addition, we discuss the policy relevance of our static and sequential analyses of the climate change problem.

170

7.1.1 Reduced-Scale Models of the Global Climate System

In Chapters 2 – 4, we emphasized the centrality of long-term climate predictions in integrated assessments of global climate change. The computational costs entailed in running large-scale climate models makes their use in decision-analytic frameworks a practical impossibility. The reduced-scale modeling approach set forth in Chapter 3 provides policy analysts and decision-makers with an instrumental basis for balancing the need for scientific adequacy and realism, on the one hand, against the need for computational efficiency and model transparency, on the other.

Central to our reduced-scale modeling approach is the idea that the *output* of such models should resemble—as closely as possible—the characteristic output of larger, more realistic models. In Chapter 4, we utilized econometric and statistical time series estimation techniques to numerically calibrate the globally-averaged one- and two-box climate models presented in Chapter 3 against transient simulations of the MIT 2D-LO global climate model. Our numerical calibration of these models utilized an experimental design that focused specifically on two key climate-change-related quantities: climate sensitivity and ocean diffusivity. By varying these variables across a range of scientifically plausible values, we obtained a range of reduced-scale model parameter estimates; these values were subsequently used to compute policy-dependent projections of future climate change.

7.1.2 Integrated Decision Analysis Framework

The IDA framework set forth in Chapters 5 and 6 imposes a formal decision-theoretic frame on the manner in which climate change response options are structured and evaluated. The static analysis presented in Chapter 5 focused on three aspects of the climate change problem:

- The economic costs of pursuing specific GHG abatement strategies. Abatement cost estimates were derived from the MIT EPPA model.

- The economic benefits of abating global climate change.

- Uncertainty concerning the level or magnitude of global climate change.

The static framework provides a nimble and computationally-efficient framework for exploring a broad range of GHG abatement policies. In addition, the framework provides a computational vehicle for exploring issues concerning the value of information and control. As we discussed in Chapter 1, the static model can also be used to guide more detailed examinations of policy choice that utilize the sequential decision framework presented in Chapter 6.

The sequential framework presented in Chapter 6 provides a more detailed and realistic basis from which to explore the various dimensions of climate policy choice under uncertainty. In

general, the framework represents several key features of the climate change decision-making problem:

- The representation of possible mid-course corrections to near-term policy choice;

- The representation of climate change as a dynamic process that evolves over time;

- The representation of uncertainty in key climate-change-related quantities;

- The representation of uncertainty in the calibration and parameterization of the functions that are used to represent climate-induced damages or impacts.

As in the static model formulation, the sequential framework draws upon outputs from the MIT IGSM. The framework also makes use of the reduced-scale modeling approach described in Chapters 3 and 4. In this way, the framework provides a computationally-efficient vehicle for structuring and evaluating sequential GHG abatement policies. Using several sensitivity analysis techniques, we were able to determine which model uncertainties and values have the greatest influence on climate policy choice. Lastly, the framework is seen to provide a flexible and transparent vehicle for exploring the potential role of learning in the evaluation of sequential GHG abatement policies.

By way of summary, the IDA framework presented in this dissertation is seen to possess several unique characteristics, which we summarize as follows:

- The models are grounded in well-established normative theories of choice under uncertainty, and are *prescriptive* in their orientation;

- The models have a distinct policy-oriented focus, and are well-attuned to the policy context in which they reside;

- The modeling approach explicitly separates the *structure* of the decision and inference problems that characterize the climate change problem from the *assessment* and *valuation* of relevant model inputs and parameters;

- The models allow for the explicit representation of uncertainty in key climate-change-related quantities and parameters;

- The models possess a reasonable balance between scientific accuracy, computational tractability, and model transparency.

7.1.3 Implications for Global Climate Change Policy

The static and sequential analyses presented in Chapters 5 and 6 yield many insights concerning a broad range of possible response options that world governments might choose to act upon

172

in their collective efforts to mitigate the potential adverse effects of anthropogenic climate change.

In the static analysis presented in Chapter 5, we determined that—relative to the other abatement policies considered—the AOSIS Protocol represents an optimal course of GHG abatement action. As part of our analysis, we noted that the 'Delayed AOSIS' policy is characterized by an expected social loss that is quite close in value to that of the AOSIS policy. In interpreting this result, we recognize that the delayed version of the AOSIS Protocol is, in actuality, a *sequential* climate policy.

The sequential analysis presented in Chapter 6 focused on sixteen sequential climate policies. In order to broaden the scope of our analysis, in addition to evaluating sequential versions of the 'AOSIS' and 'Delayed AOSIS' policies, we also considered a sequential emission stabilization policy that lies between the 'No Controls' and 'AOSIS' policies in terms of its level of stringency. Our sequential analysis suggests that delayed policy action is, indeed, warranted, *but only if followed by a global carbon emission stabilization program.* Sensitivity analysis of key model assumptions and inputs reveals that the policy prescriptions presented here are sensitive to the manner in which the model's climate-change-related uncertainties are characterized.

Finally, our exploration of the potential role of learning in the evaluation of GHG abatement policies suggests that there are positive benefits associated with policy initiatives and research programs directed at reducing or resolving key climate-change-related uncertainties, such as climate sensitivity and ocean diffusivity. However, our analysis suggests, also, that it is possible for policymakers to delay research efforts aimed at resolving these uncertainties by a deacde or more, and still realize positive benefits.

7.2 Directions for Future Research

In this section, we outline three possible directions for future research, each of which deals with a particular facet of our IDA framework.

7.2.1 Reduced-Scale Model Specification and Calibration

Possible extensions to the reduced-scale modeling approach presented in Chapters 3 and 4 fall into two general categories:

- The development of additional and, perhaps, more sophisticated reduced-scale representations of the global climate system;

- The development of statistical experimental design strategies for efficient reduced-scale model calibration.

The reduced-scale modeling approach set forth in this dissertation represent an important step towards the successful integration of such models into formal, decision-analytic frameworks. Possible extensions to the reduced-scale models presented here include the incorporation of other key features of the 2D-LO climate model into the one- and two-box models, thereby attaining added degrees of realism.[1] Of course, the manner and degree to which such extensions are incorporated into our reduced-scale modeling framework must ultimately be balanced against the need or desire for model transparency and computational-tractability.

An alternative to the reduced-scale modeling approach described here is to use the transient simulations of the 2D-LO climate model to develop statistical time series models that are able to mimic the characteristic behavior of the larger model.[2] In addition, empirical analysis of 2D-LO time series data might provide valuable insights concerning the characteristic nature of the model's dynamic behavior.

The numerical calibration procedure outlined in Chapter 4 can be expanded upon in several directions. A potentially fruitful research direction focuses on the development and specification of statistical experimental design strategies that can be used to extract maximal information from the smallest possible number of MIT IGSM transient runs. While the design strategy used in Chapter 4 can serve as a preliminary guide for subsequent IGSM runs, future designs should give explicit consideration to issues such as aliasing, balance, efficiency, resolution, and rotatability. After specifying improved experimental design strategies, attention must then focus on the task of obtaining meaningful estimates of key reduced-scale model parameters. Naturally, there are a plethora of econometric and statistical time series estimation techniques that can be brought to bear on this task.

7.2.2 Analysis of Sequential CO_2 Stabilization Policies

Several recent policy proposals aimed at mitigating the potential adverse effects associated with global climate change focus on the goal of *stabilizing* atmospheric concentrations of carbon dioxide. The driving force behind this emphasis on CO_2 stabilization is Article 2 of the United Nations Framework Convention on Climate Change, which states that

---

[1] Of course, it may also be useful to develop reduced-scale representations of other key components of the larger MIT IGSM. Webster [78] outlines a methodology for arriving at *reduced-form* representations of complex, dynamical systems. Methodologies such as this can be used to incorporate additional aspects of the IGSM into the IDA framework that might otherwise be too large and complex to incorporate directly.

[2] It might, for example, be possible to use vector ARMA models to analyze transient 2D-LO time series data. Related to this approach, one might also develop dynamic simultaneous equations models of the global climate system, much like the coupled system presented in Chapter 3.

The ultimate objective of this Convention and any related legal instruments that the Conference of Parties may adopt is to achieve, in accordance with the relevant provisions of the Convention, *stabilization* of greenhouse gas *concentrations* in the atmosphere at a level that would prevent dangerous anthropogenic interference with the climate system. Such a level should be achieved within a time frame sufficient to allow ecosystems to adapt naturally to climate change, to ensure that food production is not threatened and to enable economic development to proceed in a sustainable manner [1, emphasis added].

Most technical discussions of the stabilization problem have, to date, focused on two problem areas, the first of which we discussed earlier in Chapter 2, namely, the nature of the relation between GHG emissions and the global carbon cycle. The second problem area is a more recent topic of concern in the climate change literature, and focuses on estimating the economic costs of pursuing GHG abatement strategies aimed at achieving specific CO_2 stabilization levels.

An important theme to emerge from the stabilization literature is that GHG abatement costs are an important consideration in the selection of CO_2 concentration stabilization targets. However, abatement costs are only one facet of the stabilization problem. Ideally, abatement costs should inform the evaluation of hedging strategies that seek to balance the risks, costs, and benefits that underlie specific policy proposals aimed at stabilizing atmospheric CO_2 concentrations.

To date, most studies of the stabilization problem have focused on *static* analyses of the abatement costs associated with CO_2 stabilization policies. Consequently, most of these analyses assume that a *long-term* stabilization target is chosen today, *once-and-for-all*, with no future opportunities to amend or revise the chosen stabilization target.[3]

A potentially fruitful avenue for future research is to combine insightful economic analyses of the stabilization problem[4] with the type of sequential decision framework presented earlier in Chapter 6. In what follows, we sketch the basic elements of a decision framework for evaluating sequential CO_2 stabilization policies under uncertainty.

We begin our sequential formulation of the stabilization problem by making the assumption that the choice of a CO_2 concentration target can potentially change over time. In this way, we wish to represent the possibility of mid-course corrections to short-term policy choice. Analogous to the sequential Bayesian learning framework presented at the end of Chapter 6, we might formulate the sequential stabilization problem in terms of the TID shown in Figure 7-1. In this diagram, we focus on the evaluation of sequential GHG abatement strategies aimed at stabilizing atmospheric CO_2 concentrations. The TID is defined in terms of three decision

---

[3] See, e.g., Richels and Edmonds [65].
[4] See, e.g., Jacoby et al. [35].

175

stages: 2010-2050, 2050-2080, and 2080-2100. For each of these three periods, we specify a *control rate* on global carbon emissions. At each decision stage, we choose a global carbon emissions control rate

$$\text{Control Rate (1)} = \{L_1, M_1, H_1\},$$

where

$$L_1 \equiv 1.01;$$
$$M_1 \equiv 1.06;$$
$$H_1 \equiv 1.2.$$

Each of these three control rates defines the allowable carbon emissions for each year, as a percentage of the previous year's emissions.

In a similar fashion, we define the control rates for the second and third periods as follows:

$$\text{Control Rate (2)} = \{L_2, M_2, H_2\},$$

where

$$L_2 \equiv 1.01;$$
$$M_2 \equiv 1.03;$$
$$H_2 \equiv 1.2;$$

and

$$\text{Control Rate (3)} = \{L_3, M_3, H_3\},$$

where

$$L_3 \equiv 0.90;$$
$$M_3 \equiv 0.92;$$
$$H_3 \equiv 0.95.$$

The control rates H_i, M_i, and L_i, for $i = 1, 2, 3$, represent increasingly stringent levels of carbon emission reductions. Viewed sequentially, these control rates give rise to the decision structure depicted in Figure 7-2. In this schematic decision tree, we note that the three possible control rates in each period give rise to $3^3 = 27$ possible sequential climate policies. Using the MIT IGSM, we have chosen the control rates specified above so that, over the one hundred year time horizon of the model, sequential climate policies $< L_1, L_2, L_3 >$, $< M_1, M_2, M_3 >$, and $< H_1, H_2, H_3 >$ lead to CO_2 stabilization levels of (approximately) 450 ppmv, 550 ppmv,

176
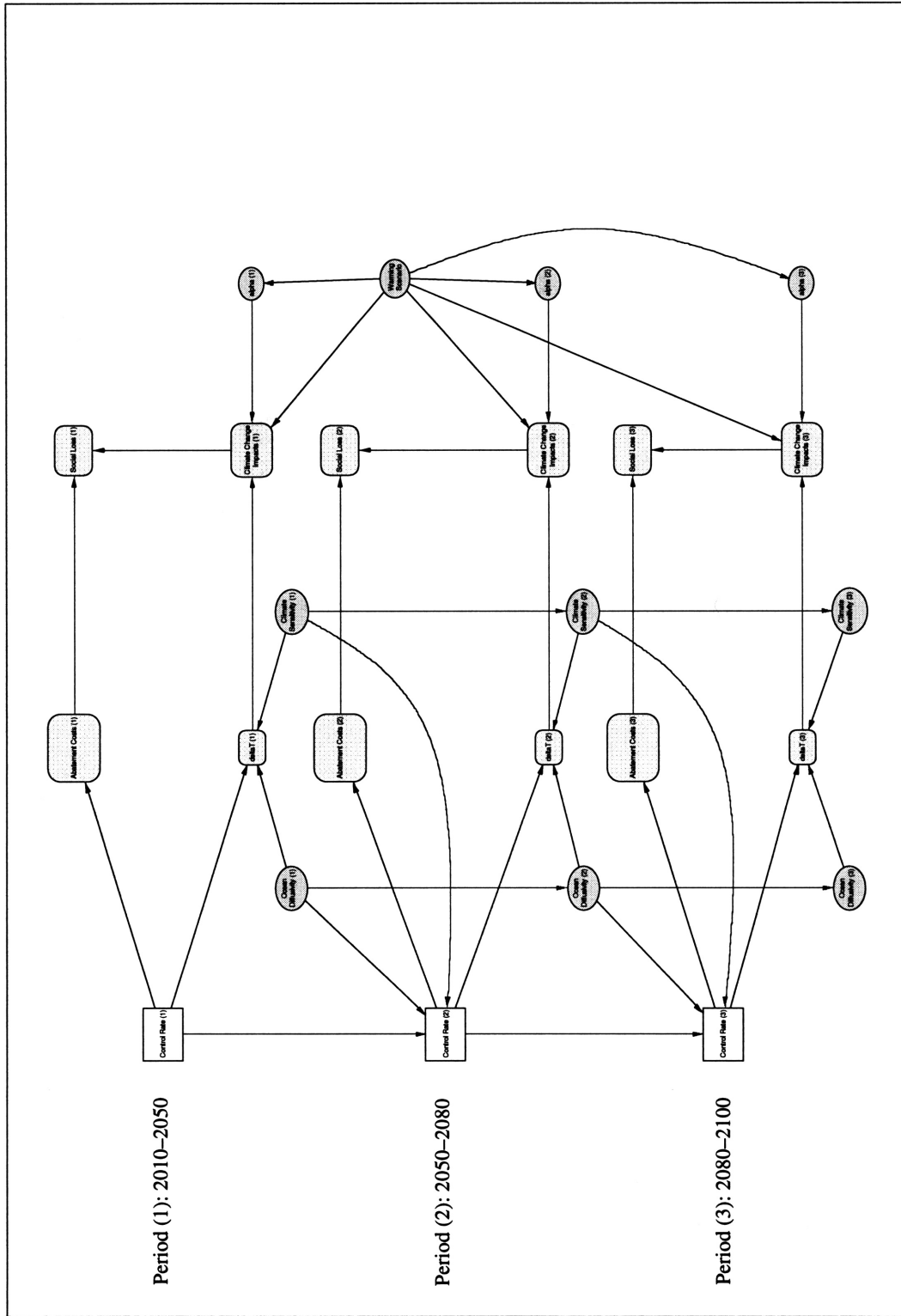
Figure 7-1: Temporal influence diagram for the evaluation of sequential CO_2 stabilization policies.
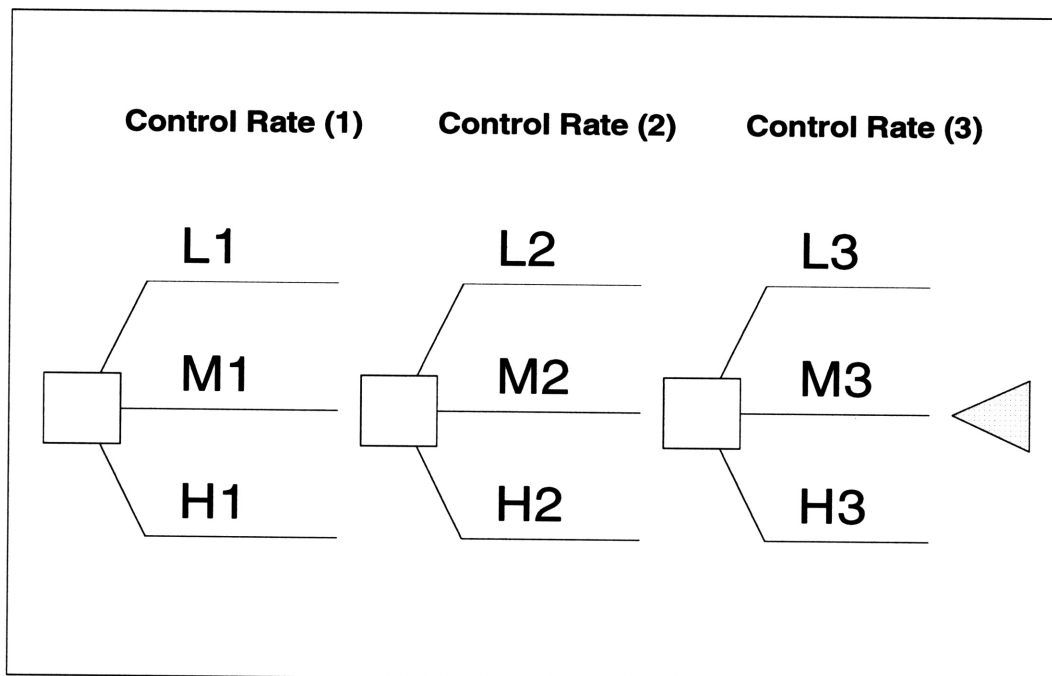
Figure 7-2: Schematic decision tree for the sequential CO_2 stabilization framework.

and 640 ppmv, respectively. Of the remaining 24 possible sequential climate policies, 14 lead to the stabilization of atmospheric CO_2 concentrations, at levels ranging from 450 ppmv to 640 ppmv. Since we are only interested in climate policies that lead to stabilization, we are able to 'trim' those branches of the decision tree shown in Figure 7-2 that do not lead to stabilization by 2100.[5] In Table 7.1, we list the 17 sequential policies that lead to specific levels of stabilization by the end of the model's one hundred year time horizon.

There are several characteristics of the sequential design outlined above that are worth noting. First, the control rates in each period are pre-defined in such a way that each of the sequential policies leads to a different level of stabilization. Looking at Table 7.1, we note that in order to achieve a CO_2 stabilization target below 500 ppmv, Control Rate L_1 must be adopted in Period 1; failure to adopt this level of control *forecloses* the option of achieving a sub-500 ppmv concentration target over the course of the model's one hundred year time horizon. Similarly, in order to achieve a stabilization target that lies in the mid-500 ppmv range, Control Rate M_1 must be adopted in Period 1. In addition, we note that in order to achieve this target, either control Rate L_2 or M_2 must be adopted in Period 2; adopting control rate H_2 in Period 2 leads to a non-stabilizing CO_2 concentration trajectory, irrespective of the

---

[5]In this way, the decision structure of our sequential stabilization framework is *asymmetric*, in that some of the paths implied by Figure 7-2 are not evaluated.

Sequential Climate Policy	Stabilization Level at 2100
$< L_1, L_2, L_3 >$	450 ppmv
$< L_1, L_2, M_3 >$	453 ppmv
$< L_1, L_2, H_3 >$	457 ppmv
$< L_1, M_2, L_3 >$	462 ppmv
$< L_1, M_2, M_3 >$	465 ppmv
$< L_1, M_2, H_3 >$	469 ppmv
$< M_1, L_2, L_3 >$	534 ppmv
$< M_1, L_2, M_3 >$	537 ppmv
$< M_1, L_2, H_3 >$	542 ppmv
$< M_1, M_2, L_3 >$	548 ppmv
$< M_1, M_2, M_3 >$	550 ppmv
$< M_1, H_2, L_3 >$	609 ppmv
$< H_1, L_2, M_3 >$	615 ppmv
$< H_1, M_2, L_3 >$	624 ppmv
$< H_1, M_2, M_3 >$	629 ppmv
$< H_1, H_2, L_3 >$	635 ppmv
$< H_1, H_2, M_3 >$	640 ppmv

Table 7.1: Atmospheric CO_2 stabilization levels for 17 sequential climate policies.

level of control that is adopted in Period 3. Lastly, we note that in order to achieve a target in the low- to mid-600 ppmv range, their is some flexibility in the control rates that can be adopted, in the limited sense that H_1 can be adopted in all but one case (609 ppmv). Also, we note that in Period 2, all three possible control rates can be adopted, without foreclosing the possibility of achieving concentration levels between 615 ppmv and 640 ppmv.

An important artifact of the sequential design presented here is that in order to achieve increasingly stringent stabilization targets, it is necessary to adopt increasingly stringent levels of control *in the near-term*. This particular feature of our sequential design is, in general, consistent with a number of recent studies that have suggested that the attainment of stringent stabilization targets is likely to require considerable near-term reductions in global carbon emissions.[6]

The complete specification of the sequential stabilization framework outlined above proceeds in a manner that is analogous to that which we outlined earlier in Chapter 6. In particular, we must specify the global carbon emission, atmospheric CO_2 concentration, and radiative

---

[6]See, e.g., Ref. [7].

179

forcing time-paths associated with each of the seventeen sequential stabilization policies listed in Table 7.1. Also, for Periods 1, 2, and 3 of the model, we must compute the projected changes in global-mean surface temperature change associated with each sequential stabilization policy. Lastly, we must assess the abatement costs and climate change impacts associated with each sequential stabilization policy.

7.2.3 Expert Judgement Elicitation

Expert judgement elicitation of key climate-change-related uncertainties has, in recent years, received a modest amount of attention in the climate change literature. Most notable in this regard are recent studies by Morgan and Keith [53] and Nordhaus [56]. The IDA framework presented in this dissertation draws upon these studies and, in addition, makes use of expert judgement elicitations conducted at MIT. Inasmuch as the IDA framework's policy prescriptions are sensitive to the manner in which key uncertainties are represented, future research must continue to explore methods and techniques for better characterizing and evaluating the scientific and economic uncertainties that underlie the greenhouse debate.

While the development of improved techniques for characterizing climate-change-related uncertainties can successfully draw upon existing frameworks and methodologies, the nature and scope of the greenhouse problem is likely to also require the exploration of alternative approaches and perspectives. A clearly discernable feature of the greenhouse debate is that credible experts disagree about substantive technical issues that have potentially broad policy implications. In highly contentious and politically-charged debates such as this, the sources of expert disagreement are oftentimes difficult to identify and resolve. As a consequence, policymakers and negotiators—not having the luxury of being able to wait until the experts are resolved in their collective judgements—must make difficult decisions in the face of complexity, expert disagreement, scientific uncertainty, limited resources, and time-constrained conditions. In this regard, an important avenue for future research concerns the examination of ways in which disagreements among experts can be resolved or otherwise successfully negotiated in the context of greenhouse policy debates.

7.3 Concluding Remarks

Programmatic efforts to confront the prospect of anthropogenic global warming require, at a base level, that we explore a broad range of possible response options. Current efforts directed along these lines focus primarily on the task of tracing-out the likely risks, costs, and benefits associated with particular climate policy proposals. On a more fundamental level, it seems important to recognize and acknowledge that such efforts—directed, as they are, at analysis and

prediction—sit in a larger set of social, political, and economic contexts. Ultimately, our best efforts to develop and improve upon the plurality of theories, methodologies, and frameworks that can be brought to bear on the policy formulation and evaluation process must be predicated on the hope and promise that such tools lead to knowledge and insights that, in turn, allow us to move towards the future with greater clarity and deliberation.

Appendix A

Computing an Upper Bound for CO$_2$-Induced Forcing

Consider the nonlinear radiative forcing function, $\rho(C_t)$, defined previously in Chapter 2 as

$$\rho(C_t) = \kappa \ln \left(\frac{C_t}{C_0} \right),$$

where $\kappa = 6.1$. For our purposes here, assume that the function ρ is both concave and differentiable on the interval $(0, \infty)$. Let

$$\rho(C_t) = \rho[(C_t - C_{t-1}) + C_{t-1}] = \rho(\Delta C_t + C_{t-1}),$$

where $\Delta C_t = C_t - C_{t-1}$, i.e., ΔC_t denotes the change in atmospheric concentration of CO$_2$ from time period $t - 1$ to period t. Because ρ is concave on $(0, \infty)$, using *Jensen's inequality*, it is possible to bound $\rho(C_t)$ from above in the following manner:

$$\rho(C_t) \le \rho(C_{t-1}) + \Delta C_t \, \rho'(C_t), \tag{A.1}$$

where ρ' denotes the first derivative of ρ, i.e.,

$$\rho'(C_{t-1}) = \frac{d\rho}{dC_{t-1}} = \frac{\kappa}{C_{t-1}}.$$

Making the relevant substitutions, Eq. (A.1) becomes

$$\rho(C_t) \le \rho(C_{t-1}) + \kappa \left(\frac{C_t - C_{t-1}}{C_{t-1}} \right). \tag{A.2}$$

The inequality given by Eq. (A.2) is valid for all values of t. Thus, it follows that

$$\rho(C_{t-1}) \le \rho(C_{t-2}) + \kappa \left(\frac{C_{t-1} - C_{t-2}}{C_{t-2}} \right),$$

182

$$\rho(C_{t-2}) \leq \rho(C_{t-3}) + \kappa \left(\frac{C_{t-2} - C_{t-3}}{C_{t-3}} \right),$$

and so on. Proceeding in this fashion, it is easily verified that

$$\rho(C_t) \leq \rho(C_0) + \kappa \sum_{j=1}^{t} \left(\frac{C_{t-j+1} - C_{t-j}}{C_{t-j}} \right),$$

which, after simplifying, becomes

$$\rho(C_t) \leq \rho(C_0) + \kappa \left[\sum_{j=1}^{t} \left(\frac{C_{t-j+1}}{C_{t-j}} \right) - t \right]. \tag{A.3}$$

Equation A.3 provides a simple and efficient means by which to compute an upper bound for CO_2-induced radiative forcing.

Appendix B

Integrated Assessment of Sequential Climate Policies

In this appendix, we provide a detailed accounting of the numerical values used in the sequential decision model presented in Chapter 6. As discussed in the main text, our formulation of the two-period decision model consists of sixteen sequential climate policies, $< a_{1i}, a_{2j} >$, where $a_{1i} \in$ Abatement Policy (1) and $a_{2j} \in$ Abatement Policy (2). The sixteen sequential climate policies are enumerated as follows:

$$< a_{11}, a_{21} > \quad < a_{12}, a_{21} > \quad < a_{13}, a_{21} > \quad < a_{14}, a_{21} >$$
$$< a_{11}, a_{22} > \quad < a_{12}, a_{22} > \quad < a_{13}, a_{22} > \quad < a_{14}, a_{22} >$$
$$< a_{11}, a_{23} > \quad < a_{12}, a_{23} > \quad < a_{13}, a_{23} > \quad < a_{14}, a_{23} >$$
$$< a_{11}, a_{24} > \quad < a_{12}, a_{24} > \quad < a_{13}, a_{24} > \quad < a_{14}, a_{24} >.$$

As Figure B-1 illustrates, we use the MIT Integrated Global System Model (IGSM) to assess the projected changes in global carbon emissions, atmospheric chemistry, and radiative forcing associated with each sequential climate policy. In the pages that follow, we tabulate the global carbon emission, atmospheric CO_2 concentration, and radiative forcing time-paths associated with each of the sixteen sequential climate policies outlined above. In addition, for Periods 1 and 2 of the sequential decision model, we summarize the projected changes in global-mean surface temperature associated with each sequential climate policy. These projections are computed using the calibrated globally-averaged one-box climate model presented in Chapters 3 and 4 of the main text.
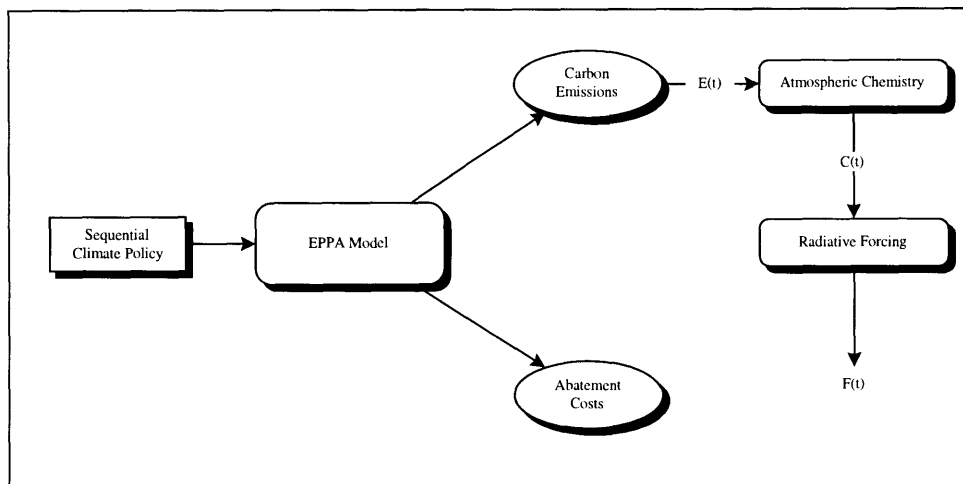
Figure B-1: Use of the MIT Integrated Global System Model to assess the changes in global carbon emissions, atmospheric chemistry, and radiative forcing associated with each sequential climate policy.

Carbon Emission, Atmospheric CO_2 Concentration, and Radiative Forcing Time-Paths

In Figures B-2 – B-5, for each sequential climate policy, $< a_{1i}, a_{2j} >$, we tabulate the global carbon emission, atmospheric CO_2 concentration, and radiative forcing time-paths for the period 1977–2050.

One-Box Model Projections of Future Climate Change

In Tables B.1 – B.8, we summarize the projected changes in global-mean surface temperature in Periods 1 and 2, for each sequential climate policy, $< a_{1i}, a_{2j} >$. These projections are tabulated for Periods 1 and 2 of the sequential decision model, and are computed using the calibrated one-box global climate model. For each sequential policy, we specify the projected values (in °C) for deltaT (1) and deltaT (2), as a function of the sequential model parameters Climate Sensitivity and Ocean Diffusivity.

	Sequential Climate Policy											
	<a_11, a_21>			<a_11, a_22>			<a_11, a_23>			<a_11, a_24>		
	E(t)	C(t)	F(t)	E(t)	C(t)	F(t)	E(t)	C(t)	F(t)	E(t)	C(t)	F(t)
1977	3.4	331.249	0.945887	3.4	331.249	0.945887	3.4	331.249	0.945887	3.4	331.249	0.945887
1978	3.756891	331.35373	0.947757	3.756891	331.35373	0.947757	3.756891	331.35373	0.947757	3.756891	331.35373	0.947757
1979	4.113782	331.62636	0.952621	4.113781	331.62636	0.952621	4.113781	331.62636	0.952621	4.113781	331.62636	0.952621
1980	4.470673	332.06419	0.960426	4.470672	332.06419	0.960426	4.470672	332.06419	0.960426	4.470672	332.06419	0.960426
1981	4.827564	332.66456	0.97111	4.827563	332.66456	0.97111	4.827563	332.66456	0.97111	4.827563	332.66456	0.97111
1982	5.184455	333.42485	0.984613	5.184453	333.42485	0.984613	5.184453	333.42485	0.984613	5.184453	333.42485	0.984613
1983	5.541346	334.34247	1.00087	5.541344	334.34247	1.00087	5.541344	334.34247	1.00087	5.541344	334.34247	1.00087
1984	5.898237	335.41488	1.019812	5.898235	335.41488	1.019812	5.898235	335.41488	1.019812	5.898235	335.41488	1.019812
1985	6.612019	336.6396	1.041371	6.612016	336.6396	1.041371	6.612016	336.6396	1.041371	6.612016	336.6396	1.041371
1986	6.737698	338.18376	1.068441	6.737696	338.18376	1.068441	6.737696	338.18376	1.068441	6.737696	338.18376	1.068441
1987	6.863377	339.76493	1.096032	6.863375	339.76493	1.096032	6.863375	339.76493	1.096032	6.863375	339.76493	1.096032
1988	6.989056	341.38252	1.124126	6.989055	341.38251	1.124126	6.989055	341.38251	1.124126	6.989055	341.38251	1.124126
1989	7.114735	343.03596	1.152706	7.114734	343.03595	1.152706	7.114734	343.03595	1.152706	7.114734	343.03595	1.152706
1990	7.240414	344.72468	1.181753	7.240414	344.72467	1.181753	7.240414	344.72467	1.181753	7.240414	344.72467	1.181753
1991	7.324721	346.44812	1.211252	7.324722	346.44811	1.211252	7.324722	346.44811	1.211252	7.324722	346.44811	1.211252
1992	7.409029	348.1861	1.240851	7.409029	348.18609	1.240851	7.409029	348.18609	1.240851	7.409029	348.18609	1.240851
1993	7.493337	349.93839	1.270545	7.493337	349.93839	1.270545	7.493337	349.93839	1.270545	7.493337	349.93839	1.270545
1994	7.577645	351.70479	1.300327	7.577645	351.70478	1.300327	7.577645	351.70478	1.300327	7.577645	351.70478	1.300327
1995	7.661953	353.48507	1.330193	7.661953	353.48507	1.330193	7.661953	353.48507	1.330193	7.661953	353.48507	1.330193
1996	7.764349	355.27904	1.360136	7.762629	355.27903	1.360136	7.762629	355.27903	1.360136	7.762629	355.27903	1.360136
1997	7.866746	357.09481	1.39029	7.863305	357.09398	1.390276	7.863305	357.09398	1.390276	7.863305	357.09398	1.390276
1998	7.969143	358.93206	1.420645	7.963981	358.9296	1.420604	7.963981	358.9296	1.420604	7.963981	358.9296	1.420604
1999	8.071539	360.79044	1.451191	8.064657	360.78555	1.451111	8.064657	360.78555	1.451111	8.064657	360.78555	1.451111
2000	8.173936	362.66963	1.48192	8.165333	362.66152	1.481788	8.165333	362.66152	1.481788	8.165333	362.66152	1.481788
2001	8.386239	364.56929	1.512822	8.341229	364.5572	1.512626	8.341229	364.5572	1.512626	8.341229	364.5572	1.512626
2002	8.598541	366.54098	1.544726	8.517125	366.50755	1.544187	8.517125	366.50755	1.544187	8.517125	366.50755	1.544187
2003	8.810844	368.58354	1.577596	8.693021	368.51169	1.576443	8.693021	368.51169	1.576443	8.693021	368.51169	1.576443
2004	9.023146	370.69581	1.611398	8.868917	370.56875	1.60937	8.868917	370.56875	1.60937	8.868917	370.56875	1.60937
2005	9.235449	372.87669	1.646095	9.044814	372.67789	1.642941	9.044814	372.67789	1.642941	9.044814	372.67789	1.642941
2006	9.377593	375.12508	1.681655	8.961428	374.83826	1.67713	9.13329	374.83826	1.67713	9.13329	374.83826	1.67713
2007	9.519738	377.4062	1.717515	8.878041	376.92489	1.709967	9.221767	377.00712	1.711257	9.221767	377.00712	1.711257
2008	9.661882	379.71955	1.753661	8.794655	378.93897	1.741489	9.310244	379.18434	1.745318	9.310244	379.18434	1.745318
2009	9.804026	382.06459	1.790079	8.711269	380.88166	1.771736	9.398721	381.36977	1.779312	9.398721	381.36977	1.779312
2010	9.946171	384.44083	1.826753	8.627883	382.75413	1.800744	9.487197	383.56329	1.813236	9.487197	383.56329	1.813236
2011	10.140968	386.84777	1.863671	8.756329	384.55751	1.828548	9.384868	385.76477	1.847088	9.354541	385.76477	1.847088
2012	10.335766	389.30985	1.901198	8.884775	386.39403	1.856729	9.282538	387.88255	1.879472	9.221885	387.86804	1.879251
2013	10.530563	391.82619	1.939308	9.013221	388.26315	1.885273	9.180209	389.91798	1.910431	9.089229	389.87468	1.909774
2014	10.725361	394.39593	1.977974	9.141667	390.16434	1.914167	9.077879	391.87238	1.940005	8.956573	391.78625	1.938705
2015	10.920158	397.01819	2.017172	9.270114	392.09711	1.943396	8.97555	393.74708	1.968235	8.823917	393.6043	1.966089
2016	11.086181	399.69213	2.056876	9.39822	394.06093	1.972947	9.045864	395.54335	1.995158	8.861879	395.33032	1.991971
2017	11.252205	402.4029	2.096858	9.526327	396.05489	2.002802	9.116179	397.34481	2.022036	8.899841	397.04718	2.017604
2018	11.418228	405.14992	2.1371	9.654433	398.07852	2.032948	9.186494	399.15139	2.048868	8.937803	398.75505	2.042992
2019	11.584252	407.93259	2.177587	9.78254	400.13132	2.063372	9.256808	400.96299	2.075654	8.975765	400.45406	2.068141
2020	11.750275	410.75035	2.218304	9.910647	402.21284	2.094063	9.327123	402.77955	2.102392	9.013727	402.14435	2.093056
2021	11.931327	413.60262	2.259237	10.04336	404.32261	2.125009	9.462275	404.60098	2.12908	9.156283	403.82608	2.11774
2022	12.112378	416.49596	2.300471	10.176073	406.4623	2.156229	9.597428	406.45815	2.156169	9.298838	405.54934	2.142928
2023	12.29343	419.42972	2.34199	10.308786	408.63143	2.187711	9.73258	408.35048	2.183643	9.441394	407.31347	2.168603
2024	12.474481	422.40325	2.383777	10.441499	410.82953	2.219444	9.867733	410.27742	2.21149	9.58395	409.1178	2.194748
2025	12.655533	425.4159	2.425814	10.574212	413.05613	2.251416	10.002885	412.2384	2.239694	9.726506	410.9617	2.221347
2026	12.793145	428.46704	2.468086	10.695153	415.31078	2.283615	10.129768	414.23287	2.268243	9.856791	412.84453	2.248385
2027	12.930758	431.53558	2.510297	10.816095	417.58769	2.315955	10.256651	416.25665	2.297071	9.987076	414.76009	2.275767
2028	13.068371	434.62124	2.552441	10.937036	419.88651	2.348429	10.383533	418.30926	2.326168	10.117361	416.70786	2.30348
2029	13.205983	437.72374	2.594515	11.057978	422.2069	2.381026	10.510416	420.39026	2.355521	10.247646	418.68733	2.331511
2030	13.343596	440.84283	2.636515	11.178919	424.5485	2.413741	10.637299	422.49917	2.38512	10.377932	420.69798	2.359849
2031	13.476322	443.97822	2.678435	11.291361	426.91098	2.446565	10.742873	424.63555	2.414954	10.487625	422.73931	2.388481
2032	13.609048	447.12734	2.720242	11.403804	429.28994	2.479435	10.848447	426.78877	2.444872	10.597319	424.80099	2.417258
2033	13.741774	450.28996	2.761933	11.516246	431.68512	2.512346	10.954022	428.95858	2.474868	10.707013	426.8827	2.446173
2034	13.8745	453.46587	2.803506	11.628689	434.09626	2.545292	11.059596	431.14469	2.504936	10.816707	428.98411	2.47522
2035	14.007226	456.65486	2.844958	11.741131	436.52311	2.578269	11.165171	433.34685	2.535072	10.926401	431.1049	2.504391
2036	14.126355	459.85671	2.886287	11.836415	438.96542	2.611271	11.262083	435.5648	2.565269	11.02534	433.24477	2.533678
2037	14.245485	463.06472	2.927408	11.931699	441.41472	2.644183	11.455467	437.79416	2.595467	11.124279	435.39827	2.563007
2038	14.364614	466.2788	2.968321	12.026984	443.87091	2.677005	11.455908	440.03473	2.625662	11.223218	437.56518	2.592372
2039	14.483743	469.49884	3.009029	12.122268	446.33389	2.709736	11.55282	442.28633	2.655851	11.322157	439.74528	2.62177
2040	14.602872	472.72475	3.049532	12.217552	448.80353	2.742375	11.649732	444.5488	2.686032	11.421096	441.93837	2.651196
2041	14.6651	475.95644	3.089832	12.283633	451.27975	2.774921	11.724315	446.82195	2.716201	11.496541	444.14423	2.680647
2042	14.727328	479.16655	3.129592	12.349714	453.74841	2.80719	11.798898	449.06541	2.746214	11.571985	446.35139	2.709968
2043	14.789555	482.35544	3.168827	12.415795	456.20965	2.839188	11.87348	451.36765	2.776073	11.64743	448.55981	2.739162
2044	14.851783	485.52344	3.207549	12.481876	458.66359	2.87092	11.948063	453.6402	2.80578	11.722874	450.7695	2.768229
2045	14.914011	488.67089	3.24577	12.547957	461.11034	2.90239	12.022646	455.91257	2.835335	11.798319	452.98042	2.79717
2046	14.98126	491.79814	3.283502	12.603236	463.55003	2.933603	12.078319	458.18474	2.864741	11.852875	455.19255	2.825986
2047	15.048509	494.90783	3.320786	12.658515	465.97753	2.964498	12.133992	460.44762	2.893883	11.907431	457.39583	2.854548
2048	15.115759	498.00026	3.357631	12.713793	468.39304	2.995081	12.189665	462.70136	2.922764	11.961987	459.59038	2.88286
2049	15.183008	501.07571	3.394048	12.769072	470.79676	3.025359	12.245338	464.94609	2.951391	12.016543	461.77636	2.910927
2050	15.250257	504.13444	3.430046	12.82435	473.18887	3.055337	12.301011	467.18198	2.979768	12.071099	463.9539	2.938755

Figure B-2: Global carbon emission, atmospheric CO_2 concentration, and radiative forcing time series for the period 1977-2050 for sequential climate policies $< a_{11}, a_{2j} >$.

	Sequential Climate Policy											
	<a_12, a_21>			<a_12, a_22>			<a_12, a_23>			<a_12, a_24>		
	E(t)	C(t)	F(t)	E(t)	C(t)	F(t)	E(t)	C(t)	F(t)	E(t)	C(t)	F(t)
1977	3.4	331.249	0.945887	3.4	331.249	0.945887	3.4	331.249	0.945887	3.4	331.249	0.945887
1978	3.756891	331.35373	0.947757	3.756891	331.35373	0.947757	3.756891	331.35373	0.947757	3.756891	331.35373	0.947757
1979	4.113781	331.62636	0.952621	4.113781	331.62636	0.952621	4.113781	331.62636	0.952621	4.113781	331.62636	0.952621
1980	4.470672	332.06419	0.960426	4.470672	332.06419	0.960426	4.470672	332.06419	0.960426	4.470672	332.06419	0.960426
1981	4.827563	332.66456	0.97111	4.827563	332.66456	0.97111	4.827563	332.66456	0.97111	4.827563	332.66456	0.97111
1982	5.184453	333.42485	0.984613	5.184453	333.42485	0.984613	5.184453	333.42485	0.984613	5.184453	333.42485	0.984613
1983	5.541344	334.34247	1.00087	5.541344	334.34247	1.00087	5.541344	334.34247	1.00087	5.541344	334.34247	1.00087
1984	5.898235	335.41488	1.019812	5.898235	335.41488	1.019812	5.898235	335.41488	1.019812	5.898235	335.41488	1.019812
1985	6.612016	336.6396	1.041371	6.612016	336.6396	1.041371	6.612016	336.6396	1.041371	6.612016	336.6396	1.041371
1986	6.737694	338.18376	1.068441	6.737694	338.18376	1.068441	6.737694	338.18376	1.068441	6.737694	338.18376	1.068441
1987	6.863372	339.76493	1.096032	6.863372	339.76493	1.096032	6.863372	339.76493	1.096032	6.863372	339.76493	1.096032
1988	6.98905	341.38251	1.124126	6.98905	341.38251	1.124126	6.98905	341.38251	1.124126	6.98905	341.38251	1.124126
1989	7.114728	343.03595	1.152706	7.114728	343.03595	1.152706	7.114728	343.03595	1.152706	7.114728	343.03595	1.152706
1990	7.240406	344.72466	1.181753	7.240406	344.72466	1.181753	7.240406	344.72466	1.181753	7.240406	344.72466	1.181753
1991	7.253725	346.4481	1.211252	7.253725	346.4481	1.211252	7.253725	346.4481	1.211252	7.253725	346.4481	1.211252
1992	7.267044	348.15211	1.240274	7.267044	348.15211	1.240274	7.267044	348.15211	1.240274	7.267044	348.15211	1.240274
1993	7.280363	349.83702	1.268831	7.280363	349.83702	1.268831	7.280363	349.83702	1.268831	7.280363	349.83702	1.268831
1994	7.293683	351.50315	1.296935	7.293683	351.50315	1.296935	7.293683	351.50315	1.296935	7.293683	351.50315	1.296935
1995	7.307002	353.15082	1.324597	7.307002	353.15082	1.324597	7.307002	353.15082	1.324597	7.307002	353.15082	1.324597
1996	7.342646	354.78034	1.351828	7.342646	354.78034	1.351828	7.342646	354.78034	1.351828	7.342646	354.78034	1.351828
1997	7.378291	356.40239	1.378809	7.378291	356.40239	1.378809	7.378291	356.40239	1.378809	7.378291	356.40239	1.378809
1998	7.413935	358.01709	1.405547	7.413935	358.01709	1.405547	7.413935	358.01709	1.405547	7.413935	358.01709	1.405547
1999	7.44958	359.62458	1.432046	7.44958	359.62458	1.432046	7.44958	359.62458	1.432046	7.44958	359.62458	1.432046
2000	7.485224	361.22498	1.458311	7.485224	361.22498	1.458311	7.485224	361.22498	1.458311	7.485224	361.22498	1.458311
2001	7.626381	362.81842	1.484346	7.626381	362.81842	1.484346	7.626381	362.81842	1.484346	7.626381	362.81842	1.484346
2002	7.767537	364.45478	1.510964	7.767537	364.45478	1.510964	7.767537	364.45478	1.510964	7.767537	364.45478	1.510964
2003	7.908693	366.13338	1.538145	7.908693	366.13338	1.538145	7.908693	366.13338	1.538145	7.908693	366.13338	1.538145
2004	8.04985	367.85352	1.565869	8.04985	367.85352	1.565869	8.04985	367.85352	1.565869	8.04985	367.85352	1.565869
2005	8.191006	369.61455	1.594119	8.191006	369.61455	1.594119	8.191006	369.61455	1.594119	8.191006	369.61455	1.594119
2006	8.28075	371.41582	1.622875	8.28075	371.41582	1.622875	8.28075	371.41582	1.622875	8.28075	371.41582	1.622875
2007	8.370495	373.23197	1.651728	8.370495	373.23197	1.651728	8.370495	373.23197	1.651728	8.370495	373.23197	1.651728
2008	8.460239	375.06276	1.680672	8.460239	375.06276	1.680672	8.460239	375.06276	1.680672	8.460239	375.06276	1.680672
2009	8.549983	376.90797	1.709701	8.549983	376.90797	1.709701	8.549983	376.90797	1.709701	8.549983	376.90797	1.709701
2010	8.639727	378.76736	1.73881	8.639727	378.76736	1.73881	8.639727	378.76736	1.73881	8.639727	378.76736	1.73881
2011	8.768315	380.64071	1.767993	8.768315	380.64071	1.767993	8.710134	380.64071	1.767993	8.679792	380.64071	1.767993
2012	8.896903	382.54613	1.797529	8.896903	382.54613	1.797529	8.780541	382.51829	1.797099	8.719858	382.50378	1.796874
2013	9.025491	384.48312	1.827404	9.025491	384.48312	1.827404	8.850948	384.40005	1.826126	8.759923	384.35673	1.825459
2014	9.154079	386.45115	1.857604	9.154079	386.45115	1.857604	8.921355	386.28591	1.855074	8.799988	386.19974	1.853754
2015	9.282667	388.44974	1.888115	9.282667	388.44974	1.888115	8.991762	388.17582	1.883943	8.840054	388.03297	1.881766
2016	9.814028	390.4784	1.918926	9.410811	390.4784	1.918926	9.062091	390.0697	1.912732	8.878834	389.85657	1.909499
2017	10.345389	392.7291	1.952922	9.538955	392.53617	1.950016	9.132421	391.96722	1.941436	8.917613	391.66984	1.936947
2018	10.876749	395.19826	1.989095	9.667099	394.62259	1.981372	9.202751	393.8683	1.970055	8.956393	393.47294	1.964115
2019	11.40811	397.88236	2.030033	9.795243	396.7372	2.012984	9.27308	395.7729	1.998589	8.995173	395.26603	1.991009
2020	11.939471	400.77794	2.072923	9.923387	398.87954	2.044839	9.34341	397.68095	2.027038	9.033953	397.04929	2.017635
2021	12.095621	403.88158	2.118553	10.056581	401.04916	2.076925	9.480332	399.59241	2.0554	9.176533	398.82287	2.043998
2022	12.25177	407.01033	2.164199	10.189775	403.24798	2.109267	9.617255	401.539	2.084145	9.319114	400.63652	2.070836
2023	12.40792	410.16378	2.209851	10.322969	405.47551	2.141851	9.754177	403.52016	2.113258	9.461694	402.48959	2.098132
2024	12.56407	413.34153	2.255501	10.456163	407.7313	2.174667	9.891099	405.53534	2.142724	9.604275	404.38144	2.12587
2025	12.720219	416.5432	2.301142	10.589358	410.01489	2.207704	10.028021	407.58398	2.17253	9.746855	406.31146	2.154034
2026	12.847525	419.7684	2.346764	10.710888	412.32583	2.240949	10.155353	409.66555	2.202662	9.877329	408.27903	2.182608
2027	12.974831	423.00326	2.392173	10.832418	414.65842	2.274317	10.282685	411.77524	2.233045	10.007803	410.27805	2.211499
2028	13.102137	426.24762	2.437367	10.953948	417.0123	2.307799	10.410017	413.91259	2.263668	10.138277	412.30803	2.240693
2029	13.229443	429.50134	2.482348	11.075478	419.38713	2.341389	10.537349	416.07717	2.29452	10.26875	414.36847	2.270179
2030	13.356749	432.76427	2.527114	11.197008	421.78259	2.375079	10.664681	418.26854	2.325592	10.399224	416.45887	2.299944
2031	13.48602	436.03626	2.571668	11.309423	424.19833	2.40886	10.776371	420.48625	2.356871	10.516646	418.57877	2.329977
2032	13.615291	439.31811	2.616021	11.421837	426.62969	2.442667	10.88806	422.72243	2.388245	10.634068	420.72144	2.360179
2033	13.744561	442.60968	2.660174	11.534252	429.0764	2.476492	10.999749	424.97677	2.419705	10.75149	422.88653	2.39054
2034	13.873832	445.9108	2.704127	11.646666	431.53824	2.510333	11.111438	427.24899	2.451247	10.868912	425.07368	2.421054
2035	14.003103	449.22132	2.747879	11.759081	434.01495	2.544184	11.223128	429.53879	2.482863	10.986334	427.28252	2.451711
2036	14.094598	452.5411	2.791431	11.854505	436.50629	2.578041	11.319654	431.84589	2.514549	11.083899	429.51272	2.482504
2037	14.186092	455.85191	2.834548	11.94993	439.00392	2.611789	11.41618	434.16278	2.546198	11.181463	431.75443	2.513296
2038	14.277587	459.1539	2.87724	12.045354	441.50772	2.645429	11.512706	436.48928	2.57781	11.279027	434.00747	2.544082
2039	14.369082	462.44722	2.919514	12.140778	444.0176	2.67896	11.609232	438.82524	2.609381	11.376591	436.27166	2.57486
2040	14.460577	465.732	2.961381	12.236203	446.53346	2.712381	11.705759	441.17052	2.64091	11.474155	438.54681	2.605627
2041	14.534558	469.0084	3.002847	12.302678	449.05521	2.745691	11.776871	443.52497	2.672394	11.546918	440.83277	2.63638
2042	14.608539	472.26811	3.043816	12.369153	451.56887	2.778709	11.847879	445.87625	2.703668	11.61968	443.11744	2.666956
2043	14.682521	475.51143	3.084299	12.435628	454.07456	2.811441	11.919095	448.2244	2.734738	11.692443	445.40085	2.697358
2044	14.756502	478.7386	3.124307	12.502104	456.57243	2.84389	11.990208	450.56947	2.765604	11.765206	447.68302	2.727589
2045	14.830483	481.9499	3.163852	12.568579	459.06259	2.876063	12.06132	452.91153	2.796271	11.837968	449.96397	2.75765
2046	14.890764	485.14559	3.202944	12.62337	461.54517	2.907965	12.112942	455.25061	2.826741	11.889357	452.24373	2.787543
2047	14.951045	488.31928	3.241512	12.678161	464.01464	2.939529	12.164564	457.57738	2.856895	11.940747	454.51202	2.817136
2048	15.011326	491.47135	3.279571	12.732953	466.47121	2.970762	12.216186	459.89204	2.886741	11.992136	456.76903	2.846437
2049	15.071607	494.60213	3.317131	12.787744	468.91509	3.00167	12.267808	462.19478	2.916285	12.043525	459.01494	2.875449
2050	15.131887	497.71197	3.354206	12.842535	471.34648	3.032261	12.31943	464.48579	2.945532	12.094914	461.24993	2.90418

Figure B-3: Global carbon emission, atmospheric CO_2 concentration, and radiative forcing time series for the period 1977–2050 for sequential climate policies $< a_{12}, a_{2j} >$.

	Sequential Climate Policy											
	<a_13, a_21>			<a_13, a_22>			<a_13, a_23>			<a_13, a_24>		
	E(t)	C(t)	F(t)	E(t)	C(t)	F(t)	E(t)	C(t)	F(t)	E(t)	C(t)	F(t)
1977	3.4	331.249	0.945887	3.4	331.249	0.945887	3.4	331.249	0.945887	3.4	331.249	0.945887
1978	3.756891	331.35373	0.947757	3.756891	331.35373	0.947757	3.756891	331.35373	0.947757	3.756891	331.35373	0.947757
1979	4.113781	331.62636	0.952621	4.113781	331.62636	0.952621	4.113781	331.62636	0.952621	4.113781	331.62636	0.952621
1980	4.470672	332.06419	0.960426	4.470672	332.06419	0.960426	4.470672	332.06419	0.960426	4.470672	332.06419	0.960426
1981	4.827563	332.66456	0.97111	4.827563	332.66456	0.97111	4.827563	332.66456	0.97111	4.827563	332.66456	0.97111
1982	5.184453	333.42485	0.984613	5.184453	333.42485	0.984613	5.184453	333.42485	0.984613	5.184453	333.42485	0.984613
1983	5.541344	334.34247	1.00087	5.541344	334.34247	1.00087	5.541344	334.34247	1.00087	5.541344	334.34247	1.00087
1984	5.898235	335.41488	1.019812	5.898235	335.41488	1.019812	5.898235	335.41488	1.019812	5.898235	335.41488	1.019812
1985	6.612016	336.6396	1.041371	6.612016	336.6396	1.041371	6.612016	336.6396	1.041371	6.612016	336.6396	1.041371
1986	6.737694	338.18376	1.068441	6.737694	338.18376	1.068441	6.737694	338.18376	1.068441	6.737694	338.18376	1.068441
1987	6.863372	339.76493	1.096032	6.863372	339.76493	1.096032	6.863372	339.76493	1.096032	6.863372	339.76493	1.096032
1988	6.98905	341.38251	1.124126	6.98905	341.38251	1.124126	6.98905	341.38251	1.124126	6.98905	341.38251	1.124126
1989	7.114728	343.03595	1.152706	7.114728	343.03595	1.152706	7.114728	343.03595	1.152706	7.114728	343.03595	1.152706
1990	7.240406	344.72466	1.181753	7.240406	344.72466	1.181753	7.240406	344.72466	1.181753	7.240406	344.72466	1.181753
1991	7.253725	346.4481	1.211252	7.253725	346.4481	1.211252	7.253725	346.4481	1.211252	7.253725	346.4481	1.211252
1992	7.267044	348.15211	1.240274	7.267044	348.15211	1.240274	7.267044	348.15211	1.240274	7.267044	348.15211	1.240274
1993	7.280363	349.83702	1.268831	7.280363	349.83702	1.268831	7.280363	349.83702	1.268831	7.280363	349.83702	1.268831
1994	7.293683	351.50315	1.296935	7.293683	351.50315	1.296935	7.293683	351.50315	1.296935	7.293683	351.50315	1.296935
1995	7.307002	353.15082	1.324597	7.307002	353.15082	1.324597	7.307002	353.15082	1.324597	7.307002	353.15082	1.324597
1996	7.342646	354.78034	1.351828	7.342646	354.78034	1.351828	7.342646	354.78034	1.351828	7.342646	354.78034	1.351828
1997	7.378291	356.40239	1.378809	7.378291	356.40239	1.378809	7.378291	356.40239	1.378809	7.378291	356.40239	1.378809
1998	7.413935	358.01709	1.405547	7.413935	358.01709	1.405547	7.413935	358.01709	1.405547	7.413935	358.01709	1.405547
1999	7.44958	359.62458	1.432046	7.44958	359.62458	1.432046	7.44958	359.62458	1.432046	7.44958	359.62458	1.432046
2000	7.485224	361.22498	1.458311	7.485224	361.22498	1.458311	7.485224	361.22498	1.458311	7.485224	361.22498	1.458311
2001	7.568354	362.81842	1.484346	7.568354	362.81842	1.484346	7.568354	362.81842	1.484346	7.568354	362.81842	1.484346
2002	7.651483	364.42702	1.510513	7.651483	364.42702	1.510513	7.651483	364.42702	1.510513	7.651483	364.42702	1.510513
2003	7.734613	366.05053	1.536806	7.734613	366.05053	1.536806	7.734613	366.05053	1.536806	7.734613	366.05053	1.536806
2004	7.817742	367.68872	1.563219	7.817742	367.68872	1.563219	7.817742	367.68872	1.563219	7.817742	367.68872	1.563219
2005	7.900872	369.34136	1.589745	7.900872	369.34136	1.589745	7.900872	369.34136	1.589745	7.900872	369.34136	1.589745
2006	7.930613	371.00821	1.61638	7.930613	371.00821	1.61638	7.930613	371.00821	1.61638	7.930613	371.00821	1.61638
2007	7.960353	372.6634	1.642711	7.960353	372.6634	1.642711	7.960353	372.6634	1.642711	7.960353	372.6634	1.642711
2008	7.990094	374.30712	1.668743	7.990094	374.30712	1.668743	7.990094	374.30712	1.668743	7.990094	374.30712	1.668743
2009	8.019835	375.93957	1.694484	8.019835	375.93957	1.694484	8.019835	375.93957	1.694484	8.019835	375.93957	1.694484
2010	8.049576	377.56092	1.719939	8.049576	377.56092	1.719939	8.049576	377.56092	1.719939	8.049576	377.56092	1.719939
2011	8.179091	379.17136	1.745116	8.179091	379.17136	1.745116	8.179091	379.17136	1.745116	8.209579	379.17136	1.745116
2012	8.308607	380.81856	1.770756	8.308607	380.81856	1.770756	8.308607	380.81856	1.770756	8.369582	380.83314	1.770983
2013	8.438122	382.50192	1.796845	8.438122	382.50192	1.796845	8.438122	382.50192	1.796845	8.529585	382.54545	1.797519
2014	8.567637	384.22088	1.823368	8.567637	384.22088	1.823368	8.567637	384.22088	1.823368	8.689587	384.30746	1.824701
2015	8.697152	385.97485	1.850309	8.697152	385.97485	1.850309	8.697152	385.97485	1.850309	8.84959	386.11839	1.852508
2016	9.368263	387.76327	1.877653	8.944314	387.76327	1.877653	8.827459	387.76327	1.877653	8.886159	387.97743	1.880919
2017	10.039374	389.84448	1.909315	9.191475	389.64163	1.906237	8.957766	389.58572	1.905388	8.922727	389.82451	1.909012
2018	10.710485	392.21374	1.945155	9.438637	391.60848	1.93602	9.088073	391.44164	1.933499	8.959296	391.65982	1.936795
2019	11.381596	394.86643	1.985026	9.685798	393.66239	1.966962	9.21838	393.33051	1.961973	8.995865	393.48355	1.964274
2020	12.052707	397.79796	2.028778	9.93296	395.80195	1.999024	9.348687	395.25179	1.990796	9.032433	395.29589	1.991456
2021	12.210549	401.00385	2.076257	10.065391	398.0258	2.032165	9.484721	397.20495	2.019953	9.17564	397.09703	2.018346
2022	12.368392	404.234	2.123713	10.197823	400.27759	2.065534	9.620754	399.19215	2.049472	9.318847	398.93808	2.045707
2023	12.526234	407.48803	2.171137	10.330254	402.55688	2.099121	9.756787	401.21284	2.079339	9.462055	400.81842	2.073521
2024	12.684077	410.76555	2.218523	10.462686	404.86323	2.132913	9.89282	403.26648	2.109538	9.605262	402.7374	2.101772
2025	12.841919	414.06619	2.265863	10.595117	407.1962	2.1669	10.028854	405.35254	2.140057	9.748469	404.69441	2.130446
2026	12.967961	417.38957	2.313148	10.718858	409.55536	2.201071	10.15871	407.4705	2.170883	9.880291	406.68882	2.159525
2027	13.094014	420.72042	2.360164	10.842599	411.93645	2.23536	10.288566	409.6172	2.201963	10.012114	408.71491	2.18892
2028	13.220062	424.05864	2.406912	10.96634	414.3391	2.26976	10.418422	411.79217	2.233288	10.143937	410.77217	2.218618
2029	13.346109	427.40409	2.453394	11.09008	416.76298	2.304262	10.548278	413.99497	2.264845	10.27576	412.86009	2.248608
2030	13.472157	430.75666	2.49961	11.213821	419.20775	2.338859	10.678134	416.22515	2.296624	10.407583	414.97818	2.278876
2031	13.590227	434.11625	2.545565	11.326073	421.67307	2.373543	10.788716	418.48226	2.328613	10.524406	417.12595	2.309411
2032	13.708297	437.47893	2.591206	11.438326	424.15312	2.40823	10.899297	420.75667	2.360674	10.64123	419.29577	2.340101
2033	13.826368	440.84466	2.636539	11.550578	426.64767	2.442916	11.009879	423.04809	2.3928	10.758053	421.48728	2.370936
2034	13.944438	444.21339	2.681568	11.66283	429.15649	2.477596	11.12046	425.35626	2.424985	10.874877	423.70013	2.401909
2035	14.062508	447.58507	2.726295	11.775083	431.67935	2.512267	11.231041	427.68091	2.457223	10.991701	425.93399	2.433013
2036	14.166971	450.95967	2.770724	11.871201	434.21602	2.546924	11.327914	430.02176	2.48951	11.08947	428.1885	2.46424
2037	14.271434	454.33061	2.814775	11.96732	436.75857	2.581458	11.424786	432.37202	2.521751	11.187239	430.45424	2.495456
2038	14.375896	457.69797	2.858454	12.063438	439.30691	2.61587	11.521659	434.73152	2.553942	11.285008	432.73101	2.52666
2039	14.480359	461.06181	2.901767	12.159557	441.86094	2.65016	11.618531	437.10012	2.586082	11.382777	435.01865	2.557847
2040	14.584821	464.42219	2.944722	12.255676	444.42057	2.684326	11.715404	439.47768	2.618169	11.480546	437.31698	2.589016
2041	14.653883	467.77915	2.987324	12.324048	446.98572	2.718369	11.788198	441.86405	2.650201	11.554541	439.62582	2.620163
2042	14.722944	471.11579	3.029366	12.39242	449.54298	2.752113	11.860992	444.24753	2.682022	11.628536	441.93361	2.651132
2043	14.792005	474.43243	3.070861	12.460792	452.09248	2.785564	11.933786	446.62817	2.713635	11.702531	444.24035	2.681927
2044	14.861066	477.72939	3.111825	12.529165	454.63436	2.818728	12.00658	449.00602	2.745043	11.776527	446.54606	2.712548
2045	14.930128	481.007	3.152268	12.597537	457.16872	2.85161	12.079374	451.38113	2.77625	11.850522	448.85077	2.742998
2046	14.988329	484.26557	3.192204	12.651148	459.69571	2.884215	12.130745	453.75353	2.807257	11.90098	451.1545	2.773279
2047	15.046531	487.50014	3.231582	12.704759	462.2083	2.916458	12.182117	456.11297	2.837935	11.951439	453.44592	2.803246
2048	15.104732	490.7111	3.270414	12.75837	464.70673	2.948345	12.233489	458.45964	2.868289	12.001898	455.72523	2.832904
2049	15.162934	493.89884	3.308715	12.811982	467.19123	2.979885	12.28486	460.79376	2.898328	12.052357	457.99265	2.862261
2050	15.221136	497.06372	3.346497	12.865593	469.66202	3.011085	12.336232	463.11553	2.928057	12.102815	460.24835	2.891322

Figure B-4: Global carbon emission, atmospheric CO_2 concentration, and radiative forcing time series for the period 1977–2050 for sequential climate policies $< a_{13}, a_{2j} >$.

	Sequential Climate Policy											
	<a_14, a_21>			<a_14, a_22>			<a_14, a_23>			<a_14, a_24>		
	E(t)	C(t)	F(t)	E(t)	C(t)	F(t)	E(t)	C(t)	F(t)	E(t)	C(t)	F(t)
1977	3.4	331.249	0.945887	3.4	331.249	0.945887	3.4	331.249	0.945887	3.4	331.249	0.945887
1978	3.756891	331.35373	0.947757	3.756891	331.35373	0.947757	3.756891	331.35373	0.947757	3.756891	331.35373	0.947757
1979	4.113781	331.62636	0.952621	4.113781	331.62636	0.952621	4.113781	331.62636	0.952621	4.113781	331.62636	0.952621
1980	4.470672	332.06419	0.960426	4.470672	332.06419	0.960426	4.470672	332.06419	0.960426	4.470672	332.06419	0.960426
1981	4.827563	332.66456	0.97111	4.827563	332.66456	0.97111	4.827563	332.66456	0.97111	4.827563	332.66456	0.97111
1982	5.184453	333.42485	0.984613	5.184453	333.42485	0.984613	5.184453	333.42485	0.984613	5.184453	333.42485	0.984613
1983	5.541344	334.34247	1.00087	5.541344	334.34247	1.00087	5.541344	334.34247	1.00087	5.541344	334.34247	1.00087
1984	5.898235	335.41488	1.019812	5.898235	335.41488	1.019812	5.898235	335.41488	1.019812	5.898235	335.41488	1.019812
1985	6.612016	336.6396	1.041371	6.612016	336.6396	1.041371	6.612016	336.6396	1.041371	6.612016	336.6396	1.041371
1986	6.737694	338.18376	1.068441	6.737694	338.18376	1.068441	6.737694	338.18376	1.068441	6.737694	338.18376	1.068441
1987	6.863372	339.76493	1.096032	6.863372	339.76493	1.096032	6.863372	339.76493	1.096032	6.863372	339.76493	1.096032
1988	6.98905	341.38251	1.124126	6.98905	341.38251	1.124126	6.98905	341.38251	1.124126	6.98905	341.38251	1.124126
1989	7.114728	343.03595	1.152706	7.114728	343.03595	1.152706	7.114728	343.03595	1.152706	7.114728	343.03595	1.152706
1990	7.240406	344.72466	1.181753	7.240406	344.72466	1.181753	7.240406	344.72466	1.181753	7.240406	344.72466	1.181753
1991	7.253725	346.4481	1.211252	7.253725	346.4481	1.211252	7.253725	346.4481	1.211252	7.253725	346.4481	1.211252
1992	7.267044	348.15211	1.240274	7.267044	348.15211	1.240274	7.267044	348.15211	1.240274	7.267044	348.15211	1.240274
1993	7.280363	349.83702	1.268831	7.280363	349.83702	1.268831	7.280363	349.83702	1.268831	7.280363	349.83702	1.268831
1994	7.293683	351.50315	1.296935	7.293683	351.50315	1.296935	7.293683	351.50315	1.296935	7.293683	351.50315	1.296935
1995	7.307002	353.15082	1.324597	7.307002	353.15082	1.324597	7.307002	353.15082	1.324597	7.307002	353.15082	1.324597
1996	7.342646	354.78034	1.351828	7.342646	354.78034	1.351828	7.342646	354.78034	1.351828	7.342646	354.78034	1.351828
1997	7.378291	356.40239	1.378809	7.378291	356.40239	1.378809	7.378291	356.40239	1.378809	7.378291	356.40239	1.378809
1998	7.413935	358.01709	1.405547	7.413935	358.01709	1.405547	7.413935	358.01709	1.405547	7.413935	358.01709	1.405547
1999	7.44958	359.62458	1.432046	7.44958	359.62458	1.432046	7.44958	359.62458	1.432046	7.44958	359.62458	1.432046
2000	7.485224	361.22498	1.458311	7.485224	361.22498	1.458311	7.485224	361.22498	1.458311	7.485224	361.22498	1.458311
2001	7.539241	362.81842	1.484346	7.539241	362.81842	1.484346	7.539241	362.81842	1.484346	7.539241	362.81842	1.484346
2002	7.593258	364.41309	1.510287	7.593258	364.41309	1.510287	7.593258	364.41309	1.510287	7.593258	364.41309	1.510287
2003	7.647275	366.00897	1.536135	7.647275	366.00897	1.536135	7.647275	366.00897	1.536135	7.647275	366.00897	1.536135
2004	7.701292	367.60604	1.561889	7.701292	367.60604	1.561889	7.701292	367.60604	1.561889	7.701292	367.60604	1.561889
2005	7.755309	369.20429	1.58755	7.755309	369.20429	1.58755	7.755309	369.20429	1.58755	7.755309	369.20429	1.58755
2006	7.755165	370.8037	1.613119	7.755165	370.8037	1.613119	7.755165	370.8037	1.613119	7.755165	370.8037	1.613119
2007	7.755021	372.37825	1.638183	7.755021	372.37825	1.638183	7.755021	372.37825	1.638183	7.755021	372.37825	1.638183
2008	7.754876	373.92833	1.662754	7.754876	373.92833	1.662754	7.754876	373.92833	1.662754	7.754876	373.92833	1.662754
2009	7.754732	375.45434	1.686844	7.754732	375.45434	1.686844	7.754732	375.45434	1.686844	7.754732	375.45434	1.686844
2010	7.754588	376.95667	1.710465	7.754588	376.95667	1.710465	7.754588	376.95667	1.710465	7.754588	376.95667	1.710465
2011	7.882855	378.43571	1.733629	7.882855	378.43571	1.733629	7.913676	378.43571	1.733629	7.882855	378.43571	1.733629
2012	8.011122	379.95304	1.757297	8.011122	379.95304	1.757297	8.072764	379.96778	1.757527	8.011122	379.95304	1.757297
2013	8.139389	381.50803	1.781456	8.139389	381.50803	1.781456	8.231852	381.55203	1.782138	8.139389	381.50803	1.781456
2014	8.267655	383.10008	1.806088	8.267655	383.10008	1.806088	8.39094	383.18761	1.807439	8.267655	383.10008	1.806088
2015	8.395922	384.72859	1.831179	8.395922	384.72859	1.831179	8.550028	384.8737	1.83341	8.395922	384.72859	1.831179
2016	9.135839	386.39299	1.856713	8.705557	386.39299	1.856713	8.710468	386.60949	1.860027	8.525183	386.39299	1.856713
2017	9.875755	388.38509	1.887131	9.015193	388.17921	1.883994	8.870908	388.39457	1.887275	8.654444	388.09291	1.882679
2018	10.615672	390.69961	1.922276	9.324828	390.0853	1.912968	9.031348	390.22815	1.915134	8.783705	389.82778	1.909062
2019	11.355588	393.33135	1.961986	9.634463	392.10932	1.94358	9.191788	392.10945	1.943582	8.912966	391.59705	1.935847
2020	12.095504	396.2752	2.006092	9.944098	394.24938	1.975775	9.352228	394.03769	1.972599	9.042227	393.40015	1.963021
2021	12.259085	399.52612	2.054419	10.074769	396.50359	2.0095	9.487794	396.01213	2.002164	9.183101	395.23654	1.990568
2022	12.422665	402.80333	2.102741	10.20544	398.78442	2.043428	9.623361	398.02004	2.032079	9.323975	397.11118	2.018557
2023	12.586246	406.1064	2.151048	10.336111	401.09144	2.077549	9.758927	400.06088	2.062331	9.464849	399.02343	2.046972
2024	12.749826	409.43492	2.199331	10.466782	403.42423	2.111851	9.894493	402.13413	2.092906	9.605724	400.9727	2.075797
2025	12.913407	412.78848	2.247582	10.597454	405.78237	2.146326	10.03006	404.23925	2.123789	9.746598	402.95839	2.105017
2026	13.039036	416.16667	2.295793	10.722889	408.16545	2.180962	10.161249	406.37575	2.154969	9.880863	404.97992	2.134617
2027	13.164664	419.55126	2.343704	10.848324	410.57088	2.215719	10.292439	408.54132	2.186407	10.015129	407.03384	2.164541
2028	13.290293	422.94213	2.391318	10.97376	412.9983	2.250588	10.423628	410.7355	2.21809	10.149394	409.11965	2.194774
2029	13.415922	426.33919	2.438638	11.099195	415.44736	2.28556	10.554818	412.95783	2.250008	10.28366	411.23684	2.225306
2030	13.541551	429.74235	2.485666	11.224631	417.91771	2.320628	10.686007	415.20786	2.282149	10.417925	413.38489	2.256122
2031	13.6596	433.1515	2.532405	11.337432	420.40901	2.355784	10.796755	417.48515	2.314503	10.535084	415.56331	2.287211
2032	13.777649	436.56293	2.578808	11.450233	422.91488	2.390937	10.907504	419.77949	2.346921	10.652244	417.76344	2.318444
2033	13.895699	439.97662	2.624881	11.563033	425.4351	2.426081	11.018252	422.0906	2.379397	10.769403	419.98494	2.349815
2034	14.013748	443.39252	2.670627	11.675834	427.96944	2.461213	11.129	424.41822	2.411926	10.886562	422.22745	2.381314
2035	14.131797	446.81061	2.716051	11.788635	430.51766	2.496328	11.239749	426.76208	2.444502	11.003721	424.49065	2.412935
2036	14.236151	450.23084	2.761157	11.885139	433.07956	2.531422	11.336917	429.12192	2.47712	11.102264	426.7742	2.44467
2037	14.340505	453.64665	2.805864	11.981643	435.64711	2.566387	11.434086	431.491	2.509686	11.200807	429.06886	2.476389
2038	14.44486	457.05809	2.850179	12.078147	438.22022	2.601221	11.531255	433.86916	2.542197	11.29935	431.37448	2.508088
2039	14.549214	460.46524	2.894109	12.17465	440.79882	2.635924	11.628423	436.25626	2.574652	11.397893	433.69086	2.539766
2040	14.653568	463.86818	2.937662	12.271154	443.3828	2.670497	11.725592	438.65216	2.607048	11.496437	436.01783	2.571418
2041	14.721305	467.26698	2.980844	12.340197	445.97209	2.70494	11.798468	441.05672	2.639384	11.570561	438.35524	2.603043
2042	14.789042	470.64413	3.023441	12.40924	448.55343	2.739078	11.871345	443.45814	2.671502	11.644686	440.69118	2.63448
2043	14.85678	474.00001	3.065468	12.478283	451.12694	2.772918	11.944221	445.85646	2.703406	11.718811	443.02569	2.665731
2044	14.924517	477.33494	3.106939	12.547327	453.69276	2.806465	12.017097	448.25175	2.735099	11.792936	445.35878	2.6968
2045	14.992254	480.64927	3.147867	12.61637	456.251	2.839724	12.089973	450.64406	2.766583	11.867061	447.69049	2.727688
2046	15.049293	483.94333	3.188267	12.669289	458.8018	2.872702	12.141674	453.03343	2.797862	11.918094	450.02084	2.758397
2047	15.106333	487.21227	3.228088	12.722208	461.33749	2.905303	12.193375	455.40971	2.828807	11.969127	452.33873	2.788785
2048	15.163372	490.45649	3.267344	12.775127	463.85831	2.937536	12.245076	457.77311	2.859425	12.020161	454.64437	2.818859
2049	15.220412	493.67639	3.30605	12.828046	466.36451	2.969409	12.296777	460.12385	2.889722	12.071194	456.93796	2.848624
2050	15.277451	496.87236	3.344219	12.880965	468.85633	3.000929	12.348477	462.46212	2.919705	12.122227	459.21969	2.878087

Figure B-5: Global carbon emission, atmospheric CO_2 concentration, and radiative forcing time series for the period 1977–2050 for sequential climate policies $< a_{14}, a_{2j} >$.

Sequential Climate Policy	Climate Sensitivity	Ocean Diffusivity	deltaT (1)	deltaT (2)
$< a_{11}, a_{21} >$	1.5°C	1/50	0.535	1.077
		1	0.501	0.990
		5	0.480	0.916
		50	0.470	0.876
	2.5°C	1/50	0.895	1.824
		1	0.731	1.523
		5	0.652	1.325
		50	0.575	1.094
	4.5°C	1/50	1.340	2.913
		1	0.907	2.025
		5	0.743	1.576
		50	0.649	1.286
$< a_{11}, a_{22} >$	1.5°C	1/50	0.535	0.974
		1	0.501	0.904
		5	0.480	0.842
		50	0.470	0.809
	2.5°C	1/50	0.895	1.646
		1	0.731	1.398
		5	0.652	1.229
		50	0.575	1.026
	4.5°C	1/50	1.340	2.660
		1	0.907	1.887
		5	0.743	1.483
		50	0.649	1.218

Table B.1: One-box climate model projections (in °C) of global-mean surface temperature change for Periods 1 and 2 under sequential policies $< a_{11}, a_{21} >$ and $< a_{11}, a_{22} >$, as a function of Climate Sensitivity and Ocean Diffusivity.

Sequential Climate Policy	Climate Sensitivity	Ocean Diffusivity	deltaT (1)	deltaT (2)
$< a_{11}, a_{23} >$	1.5°C	1/50	0.535	0.956
		1	0.501	0.890
		5	0.480	0.831
		50	0.470	0.799
	2.5°C	1/50	0.895	1.615
		1	0.731	1.379
		5	0.652	1.215
		50	0.575	1.017
	4.5°C	1/50	1.340	2.619
		1	0.907	1.869
		5	0.743	1.471
		50	0.649	1.209
$< a_{11}, a_{24} >$	1.5°C	1/50	0.535	0.945
		1	0.501	0.880
		5	0.480	0.823
		50	0.470	0.792
	2.5°C	1/50	0.895	1.595
		1	0.731	1.366
		5	0.652	1.205
		50	0.575	1.010
	4.5°C	1/50	1.340	2.592
		1	0.907	1.854
		5	0.743	1.461
		50	0.649	1.202

Table B.2: One-box climate model projections (in °C) of global-mean surface temperature change for Periods 1 and 2 under sequential policies $< a_{11}, a_{23} >$ and $< a_{11}, a_{24} >$, as a function of Climate Sensitivity and Ocean Diffusivity.

191

Sequential Climate Policy	Climate Sensitivity	Ocean Diffusivity	deltaT (1)	deltaT (2)
$< a_{12}, a_{21} >$	1.5°C	1/50	0.524	1.044
		1	0.493	0.958
		5	0.473	0.885
		50	0.464	0.847
	2.5°C	1/50	0.873	1.769
		1	0.720	1.471
		5	0.643	1.281
		50	0.569	1.060
	4.5°C	1/50	1.315	2.816
		1	0.896	1.959
		5	0.736	1.528
		50	0.644	1.249
$< a_{12}, a_{22} >$	1.5°C	1/50	0.524	0.962
		1	0.493	0.892
		5	0.473	0.831
		50	0.464	0.798
	2.5°C	1/50	0.873	1.627
		1	0.720	1.379
		5	0.643	1.211
		50	0.569	1.012
	4.5°C	1/50	1.315	2.624
		1	0.896	1.860
		5	0.736	1.462
		50	0.644	1.202

Table B.3: One-box climate model projections (in °C) of global-mean surface temperature change for Periods 1 and 2 under sequential policies $< a_{12}, a_{21} >$ and $< a_{12}, a_{22} >$, as a function of Climate Sensitivity and Ocean Diffusivity.

Sequential Climate Policy	Climate Sensitivity	Ocean Diffusivity	deltaT (1)	deltaT (2)
$< a_{12}, a_{23} >$	1.5°C	1/50	0.524	0.939
		1	0.493	0.872
		5	0.473	0.814
		50	0.464	0.783
	2.5°C	1/50	0.873	1.587
		1	0.720	1.351
		5	0.643	1.190
		50	0.569	0.998
	4.5°C	1/50	1.315	2.567
		1	0.896	1.830
		5	0.736	1.442
		50	0.644	1.188
$< a_{12}, a_{24} >$	1.5°C	1/50	0.524	0.927
		1	0.493	0.863
		5	0.473	0.806
		50	0.464	0.776
	2.5°C	1/50	0.873	1.567
		1	0.720	1.337
		5	0.643	1.180
		50	0.569	0.990
	4.5°C	1/50	1.315	2.539
		1	0.896	1.816
		5	0.736	1.432
		50	0.644	1.181

Table B.4: One-box climate model projections (in °C) of global-mean surface temperature change for Periods 1 and 2 under sequential policies $< a_{12}, a_{23} >$ and $< a_{12}, a_{24} >$, as a function of Climate Sensitivity and Ocean Diffusivity.

Sequential Climate Policy	Climate Sensitivity	Ocean Diffusivity	deltaT (1)	deltaT (2)
$< a_{13}, a_{21} >$	1.5°C	1/50	0.522	1.037
		1	0.492	0.951
		5	0.472	0.879
		50	0.464	0.841
	2.5°C	1/50	0.871	1.759
		1	0.718	1.461
		5	0.643	1.272
		50	0.569	1.053
	4.5°C	1/50	1.313	2.796
		1	0.895	1.944
		5	0.735	1.517
		50	0.643	1.241
$< a_{13}, a_{22} >$	1.5°C	1/50	0.522	0.952
		1	0.492	0.882
		5	0.472	0.821
		50	0.464	0.789
	2.5°C	1/50	0.871	1.610
		1	0.718	1.363
		5	0.643	1.198
		50	0.569	1.002
	4.5°C	1/50	1.313	2.594
		1	0.895	1.841
		5	0.735	1.448
		50	0.643	1.192

Table B.5: One-box climate model projections (in °C) of global-mean surface temperature change for Periods 1 and 2 under sequential policies $< a_{13}, a_{21} >$ and $< a_{13}, a_{22} >$, as a function of Climate Sensitivity and Ocean Diffusivity.

Sequential Climate Policy	Climate Sensitivity	Ocean Diffusivity	deltaT (1)	deltaT (2)
$< a_{13}, a_{23} >$	1.5°C	1/50	0.522	0.930
		1	0.492	0.864
		5	0.472	0.807
		50	0.464	0.776
	2.5°C	1/50	0.871	1.573
		1	0.718	1.338
		5	0.643	1.180
		50	0.569	0.990
	4.5°C	1/50	1.313	2.543
		1	0.895	1.814
		5	0.735	1.431
		50	0.643	1.179
$< a_{13}, a_{24} >$	1.5°C	1/50	0.522	0.921
		1	0.492	0.857
		5	0.472	0.800
		50	0.464	0.770
	2.5°C	1/50	0.871	1.556
		1	0.718	1.328
		5	0.643	1.172
		50	0.569	0.984
	4.5°C	1/50	1.313	2.521
		1	0.895	1.803
		5	0.735	1.424
		50	0.643	1.174

Table B.6: One-box climate model projections (in °C) of global-mean surface temperature change for Periods 1 and 2 under sequential policies $< a_{13}, a_{23} >$ and $< a_{13}, a_{24} >$, as a function of Climate Sensitivity and Ocean Diffusivity.

Sequential Climate Policy	Climate Sensitivity	Ocean Diffusivity	deltaT (1)	deltaT (2)
$< a_{14}, a_{21} >$	1.5°C	1/50	0.522	1.035
		1	0.491	0.948
		5	0.472	0.876
		50	0.463	0.838
	2.5°C	1/50	0.870	1.754
		1	0.718	1.455
		5	0.642	1.267
		50	0.569	1.049
	4.5°C	1/50	1.311	2.786
		1	0.895	1.937
		5	0.735	1.512
		50	0.643	1.237
$< a_{14}, a_{22} >$	1.5°C	1/50	0.522	0.947
		1	0.491	0.877
		5	0.472	0.817
		50	0.463	0.785
	2.5°C	1/50	0.870	1.602
		1	0.718	1.355
		5	0.642	1.192
		50	0.569	0.998
	4.5°C	1/50	1.311	2.579
		1	0.895	1.831
		5	0.735	1.441
		50	0.643	1.187

Table B.7: One-box climate model projections (in °C) of global-mean surface temperature change for Periods 1 and 2 under sequential policies $< a_{14}, a_{21} >$ and $< a_{14}, a_{22} >$, as a function of Climate Sensitivity and Ocean Diffusivity.

Sequential Climate Policy	Climate Sensitivity	Ocean Diffusivity	deltaT (1)	deltaT (2)
$< a_{14}, a_{23} >$	1.5°C	1/50	0.522	0.926
		1	0.491	0.860
		5	0.472	0.803
		50	0.463	0.773
	2.5°C	1/50	0.870	1.566
		1	0.718	1.332
		5	0.642	1.174
		50	0.569	0.986
	4.5°C	1/50	1.311	2.531
		1	0.895	1.806
		5	0.735	1.425
		50	0.643	1.175
$< a_{14}, a_{24} >$	1.5°C	1/50	0.522	0.915
		1	0.491	0.850
		5	0.472	0.795
		50	0.463	0.765
	2.5°C	1/50	0.870	1.546
		1	0.718	1.318
		5	0.642	1.164
		50	0.569	0.978
	4.5°C	1/50	1.311	2.503
		1	0.895	1.791
		5	0.735	1.415
		50	0.643	1.168

Table B.8: One-box climate model projections (in °C) of global-mean surface temperature change for Periods 1 and 2 under sequential policies $< a_{14}, a_{23} >$ and $< a_{14}, a_{24} >$, as a function of Climate Sensitivity and Ocean Diffusivity.

Bibliography

[1] *Draft Protocol to the United Nations Framework Convention on Climate Change on Greenhouse Gas Emission Reduction.* United Nations, Framework Convention on Climate Change, 1994.

[2] ADA Decision Systems. *DPL: Advanced Version User Guide.* Duxbury Press: Belmont, California, 1995.

[3] S. Arrhenius. On the influence of carbonic acid in the air upon the temperature of the ground. *Philosophical Magazine,* 41:237–276, 1896.

[4] Robert C. Balling, Jr. *The Heated Debate: Greenhouse Predictions Versus Climate Reality.* Pacific Research Institute for Public Policy, San Francisco, California, 1992.

[5] R. E. Barlow. Using influence diagrams. In C. A. Clarotti and D. V. Lindley, editors, *Accelerated Life Testing and Experts' Opinions in Reliability,* pages 145–157. North-Holland Physics Publishing, 1988.

[6] Jose' M. Bernardo and Adrian F. M. Smith. *Bayesian Theory.* John Wiley & Sons, New York, 1994.

[7] Bert Bolin, John Houghton, and L. Gylvan Meira Filho. *Radiative Forcing of Climate Change: The 1994 Report of the Scientific Assessment Working Group of IPCC, Summary for Policymakers.* Intergovermental Panel on Climate Change, 1994.

[8] W. Broecker. A revised estimate for the radiocarbon age of North Atlantic deep water. *Journal of Geophysical Research,* 84:3218–3226, 1979.

[9] J. Bruce, Hoesung Lee, and E. Haites, editors. *Climate Change 1995: Economics and Social Dimensions of Climate Change.* Cambridge University Press, New York, 1996.

[10] M. I. Budyko. The effect of solar radiation variations on the climate of the Earth. *Tellus,* 21(5):611–619, 1969.

[11] H. J. Call and W. A. Miller. A comparison of approaches and implementations for automating decision analysis. *Reliability Engineering and System Safety*, 30:115-162, 1990.

[12] R. D. Cess et al. Uncertainties in carbon dioxide radiative forcing in atmospheric general circulation models. *Science*, 262:1252-1255, 1993.

[13] Robert T. Clemen. *Making Hard Decisions: An Intorduction to Decision Analysis*. Duxbury Press, Belmont, California, second edition, 1996.

[14] William R. Cline. *The Economics of Global Warming*. Institute for International Economics, Washington, D.C., 1992.

[15] U. Cubasch and R. D. Cess. Processes and modelling. In J. T. Houghton, G. J. Jenkins, and J. J. Ephraums, editors, *Climate Change: The IPCC Scientific Assessment*, pages 69-92. Cambridge University Press, New York, 1990.

[16] H. Dezhbaksh. The inappropriate use of serial correlation tests in dynamic linear models. *Review of Economics and Statistics*, 72:126-132, 1990.

[17] Hadi Dowlatabadi. Integrated assessment models of climate change: An incomplete overview. *Energy Policy*, 23(4-5):289-296, 1995.

[18] Hadi Dowlatabadi and M. Granger Morgan. Integrated assessment of climate change. *Science*, 259:1813, 1993.

[19] Hadi Dowlatabadi and M. Granger Morgan. A model framework for integrated studies of the climate problem. *Energy Policy*, pages 209-221, March 1993.

[20] J. Durbin. Testing for serial correlation in least-squares regression when some of the regressors are lagged dependent variables. *Econometrica*, 38:410-421, 1970.

[21] R. C. Fair. The estimation of simultaneous equation models with lagged endogenous variables and first order serially correlated errors. *Econometrica*, 38:507-516, May 1970.

[22] J. B. Fourier. Temperature du globe terrestre et des espace planetaires. In G. Darboux, editor, *Fourier, J. B., Ouvres*, volume 2, pages 97-125. Gauthier-Villars, Paris, 1888.

[23] William H. Greene. *Econometric Analysis*. Prentice Hall, Englewood Cliffs, New Jersey, second edition, 1993.

[24] James D. Hamilton. *Time Series Analysis*. Princeton University Press, Princeton, New Jersey, 1994.

[25] James K. Hammitt. Outcome and value uncertainties in global-change policy. *Climatic Change*, 1996.

[26] James K. Hammitt, Robert J. Lempert, and Michael E. Schlesinger. A sequential-decision strategy for abating climate change. *Nature*, 357:315–318, 1992.

[27] J. Hansen et al. Climate response times: Dependence on climate sensitivity and ocean mixing. *Science*, 229:857–859, 1985.

[28] J. Hansen et al. Global climate changes as forecast by Goddard Institute for Space Studies three-dimensional model. *Journal of Geophysical Research*, 93(D8):9341–9364, August 1988.

[29] L. D. D. Harvey. Managing atmospheric CO_2. *Climatic Change*, 15:343–381, 1989.

[30] A. Henderson-Sellers and K. McGuffie. *A Climate Modelling Primer*. John Wiley & Sons, New York, 1987.

[31] J. T. Houghton, B. A. Callander, and S. K. Varney, editors. *Climate Change 1992: The Supplementary Report to the IPCC Scientific Assessment*. Cambridge University Press, New York, 1992.

[32] J. T. Houghton, G. J. Jenkins, and J. J. Ephraums, editors. *Climate Change: The IPCC Scientific Assessment*. Cambridge University Press, New York, 1990.

[33] Ronald A. Howard. From influence to relevance to knowledge. In Robert M. Oliver and James Q. Smith, editors, *Influence Diagrams, Belief Nets and Decision Analysis*, Wiley Series in Applied Probability and Statistics, chapter 1, pages 3–23. John Wiley & Sons, New York, 1990.

[34] H. D. Jacoby, G. M. Kaufman, and L. J. Valverde A., Jr. Formulation of climate policy for use in uncertainty analysis. Technical report, MIT Joint Program on the Science and Policy of Global Change, May 1996.

[35] H. D. Jacoby, R. Schmalensee, and D. M. Reiner. What does stabilizing greenhouse gas concentrations mean? Technical report, MIT Joint Program on the Science and Policy of Global Change, October 1996.

[36] Henry D. Jacoby and Ronald G. Prinn. Uncertainty in climate change policy analysis. Technical Report 1, MIT Joint Program on the Science and Policy of Global Change, December 1994.

[37] Richard C. Jeffrey. *The Logic of Decision*. The University of Chicago Press, Chicago, second edition, 1993.

[38] Joint Program on the Science and Policy of Global Change, Massachusetts Institute of Technology. *Design Report: An Improved Framework for Analysis of Global Warming*, August 1993.

[39] C. D. Keeling, R. B. Bacastow, A. F. Carter, S. C. Piper, T. P. Whorf, M Heimann, W. G. Mook, and H. Roeloffzen. A three dimensional model of atmospheric CO_2 transport based on observed winds: 1. analysis of observational data. In *Aspects of Climate Variability in the Pacific and the Western Americas*, volume 55 of *Geophysical Monograph*. American Geophysical Union, 1989.

[40] Charles D. Kolstad. George Bush versus Al Gore: Irreversibilities in greenhouse gas accumulation and emission control investment. *Energy Policy*, 22(9):771-778, 1994.

[41] Robert J. Lempert, Michael E. Schlesinger, and James K. Hammitt. The impact of potential abrupt climate changes on near-term policy choices. *Climatic Change*, 26:351-376, 1994.

[42] Richard S. Lindzen. Climate dynamics and global change. Technical Report 28, Center for Global Change Science, Massachusetts Institute of Technology, March 1994.

[43] Lester Machta. The role of the oceans and biosphere in the carbon dioxide cycle. In *Nobel Symposium*, volume 20, pages 121-145. 1972.

[44] A. Madansky. On the efficiency of three-stage least squares estimation. *Econometrica*, 32:55, 1964.

[45] E. Maier-Reimer and K. Hasselmann. Transport and storage of CO_2 in the ocean — An inorganic ocean-circulation carbon cycle model. *Climate Dynamics*, 2:63-90, 1987.

[46] S. Manabe and R. Stouffer. Century-scale effects of increased atmospheric CO_2 on the ocean-atmosphere system. *Nature*, 364:215-218, 1993.

[47] Alan S. Manne. Hedging strategies for global carbon dioxide abatement: A summary of poll results EMF 14 Subgroup - analysis for decisions under uncertainty. In N. Nakićenović, W. D. Nordhaus, R. Richels, and F. L. Toth, editors, *Climate Change: Integrating Science, Economics, and Policy*, pages 207-228. International Institute for Applied Systems Analysis, Laxenburg, Austria, December 1996.

[48] Alan S. Manne and Richard G. Richels. *Buying Greenhouse Insurance: The Economic Costs of Carbon Dioxide Emission Limits*. MIT Press, Cambridge, Massachusetts, 1992.

[49] Howard Margolis. *Patterns, Thinking, and Cognition: A Theory of Judgment*. University of Chicago Press, Chicago, Illinois, 1987.

[50] James E. Matheson. Using influence diagrams to value information and control. In Robert M. Oliver and James Q. Smith, editors, *Influence Diagrams, Belief Nets and Decision Analysis*, Wiley Series in Applied Probability and Statistics, chapter 2, pages 25-47. John Wiley & Sons, New York, 1990.

[51] Izhar Matzkevich and Bruce Abramson. Decision analytic networks in artificial intelligence. *Management Science*, 41(1):1-22, January 1995.

[52] Jon R. Miller and Frank Lad. Flexibility, learning, and irreversability in environmental decisions: A Bayesian approach. *Journal of Environmental Economics and Management*, 11:161-172, 1984.

[53] M. Granger Morgan and David W. Keith. Subjective judgments by climate experts. *Environmental Science and Technology*, 29(10):468-476, 1995.

[54] National Academy of Sciences. *Policy Implications of Greenhouse Warming*. National Academy Press, Washington, D.C., 1992.

[55] William D. Nordhaus. The cost of slowing climate change: A survey. *The Energy Journal*, 12(1):37-65, 1991.

[56] William D. Nordhaus. Expert opinion on climatic change. *American Scientist*, 82:45-51, January 1994.

[57] William D. Nordhaus. *Managing the Global Commons: The Economics of Climate Change*. MIT Press, Cambridge, Massachusetts, 1994.

[58] Edward A. Parson. Integrated assessment and environmental policy making: In pursuit of usefulness. *Energy Policy*, 23(4-5):463-475, 1995.

[59] Judea Pearl. *Probabilistic Reasoning in Intelligent Systems: Networks of Plausible Inference*. Series in Representation and Reasoning. Morgan Kaufmann Publishers, Inc., San Mateo, California, 1988.

[60] Stephen C. Peck and Thomas J. Teisberg. Global warming uncertainties and the value of information: An analysis using CETA. *Resource and Energy Economics*, 15:71-97, 1993.

[61] Robert S. Pindyck and Daniel L. Rubinfeld. *Econometric Models and Economic Forecasts*. McGraw-Hill, Inc., New York, third edition, 1991.

[62] R. Prinn et al. Integrated Global System Model for climate policy analysis: I. Model framework and sensitivity studies. Technical Report 7, MIT Joint Program on the Science and Policy of Global Change, June 1996.

[63] Howard Raiffa. *Decision Analysis: Introductory Lectures on Choices Under Uncertainty.* Random House, New York, 1968.

[64] R. Revelle and H. E. Suess. Carbon dioxide exchange between atmosphere and ocean and the question of an increase of atmospheric CO_2 during past decades. *Tellus*, 9:18-27, 1957.

[65] Richard Richels and Jae Edmonds. The economics of stabalizing atmospheric CO_2. *Energy Policy*, 23(4-5):373-378, 1995.

[66] Leonard J. Savage. *The Foundations of Statistics.* Wiley, New York, second edition, 1954.

[67] Stephen H. Schneider and Starley L. Thompson. Atmospheric CO_2 and climate: Importance of the transient response. *Journal of Geophysical Research*, 86(C4):3135-3147, 1981.

[68] Frederick Seitz. *Global Warming and Ozone Hole Controversies: A Challenge to Scientific Judgment.* George C. Marshall Institute, Washington, D.C., 1994.

[69] William D. Sellers. A global climate model based on the energy balance of the Earth-atmosphere system. *Journal of Applied Meteorology*, 8:392-400, 1969.

[70] Ross D. Shachter. Evaluating influence diagrams. *Operations Research*, 33(6), 1986.

[71] K. P. Shine et al. Radiative forcing of climate. In J. T. Houghton, G. J. Jenkins, and J. J. Ephraums, editors, *Climate Change: The IPCC Scientific Assessment*, pages 41-68. Cambridge University Press, New York, 1990.

[72] Andrei P. Sokolov and Peter H. Stone. Description and validation of the MIT version of the GISS 2-D model. Technical Report 2, MIT Joint Program on the Science and Policy of Global Change, June 1995.

[73] Andrei P. Sokolov and Peter H. Stone. Global warming projections: Sensitivity to deep ocean mixing. Technical Report 11, MIT Joint Program on the Science and Policy of Global Change, September 1996.

[74] R. Stouffer et al. Century-scale effects of increased atmospheric CO_2 on the ocean-atmosphere system. *Nature*, 367:634-640, 1994.

[75] Gilbert Strang. *Linear Algebra and its Applications.* Harcourt Brace Jovanovich, San Diego, 1988.

[76] Ferenc L. Toth. Practice and progress in integrated assessments of climate change. *Energy Policy*, 23(4-5):253-267, 1995.

[77] S. G. Warren and S. H. Schneider. Seasonal simulation as a test for uncertainties in the parameterization of a Budyko-Sellars zonal climate model. *Journal of Atmospheric Science*, 36:1377–1391, 1979.

[78] Mort D. Webster. Analysis of uncertainty in large models with application to climate policy. Master's thesis, MIT, Technology and Policy Program, June 1996.

[79] T. M. L. Wigley. A simple inverse carbon cycle model. *Global Biochemical Cycles*, 5(4):373–382, 1991.

[80] Z. Yang et al. The MIT Emissions Prediction and Policy Analysis (EPPA) model. Technical Report 6, MIT Joint Program on the Science and Policy of Global Change, 1996.